SSC - 1400 Draft Report

MODELING STRUCTURAL DAMAGE IN SHIP COLLISIONS

SHIP STRUCTURE COMMITTEE

2002

Inside Cover

Chairman of SSC Letter

Blank

Technical Report Documentation Page

1. Report No. SSC-Draft Report	2. Government Accession No. PB98-172455	3. Recipient's Catalog No.	
4. Title and Subtitle Modeling Structural Damage in Ship Collisions		5. Report Date June 2001	
		6. Performing Organization Code	
7. Author(s) Brown, A.J.		8. Performing Organization Report No. SR-1400	
9. Performing Organization Name and Address Department of Aerospace and Ocean Engineering. Virginia Polytechnic Institute and State University Blacksburg, VA 24061-0203		10. Work Unit No. (TRAIS)	
		11. Contract or Grant No. DTCG32-98-P-E00281 mod 0001	
12. Sponsoring Agency Name and Address Ship Structure Committee US Coast Guard C/O US Coast Guard Research & Development Ctr. 2100 Second Street, SW 1082 Shennecossett Road Washington, DC 20593 Groton, Connecticut 06340		13. Type of Report and Period Covered Draft Report 9/98-6/01	
		14. Sponsoring Agency Code G-M	
15. Supplementary Notes The R&DC technical point of contact is Walt Lincoln, 860-441-2865			

16. Abstract

This project has two primary objectives. The first is to develop, validate and assess a probabilistic ship-collision damage model to support ongoing work by the Society of Naval Architecture and Marine Engineering (SNAME) Ad Hoc Panel 6 and IMO working groups. The second is to address the shortcomings in the IMO Interim Guidelines using physics-based models to predict probabilistic damage in collision, vice basing damage prediction on a single set of limited data. It is generally agreed that structural design has a major influence on tanker oil outflow and damaged stability in grounding and collision, but crashworthiness is not considered in present regulations. The proposed methodology provides a practical means of considering structural design in a regulatory framework, and when implemented would improve the safety and environmental performance of ships. This project continues the development and applies a Simplified Collision Model (SIMCOL) to calculate damage extent and oil outflow in ship collisions. SIMCOL is sufficiently fast to be applied to thousands of collision cases as is required for a probabilistic analysis. The following specific tasks were completed using SIMCOL in support of this project:

1. Completed the development of SIMCOL Version 2.11.
2. Developed the capability to model collision events using LSDYNA.
3. Validated SIMCOL. Due to the lack of sufficient actual or test data for proper model validation, validation was accomplished by comparison to results from two other simplified models and two finite element models.
4. Defined probabilistic oil tanker collision events. Probabilities and probability density functions were developed for important collision event parameters.
5. Predicted probabilistic structural damage and oil outflow for four notional oil tankers. Collision damage and outflow were calculated for ten thousand collision events. Mean values and response surfaces were developed for each tanker. Sensitivity to collision scenario variables was explored.

17. Key Words ship collisions, probabilistic methods, ship damage		18. Distribution Statement Distribution is available to the public through: National Technical Information Service U.S. Department of Commerce Springfield, VA 22151 Ph. (703) 487-4650	
19. Security Classification (of this report) Unclassified	20. Security Classification (of this page) Unclassified	21. No. of Pages 164	22. Price

CONVERSION FACTORS
(Approximate conversions to metric measures)

To convert from	to	Function	Value
LENGTH			
inches	meters	divide	39.3701
inches	millimeters	multiply by	25.4000
feet	meters	divide by	3.2808
VOLUME			
cubic feet	cubic meters	divide by	35.3149
cubic inches	cubic meters	divide by	61,024
SECTION MODULUS			
$inches^2$ $feet^2$	$centimeters^2$ $meters^2$	multiply by	1.9665
$inches^2$ $feet^2$	$centimeters^3$	multiply by	196.6448
$inches^4$	$centimeters^3$	multiply by	16.3871
MOMENT OF INERTIA			
$inches^2$ $feet^2$	$centimeters^2$ meters	divide by	1.6684
$inches^2$ $feet^2$	$centimeters^4$	multiply by	5993.73
$inches^4$	$centimeters^4$	multiply by	41.623
FORCE OR MASS			
long tons	tonne	multiply by	1.0160
long tons	kilograms	multiply by	1016.047
pounds	tonnes	divide by	2204.62
pounds	kilograms	divide by	2.2046
pounds	Newtons	multiply by	4.4482
PRESSURE OR STRESS			
$pounds/inch^2$	$Newtons/meter^2$ (Pascals)	multiply by	6894.757
kilo $pounds/inch^2$	mega $Newtons/meter^2$ (mega Pascals)	multiply by	6.8947
BENDING OR TORQUE			
foot tons	meter tons	divide by	3.2291
foot pounds	kilogram meters	divide by	7.23285
foot pounds	Newton meters	multiply by	1.35582
ENERGY			
foot pounds	Joules	multiply by	1.355826
STRESS INTENSITY			
kilo $pound/inch^2$ $inch^{½}$ ($ksi\sqrt{in}$)	mega Newton $MNm^{3/2}$	multiply by	1.0998
J-INTEGRAL			
kilo pound/inch	$Joules/mm^2$	multiply by	0.1753
kilo pound/inch	kilo $Joules/m^2$	multiply by	175.3

TABLE OF CONTENTS

LIST OF FIGURES

LIST OF TABLES

Blank

CHAPTER 1 Motivation and Introduction

1.1 Motivation

The serious consequences of ship grounding and collision necessitate the development of regulations and requirements for the subdivision and structural design of ships to reduce damage and environmental pollution, and improve safety. This report addresses primarily oil tanker damage and oil pollution, but the process and damage calculations are directly applicable to damage stability calculations and regulations.

The International Maritime Organization (IMO) is responsible for regulating the design of oil tankers and other ships to provide for ship safety and environmental protection. Their ongoing transition to probabilistic performance-based standards requires the ability to predict the environmental performance and safety of specific ship designs. This is a difficult problem requiring the application of fundamental engineering principles and risk analysis [1,2,3,4].

IMO's first attempt at probabilistic performance-based standards for oil tankers was in response to the U.S. Oil Pollution Act of 1990 (OPA 90). In OPA 90, the U.S. requires that all oil tankers entering the U.S. waters must have double hulls. IMO responded to this unilateral action by requiring double hulls or their equivalent. Equivalency is determined based on probabilistic oil outflow calculations specified in the "Interim Guidelines for the Approval of Alternative Methods of Design and Construction of Oil Tankers Under Regulation 13F(5) of Annex I of MARPOL 73/78" [4], hereunder referred to as the Interim Guidelines.

The Interim Guidelines are an excellent beginning, but they have a number of significant shortcomings:

- They use a single set of damage extent probability density functions (pdfs) from limited single-hull accident data applied to all ships, independent of structural design.
- IMO damage pdfs consider only damage significant enough to breach the outer hull. This penalizes structures able to resist rupture.
- Damage extents are treated as independent random variables when they are actually dependent variables, and ideally should be described using a joint pdf.
- Damage pdfs are normalized with respect to ship length, breadth and depth when damage may depend largely on local structural features and scantlings vice global ship dimensions.

This project has two primary objectives. The first is to develop, validate and assess a probabilistic collision damage model to support ongoing work by the Society of Naval Architecture and Marine Engineering (SNAME) Ad Hoc Panel #6 and IMO working groups. The second is to address the shortcomings in the IMO Interim Guidelines using physics-based models to predict probabilistic damage in collision, vice basing damage prediction on a single set of limited data.

It is generally agreed that structural design has a major influence on tanker oil outflow and damaged stability in grounding and collision, but crashworthiness is not considered in present regulations. The proposed methodology provides a practical means of considering structural

design in a regulatory framework, and when implemented would improve the safety and environmental performance of ships.

Specific objectives are:

- To support ongoing work by SNAME Ad Hoc Panel #6 (Structural Design and Response in Collision and Grounding).
- To assess and integrate existing simplified collision-damage models and mechanisms into a single Simplified Collision Model (SIMCOL). This model will be used to predict probabilistic collision damage extents given a probabilistic description of collision scenarios. This requires that sub-model physics be sufficiently simple to support overall computational efficiency in probabilistic applications where thousands of runs are required. (Chapters 3 and 4)
- To identify and apply probabilistic collision scenarios and assess their relative impact on collision damage extents. (Chapter 7)
- To validate SIMCOL in the context of a realistic collision simulation using real and finite element model data. (Chapters 5 and 6)
- To achieve international acceptance of this validation by publishing results and making all data and aspects of the research open for discussion and collaboration through SNAME and the Ship Structure Committee.
- To demonstrate the process. Predict probabilistic structural damage and oil outflow for four notional oil tankers. Identify important ship global and structural characteristics that impact collision damage extents and quantify their relative impact through sensitivity analysis. (Chapter 8)
- To provide the basis for further work in which a parametric analysis of probabilistic results would be incorporated in IMO oil outflow and damage stability regulations. (Chapter 9)

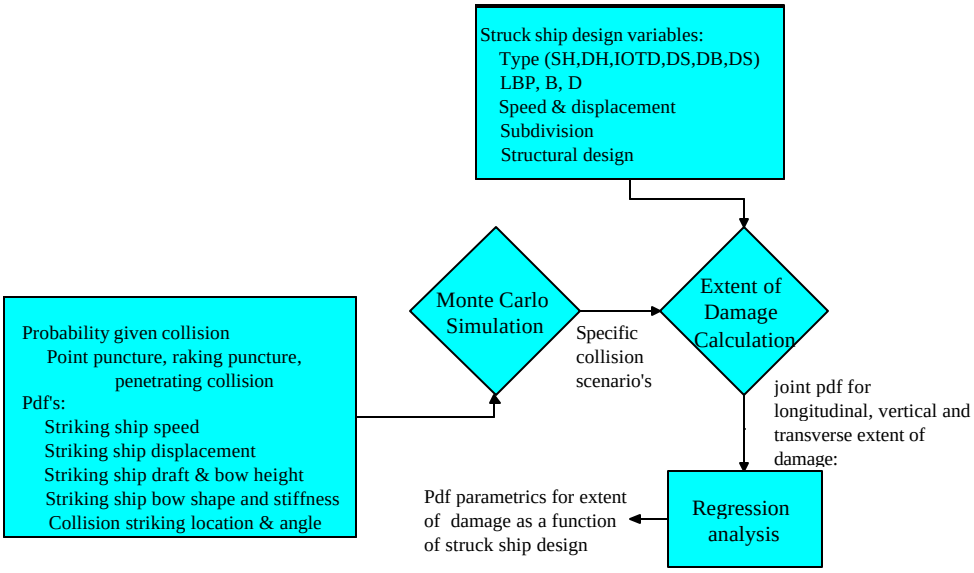

Figure 1 - Methodology to Predict Probabilistic Damage in Collision [3]

Figure 1 illustrates the overall process proposed to predict probabilistic damage as a function of ship structural design. The process begins with a set of probabilities and probability density functions (pdfs) defining possible collision scenarios (Chapter 7). Based on these pdfs, specific scenarios are selected in a Monte Carlo simulation, and, together with a specific ship structural design, provide the necessary input to predict damage using SIMCOL (Chapter 3). In the future, this process will be repeated for thousands of scenarios and a range of structural designs until sufficient data is generated to build a set of parametric equations relating probabilistic damage extent to structural design. These parametric equations can then be used in oil outflow or damage stability calculations. In this project only four structural designs are considered. This will be extended to a full range of structural design parameters in a subsequent project. Critical to this process are a simple, but sufficient probabilistic definition of the collision scenario, including the striking ship, and a fast, but sufficient structural model to predict damage.

1.2 SIMCOL

The damage calculation is the most difficult step in the Figure 1 process. The simplified collision model (SIMCOL) performs this function. There are 3 major ship-to-ship collision classifications: puncture, raking and penetrating. SIMCOL models penetrating collisions. SIMCOL is sufficiently fast to be applied to thousands of collision cases as is required for a probabilistic analysis, and is sufficient for a regulatory application. A simple and fast model is important in probabilistic analysis because thousands of different scenarios must be run to develop statistically significant results.

In 1979, the Ship Structure Committee (SSC) conducted a review of collision research and design methodologies [5,6,7]. They concluded that the most promising simplified collision analysis alternative was to extend Minorsky's original analysis of high-energy collisions by including consideration of shell membrane energy absorption.

A more recent review of the literature and of the applicability of available methods for predicting structural performance in collision and grounding was made at the 1997 International Ship and Offshore Structures Congress (ISSC 97) by Specialist Panel V.4 [8]. Their report states: "Knowledge of behavior on a global level only (i.e., total energy characteristics like the pioneering Minorsky formula) is not sufficient. The designer needs detailed knowledge on the component behavior (bulkheads, girders, plating, etc.) in order to optimize the design for accident loads."

The approach taken in this project is to progressively increase the complexity of SIMCOL starting with a modified Minorsky approach until results with sufficient accuracy and sensitivity to design characteristics is obtained. SIMCOL V2.11 represents the most recent product of this evolution.

CHAPTER 2 Existing Analysis Methods and Models

Models for analyzing ship collisions were initially developed in the 1950s for ships transporting radioactive materials, and later were applied to other types of ships, including barges, tankers and LPG/LNG carriers. SSC Reports 283, 284 and 285 provide an excellent summary of collision models developed before 1979 [5,6,7]. A more recent review was conducted by the 1997 International Ship and Offshore Structures Congress (ISSC 97), Specialist Panel V.4 [8].

Collision analysis models include three primary elements:

- External ship dynamics sub-model;
- Internal sub-model of structural mechanics for the struck and striking ships; and
- Simulation approach that couples the internal and external sub-models.

Various existing models use different sub-models and coupling approaches. These are discussed in the following sections.

2.1 External Ship Dynamics

The external sub-model calculates the ship dynamics in collision. Different models have been developed from different assumptions and for different purposes. The simplest is the one-dimensional approach (striking ship surge, struck ship sway) proposed by Minorsky [9]. MIT's collision analysis software, DAMAGE [10], adds an additional degree of freedom (struck ship yaw) and is more suitable for strikes away from the center of gravity of the struck ship. More sophisticated models consider three degrees of freedom (surge, sway and yaw) for both ships, as in Crake [2, 11], Hutchison [12], Zhang [13] and Pedersen and Zhang [14].

2.1.1 One and Two Degree-of-Freedom Models

2.1.1.1 Minorsky Method

Collision analysis models were first developed for analyzing the design of ships transporting nuclear materials. The crashworthiness of these ships under worse case conditions was the primary concern. A totally inelastic right angle collision with the struck ship at rest was considered the "worse case". Hence, most currently available models consider only right angle collisions, and assume that the effect of the kinetic energy parallel to the struck ship's centerline is small. The most popular of these approaches is the one proposed by Minorsky [9].

V.U. Minorsky conducted the first and best known of the empirical collision studies based on actual data. His method relates the energy dissipated in a collision event to the volume of damaged structure. Actual collisions in which ship speeds, collision angle, and extents of damage are known were used to empirically determine a linear constant. This constant relates damage volume to energy dissipation. In the original analysis the collision is assumed to be totally inelastic, and motion is limited to a single degree of freedom. Under these assumptions, a closed form solution for damaged volume can be obtained.

Minorsky's approach is based on the following assumptions:

- The collision is totally inelastic.
- The effect of the system kinetic energy along the struck ship's longitudinal direction is small.
- The rotations of the struck and striking ships (yaw) are small and can be neglected.

The first two assumptions define the so-called "worse case". The third is based on the observation that only small rotations occur in actual collisions.

With these assumptions, the motion is one-dimensional and the final velocities of both striking and struck ships are derived as follows based on conservation of momentum:

$$(M_A + M_B + dm_A)v = M_B v_B$$
$$v = \frac{M_B v_B}{M_A + M_B + dm_A} \tag{2.1}$$

where:

M_A	-	mass of the struck ship;
M_B	-	mass of the striking ship;
dm_A	-	added mass of the struck ship in the sway direction;
v	-	final velocity in Y direction, normal to the struck ship's centerline;
v_B	-	initial velocity in Y direction of the striking ship.

The total kinetic energy absorbed in the collision, ΔKE, is:

$$\Delta KE = \frac{1}{2} M_B v_B^2 - \frac{1}{2}(M_A + M_B + dm_A)v^2 = \frac{M_B (M_A + dm_A)}{2(M_A + M_B + dm_A)} v_B^2 \tag{2.2}$$

Minorsky estimated the added mass in sway, dm_A, to be $0.4M_A$. The collision angle, ϕ, is introduced to calculate the velocity and kinetic energy of the striking ship in the sway direction of the struck ship when the collision is not at a right angle. Energy in the struck ship longitudinal (surge) direction is ignored. The absorbed kinetic energy in the struck ship transverse direction is then:

$$\Delta KE = \frac{M_A M_B}{2M_A + 1.43M_B}(V_B \sin f)^2 \tag{2.3}$$

where V_B is the velocity of the striking ship at impact.

It is important to note that a right angle collision may not be the "worse case". Equations (2.2) and (2.3) may underestimate the kinetic energy absorbed in collisions at oblique angles (by the bow) when the struck ship has forward speed. External dynamics may also substantially affect absorbed energy. This is investigated in later sections of this report.

2.1.1.2 DAMAGE

The computer program DAMAGE was developed at MIT under the Joint MIT-Industry Program on Tanker Safety. This project, lead by Professor Tomasz Wierzbicki, was initiated in 1991, and in addition to the program DAMAGE, the project produced more than 70 technical reports about

prediction of grounding and collision damage. The program DAMAGE Version 5.0 can be used to predict structural damage in the following accident scenarios [10]:

- Ship grounding on a conical rock with a rounded tip (rigid rock, deformable bottom)
- Right angle ship-ship collisions (deformable side, deformable bow)

Compared to previous models for prediction of grounding and collision damage, a major advantage of DAMAGE is that the theoretical models are hidden behind a modern graphical user interface (GUI). The program has been developed with the objective of making crash analysis of ship structures feasible for engineers that do not have any particular experience in the field of crashworthiness.

The DAMAGE Collision Module calculates velocities and lost kinetic energy after impact using conservation of linear momentum, angular momentum and energy as shown in Equations (2.4) and (2.5):

$$\begin{aligned} & M_{1y}v_1^a + M_{2x}v_2^a = M_{2x}v_2 \\ & I_{1z}w_1^a + M_{2x}x_1v_2^a = M_{2x}x_1v_2 \\ & v_2^a = v_1^a + x_1w_1^a \\ & v_1^a = v_2\frac{1}{1+M_{1y}x_1^2/I_{1z}+M_{1y}/M_{2x}} \\ & w_1^a = v_2\frac{M_{1y}x_1/I_{1z}}{1+M_{1y}x_1^2/I_{1z}+M_{1y}/M_{2x}} \end{aligned} \tag{2.4}$$

where:

M_{1y}	-	virtual mass of the struck ship including added mass in sway;
M_{2x}	-	virtual mass of the striking ship including added mass in surge;
I_{1z}	-	virtual moment of inertia in yaw of the struck ship including yaw added mass (moment of inertia);
$v_1{}^a$	-	final velocity of struck ship in the sway direction;
$\omega_1{}^a$	-	final angular velocity of struck ship;
v_2	-	initial velocity of striking ship;
$v_2{}^a$	-	final velocity of striking ship in the sway direction of the struck ship; and
x_1	-	impact point to the midship point of struck ship.

The kinetic energy absorbed in the collision is then:

$$\Delta KE = \frac{1}{2}M_{1y}v_1^{a\,2} + \frac{1}{2}M_{2x}v_2^{a\,2} + \frac{1}{2}I_{1z}w_1^{a\,2} - \frac{1}{2}M_{2x}v_2{}^2 \tag{2.5}$$

Deformation of the bow and the side are calculated separately by moving the striking ship into the struck ship in small increments. In each increment, the total resistance forces from crushing of the bow and penetration into the side are compared. The actual crushing/penetration increment takes place in the ship with lowest resistance. Absorbed energy is calculated. This process continues until absorbed structural energy equals the lost kinetic energy calculated previously. DAMAGE cannot analyze collisions with an oblique striking angle or an initial struck ship

velocity. DAMAGE considers the material and structural scantlings of all major structural components of the side structure. The model for the internal mechanics is based on the direct contact deformation of super-elements. The super-elements used to model the side in DAMAGE are:

- Shell and inner side plating panels (laterally loaded plastic membranes)
- Deck panels and girders (crushing)
- Beams (loaded by a concentrated load)
- X-, L- and T-form intersections crushed in the axial direction

2.1.2 Models with Three Degrees of Freedom

2.1.2.1 Hutchison

Hutchison generalized the Minorsky method to include all horizontal degrees of freedom (surge, sway, yaw) and hull membrane resistance. The resulting model is used to study collisions with barges carrying radioactive material (RAM) [12]. Twenty-five hundred barge collision scenarios were developed for each of five classifications of US navigable waters. These were used in a Monte Carlo simulation to estimate the conditional probabilities of RAM container damage.

Hutchison uses a global coordinate system with three degrees of freedom. The virtual masses of both struck and striking ships are developed in matrix form, including the added mass terms. The kinetic energy and momentum of the ships is determined from the velocity vector and virtual mass matrix. A similar model is used by Crake and Brown [2,11].

It is necessary to calculate the final velocities of both struck and striking ships to determine the lost kinetic energy. Hutchison accomplishes this using conservation of momentum with the following assumptions:

- Changes in the global orientation angles, or rotation angles of the ships during the collision are small and can be neglected in certain parts of the analysis.
- There is no change in the distribution of mass after the initial contact.
- After the "inelastic" collision, the striking ship is attached to the struck ship and both ships move together as a single body.

Similar three degree of freedom dynamics are used in SIMCOL, and these are described in detail in Chapter 3. Hutchison and SIMCOL calculate external dynamics simultaneously with internal mechanics in a time-stepping solution. This is an important distinction compared to other models.

2.1.2.2 Pedersen and Zhang

Pedersen and Zhang derive expressions for absorbed energy uncoupled from internal mechanics [13,14]. They apply three local coordinate systems to the striking ship, the struck ship and the impact point separately as shown in Figure 2. By analyzing the motions and impulses around the impact point, the absorbed kinetic energy is derived in both the longitudinal and transverse directions relative to the struck ship. Important assumptions in this analysis include: 1) small rotation during the collision (the angles α and β in Figure 2 are considered constant); and 2) a constant ratio of absorbed plastic deformation energy for the transverse and longitudinal directions is assumed for the entire collision event. The absorbed energy is calculated uncoupled from the internal mechanics problem.

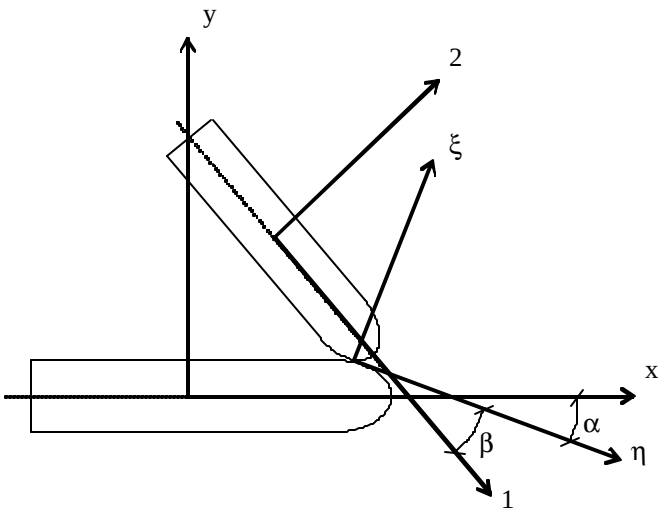

Figure 2 – DTU Ship Dynamics Model

Collision absorbed energies in the ξ (transverse) and η (longitudinal) directions are:

$$E_x = \int_0^{x_{\max}} F_x dx = \frac{1}{2}\frac{1}{D_x + mD_h}\dot{x}(0)^2$$

$$E_h = \int_0^{h_{\max}} F_h dh = \frac{1}{2}\frac{1}{\frac{1}{m}K_x + K_h}h(0)^2 \qquad (2.6)$$

$$E_{total} = E_x + E_h$$

where the coefficients D_ξ, D_η, K_ξ, K_η are algebraic expressions that are a function of the ship masses, strike location, collision angle, and added mass coefficients. Added mass coefficients are assumed to be 0.05 in surge, 0.85 in sway and 0.21 in yaw. $h(0)$ and $\dot{x}(0)$ are the relative longitudinal and transverse velocities between the two ships just prior to impact. Equation (2.6) assumes that the two ships stick together on impact. Whether the two ships slide or stick is determined by the ratio of transverse to longitudinal force-impulses at impact. If this ratio exceeds the coefficient of static friction, it is assumed that the two ships slide. The impulse ratio at impact is assumed constant for the entire process. This approach is used in the Technical University of Denmark (DTU) collision simulation model.

2.2 Internal Mechanics

Methods for analyzing internal collision mechanics may be categorized as:

- Correlation of actual collision data;
- Direct simplified calculations;
- Finite element analysis; and
- Model experiments.

2.2.1 Correlation Of Actual Collision Data

2.2.1.1 Minorsky Method

The Minorsky method [9] is representative of empirical formulae derived from data of actual accidents. Based on an investigation of 26 ship-ship collisions, Minorsky relates the volume of damaged structural steel to the energy absorbed during the collision as illustrated in Figure 3.

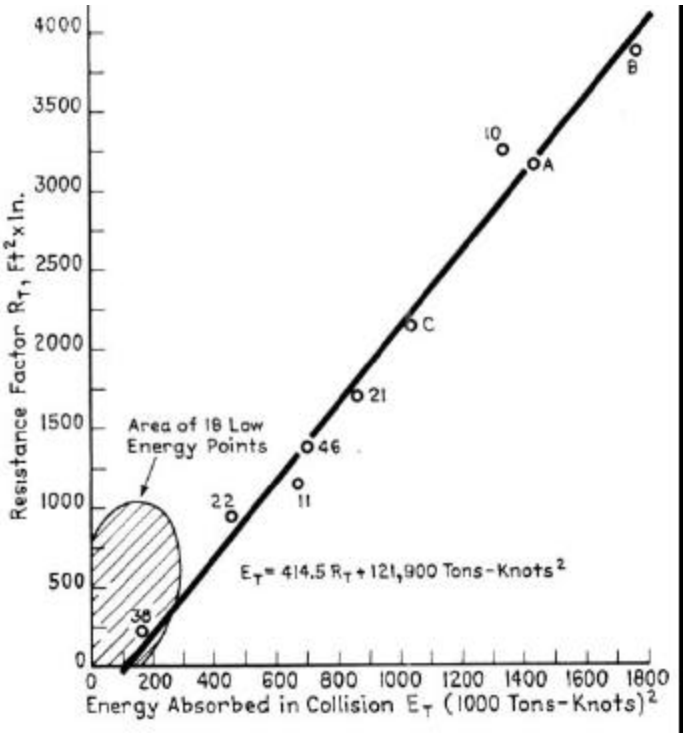

Figure 3 - Minorsky's Correlation [15]

The straight-line correlation between the damaged volume of ship structure and absorbed energy was found to be:

$$E_T = 414.5R_T + 121{,}900 \tag{2.7}$$

where:

E_T - energy absorbed in collision (ltons-knots^2); and
R_T - resistance factor or damaged volume of structural steel (ft^2 in).

Reardon and Sprung [15] revalidated Minorsky's approach by including 16 additional collisions and proposed the following correlation in metric units:

$$\Delta KE = (47.1 \pm 8.8)R_T + 28.4 \tag{2.8}$$

where:

ΔKE - lost kinetic energy in MJ; and
R_T - resistance factor in m^3.

Low energy collisions are not modeled well with the Minorsky method. The intercept term, 121,900 ltons-knots^2, in the original Minorsky's formula, and 28.4 MJ, in Reardon and Sprung, is the energy expended bending, stretching, puncturing and tearing the shell of the struck ship. This value varies significantly in the collision data reflecting different designs and dependence on variables other than damage volume.

2.2.1.2 Extensions of Minorsky Method

To correct the limitation of Minorsky's method at the low energy end, several approaches have been developed.

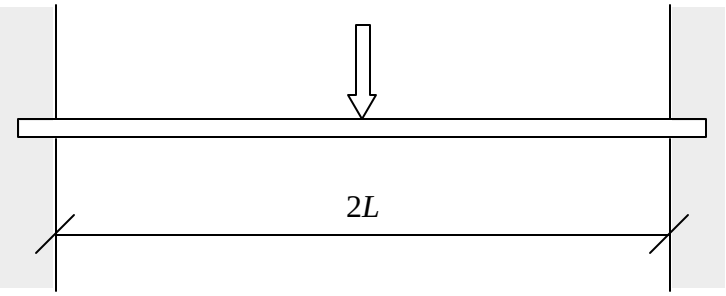

Figure 4 – Jones' Beam Model

A simplified procedure introduced by Jones [6] extended the Minorsky correlation by modeling the ship's side shell as a clamped beam subjected to a concentrated load at mid-span as shown in Figure 4. It is also assumed that membrane behavior occurs from the beginning of deformation. Bending is neglected.

This results in the following equations for predicting the low-energy structural response:

$$E_T = 0.030288 s_y \left(\frac{w}{L}\right)^2 R_T$$
$$R_T = \frac{2LB_e t}{144} \tag{2.9}$$

where:

σ_y	-	yielding strength of the beam (psi);
w	-	deformation of the beam at mid-span (in);
L	-	one half of unsupported span of the beam (in);
B_e	-	breadth of the beam (in); and
t	-	thickness of the beam (in).

Based on a study by McDermott, Van Mater extended Jones' analysis to off-center striking as shown in Figure 5 and derived the maximum deflection of the side panel based on a rupture strain of 0.1 [6,16]:

$$E_{(a,b)} = E_{CL} \frac{a}{b}$$
$$w_m = 0.453a \tag{2.10}$$

where:

$E_{(a,b)}$	-	absorbed energy, striking point away from mid-span (lton-knots^2);
E_{CL}	-	absorbed energy derived by Jones (lton-knots^2);
a	-	distance from striking point to the close support (in);
b	-	distance from striking point to the far support (in); and
w_m	-	maximum deformation of the side panel (in).

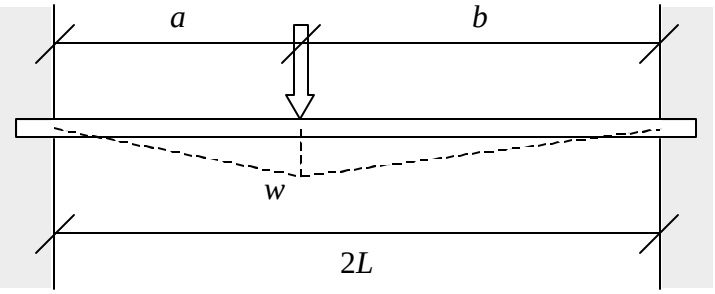

Figure 5 - Van Mater's Beam Model

Woisin also proposed an alternative to the intercept term in Minorsky's correlation [17]. He suggested the energy absorbed by the ruptured shell be calculated as follows:

$$b = 0.5 \sum H t_s^2 \tag{2.11}$$

where:

b	-	absorbed energy by ruptured side shell and longitudinal bulkheads (MJ);
H	-	height of broken or heavily deformed side shell and bulkheads (m); and
t_s	-	thickness of side shell and longitudinal bulkheads (cm).

With these improvements, the Minorsky method is more effective for estimating damage extents of ships in past collisions. A major limitation in these improvements is that they do not consider many important side shell design parameters, and they cannot properly be applied to new and unique designs including double hulls.

2.2.2 Direct Simplified Calculations

Collision research continues to develop new methods to predict the structural response of ships in collision from first principles. There are several analysis schemes available today. The basic approach behind these methods is similar. They decompose the struck ship into simple substructures or components, such as plates, stiffeners, web frames and panels, etc. The energy absorbed in each substructure during the collision process is calculated separately. The total absorbed energy up to rupture of the cargo boundary is obtained by summing up the absorbed energy for all components.

A number of these methods are based on plastic membrane tension analysis. These include methods proposed by McDermott [16], Rosenblatt [18] and Reckling [19]. These schemes were developed primarily for minor ship collisions before rupture of cargo boundaries. Others are derived based on the energy absorbed during plastic deformation of basic structural elements such as angles, T-sections and cruciforms. MIT's DAMAGE and the DTU model are examples of energy-based methods.

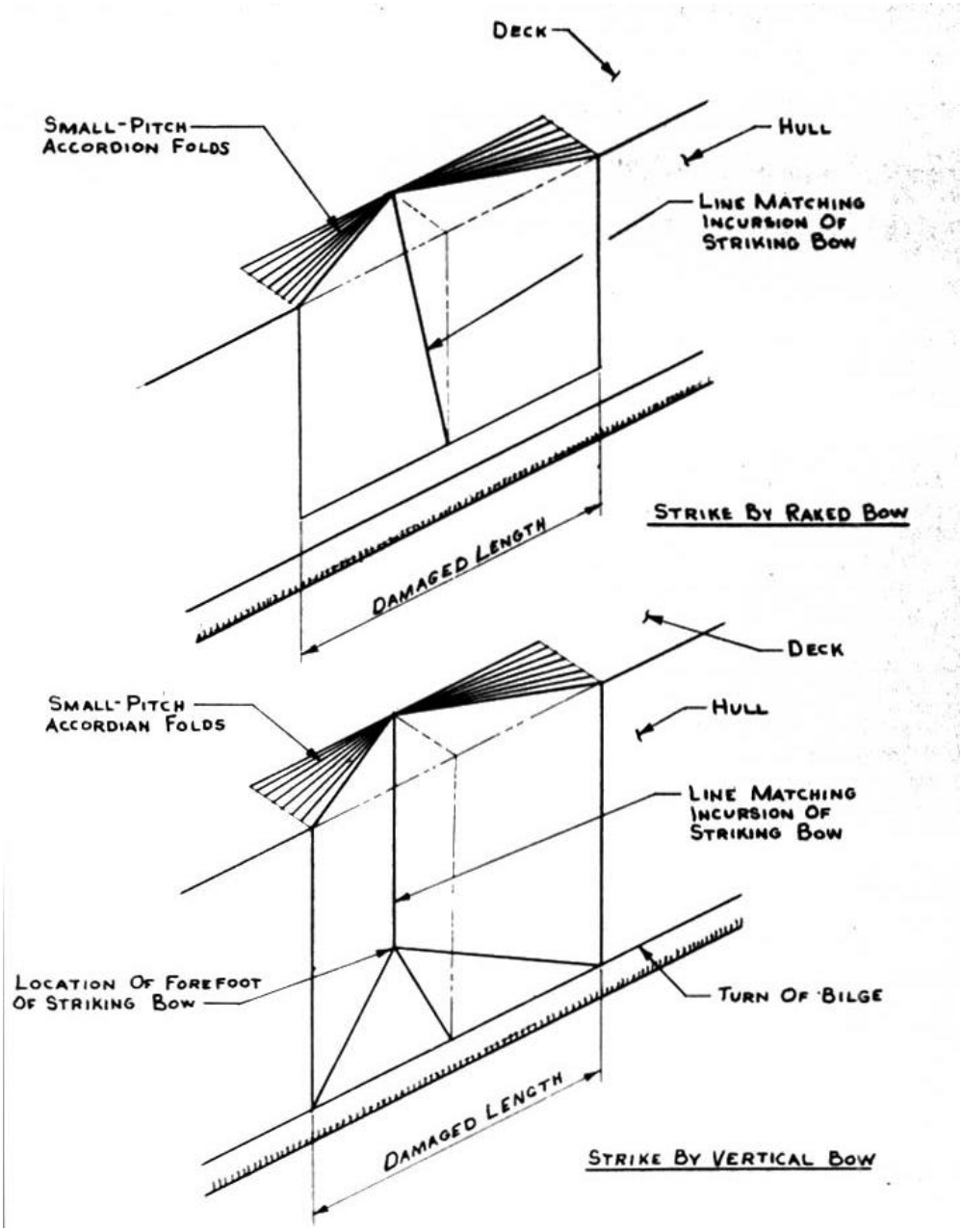

Figure 6 - Idealized Collision Damage [18]

2.2.2.1 Rosenblatt Study

M. Rosenblatt and Son performed a study for the US Coast Guard in 1976 on the Evaluation of Tanker Structure in Collision. The objective of this project was to model and evaluate phenomena that contribute to the ability of a longitudinally stiffened ship, particularly a tanker, to withstand a minor collision [18]. The models and methods used in this project were developed and summarized by McDermott et al. [16]. They were developed for analyzing minor collisions, which are defined as collisions without rupture of cargo boundaries. Their purpose is to calculate the maximum kinetic energy that can be absorbed in the tanker side structure without

rupture so that the structure can be optimized for crashworthiness in the design stage. They assume that the bow of the striking ship is infinitely stiff and that only the struck ship absorbs plastic energy.

The collision process is decomposed into a series of deformation mechanisms, including bending of the stiffened hull plating, membrane stretching, web frame failures, and deck folding, until rupture of the cargo boundary. Figure 6 shows the assumed idealized collision imprint into the struck ship. Possible side structure plastic deformation mechanism options for a single-hull ship are listed in Figure 7. Deformation mechanisms considered for double hull ships are listed in Figure 8. The analysis procedure follows the consequence of these deformation mechanisms.

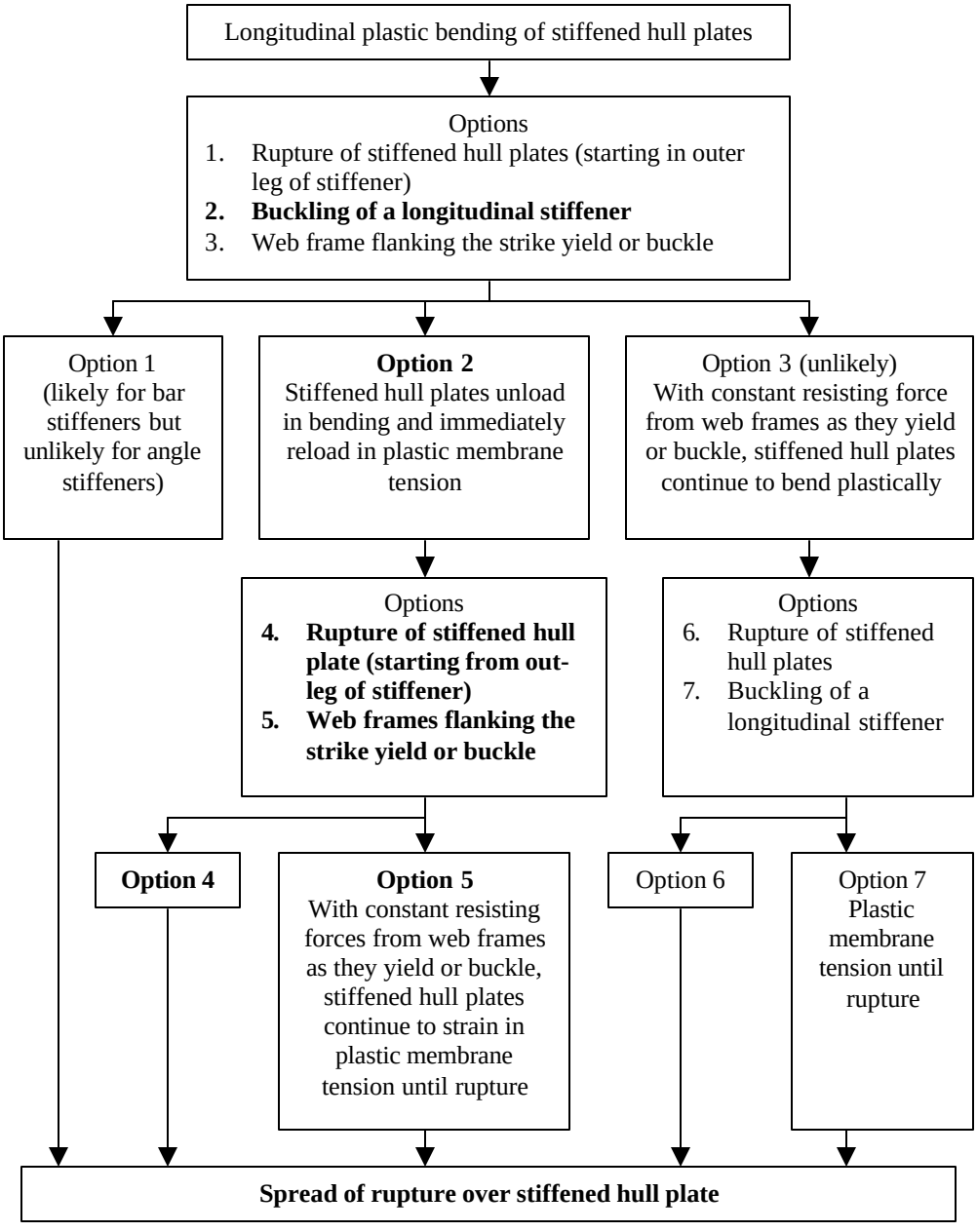

Figure 7 - Deformation Analysis of a Single Hull [18]

The rupture of plates under membrane tension is determined by the following criteria:

- The strain in the plate reaches the rupture strain, ε_r, which is taken as 10% for ABS steel; or
- The bending angle at a support reaches the critical value as defined in the following formula developed based on a series of tests by Rosenblatt [18]:

$$e_m = \frac{4}{3}\frac{s_m}{s_u - s_m \cos q_c}\sin q_c \tan q_c = 1.5D \tag{2.12}$$

where:

ε_m	-	maximum bending and membrane-tension strain at hull rupture;
σ_m	-	in-plate stress under membrane-tension (MPa);
σ_u	-	ultimate stress of the plate (MPa);
θ_c	-	critical bending angle; and
D	-	tension test ductility in a 2-in gage length, 32% for ABS steel.

The in-plate stress during the plastic membrane-tension phase, σ_m, is assumed to be:

$$s_m = \frac{1}{2}(s_u + s_y) \tag{2.13}$$

SIMCOL 1.1 and subsequent versions use various mechanisms developed in this study. Details are provided in Chapter 3.

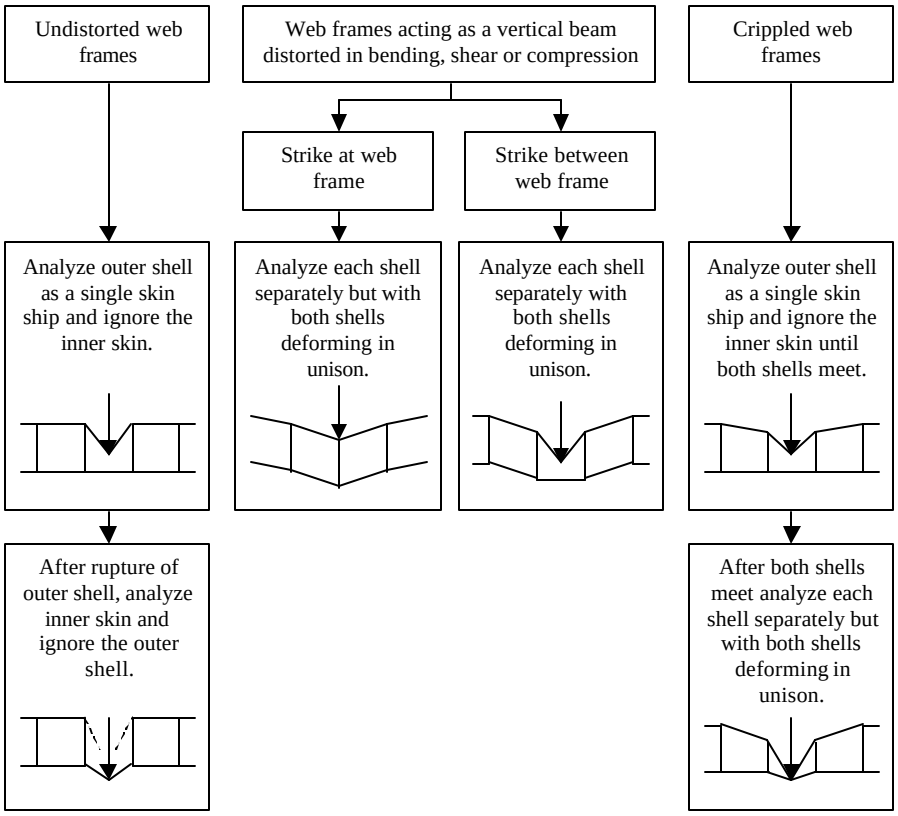

Figure 8 - Deformation Analysis of a Double Hull [18]

2.2.2.2 Reckling Model

Reckling provides an extension of the Rosenblatt methods [19]. In his model, the striking bow is allowed to deform. The collision force exerted by the deformed striking bow is distributed over the struck ship elements. To determine the resistant force and deformation of the striking bow, Reckling introduces detailed calculations of crushing loads of different shapes of plates under different loads. Deformations of both striking and struck ships are determined by comparing their collision resistant forces. Reckling also suggests a 5% rupture strain instead of the 10% strain used in the Rosenblatt method.

2.2.2.3 Super-Element Methods

Both DAMAGE and the DTU model calculate the absorbed energy for direct contact deformation of struck ship super-elements by the striking ship bow. This is not a finite element method. Deformation away from the actual striking ship penetration is not considered. Both models are based on the deformation and energy evaluation procedure and folding mechanisms proposed by Wierzbicki [20]. By summing the deformation energy absorbed by various sections and intersections during the folding process, i.e. angles, T-sections and cruciforms, the total energy absorbed and the total crushing force is obtained (Figure 9). These sections and intersections are called Super-Elements.

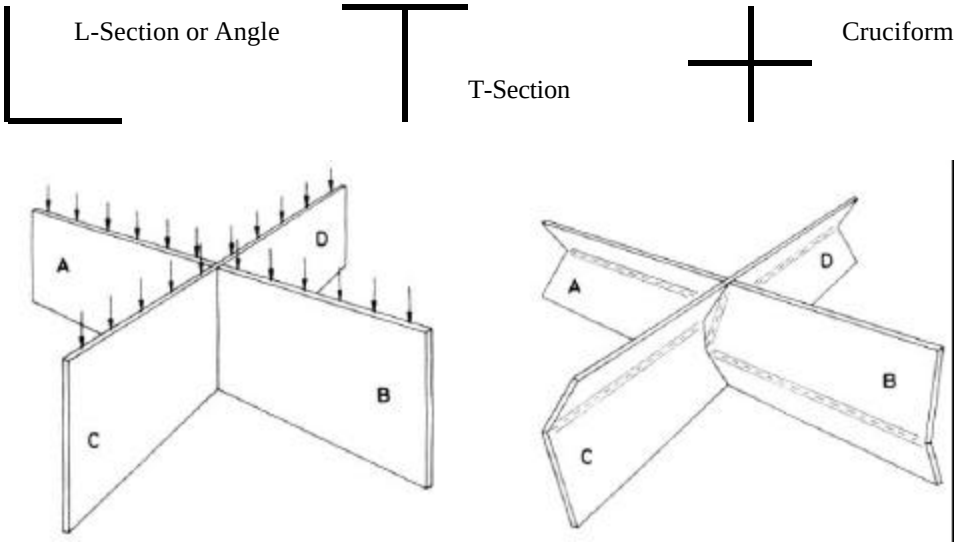

Crushing Mechanism of cruciformed structural element

Figure 9 – Basic Structural Elements and Crushing Mechanisms [23]

Wierzbicki provides closed-form solutions for the mean crushing strengths and the cutting resistance of plated structures during collision [20]. Based on these solutions derived for unstiffened structures, an extension is proposed for longitudinally and/or transversely stiffened structures. The process of ship collision is dynamic in nature and the applicability of the formulations derived under quasi-static loading conditions to analyze the crushing and cutting damage of the structure in the dynamic situations is also discussed.

The general solutions, which can be used for both stiffened and unstiffened intersections in both bow and side structure are:

For T-sections:

$$\frac{s_m}{s_y} = \frac{1.1608}{h}\left(\frac{t_{eq}}{b}\right)^{2/3} \tag{2.14}$$

For X-sections:

$$\frac{s_m}{s_y} = \frac{0.7606}{h}[0.87\left(\frac{t_{eq}}{b}\right) + 0.63\left(\frac{t_{eq}}{b}\right)^{3/4}]^{2/3} \tag{2.15}$$

For L-sections:

$$\frac{s_m}{s_y} = \frac{2.3910}{h}\left(\frac{t_{eq}}{b}\right)^{2/3} \tag{2.16}$$

where:

σ_m	-	static mean crushing strength (stress)
σ_y	-	static yield strength (stress) of the material
η	-	normalized effective crushing length of unit without transverse stiffeners
t_{eq}	-	equivalent plate thickness
b	-	plate width

Paik and Wierzbicki derive a general equation for individual stiffened plate units based on the Wierzbicki models: [21]

$$\frac{s_m}{s_y} = \frac{1}{h}[1.4245\left(\frac{t_{eq}}{b}\right)^{0.5} + 0.2673\left(\frac{t_{eq}}{b}\right)] \tag{2.17}$$

The most recent DTU model and DAMAGE 5.0 also consider deformation of the striking ship bow. These calculations are based on Pedersen's study of bow collisions [22]. In Pedersen's study, Amdahl's method [23] and Yang and Caldwell's method [24] for estimating bow-crushing force as a function of penetration are investigated and compared. Striking ship bow models are discussed in Chapter 4 of this report.

2.2.3 Finite Element Analysis

Many structural problems can be solved using finite element methods. Because of the size and complexity of the ship structure, a finite element analysis may take hundreds of hours to create and solve. This is a significant disadvantage and much effort has been applied to simplifying these models.

In the 1980s, Ito, et al. [25, 26, 27] carried out a series of theoretical and experimental studies to develop a simplified finite element method (FEM). Since most deformation in collisions is local, instead of modeling the whole struck ship or a whole segment of it, Ito only modeled a piece of the side panel with coarse triangular elements. The principle of stationary potential energy was applied to analyze the deformation and energy at the point of rupture.

Another simplified method, the Idealized Structural Unit Method (ISUM), was developed by Paik [28, 29]. ISUM is an idealized non-linear stress-strain FEM. A coarse mesh is used to model a segment of the struck ship with elements the size of whole panels supported by web frames and stringers. These are super-elements, but solved in a finite element matrix vice by direct contact. ISUM considers the coupling between local and global deformation and failure modes inside the model. Based on ISUM, Paik developed the collision simulation software, ALPS/SCOL. With these simplifications, the computing time is reduced dramatically, and in the case of Paik's model, the time is reduced to a fraction of hour to run a single collision case.

A number of researchers have used LSDYNA or DYNA-3D. LSDYNA is a general-purpose, explicit finite element program used to analyze the nonlinear dynamic response of three-dimensional inelastic structures. Its fully automated contact analysis capability and error-checking features enable users to solve complex crash and forming problems [30,31,32]. It was developed primarily for automotive collision applications, but can also be used for ship to ship collisions as described in Chapter 5 of this report.

2.2.4 Model Experiments

Because of the complexity of the ship structure and collision mechanisms, and the lack of accurate and detailed data of actual collisions, it is often necessary to conduct experiments to understand the internal mechanics behind collisions. An important example is the German GKSS experiments [17]. Based on these experiments, Woisin developed his extension to Minorsky's correlation and proposed methods to improve the crashworthiness of several types of ships.

To adequately simulate the structural response of ships in collisions, it is necessary to use full scale or at least large-scale models so that the structural behavior of the model represents that of a real ship. These experiments are extremely expensive. Therefore, experiments are more often used as a tool to verify theoretical results derived from other methods rather than as a direct simulation approach.

Experiments conducted at the US Steel Research Laboratory were used extensively in the Rosenblatt study [18]. On the basis of the results of a series model tests, Ito et al. generated and verified their simplified method to analyze the response of double hull structures in minor collisions [25-27]. Recently, Paik has also completed an experimental study of internal collision mechanics to demonstrate the accuracy of his ISUM model [28,29].

In the early 1990's the Japanese Association for the Structural Improvement of the Shipbuilding Industry (ASIS) in collaboration with the Netherlands Foundation for the Coordination of Maritime Research conducted a series of full scale grounding and collision tests. The collision tests included four experiments that were carried out using two inland waterway tankers of approximately 1000 tonnes displacement [33,34]. In each experiment, a rigid bow struck a test side section at a right angle. Three types of side structure were tested: single hull, double hull with stringers and double hull with stringer deck. Collision forces, motions and penetration depths were measured.

2.3 Coupling Internal and External Models

Most previous and current work in collision analysis, including Minorsky [9], DAMAGE [10], the DTU model [13] and ALPS/SCOL [28,29], determine the lost kinetic energy in an uncoupled solution of the external problem, then calculate the deformation energy of the colliding structures with increasing penetration, and finally find the maximum penetration by matching the deformation energy to the lost kinetic energy. This approach relies on the solution of final velocities of struck and striking ships by an external model. This uncoupled quasi-static solution requires significant simplifying assumptions, and/or restricting degrees of freedom of the system.

The analysis can also be done in the time domain with a fully coupled time-stepping dynamic solution similar to Hutchison [12] and Crake [11]. Starting with the initial external condition, impact forces are calculated based on internal structural mechanics at each time step and applied to the struck and striking ships in the external model until the forces approach zero. This is the method used in the continued evolution of SIMCOL presented in this report. A comparison of longitudinal and transverse absorbed energy as calculated by SIMCOL and the DTU model, contrasting these two methods, is provided in Chapter 8 of this report.

CHAPTER 3 Simplified Collision Model (SIMCOL)

3.1 SIMCOL Description

SIMCOL uses a time-domain simultaneous solution of external ship dynamics and internal deformation mechanics similar to that originally proposed by Hutchison [12].

SIMCOL Version 0.0 was developed as part of the work of SNAME Ad Hoc Panel #3 [2,11]. Based on further research, test runs and the need to make the model sensitive to a broader range of design and scenario variables, improvements were progressively made at Virginia Tech [35]. A sweeping segment method was added to the model in SIMCOL Version 1.0 to improve the calculation of damage volume and the direction of damage forces. Models from Rosenblatt [16,18] were applied in Version 1.1 assuming rigid web frames. In Version 2.0, the lateral deformation of web frames was included. In Version 2.1, the vertical extent of the striking ship bow is considered. Table 1 summarizes the evolution of SIMCOL over the last five years. Version 2.1 is described in this Chapter and used to obtain the results presented in this report.

Table 1 - SIMCOL Evolution

<table>
<tr><td colspan="2">Version</td><td>0.1</td><td>1.0</td><td>1.1</td><td>2.0</td><td>2.1</td></tr>
<tr><td colspan="2">Simulation</td><td colspan="5">Simulation in time domain</td></tr>
<tr><td colspan="2">External Model</td><td colspan="5">Three degrees of freedom
(Hutchison and Crake)</td></tr>
<tr><td rowspan="5">Internal Model</td><td rowspan="2">Horizontal Members</td><td colspan="5">Minorsky mechanism as re-validated by Reardon and Sprung</td></tr>
<tr><td>Crake’s model</td><td colspan="4">Sweeping segment method to calculate damaged area and resulting forces and moments</td></tr>
<tr><td rowspan="2">Vertical Members w/o rupture of plate</td><td colspan="2">Jones and Van Mater</td><td colspan="3">McDermott / Rosenblatt Study methods</td></tr>
<tr><td>Crake’s model (Jones)</td><td>Van Mater’s extension of Jones</td><td>Does not consider deforma-tion of webs, friction force and the force to propagate yielding zone</td><td>Considers deforma-tion of webs, friction force and the force to propagate yielding zone</td><td>Striking bow with limited depth</td></tr>
<tr><td>Vertical Members w/ ruptured plate</td><td colspan="3">Neglected</td><td colspan="2">Minorsky method for calculating absorbed energy due to longitudinal motion</td></tr>
</table>

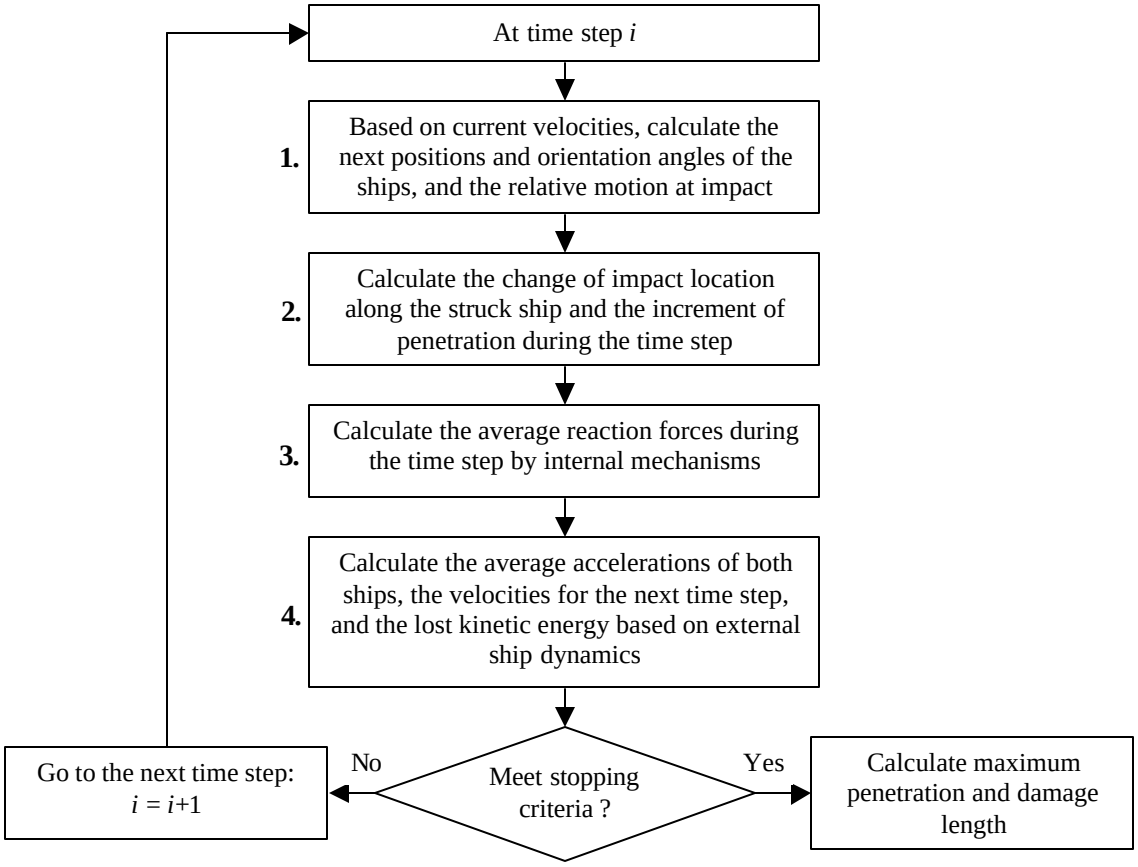

Figure 10 - SIMCOL Simulation Process

Figure 10 shows the SIMCOL simulation process. The Internal Sub-Model performs Steps 2 and 3 in this process. It calculates internal deformation due to the relative motion of the two ships and the internal reaction forces resulting from this deformation. The External Sub-Model performs Steps 1 and 4 in this process. It applies the internal forces to the global motion of the two ships and calculates the resulting accelerations, velocities and motions of the two ships during a time step.

3.1.1 SIMCOL External Dynamics Sub-Model

The External Dynamics Sub-Model uses a global coordinate system shown in Figure 11. Its origin is at the initial (time of strike) center of gravity of the struck ship with the *x*-axis towards the bow of the struck ship. The initial locations and orientations of the struck and striking ships in the global coordinate system are:

$$
\begin{aligned}
&x_{1,0} = 0 \qquad y_{1,0} = 0 \qquad q_{1,0} = 0 \\
&x_{2,0} = -l_0 + \frac{L_{BP2}}{2}\cos f_0 \\
&y_{2,0} = \frac{B_1}{2} + \frac{L_{BP2}}{2}\sin f_0 \\
&q_{2,0} = f_0 - p
\end{aligned}
\tag{3.1}
$$

where:

x_1, y_1	-	center of gravity of the struck ship (m), assumed at midship;
θ_1	-	heading of the struck ship;
x_2, y_2	-	center of gravity of the striking ship (m), assumed at midship;
θ_2	-	heading of the striking ship;
L_{BP2}	-	length between perpendiculars of the striking ship (m);
B_1	-	breadth of the struck ship (m); and
ϕ	-	collision angle.

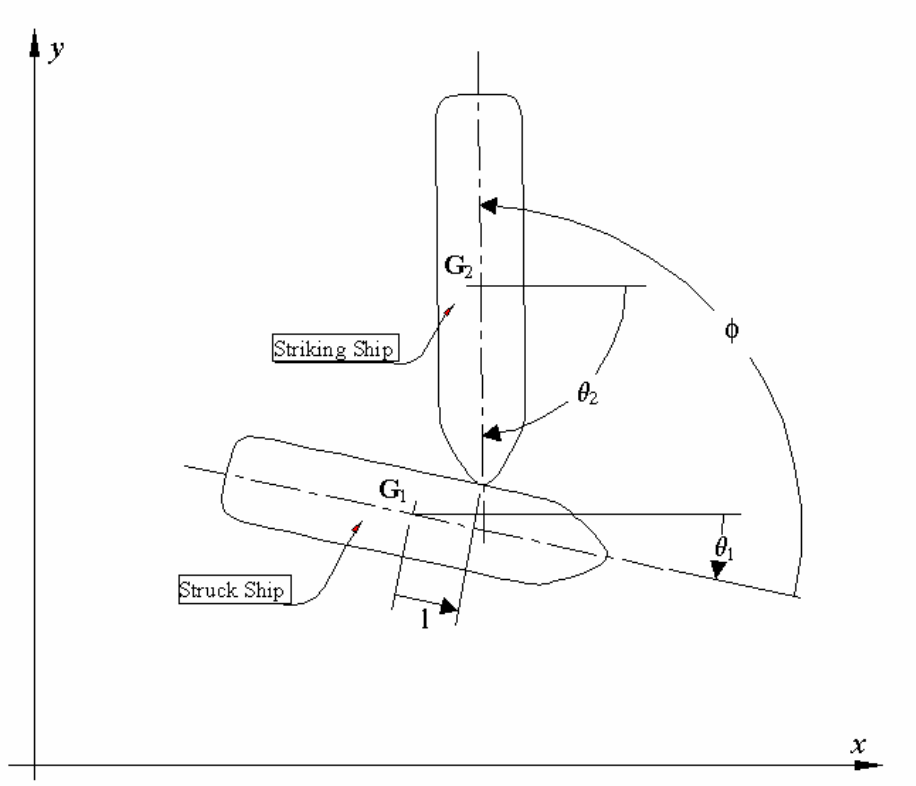

Figure 11 - SIMCOL External Ship Dynamics

A local damage coordinate system, ξ-η, is established on the struck ship to calculate relative movement and collision forces. The origin of this system is set at midship on the shell plate of the damaged side of the struck ship. Axes ξ and η point aft and inboard relative to the struck ship. Local coordinate systems are also established at the centers of gravity of both struck and striking ships.

Forces and moments in the local systems are transformed to the global *x*-*y* system for solution of the ship dynamics.

In the local ship systems, the hydrodynamic added mass for each ship is a tensor in the form:

$$\mathbf{A} = \begin{bmatrix} a_{11} & a_{12} & a_{13} \\ a_{21} & a_{22} & a_{23} \\ a_{31} & a_{32} & a_{33} \end{bmatrix} \tag{3.2}$$

Considering the approximate symmetry of the ships, and with the center of gravity of the ships assumed to be at midship, the off-diagonal terms of the added mass tensor for each ship are zeros:

$$\mathbf{A}_s = \begin{bmatrix} a_{11} & 0 & 0 \\ 0 & a_{22} & 0 \\ 0 & 0 & a_{33} \end{bmatrix} \tag{3.3}$$

where:

a_{11} - added mass in the surge direction (kg);

a_{22} - added mass in the sway direction (kg); and

a_{33} - added mass in the yaw direction (kg-m^2).

The added mass tensor is transformed in accordance with the orientation of each ship to the global coordinate system. The transformed tensor, $\mathbf{A}_\theta$, for each ship is:

$$\mathbf{A}_q = \begin{bmatrix} a_{11}\cos^2 q + a_{22}\sin^2 q & (a_{11} - a_{22})\cos q \sin q & 0 \\ (a_{11} - a_{22})\cos q \sin q & a_{11}\sin^2 q + a_{22}\cos^2 q & 0 \\ 0 & 0 & a_{33} \end{bmatrix} \tag{3.4}$$

The added mass in surge is approximated by the added mass of a circumscribed cylinder [12]. The added mass in surge, a_{11}, for each ship is:

$$a_{11} = \frac{4}{3} r p \left(\frac{BT}{p}\right)^{\frac{3}{2}} = 0.75225\, r (BT)^{\frac{3}{2}} \tag{3.5}$$

where:

ρ - density of sea water, 1025 kg/m^3;

B - breadth of the ship (m); and

T - draft of the ship (m).

The added mass in sway is approximated assuming that the cross sections of ships are rectangular [12]. The added mass in sway, a_{22}, for each ship is:

$$a_{22} = 1.189\, r T^2 L_{BP} \tag{3.6}$$

Similarly, by assuming that the waterplanes are rectangular, the added mass in yaw, a_{33}, is [12]:

$$a_{33} = \frac{2.378\, r T^2 L_{BP}{}^3}{24} = 0.0991\, r T^2 L_{BP}{}^3 \tag{3.7}$$

Instead of calculating added mass directly, added mass coefficients may be used where:

$$\begin{aligned} a_{11} &= c_{11} m_s \\ a_{22} &= c_{22} m_s \\ a_{33} &= c_{33} I_{s33} \end{aligned} \tag{3.8}$$

Coefficients are used in this report to standardize results when compared to other models. Assumed added mass coefficients are 0.05 in surge (c_{11}), 0.85 in sway (c_{22}) and 0.21 in yaw (c_{33}).

The actual mass for each ship is also represented by a tensor:

$$\mathbf{M}_{ship} = \begin{bmatrix} m_s & 0 & 0 \\ 0 & m_s & 0 \\ 0 & 0 & I_{s33} \end{bmatrix} \tag{3.9}$$

where:

m_s - ship mass (kg); and
I_{s33} - mass moment of inertia about the yaw axes of each ship (kg-m^2).

The virtual mass, $\mathbf{M}_V$, for each ship is then:

$$\begin{aligned} \mathbf{M}_{Vq} &= \mathbf{M}_{ship} + \mathbf{A}_q = \begin{bmatrix} m_{V11} & m_{V12} & 0 \\ m_{V21} & m_{V22} & 0 \\ 0 & 0 & I_{V33} \end{bmatrix} \\ &= \begin{bmatrix} m_s + a_{11}\cos^2 q + a_{22}\sin^2 q & (a_{11} - a_{22})\cos q \sin q & 0 \\ (a_{11} - a_{22})\cos q \sin q & m_s + a_{11}\sin^2 q + a_{22}\cos^2 q & 0 \\ 0 & 0 & I_{s33} + a_{33} \end{bmatrix} \end{aligned} \tag{3.10}$$

In Steps 2 and 3, the Internal Model calculates the resulting deformation, and the average forces and moments generated by this deformation over the time step. In Step 4, these forces and moments are applied to each ship. The new acceleration for each ship is:

$$\mathbf{V_s}' = \frac{\mathbf{F}}{\mathbf{M}_{VJ}} \tag{3.11}$$

or:

$$\begin{aligned} u' &= \frac{F_x m_{V22} - F_y m_{V12}}{m_{V11} m_{V22} - m_{V12}^2} \\ v' &= \frac{F_y m_{V11} - F_x m_{V12}}{m_{V11} m_{V22} - m_{V12}^2} \\ w' &= \frac{M}{I_{V33}} \end{aligned} \tag{3.12}$$

where:

$\mathbf{F}$ - forces exerted on each ship in the global system, $\mathbf{F} = \{F_x, F_y, M\}^T$;
F_x - force in the X direction in the global coordinate system (N);
F_y - force in the Y direction in the global coordinate system (N);
M - moment about the center of gravity of each ship (N-m);
$\mathbf{V}_s'$ - ship acceleration, $\mathbf{V}_s' = \{u', v', \omega'\}^T$;
u' - acceleration in the X direction in the global coordinate system (m/s^2);
v' - acceleration in the Y direction in the global coordinate system (m/s^2); and
ω' - angular acceleration of each ship in yaw (degree/s^2).

The new velocities for each ship at the end of the time step are:

$$\mathbf{V}_{s,n+1} = \mathbf{V}_{s,n} + \mathbf{V}_s' t \tag{3.13}$$

where:

n - time step number; and
τ - length of the time step (second).

Referring to Figure 10, Step 1, the velocities from the previous time step are applied to the ships to calculate their positions at the end of the current time step:

$$\mathbf{X}_{n+1} = \mathbf{X}_n + \mathbf{V}_{sn} t \tag{3.14}$$

where:

$\mathbf{X}$ - location and orientation of each ship in the global system, $\mathbf{X} = \{x, y, \theta\}^T$.

3.1.2 SIMCOL Internal Sub-Model

Referring to Figure 10, Steps 2 and 3, the Internal Sub-Model calculates the struck ship deformation resulting from the ships' relative motion, and the average internal forces and moments generated by this deformation over the time step. The Internal Sub-Model determines reacting forces from side and bulkhead (vertical) structures using detailed mechanisms adapted from Rosenblatt [16,18]. It determines absorbed energy and forces from the crushing and tearing of decks, bottoms and stringers (horizontal structures) using the Minorsky correlation [9] as modified by Reardon and Sprung [15]. Total forces are the sum of these two mechanisms. In SIMCOL Version 2.1, the striking ship bow is assumed to be wedge-shaped with upper and lower extents determined by the bow height of the striking ship and the relative drafts of the two ships. Deformation is only considered in the struck ship. The striking ship is assumed to be rigid.

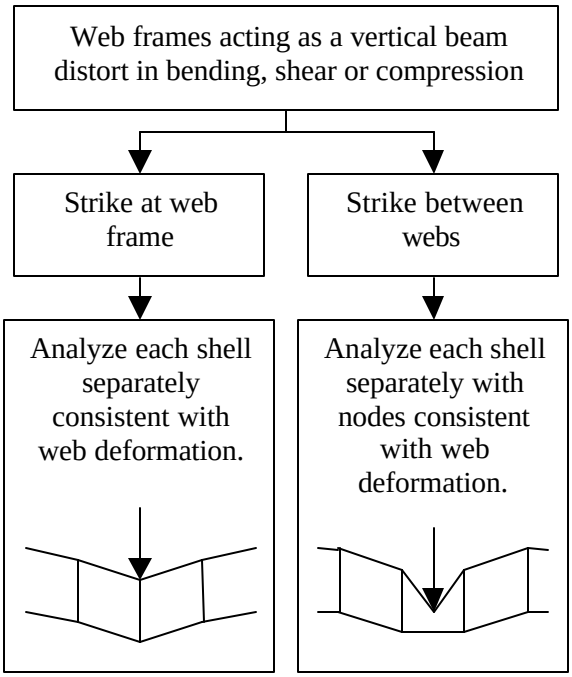

Figure 12 - Web Deformation in SIMCOL 2.0 and Later [16,18]

Penetration of the struck ship begins with the side shell plating and webs (vertical structures). Figure 12 illustrates the two basic types of strike determined by the strike location relative to the webs. The following assumptions are made consistent with Rosenblatt [18]:

- Plastic bending of shell plating is not considered - The contribution of plastic bending in the transverse deformation of longitudinally stiffened hull plates is negligible. The sample calculation sheets in Rosenblatt [18] support this argument. In six test cases, the energy absorbed in plastic bending never exceeds 0.55% of the total absorbed energy when the cargo boundary is ruptured. It is a good assumption that the plastic membrane tension phase starts from the beginning of collision penetration and is the primary shell energy-absorption mechanism.
- Rupture of stiffened hull plates starting in the stiffeners is not considered - As suggested in McDermott [16], this mechanism is unlikely for most structures except for flat-bar stiffened plates. It is a standard practice to use angles instead of flat bar for longitudinal stiffeners of side shell and longitudinal bulkheads, therefore, this option is not considered in SIMCOL.
- Web frames do not yield or buckle before plates load in membrane tension - McDermott demonstrates that this mechanism is unlikely and does not contribute significantly to absorbed energy in any case. This mechanism requires very weak web frames that would not be sufficient to satisfy normal sea and operational loads.

SIMCOL Version 1.1 assumes that flanking web frames are rigid. Version 2.0 and subsequent versions used for this report consider the transverse deformation of webs.

In a right-angle collision case, Equation (3.15) gives the total plastic energy absorbed in membrane tension in time step *n*. This assumes that the plate is not ruptured, that flanking webs

do not deflect in the longitudinal direction, and that compression in the side shell caused by longitudinal bending of ship hull girder is small.

$$E_n = T_m \, e_{tn}$$
$$T_m = s_m \, t \, B_e \tag{3.15}$$

where:

E_n - plastic energy absorbed by side shell or longitudinal bulkhead (J);
T_m - membrane tension (N);
σ_m - yield stress of side shell or bulkhead adjusted for strain rate (Pa);
e_{tn} - total elongation of shell or bulkhead structure within the web spacing;
t - smeared thickness of side shell or bulkhead (m);
B_e - effective breadth (height) of side shell or bulkhead (m);

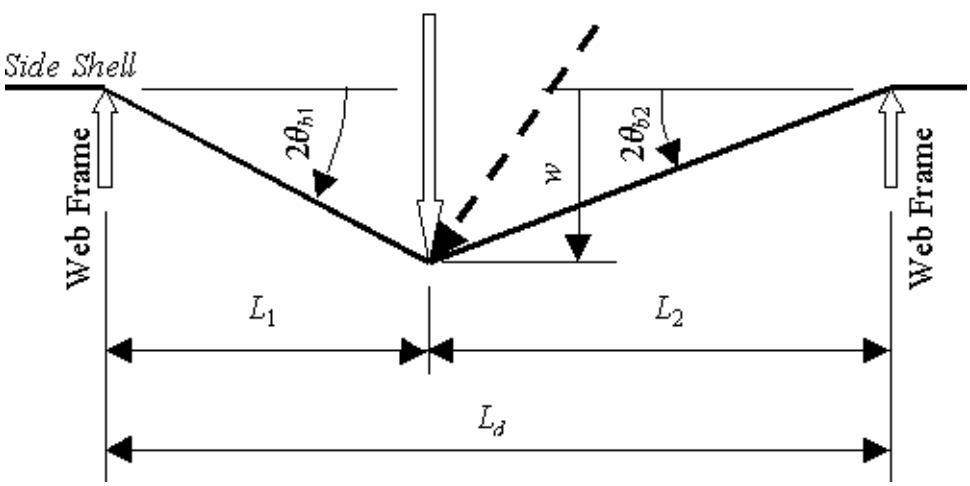

Figure 13 – Membrane Geometry

Figure 13 illustrates the membrane geometry for calculation of elongation where e_1 and e_2 are the elongation of legs L_1 and L_2 respectively:

$$e_i = \sqrt{L_i^2 + w^2} - L_i \cong \frac{w^2}{2L_i}$$
$$e_t = e_1 + e_2 = \frac{L_d}{2L_1L_2} w^2 \tag{3.16}$$

where:

L_d - damage length, or distance between adjacent webs (m);
w_n - deflection of side shell or bulkhead at time step n (m).

Side shell rupture due to membrane tension is determined using the following criteria:

- The strain in the side shell reaches the rupture strain, ε_r, which is taken as 10% in ABS steel;
- The bending angle at a support reaches the critical value as defined in Equation (3.17) [18]:

$$e_m = \frac{4}{3} \frac{s_m}{s_u - s_m \cos q_c} \sin q_c \tan q_c = 1.5D \tag{3.17}$$

where:

ε_m - maximum bending and membrane-tension strain at hull rupture;
σ_m - in-plate stress under membrane-tension (MPa);
σ_u - ultimate stress of the plate (MPa);
θ_c - critical bending angle; and
D - tension test ductility in a 2-in gage length, 32% for ABS steel.

The criteria for rupture is then:

$$e_i = \frac{e_i}{L_i} \le e_r$$
$$q_{bi} = \frac{1}{2}\arctan\frac{w}{L_i} \cong \frac{w}{2L_i} \le q_c \qquad (3.18)$$

where:

ε_i - strain in leg i; and
θ_{bi} - bending angle at flanking web frames of leg i.

Since the striking bow normally has a generous radius, the bending angle at the impact location is not considered in the rupture criteria. From these equations, it can be seen that only the strain and bending angle in the shorter leg need be considered for right angle collisions. Based on material properties of ABS steel, the critical bending angle θ_c from Equation (3.17) is 19.896, 17.318 or 16.812 degrees for MS, H32 or H36 grades respectively. Once either of the rupture criteria is reached, the side shell or longitudinal bulkhead is considered ruptured and does not continue to contribute to the reacting force.

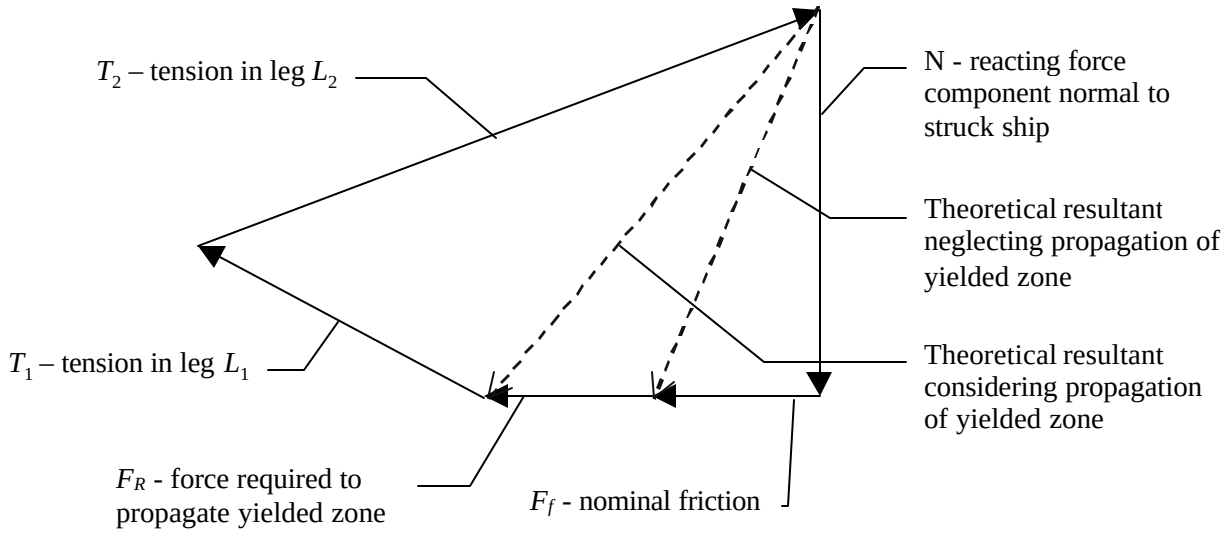

Figure 14 - Force Diagram for an Oblique Angle Collision [18]

For collisions at an oblique angle, the membrane tension is only fully developed in the leg behind the strike, L_2 in Figure 13. This is demonstrated in the force diagram shown in Figure 14, where T_1 is much smaller than T_2. It is also assumed that all the plastic strain developed from membrane tension is behind the striking point.

The first rupture criterion in Equation (3.18) becomes:

$$e_b = \frac{e_t}{L_b} \le e_r \tag{3.19}$$

where ε_b and L_b represent the strain and length of the leg behind the striking.

In SIMCOL Version 2.0 and later, transverse deformation of web frames is also considered. Web failure modes include bending, shear, and compression. Web frames are allowed transverse deformation while keeping their longitudinal locations. The resisting force is assumed constant (plastic) at a distorted flanking web frame, and the transverse deformation of the web frame is assumed uniform from top to bottom. The magnitude of this force is its maximum elastic capacity. From Figure 13, the applied force on a rigid flanking web frame is:

$$P_i = T_i \frac{w}{L_i} \tag{3.20}$$

where P_i and T_i are referred to the particular leg L_i. If the applied force, P_i, is greater than the maximum elastic capacity of the flanking web, P_{wf}, the particular web frame is deformed as in Figure 15. The change of angle, γ_c, at the distorted web is:

$$g_{ci} \cong \frac{P_{wf}}{T_i} \tag{3.21}$$

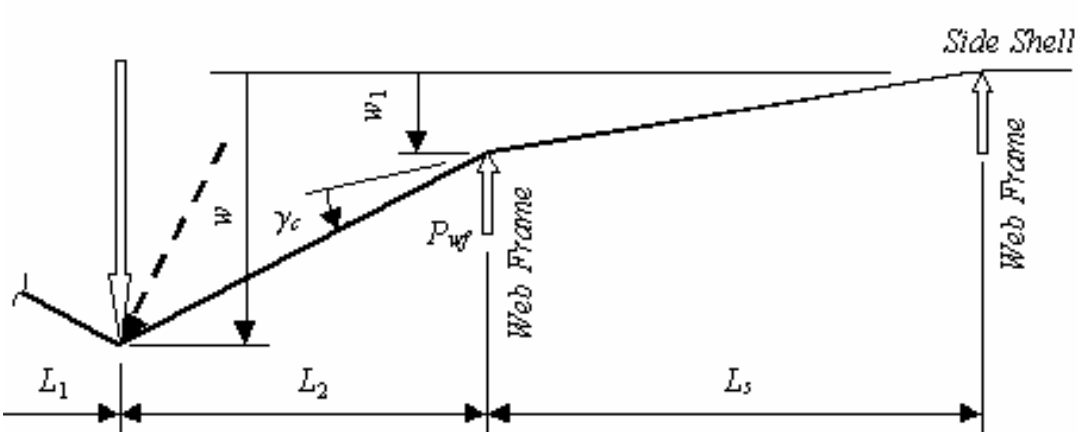

Figure 15 - Deflection and Forces in Distorted Web Frames

Rosenblatt [18] proposes an approach to determine whether P_i exceeds the capacity P_{wf}, and to estimate the value of P_{wf}. First, the allowable bending moment and shear force of the web frame at each support, the crushing load of the web, and the buckling force of supporting struts are calculated. Then, the load, P_i, is applied to the web frame, and the induced moments, shear forces and compression of the web frame and struts are calculated, considering the web frame as a beam with clamped ends. The ratios of the induced loads to the allowable loads are determined using Equation (3.22). If the maximum ratio, R_m, is greater than unity, the load, P, exceeds the capacity, and the web frame deforms.

$$R_m = \frac{P}{P_{wf}} \tag{3.22}$$

The deflection at the outermost distorted web frame is:

$$w_n = \frac{L_s}{L_i + nL_s}\{w - g_{c2}[nL_i + \frac{1}{2}(n-1)nL_s]\} \tag{3.23}$$

where:

n - total number of deformed web frames on the L_i side; and
L_s - web frame spacing (m).

The deflection at other deformed web frames is:

$$w_j = (n - j + 1)w_n + \frac{1}{2}(n - j)(n - j + 1)g_{c2}L_s \tag{3.24}$$

where j is the number of web frames counted from the striking point. The elongation in adjacent webs is:

$$e_j = \sqrt{(w_j - w_{j+1})^2 + L_s^2} - L_s \tag{3.25}$$

and the elongation in the struck web is:

$$e_{0i} = \sqrt{(w - w_1)^2 + L_i^2} - L_i \tag{3.26}$$

With these elongation and deformation results, the same rupture criteria given in Equations (3.17) and (3.19) are applied to all deformed webs. The total elongation on the L_i side is:

$$e_{ti} = e_{0i} + \sum_{j=1}^{n} e_{ji} \tag{3.27}$$

and the energy absorbed in membrane tension and web deformation is:

$$E_i = T_i e_{ti} + P_{wf} \sum_{j=1}^{n} w_{ji} \tag{3.28}$$

For right angle collisions, T_i always equals T_m as calculated in Equation (3.15). In oblique angle collisions, T_i equals T_m if L_i is on the side behind the strike. Based on experimental data, Rosenblatt [18] suggests using ½ T_m ahead of the strike and this is used in SIMCOL 2.1.

For double hull ships, if the web frames are distorted because of bending, shearing and buckling of supporting struts, the deformed web frames push the inner skin into membrane tension as shown in Figure 12, and the right angle collision mechanism is applied to the inner hull. Inner skin integrity is checked using Equations (3.18) and (3.19), and the energy absorbed in inner skin membrane tension is calculated using Equation (3.15).

In the simulation, the energy absorbed in membrane tension and web deformation during a time step is:

$$\Delta KE_n = (E_{1,n+1} + E_{2,n+1}) - (E_{1n} + E_{2,n}) \tag{3.29}$$

Considering the friction force, F_f, in Figure 14, and assuming the dynamic coefficient of friction has a constant value of 0.15, the reacting forces and moments are calculated:

$$\begin{aligned}
\Delta KE_n &= N_n(w_{n+1} - w_n) + F_{fn}\left| l_{n+1} - l_n \right| = N_n\left[(w_{n+1} - w_n) + 0.15\left| l_{n+1} - l_n \right|\right] \\
F_{hn} &= N_n = \frac{(E_{1,n+1} + E_{2,n+1}) - (E_{1n} + E_{2,n})}{(w_{n+1} - w_n) + 0.15\left| l_{n+1} - l_n \right|} \\
F_{xn} &= F_f \frac{(l_{n+1} - l_n)}{\left| l_{n+1} - l_n \right|} = 0.15 F_{hn} \frac{(l_{n+1} - l_n)}{\left| l_{n+1} - l_n \right|} \\
M_n &= -F_{xn} d_n + F_{hn} l_n
\end{aligned} \tag{3.30}$$

where:

$N_n = F_{hn}$	-	Force on struck ship normal (transverse) to centerline (N)
F_{xn}	-	Force on struck ship parallel (longitudinal) to centerline (N)
M_n	-	Yaw moment on struck ship (N m)
d_n	-	Distance of longitudinal line of force from centerline (m)
l_n	-	Distance of transverse line of force from midship (m)

In addition to the friction force, another longitudinal force, F_R, the force to propagate the yielding zone, is considered, as shown in Figure 14. McDermott provides an expression for this force [16]:

$$F_R = \frac{s_y d'}{R}\left[d' t_w \left(1 - \frac{s_y R}{d' E} \right)^2 + t_f (b - t_w)\left(\frac{d' - 0.5 t_f}{d'} - \frac{s_y R}{d' E} \right)\right] \tag{3.31}$$

where:

d'	-	depth of side shell longitudinal stiffeners;
R	-	radius of the striking bow;
t_w	-	thickness of side shell stiffener webs;
t_f	-	thickness of side shell stiffener flanges;
b	-	width of side shell stiffener flanges; and
E	-	modulus of elasticity.

or when simplified:

$$\begin{aligned}
c_F &= \frac{F_R}{s_y A_{stiff}} \\
c_A &= \frac{A_{stiff}}{A_{total}} \\
F_R &= c_F c_A s_y t B
\end{aligned} \tag{3.32}$$

where:

c_F	-	force coefficient;
c_A	-	ratio of sectional areas;
A_{stiff}	-	sectional area of stiffeners; and
A_{total}	-	total sectional area of stiffeners and their attached plate.

The full implementation of this equation requires structural details that are not appropriate for a simplified analysis. In this study, based on a sampling of typical side shell scantlings, a simplified calculation is used where $c_F c_A$ is assumed to have a constant value of 0.025.

Since F_R also effects membrane tension energy, Equations (3.30) become:

$$\begin{aligned}
\Delta KE_n &= F_{hn}\left[(w_{n+1}-w_n)+0.15\left|l_{n+1}-l_n\right|\right]+F_R(l_{n+1}-l_n)\\
F_{hn} &= \frac{(E_{1,n+1}+E_{2,n+1})-(E_{1n}+E_{2,n})-F_R(l_{n+1}-l_n)}{(w_{n+1}-w_n)+0.15\left|l_{n+1}-l_n\right|}\\
F_{xn} &= (F_R+0.15F_{hn})\frac{(l_{n+1}-l_n)}{\left|l_{n+1}-l_n\right|}\\
M_n &= -F_{xn}d_n+F_{hn}l_n
\end{aligned} \tag{3.33}$$

The Internal Sub-Model determines absorbed energy and forces from the crushing and tearing of decks, bottoms and stringers (horizontal structures) in a much more simplified manner using the Minorsky correlation [9] as modified by Reardon and Sprung [15].

Step 2 in the SIMCOL collision simulation process calculates damaged area and volume in the struck ship given the relative motion of the two ships calculated in Step 1 by the External Sub-Model. Figure 16 illustrates the geometry of the sweeping segment method used for this calculation in SIMCOL Version 2.1.

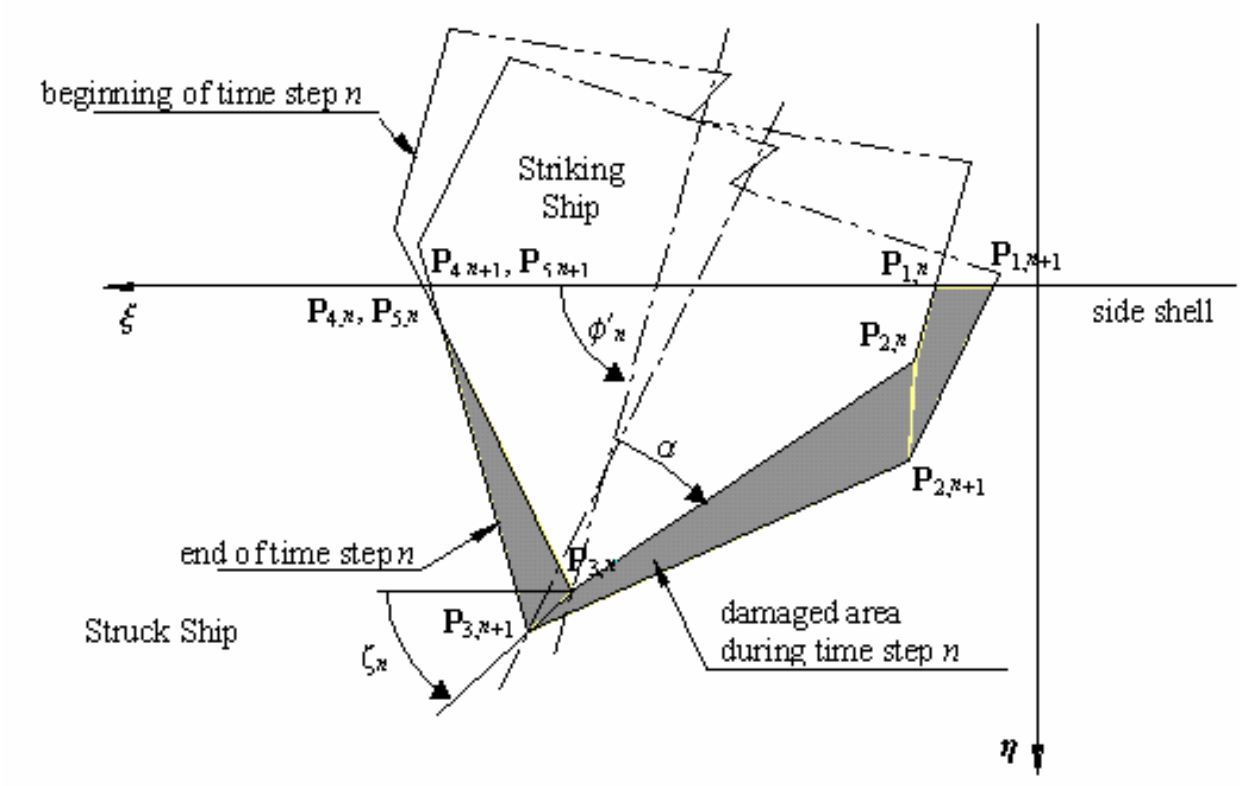

Figure 16 - Sweeping Segment Method

The intrusion portion of the bow is described with five nodes, as shown in Figure 16. The shaded area in Figure 16 is the new damaged area of decks and/or bottoms during the time step. Coordinates of the five nodes in the ξ-η system at each time step are derived from the penetration and location of the impact, the collision angle, ϕ, and the half entrance angle, α, of the striking bow.

$\mathbf{P}_3$ is specified by the penetration and location of the striking ship relative to the struck ship:

$$\begin{aligned} \mathbf{P}_3 &= \{x_3, h_3\} = \{l, d\} \\ f' &= p - f \end{aligned} \tag{3.34}$$

If the parallel body of the striking ship has not penetrated into the struck ship then:

$$\overline{\mathbf{P}_2\mathbf{P}_3} \le \frac{B_2}{2\sin a} \text{ or } \overline{\mathbf{P}_3\mathbf{P}_4} \le \frac{B_2}{2\sin a}, \text{ and}$$

$$\begin{aligned} \mathbf{P}_2 &= \{x_2, h_2\} = \left\{x_3 - \frac{h_3}{\tan(-a + f')}, 0\right\} \\ \mathbf{P}_1 &= \{x_1, h_1\} = \mathbf{P}_2 \\ \mathbf{P}_4 &= \{x_4, h_4\} = \left\{x_3 - \frac{h_3}{\tan(a + f')}, 0\right\} \\ \mathbf{P}_5 &= \{x_5, h_5\} = \mathbf{P}_4 \end{aligned} \tag{3.35}$$

If the parallel body of the striking ship has penetrated into the struck ship then:

$$\overline{\mathbf{P}_2\mathbf{P}_3} > \frac{B_2}{2\sin a} \text{ or } \overline{\mathbf{P}_3\mathbf{P}_4} > \frac{B_2}{2\sin a}, \text{ and}$$

$$\begin{aligned} \mathbf{P}_2 &= \{x_2, h_2\} = \left\{x_3 - \frac{B_2}{2\sin a}\cos(-a + f'), h_3 - \frac{B_2}{2\sin a}\sin(-a + f')\right\} \\ \mathbf{P}_1 &= \{x_1, h_1\} = \left\{x_2 - \frac{h_2}{\tan f'}, 0\right\} \\ \mathbf{P}_4 &= \{x_4, h_4\} = \left\{x_3 - \frac{B_2}{2\sin a}\cos(a + f'), h_3 - \frac{B_2}{2\sin a}\sin(a + f')\right\} \\ \mathbf{P}_5 &= \{x_5, h_5\} = \left\{x_4 - \frac{h_4}{\tan f'}, 0\right\} \end{aligned} \tag{3.36}$$

where:

$\mathbf{P}_i$ - node of penetrated bow;

ξ_i, η_i - coordinates of node in ξ-η system (m); and

B_2 - breadth of the striking ship (m).

Once the node coordinates before and after the time step are calculated, the segment of the bow plan that has caused further damage during the time step and the area swept by a specific segment are determined. In the case of the segment $\mathbf{P}_1\mathbf{P}_2$ in Figure 16, the out-sweeping area, A_1, during time step n is calculated as follows:

$$A_{1,n} = \frac{1}{2}\left(\begin{vmatrix} x_{2,n} & x_{1,n} \\ h_{2,n} & h_{1,n} \end{vmatrix} + \begin{vmatrix} x_{2,n+1} & x_{2,n} \\ h_{2,n+1} & h_{2,n} \end{vmatrix} + \begin{vmatrix} x_{1,n+1} & x_{2,n+1} \\ h_{1,n+1} & h_{2,n+1} \end{vmatrix} + \begin{vmatrix} x_{1,n} & x_{1,n+1} \\ h_{1,n} & h_{1,n+1} \end{vmatrix} \right) \tag{3.37}$$

The damaged plating thickness t is the sum thickness of deck, stringer and/or bottom structures that are within the upper and lower extents of the striking bow. Given the damaged material volume, the Minorsky force is calculated based on the following assumptions:

- The resistant force acting on each out-sweeping segment is in the opposite direction of the average movement of the segment. The force exerted on the struck ship is in the direction of this average movement.
- The work of the resistant force is done over the distance of this average movement.
- The total force on each segment acts through the geometric center of the sweeping area.

Using the Minorsky relation, Equation (2.8), the energy absorbed by the sweeping segment $\mathbf{P}_1\mathbf{P}_2$ is then:

$$\Delta KE_{1,n} = 47.1\times10^6 R_{T1,n} = 47.1\times10^6 A_{1,n}\ t \tag{3.38}$$

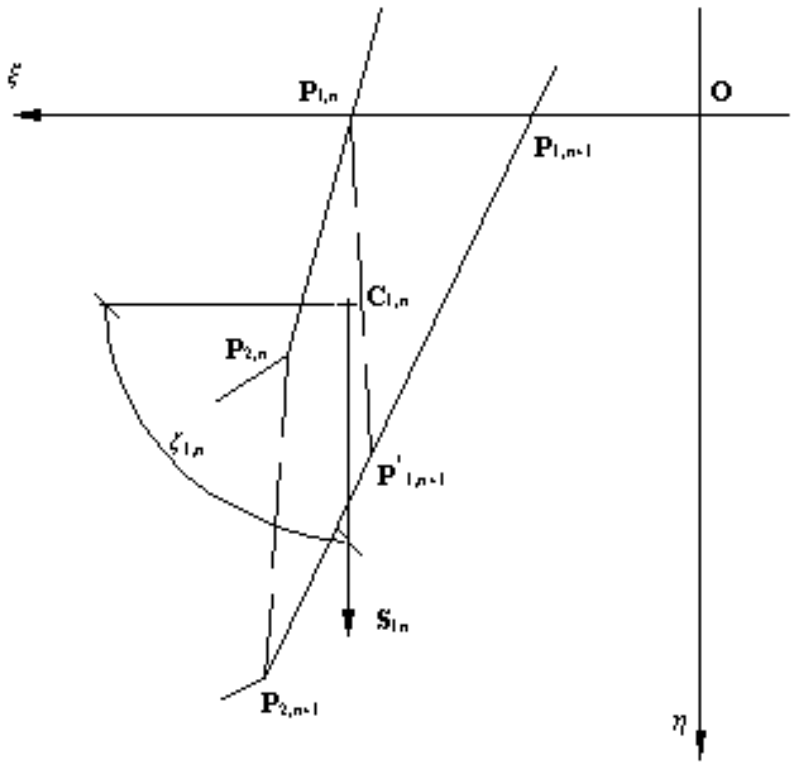

Figure 17 - Sweeping Segment Geometry

The average motion, $\mathbf{S}_1$, and the geometric center of the sweeping area, $\mathbf{C}_1$, for the segment $\mathbf{P}_1\mathbf{P}_2$ in time step n are approximated as follows (Figure 16 and Figure 17):

$$\text{Select } \mathbf{P}^*_{1,n+1} \text{ on } \mathbf{P}_{1,n+1}\mathbf{P}_{2,n+1}, \text{ so that } \overline{\mathbf{P}^*_{1,n+1}\mathbf{P}_{2,n+1}} = \overline{\mathbf{P}_{1,n}\mathbf{P}_{2,n}}$$

$$\begin{aligned}
\mathbf{S}_{1,n} &= \frac{1}{2}(\mathbf{P}_{2,n}\mathbf{P}_{2,n+1}\text{`} + \mathbf{P}_{1,n}\mathbf{P}^*_{1,n+1}\text{`}) \\
&= \frac{1}{2}[\mathbf{P}_{2,n+1} - \mathbf{P}_{2,n} + (\mathbf{P}_{2,n+1} - \mathbf{P}_{1,n+1})\frac{\overline{\mathbf{P}_{1,n}\mathbf{P}_{2,n}}}{\overline{\mathbf{P}_{1,n+1}\mathbf{P}_{2,n+1}}} - \mathbf{P}_{1,n}] \qquad (3.39) \\
\mathbf{C}_{1,n} &= \frac{1}{4}(\mathbf{P}_{1,n} + \mathbf{P}_{2,n} + \mathbf{P}_{1,n+1} + \mathbf{P}_{2,n+1})
\end{aligned}$$

The force exerted through the segment $\mathbf{P}_1\mathbf{P}_2$ on the struck ship, $\mathbf{F}_{1,n}$, and the moment to the origin of the local coordinate system, $M_{1,n}$, are then:

$$\begin{aligned}
F_{1,n} &= \left|\mathbf{F}_{1,n}\right| = \frac{\Delta KE_{1,n}}{s_{1,n}} \\
\mathbf{F}_{1,n} &= \begin{pmatrix} F_{x1,n} \\ F_{h1,n} \end{pmatrix} = \begin{pmatrix} F_{1,n}\cos z_{1,n} \\ F_{1,n}\sin z_{1,n} \end{pmatrix} \qquad (3.40) \\
M_{1,n} &= \mathbf{OC}_{1,n}\text{`} \times \mathbf{F}_{1,n}
\end{aligned}$$

where $s_{1,n} = \left|\mathbf{S}_{1,n}\right|$ and $\zeta_{1,n}$ is the direction of $\mathbf{S}_{1,n}$.

Forces and moments acting on other segments are calculated similarly. The total exerted force, $\mathbf{F}_n$, is the sum of the forces and moments on each segment:

$$\mathbf{F}_n = \sum_{i=1}^{4} \{F_{xi,n}, F_{hi,n}, M_{i,n}\} \qquad (3.41)$$

These forces are added to the side shell, bulkhead and web forces. Internal forces and moments are calculated for the struck ship in the local coordinate system, i.e. the ξ-η system, and converted to the global system. The forces and moments on the striking ship have the same magnitude and the opposite direction from those on the struck ship.

The damage length, L_D, is:

$$L_D = \max(x_{i,j}) - \min(x_{i,j}) \qquad i = 1, \ldots, 5 \qquad j = 1, \ldots, m \qquad (3.42)$$

where m is the time step.

3.1.3 SIMCOL Input Data Requirements and Description

SIMCOL requires two types of input data:

- Data describing the struck ship
- Data Describing the collision scenario

For a single hull tanker, the struck ship data includes:

SHIP_TYPE - struck ship type (1 for single hull)

LBP1 - struck ship length (m)

B1 - struck ship breadth (m)

D1 - struck ship depth (m)

T1 - struck ship draft (m)

DISP1 - struck ship displacement (kg)

WEB_SPC - struck ship transverse web spacing (m)

TBHD_NUM - number of transverse bulkheads including FP and AP

TBHD_LOC - the location of transverse bulkheads, input measured aft of FP (m)

LBHD_NUM - number of longitudinal bulkheads including side shells

LBHD_LOC - the location of side shell and longitudinal bulkheads, measured from CL, starting outboard, one side and CL only (m)

LBHD_THK - smeared plate thickness, side shell and longitudinal bulkheads (m)

LBHD_MAT - material grade of side shell and longitudinal bulkheads

DECK_THK - smeared plate thickness of decks (m)

BTM_THK - smeared plate thickness of bottom (m)

STRG_NUM - number of side stringers

STRG_WID - stringer width (m)

STRG_LOC - stringer location measured above baseline (m)

STRG_THK - stringer thickness (m)

WEB_SUP - number of supports including decks, bottom, and struts

WEB_DEP - depth (transverse width) (m)

WEB_STF - web horizontal stiffener spacing (m)

WEB_MAT - web material grade at each support

WEB_THK - web thickness at each support (m)

WEB_SMZ - web section modulus at each support (m^4)

WEB_SPN - unsupported web span (vertical distance) between each support (m)

WEB_GAP - supported length at each support (bracket) (m)

SUP_MAT - material grade of each intermediate web support (strut)

SUP_ARA - cross section area of each intermediate web support (m^2)

SUP_GRA - gyration radius of each intermediate web support (m)

SUP_LEN - critical length of each intermediate support (m)

STF_THK - smeared thickness of web stiffeners (m)

STF_GRA - gyration radius of each stiffener w/ attached web plate (m)

VOLTANK - Cargo tank volumes (98%) (m^3)

For a double hull tanker, the struck ship data includes:

SHIP_TYPE - struck ship type (2 for double hull)

LBP1 - struck ship length (m)

B1 - struck ship breadth (m)

D1 - struck ship depth (m)

T1 - struck ship draft (m)

DISP1 - struck ship displacement (kg)

WEB_SPC - struck ship transverse web spacing (m)

TBHD_NUM - number of transverse bulkheads including FP and AP

TBHD_LOC - the location of transverse bulkheads, input measured aft of FP (m)

LBHD_NUM - number of longitudinal bulkheads including side shells

LBHD_LOC - the location of side shell and longitudinal bulkheads, measured from CL, starting outboard, one side and CL only (m)

LBHD_THK - smeared plate thickness, side shell and longitudinal bulkheads (m)

LBHD_MAT - material grade of side shell and longitudinal bulkheads

DECK_THK - smeared plate thickness of decks (m)

IBTM_THK - smeared plate thickness of inner bottom (m)

BTM_THK - smeared plate thickness of bottom (m)

DBL_HT - double bottom height (vertical) (m)

STRG_NUM - number of side stringers

STRG_LOC - stringer location measured above baseline (m)

STRG_THK - stringer thickness (m)

WEB_SUP - number of supports including decks, bottom, and struts

WEB_DEP - depth (transverse width) (m)

WEB_STF - web horizontal stiffener spacing (m)

WEB_MAT - web material grade at each support

WEB_THK - web thickness at each support (m)

WEB_SMZ - web section modulus at each support (m^4)

WEB_SPN - unsupported web span (vertical distance) between each support (m)

WEB_GAP - supported length at each support (bracket) (m)

SUP_MAT - material grade of each intermediate web support (strut)

SUP_ARA - cross section area of each intermediate web support (m^2)

SUP_GRA - gyration radius of each intermediate web support (m)

SUP_LEN - critical length of each intermediate support (m)

STF_THK - smeared thickness of web stiffeners (m)

STF_GRA - gyration radius of each stiffener w/ attached web plate (m)

VOLTANK - Cargo tank volumes (98% full) (m^3)

The collision scenario data includes:

VEL1 - speed of the struck ship (knots)

VEL2 - speed of the striking ship (knots)

LOC - impact point location measured after of midships in the struck ship (m)

PHI - collision angle (degrees)

SHPTPE - striking ship type

DISP2 - striking ship displacement (kg)

SIMCOL calculates striking ship length, beam, draft, bow height and half entrance angle as a function of the striking ship type and displacement using the relationships presented in Chapter 7.

3.2 SIMCOL Simplified Oil Outflow Calculation

Current hypothetical outflow and tank size requirements for oil tankers are found in Regulations 22-24 of Annex I of MARPOL 73/78. Recognizing that these regulations do not actually assess the environmental performance of tankers, IMO instructed its BLG (Bulk Liquids and Gases) Sub-Committee to develop a new accidental oil outflow regulation modeled after the probabilistic methodology contained in the IMO Guidelines [4]. This new regulation will still not consider the crashworthiness of the structural design. One of the primary objectives of this SSC project is to provide a methodology and model that does consider crashworthiness for potential application in future IMO regulations. The IMO Guidelines provide a probabilistic-based procedure for assessing the oil outflow performance of an alternative tanker design. The alternative design is compared to selected reference double hull design based on a pollution prevention index.

The IMO Guidelines present two procedures for evaluating the oil outflow. The “conceptual” method, applicable for conceptual design approval, assumes the ship survives the damage. For bottom damage, the ship is assumed to rest on the ground at its initial intact drafts, with zero trim and heel. The “survivability” method, applicable to final designs, requires damage stability calculations. For damage cases that fail to satisfy the specified survivability criterion, it is assumed that the ship is lost and 100% of all cargo oil onboard outflows to the sea.

A fully probabilistic evaluation of a specific vessel on a specific route would require development of the following probabilities:

- The probability that the ship will have a grounding or collision accident
- The conditional probability density function for damage location and extent;
- The expected consequences (i.e. quantity of outflow).

The IMO Guidelines do not specifically deal with the probability of whether the ship will have an accident. Rather, it is acknowledged that the risk exists, and it is assumed that the vessel is involved in a grounding or collision event significant enough to breach the outer hull. This is because data for accidents where the outer hull is not breached is rarely recorded. The resulting oil outflow is therefor conditional on an accident significant enough to breach the outer hull. The SIMCOL methodology is conditional only on a collision accident occurring. SIMCOL considers accidents that do not breach the outer hull. This better reflects the true crashworthiness of a structural design.

Rigorous application of the probabilistic oil outflow methodology contained in the IMO Guidelines is a calculation intensive effort based on an empirical description of damage extent and location. SIMCOL follows the basic steps of the IMO methodology, but assembles the damage cases using a Monte Carlo simulation with a probabilistic description of the accident scenarios as the primary input. The following steps are followed in the SIMCOL process:

Step 1: Assemble Damage Cases

For each collision case in the Monte Carlo simulation, SIMCOL calculates damage extent. Once collision damage calculations are completed, SIMCOL determines which cargo tanks have been penetrated and ruptured by comparing damage extents to cargo tank subdivision boundaries specified in the SIMCOL input. In addition to depth and length of penetration, SIMCOL also flags when a tank boundary is ruptured. It is assumed in side damage that if a tank is penetrated and ruptured, its entire contents are spilled. The volume of oil in each tank is specified in the SIMCOL input. For a specified collision case, SIMCOL sums the outflow from all ruptured tanks to determine the total outflow for the case.

Step 2: Calculate Oil Outflow

Consistent with the IMO analysis approach, 100% outflow for all cargo tanks sustaining side damage is assumed.

Step 3: Calculate Oil Outflow Parameters

- The *probability of zero outflow*, P_0, represents the likelihood that no oil will be released into the environment, given a collision or grounding accident. P_0 equals the cumulative probability of all damage cases without outflow.
- The *mean outflow parameter,* O_M, is the non-dimensionalized mean or expected outflow, and provides an indication of a design's overall effectiveness in limiting oil outflow. The mean outflow equals the sum of the products of each damage case probability and the associated outflow. O_M equals the mean outflow divided by the total quantity of oil onboard the vessel.

- The extreme *outflow parameter*, O_E, is the non-dimensionalized extreme outflow, and provides an indication of the expected oil outflow from particularly severe casualties. The extreme outflow is the weighted average of the upper 10% of all casualties (i.e. all damage cases within the cumulative probability range from 0.9 to 1.0).

Step 4: Compute the Pollution Prevention Index

The Pollution Prevention Index is calculated as in the IMO Guidelines.

Alternative designs are compared to reference double hull designs by substituting the outflow parameters for the reference design and the alternative design into the following formula:

$$E = \frac{(0.5)(P_O)}{P_{OR}} + \frac{(0.4)(0.01 + O_{MR})}{0.01 + O_M} + \frac{(0.1)(0.025 + O_{ER})}{0.025 + O_E} \tag{3.43}$$

P_0, O_M, and O_E are the oil outflow parameters for the alternative design, and P_{0R}, O_{MR}, and O_{ER} are the oil outflow parameters for the IMO reference ship of equivalent size.

CHAPTER 4 Striking Ship Bow

There are two basic types of bow models: rigid and deformable. Rigid models are defined only by the external geometry of the bow. Deformable models require definition of the internal structure of the bow or the resulting stiffness relative to external deformation. Deformable models have been developed from actual collision data, quasi-static and dynamic model tests, basic principles and finite element analysis. This Chapter presents existing models and data, provides additional finite element results, compares results, draws conclusions, and proposes bow models for future application in SIMCOL.

4.1 Rigid Bows

4.1.1 Hutchison and SIMCOL 1.0

Hutchison uses a sharp, rigid, wedge-shaped bow with a half-entrance angle of α and infinite vertical extent [12]. Hutchison states that these assumptions are conservative, and not unreasonable, particularly when the collision is between a large ship and a barge. Figure 18 shows the geometry of the simple bow model used by Hutchison.

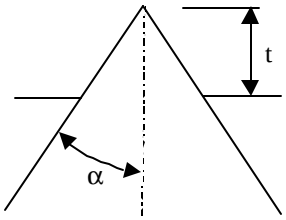

Figure 18 - Rigid Wedge-Shaped Bow Model used by Hutchison [12]

4.1.2 Ito

Ito investigates the effect of various design parameters on the strength of double-hulled structures in collision [25,26,27]. Collisions are classified into five types as shown in Figure 19. Types a, b and c are generally the most critical of all cases based on damage in actual collisions. Only types b (bulb strike) and c (stem strike) are analyzed in the Ito study.

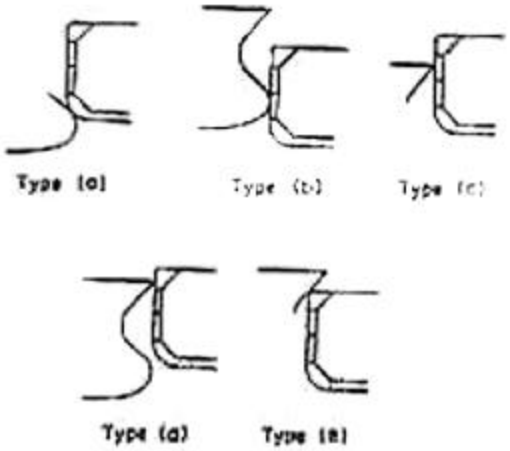

Figure 19 - Ito Collision Types [25]

Figure 20 shows the rigid indenters used in Ito's model tests. Figure 20 (a) shows the stem indenter and Figure 20 (b) shows the bulb indenter.

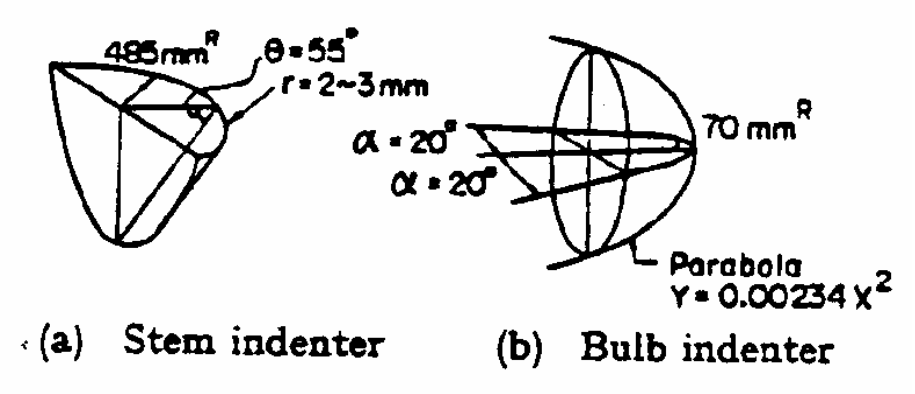

Figure 20 - Ito Bow Model Test Indenters [25]

The bow model indenters are gradually pushed into the double-hull structure using a hydraulic jack. Measurements of load, penetration, deformation and strain are made and presented.

4.1.3 Wierzbicki

Wierzbicki provides closed-form solutions for the mean crushing strengths and the cutting resistance of plated structures during collision [20] as discussed in Section 2.2.2.3. Figure 21 shows the wedge-like rigid bow model used by Wierzbicki in his experiments. His experiments and DAMAGE 4.0 [10] use a rigid bow.

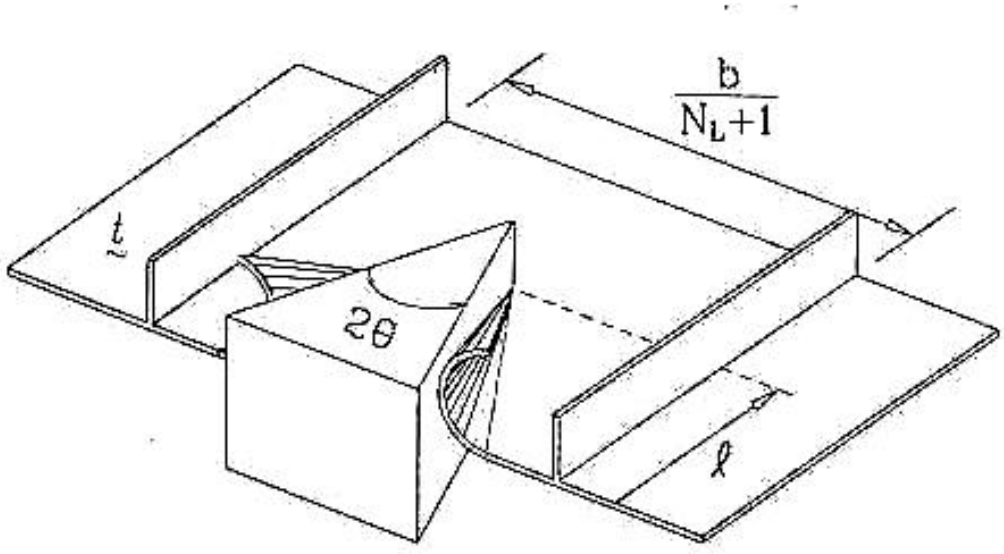

Figure 21 - Wedge-like Bow model used by Wierzbicki [20]

4.1.4 DAMAGE 4.0

DAMAGE 4.0 uses a rigid bow with significant geometrical detail. Figure 22 shows the bow geometry as idealized in DAMAGE 4.0. Figure 23 shows an Excel surface plot of the bow model used by DAMAGE.

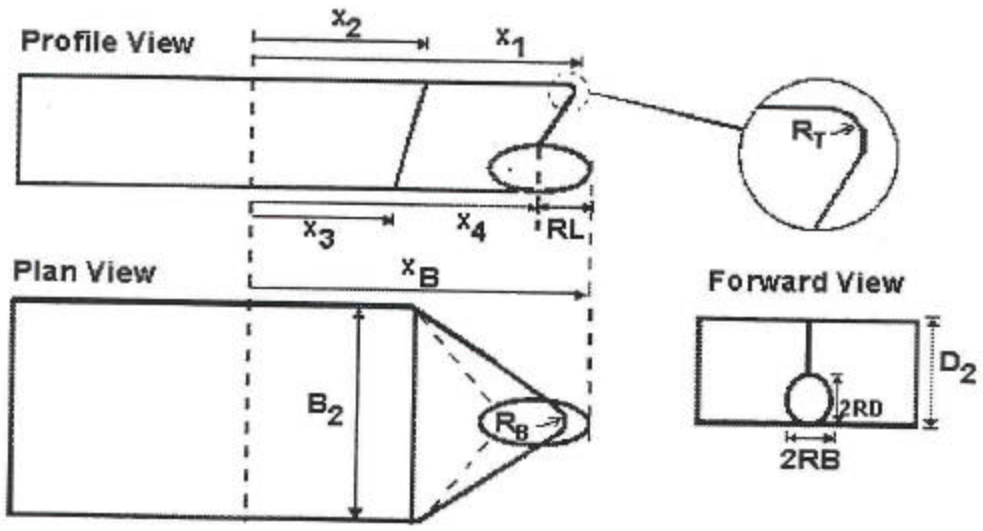

Figure 22 - Idealization of a Bulbous Bow in DAMAGE 4.0 [10]

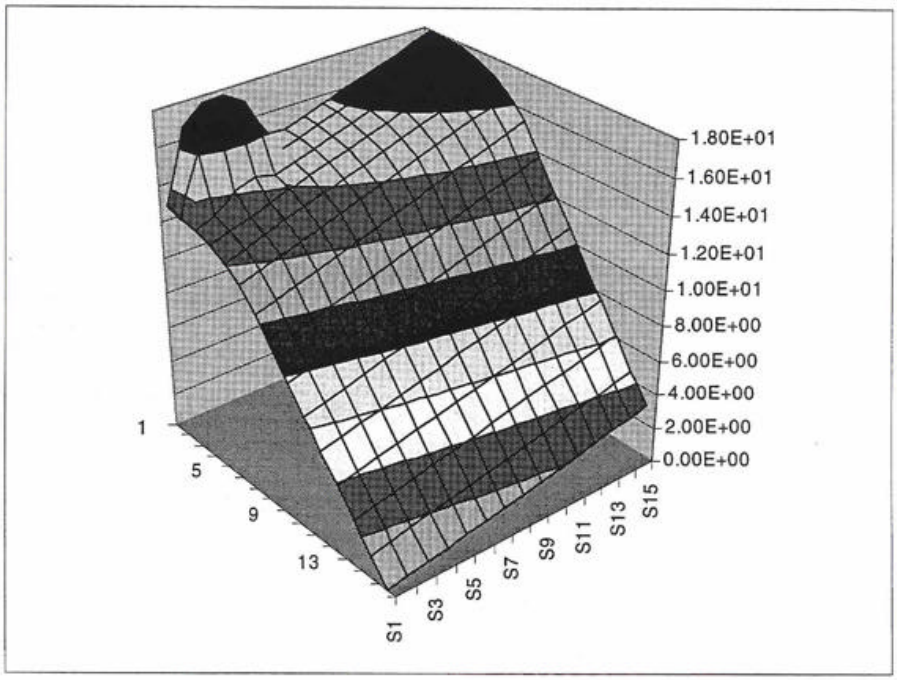

Figure 23 - Excel Surface Plot of Bow Model [10]

4.1.5 SIMCOL 2.11

SIMCOL Versions 0.0 to 2.0 assume that the striking bow is rigid with a wedge-shape defined only by a half-entrance angle, and with infinite vertical extents. SIMCOL Version 2.1 considers the upper and lower extents of the bow relative to the struck ship as shown in Figure 24. This new model provides results similar to other simplified models with rigid bows of more complex geometry as discussed in Chapter 6. The infinite wedge model used in SIMCOL 1.0 did not provide satisfactory results.

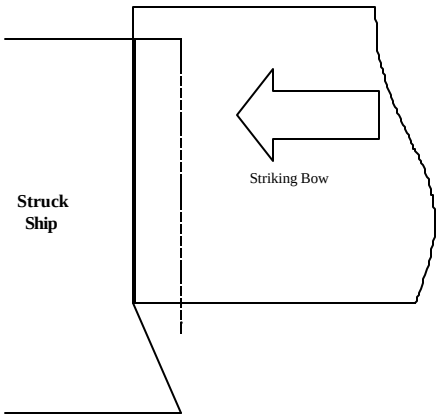

Figure 24 - SIMCOL Version 2.1 Bow Model

4.1.6 ASIS and Netherlands Foundation for the Coordination of Maritime Research

The Japanese Association for the Structural Improvement of the Shipbuilding Industry (ASIS) and Netherlands Foundation for the Coordination of Maritime Research tests included four experiments which were carried out using two inland waterway tankers of approximately 1000 tonnes displacement [33,34]. In each experiment, a rigid bow strikes a test side section at a right angle. Three types of side structure were tested: single hull, double hull with stringers and double hull with stringer deck. Collision forces, motions and penetration depths were measured.

4.2 Deformable Bows

4.2.1 Data from Bows in Actual Collisions - Minorsky

Minorsky's resistance factor, R_T, plotted with absorbed energy for 9 collisions in Figure 3, considers the deformation of structural members in both ships having depth in the direction of penetration including:

- Decks, flats and double bottoms in both struck and striking vessels
- Transverse bulkheads in the struck vessel
- Longitudinal bulkheads in the striking vessel
- Component in the direction of collision of the shell of the striking vessel (assumed at 0.7 of the shell area)

Minorsky calculates resistance factor using the equation:

$$R_T = \sum P_N L_N t_N + \sum P_n L_n t_n \tag{4.1}$$

where:

P_N - depth of damage in the Nth member of the striking vessel;
L_N - length of damage in the Nth member of the striking vessel;
t_N - thickness of the Nth member of the striking vessel;
P_n - depth of damage in the nth member of the struck vessel;
L_n - length of damage in the nth member of the struck vessel;
t_n - thickness of the nth member of the struck vessel

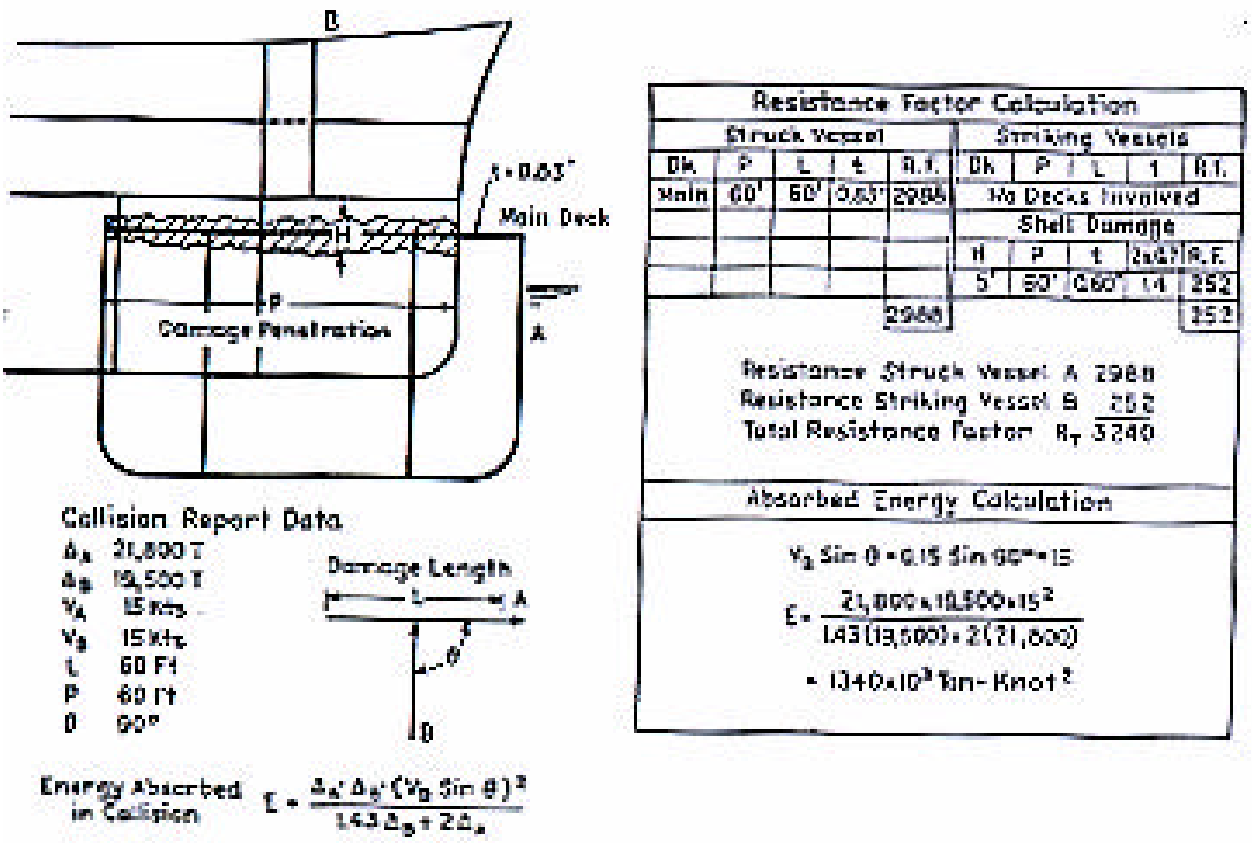

Figure 25 - Resistance Factor Calculations [9]

Figure 25 shows the Minorsky resistance factor and absorbed energy calculation for Collision Number 11. A similar figure was made for each collision that Minorsky studied. This data is not available for the other collisions, however Reardon and Sprung [15] discovered a tabular summary for the same ships in a 1960 Gibbs and Cox report [36]. Table 2 presents this data for six collision cases that were originally from Minorsky, and for the Andria Doria collision which was also identified in Minorsky.

Using this data, the percentage of energy absorbed in the striking ship bow for these seven actual collision cases can be reproduced as follows:

1. The struck ship resistance factors are calculated using Table 2 data and Equation (4.1).

2. The total resistance factors for these seven collisions are taken from Figure 3.

3. The bow resistance factors are calculated by subtracting the struck ship resistance factors from the total-ship resistance factors.

4. Since absorbed energy and resistance factor are assumed to have a linear relationship, the percentage of the total absorbed energy by the striking ship bow is the bow resistance factor divided by the total resistance factor. These results are also listed in Table 2.

Table 2 - Percentage of energy absorbed by striking ship [15,36]

MINORSKY COLLISION CASE		Displacement (lton) [15,36]	n	t (in) [15,36]	V (knots) [15,36]	q(deg) [15,36]	width (ft) [15,36]	penetration (ft) [15,36]	Struck Ship R_T (ft^2in)	Minirsky Total R_T (ft^2in) [9]	Bow R_T (ft^2in)	% Energy Absorbed in Bow
10	**Esso Greensboro**	21800	1	0.83	15	90	60	60	2988	3250	262	8.1
	Esso Suez	19500			15							
11	**Tullahoma**	21900	2	0.8	10	90	20	25	800	1100	300	27.3
	P&T Adventurer	8900			14							
21	**Gulf Glow**	21900	2	0.8	0	65	20	38	1216	1700	484	28.5
	Imperial Toronto	16000			14							
22	**Mojave**	5600	2	0.5	10	70	28	23	644	900	256	28.4
	Prometed	16000			14							
38	**Catawba Ford**	21800	1	0.8	10	90	27	10	216	250	34	13.6
	Hoegh Clair	6600			8							
46	**David E Day**	8700	2	0.7	16.3	55	35	17	833	1300	467	35.9
	Marine Flyer	20400			16.5							
B	**Andria Doria**	20900	6	0.375	15	90	50	30	3375	3800	425	11.2
	Stockholm	16200			18							

In these cases, the percentage of energy absorbed by the striking ship is significant and is not constant. This supports the hypothesis that the striking bow can absorb significant energy in a collision, and must be considered.

4.3 Bows in Dynamic Model Tests

4.3.1 Woisin

Woisin analyzed the structural design of nuclear ships to reduce damage from collision in a series of tests by GKSS in Germany [17]. Twelve pairs of collision models were tested in Hamburg from 1967 to 1976. Figure 26 shows a schematic diagram of the dynamic collision model tests performed in Hamburg. These tests used deformable bows. He proposes a theory of "soft bows" to minimize penetration into other ships.

The test stand consists of a carriage of up to 25 tonnes with a fore-ship model attached to its forward end, which rams a ship's side model attached to a rigid counter bearing. The necessary velocity and energy of impact are achieved by an incline on which the carriage, after release of

an arresting device, accelerates until it coasts without acceleration on a horizontal plane. Significant damage is caused to the bow model. Model scales were 1:12 and 1:7.5. Results showed a significant difference in impact force with bow structural design.

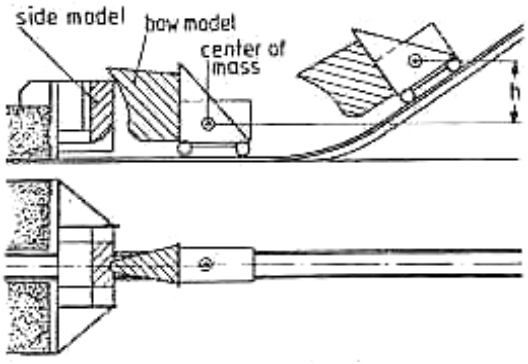

Figure 26 - Schematic Diagram of Test Techniques in Hamburg [17]

Based on these tests, Woisin proposes a number of potential methods for designing soft bows:

- transverse, instead of longitudinal stiffeners
- water filling
- fewer breast hooks and reduced stem plate thickness
- no hard points
- design of bulbous bows and raking parts above water as crushable zones

Woisin also proposes the following formula for predicting the maximum collision force P_{max} of typical bow structures, as a function of the dwt of the striking ship:

$$P_{max} = 0.88\sqrt{DWT} \pm 50\% \tag{4.2}$$

One of the GKSS tests used a 1:12 scale model of the Esso Malaysia bow against a rigid side [17,37]. The impact speed was 6.51 meters/second with a total weight of 18 tonne. The bow crushing indentation was 0.5 meters. The actual ship has the following principal characteristics:

LOA	-	323.7 m
LBP	-	304.9 m
B	-	47.2 m
D	-	23.7 m
T	-	18.4 m
Δ	-	194 tonne

The bow model plating thicknesses were as follows:

Shell plate forward frame 158	-	2.75 mm
Shell plate frame 147-158	-	2.0 mm
Bottom shell frame 143-147 below 0.145 m	-	2.0 mm
Shell plate frame 143-147 above 0.145 m	-	1.5 mm
Center bulkhead, decks and inner structure	-	1.0 mm

Figure 27 shows the details of the model structure. Figure 28 and Figure 29 show the model before and after damage. Figure 30 shows the results of Kierkegaard's numerical model for this same test case.

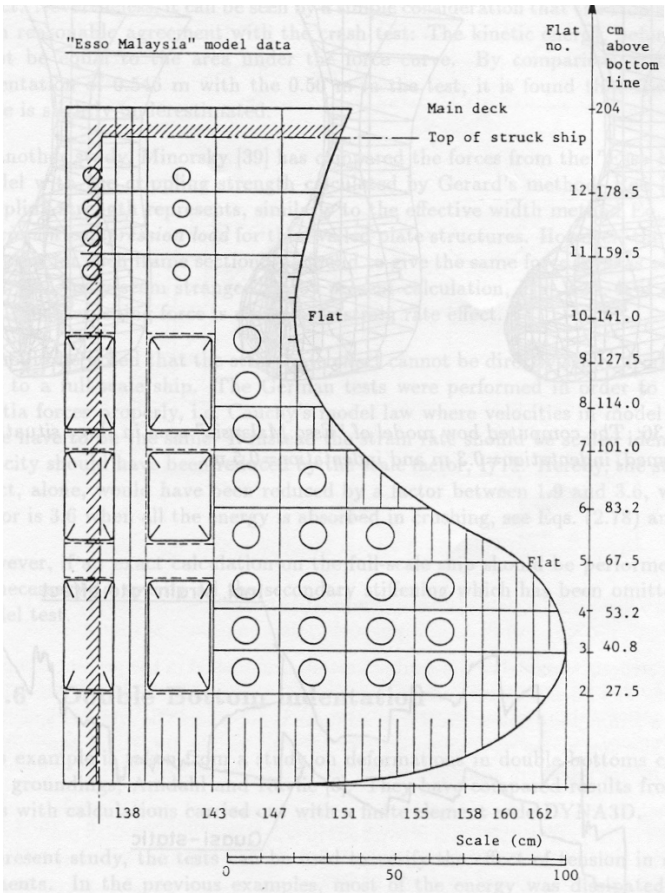

Figure 27 - Structural Details of Esso Maylasia Model [37]

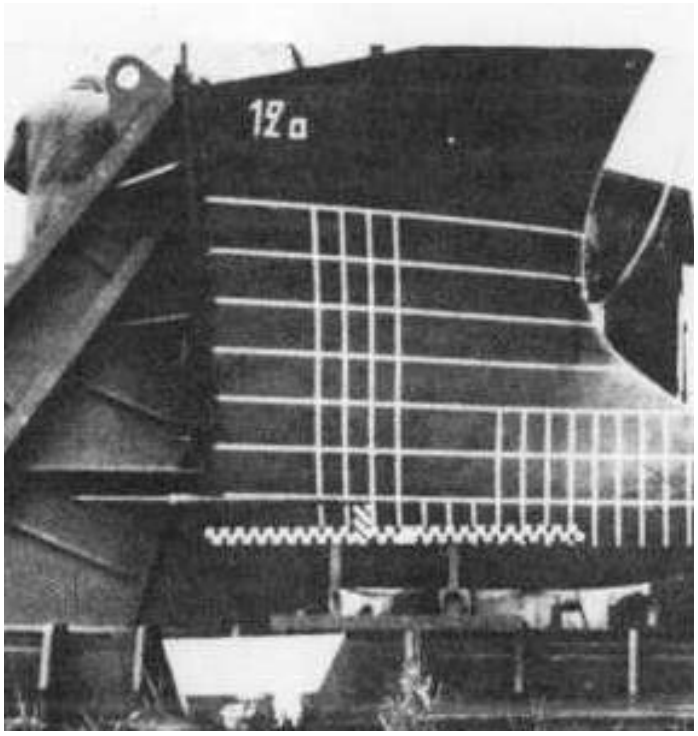

Figure 28 - Esso Malaysia Bow Model [37]

Figure 29 - Esso Malaysia Model after Damage [37]

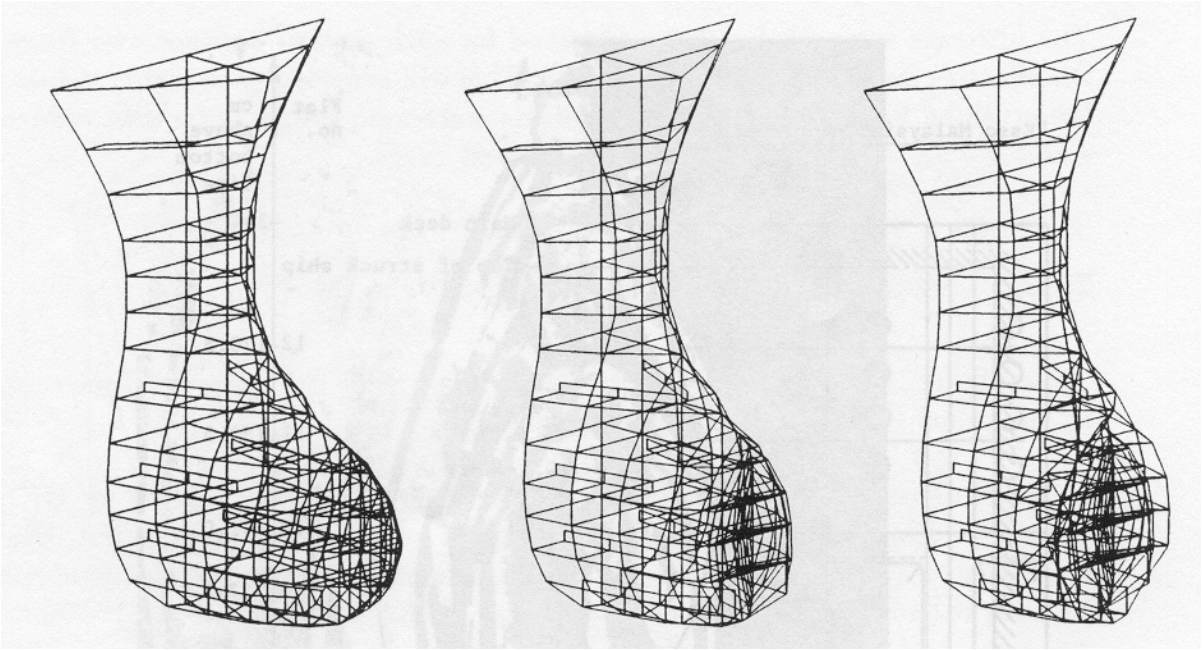

Figure 30a - Kierkegaard Model Results for Esso Malaysia Model Test [37]

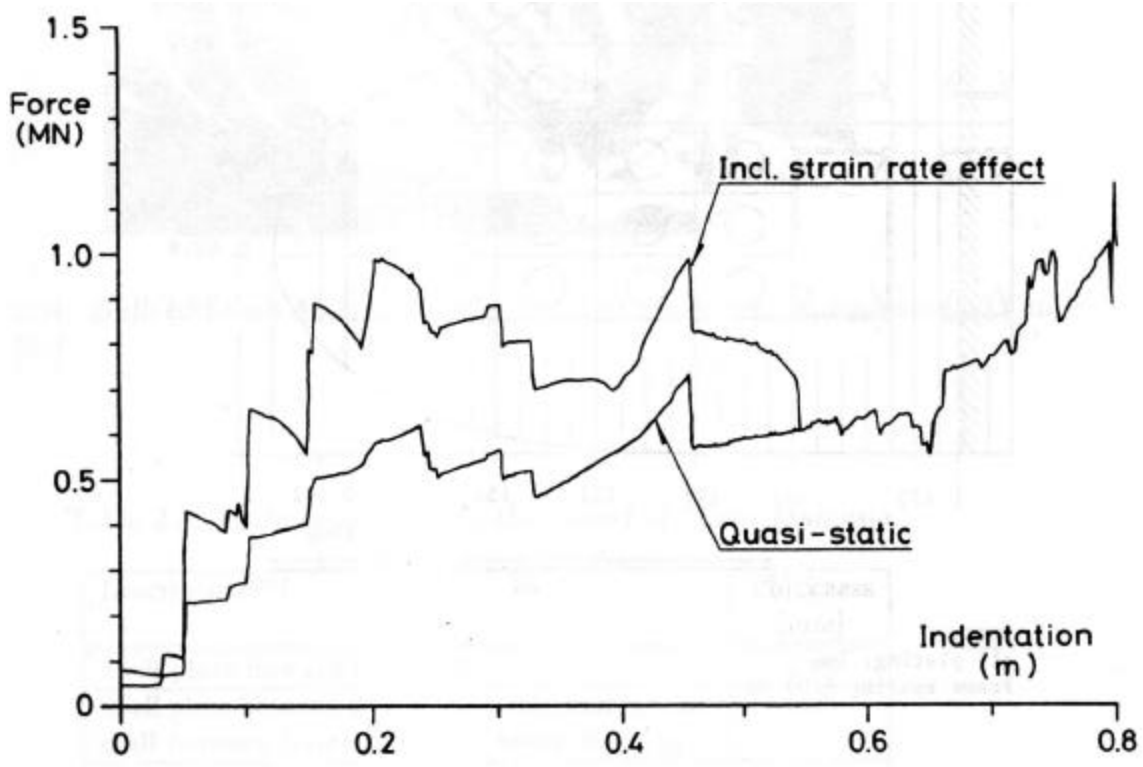

Figure30b - Kierkegaard Model Results for Esso Malaysia Model Test [37]

4.4 Bows in Quasi-Static Model Tests

4.4.1 Amdahl

Amdahl performed a series of model tests with simplified bow models (Figure 31) [23, 37]. The models included:

1. Box-shaped with transverse frames
2. Wedge-shaped with transverse frames
3. Wedge-shaped with transverse frames, deck and longitudinal bulkhead
4. Wedge-shaped with transverse frames, three stringer decks and longitudinal bulkhead
5. Wedge-shaped with transverse frames, deck, longitudinal bulkhead and longitudinal stiffeners
6. Raked bow with transverse frames

A longitudinal quasi-static compression is applied to each. The resulting load-displacement curves for models 1-3, 5 and 6 are provided in Figure 32a-e.

4.4.2 Kitamura and Akita

Kitamura and Akita report on a series of quasi-static bow model tests conducted in Japan [37,38]. Six bow w/stem models were crushed into a rigid nuclear-ship side model. These models are shown in Figure 33. Load/indentation results are shown in Figure 34 with Kierkegaard's model results, discussed in Section 4.5.18.

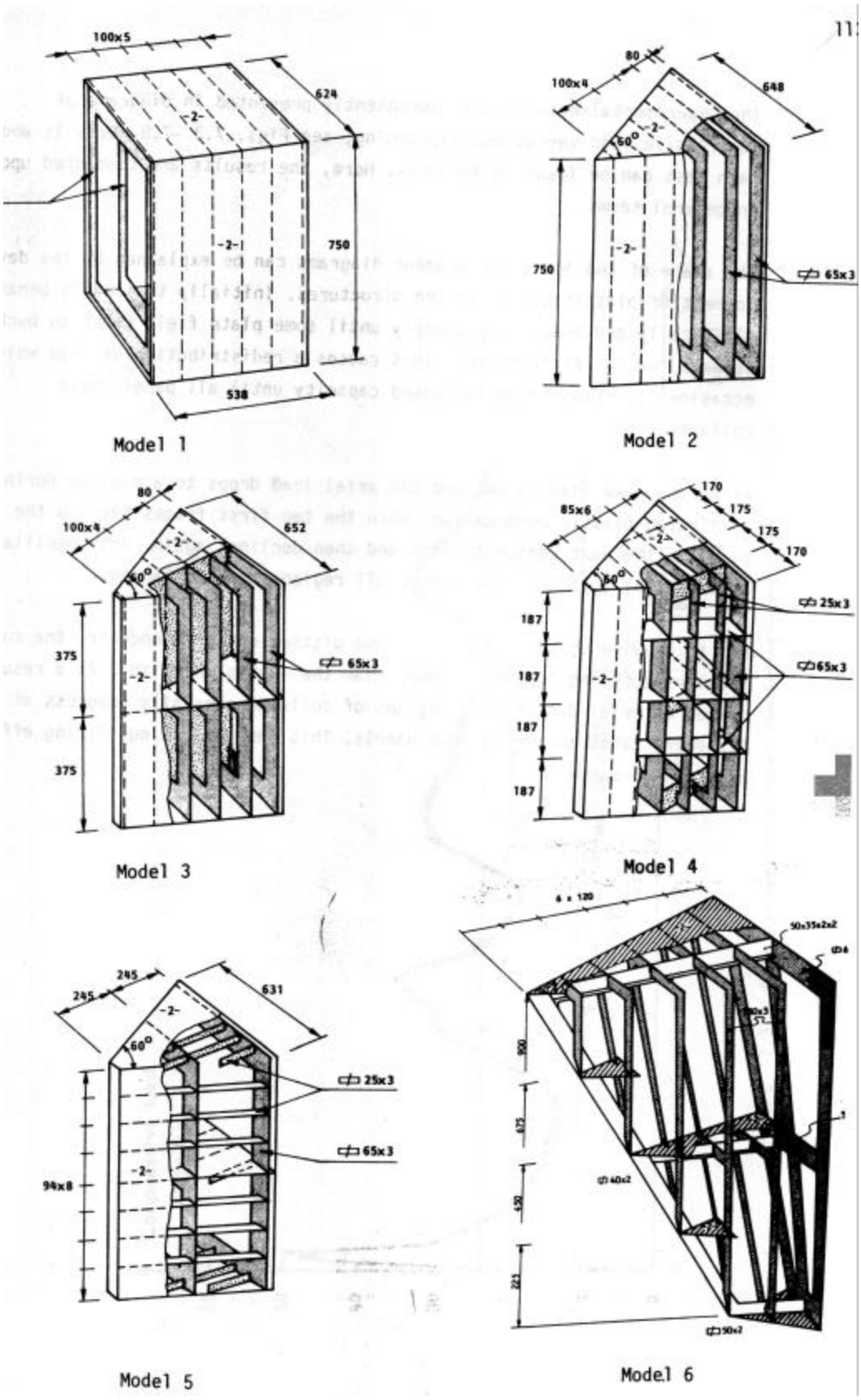

Figure 31 - Amdahl Bow Model Tests [23]

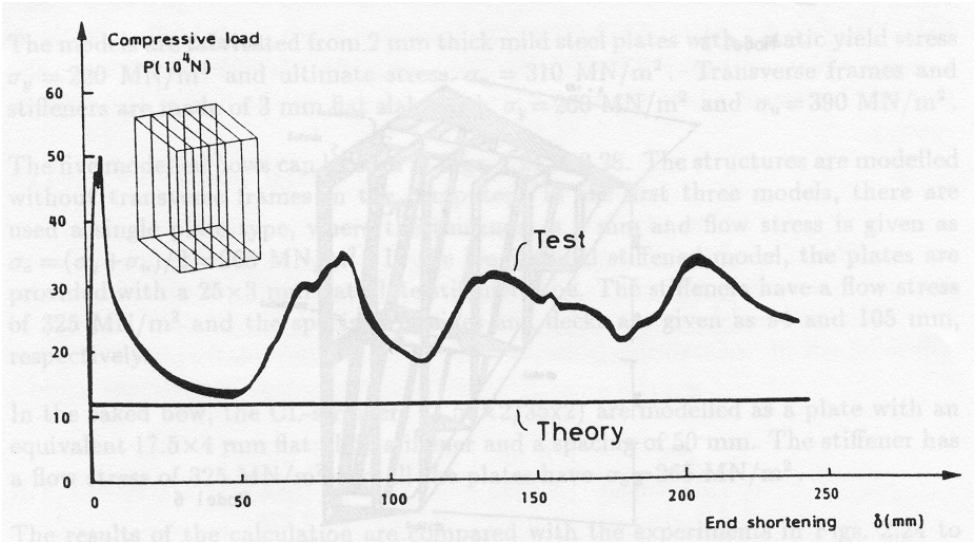

Figure 32a - Amdahl Bow Model Test Results Model #1 [37, 23]

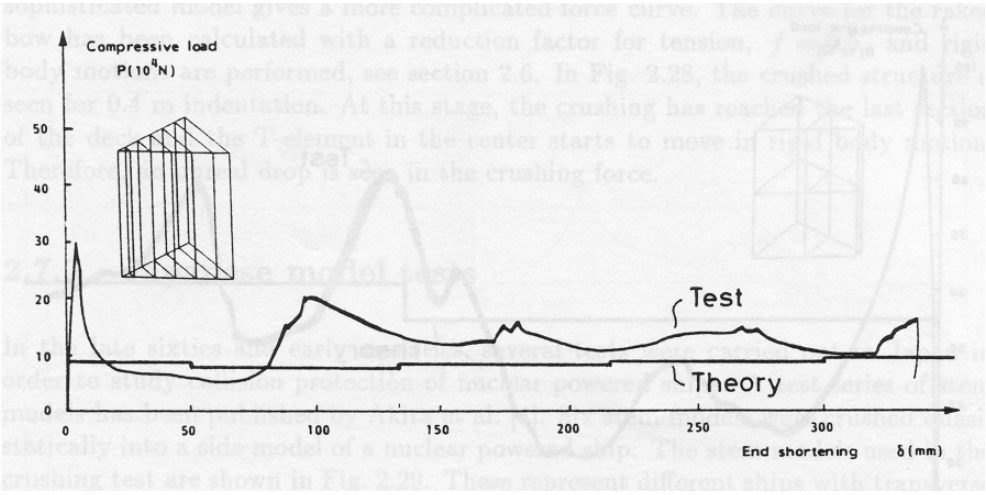

Figure 32b - Amdahl Bow Model Test Results Model #2 [37, 23]

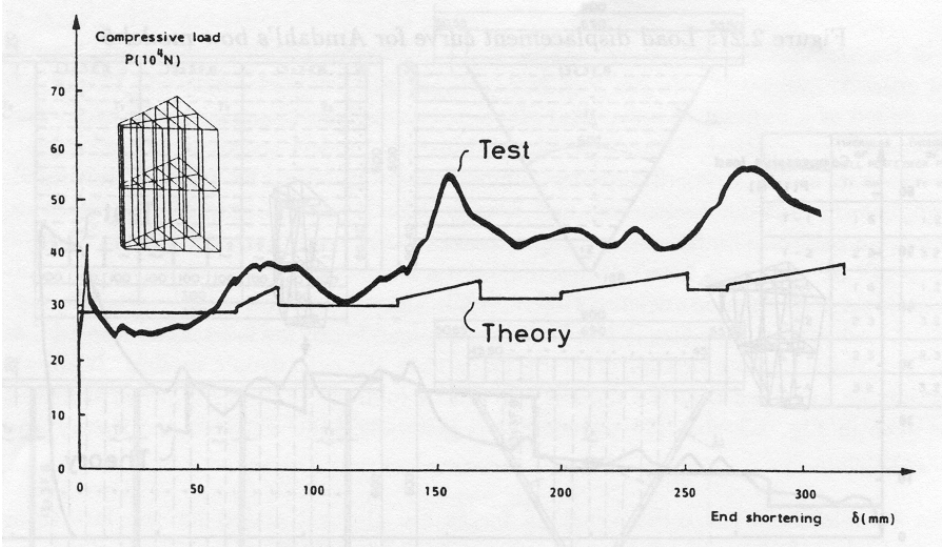

Figure 32c - Amdahl Bow Model Test Results Model #3 [37, 23]

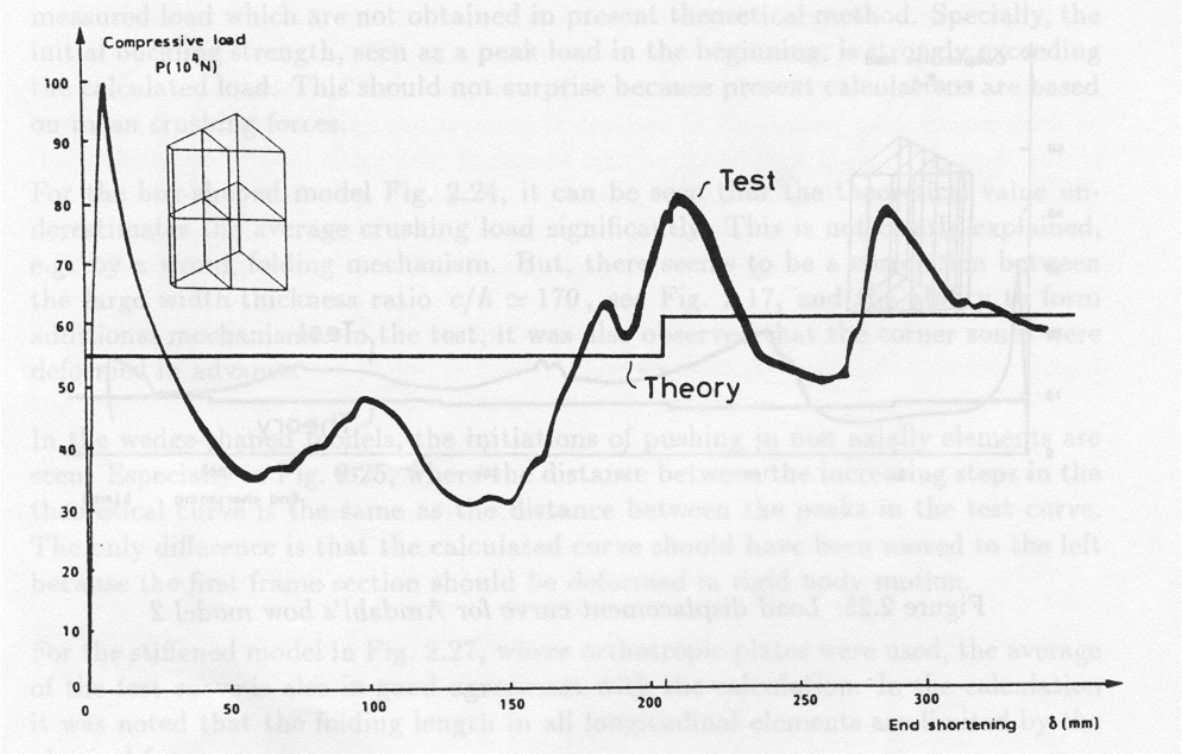

Figure 32d - Amdahl Bow Model Test Results Model #5 [37, 23]

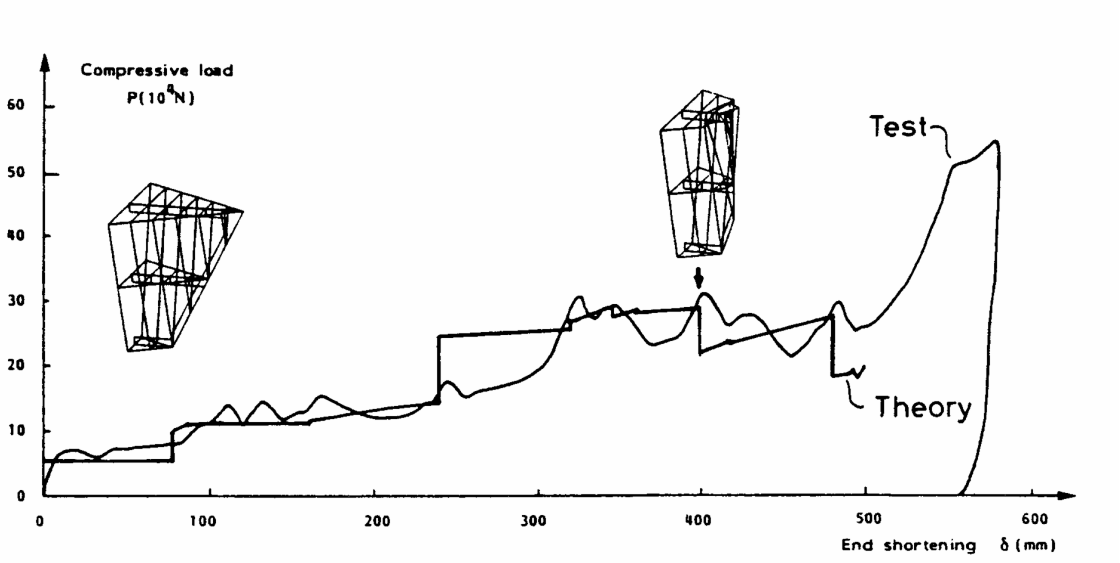

Figure 32e - Amdahl Bow Model Test Results Model #6 [37, 23]

4.4.3 Hagiwara

Hagiwara conducted a 1:5 scale model test of a 17000 dwt cargo ship bow with transverse framing shown in Figure 35 with Kierkegaard's finite element model. Test results are shown in Figure 36 with the results of Kierkegaard's analysis of the same structure [39, 37], discussed in Section 4.5.18.

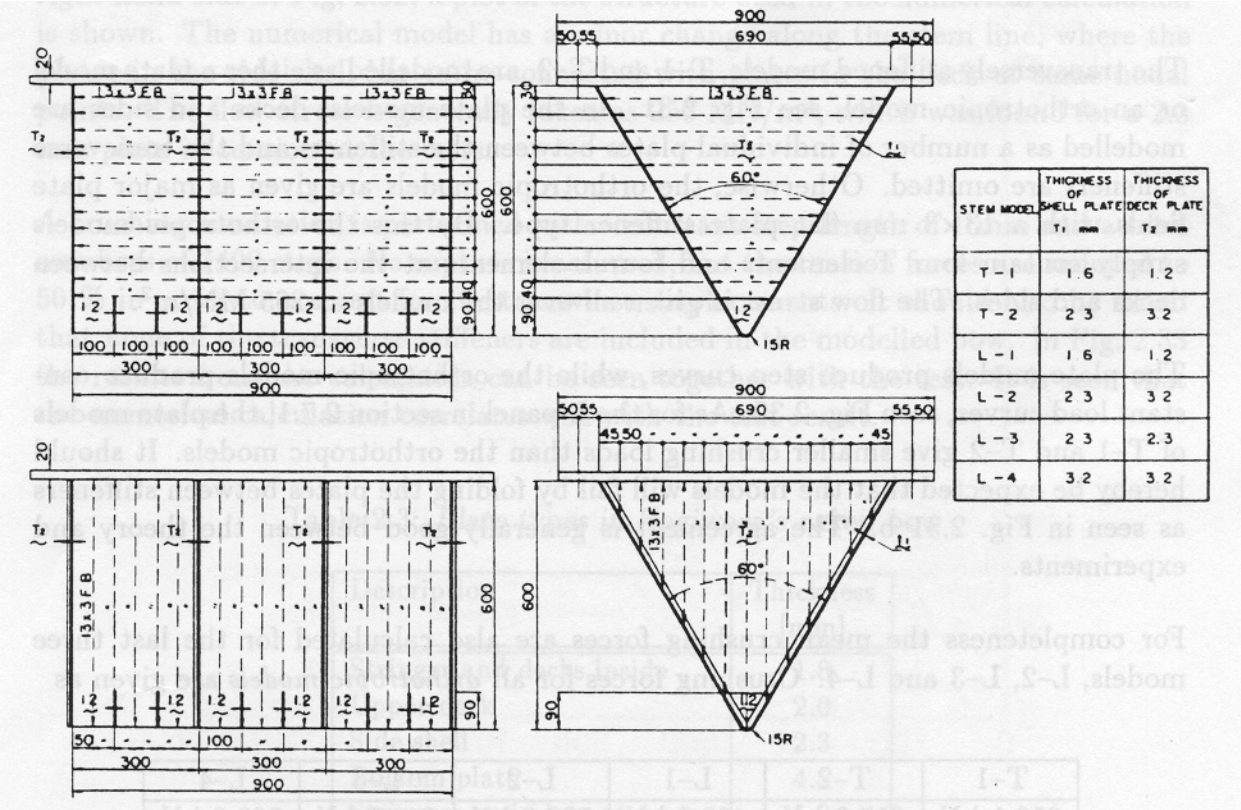

STEM MODEL	THICKNESS OF SHELL PLATE T_1 mm	THICKNESS OF DECK PLATE T_2 mm
T-1	1.6	1.2
T-2	2.3	3.2
L-1	1.6	1.2
L-2	2.3	3.2
L-3	2.3	2.3
L-4	3.2	3.2

Figure 33 - Kitamura and Akita Bow with Stem Models [37, 38]

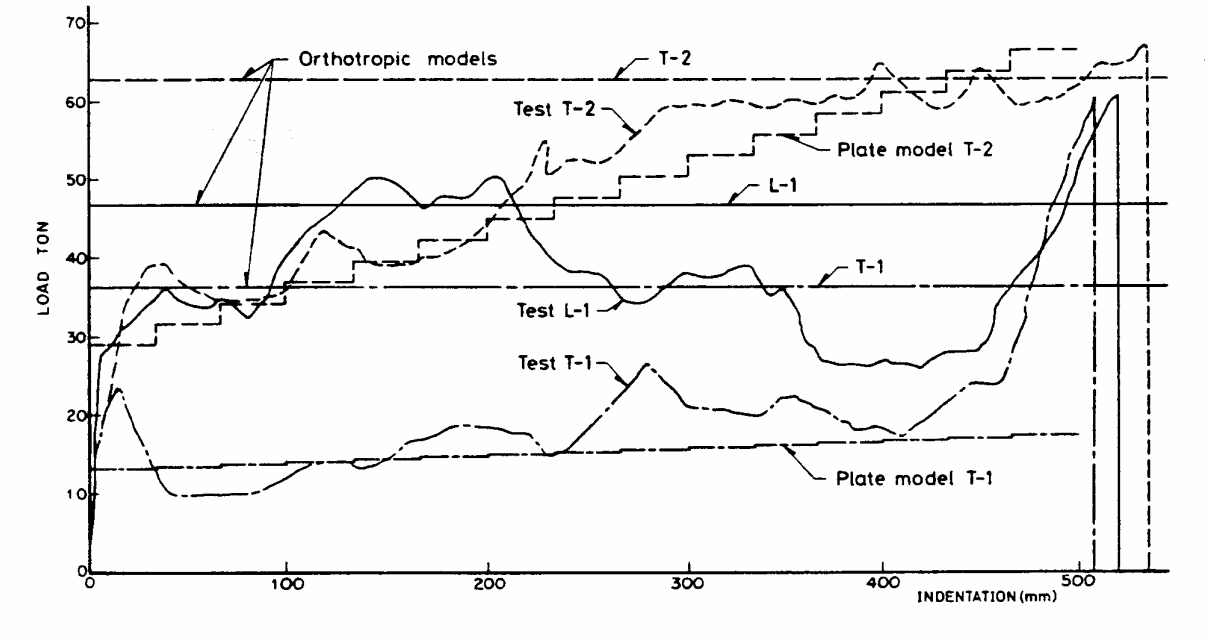

Figure 34 - Kitamura and Akita Bow with Stem Model Load/Indentation Results [37, 38]

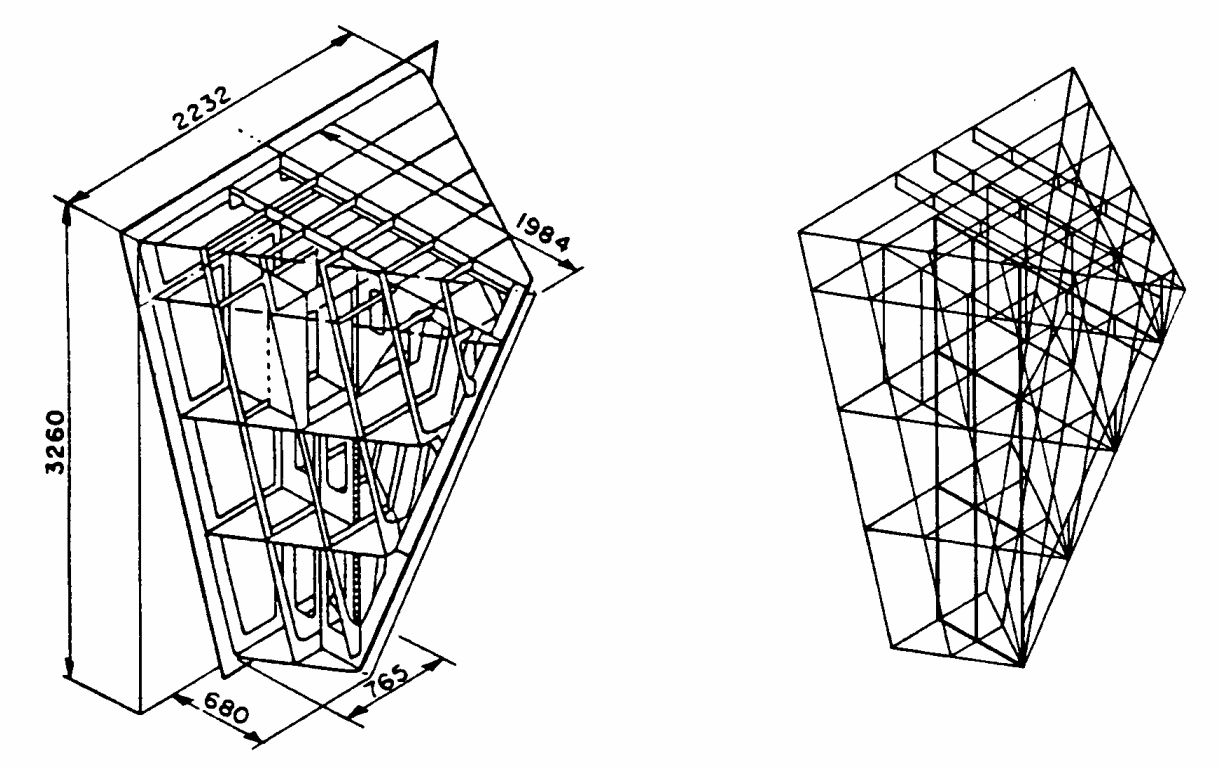

Figure 35 - Hagiwara Bow Test Model and Kierkegaard FEM [37, 39]

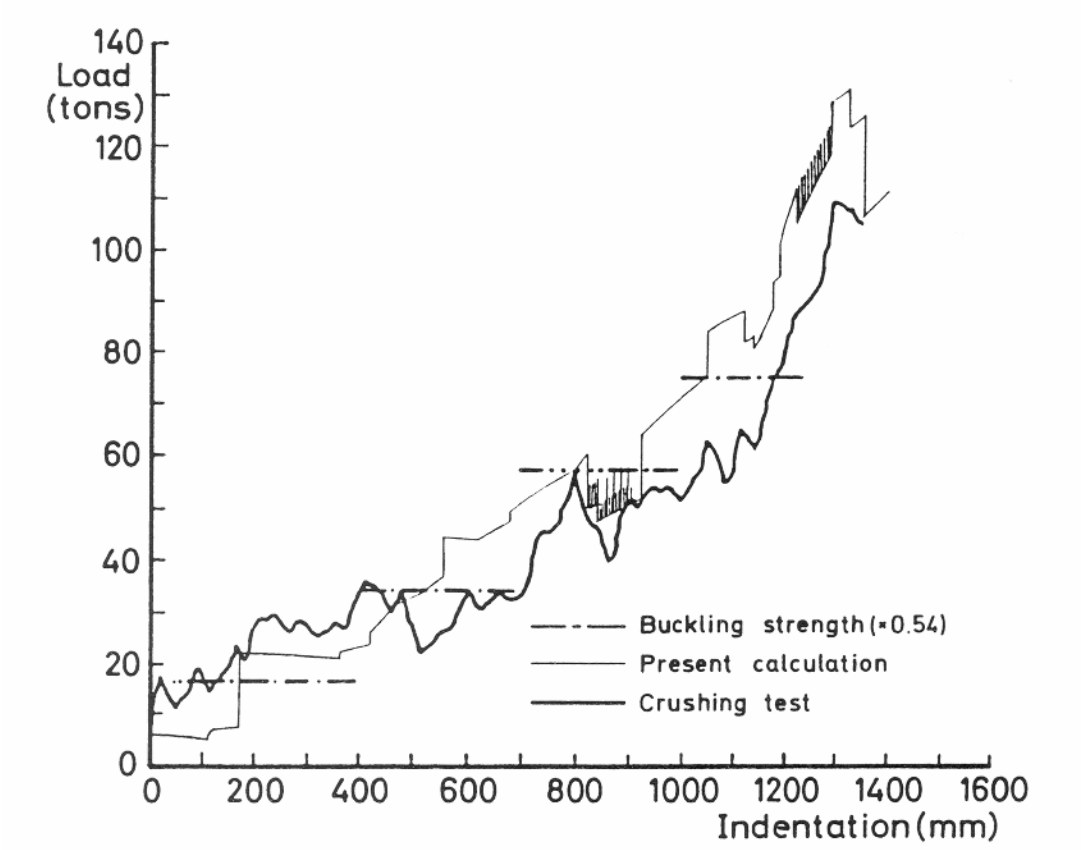

Figure 36 - Hagiwara Results with Kierkegaard Model Results [39,37]

4.5 Deformable Bow Models from Basic Principles

4.5.1 Kim and Gooding

Kim and Gooding consider the finite strength of the striking bow in the overall collision simulation [40,41,42]. Kim develops two simple structural models by identifying localized zones of plastic deformation from photographs of damaged ships (Figure 37). The bow structural members considered are the side shell and the decks. Transverse and longitudinal stiffeners are considered using a smearing technique. Five scale model tests are run and the force-deflection characteristics are recorded and compared showing good correlation. A model with inward folds (Model B) gives superior results compared to a model with outward folds (Model A).

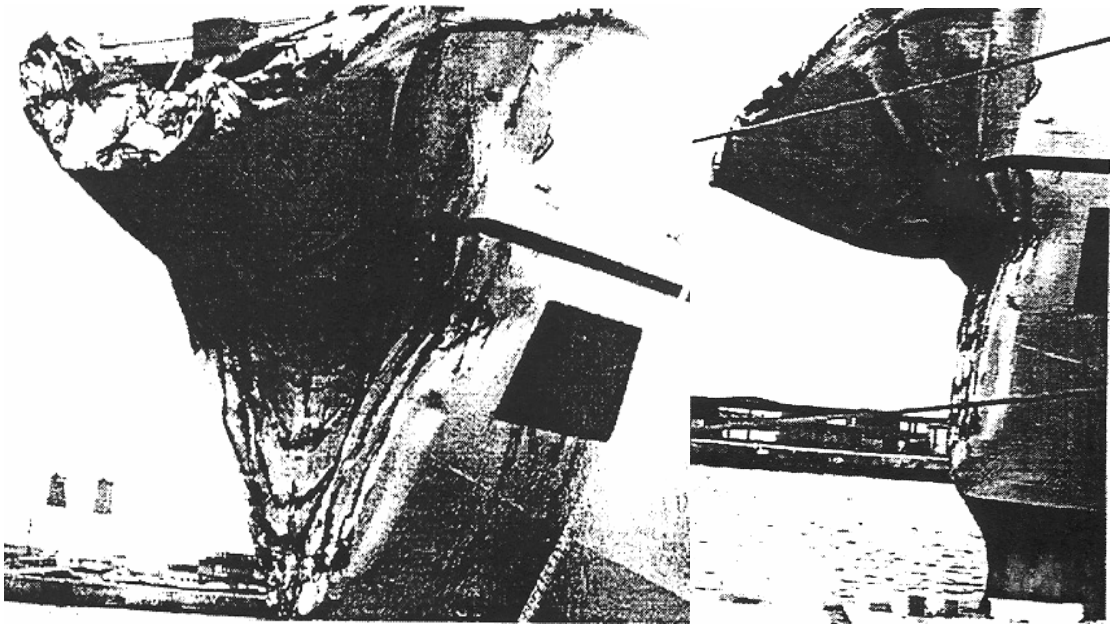

Figure 37 – Photographs of Actual Collision [40]

Since the bow has complex three-dimensional geometry, it is necessary to simplify the bow geometry. First, the contact point between the ship and the rigid obstacle is specified. It is observed from actual accidents and tests that the contact point divides the bow length in two parts with the same length and the vertical extension of the line from the end of the bow length to the deck plate gives the boundary of the deforming part of the bow. The bow model in this study is defined using three independent variables, bow length (l), bow angle (ϕ) and deck angle (θ). All edge lines in the bow are then defined in terms of these 3 parameters.

Photographs of the actual collision shown in Figure 37 show quite a complex deformation mode. However, by careful inspection, it is observed that there are four major internal energy dissipation areas, which are side shell folding, deck tilting, frontal bow stretching and side shell stretching. It is also noticed that one fold of the side shell of the bow matches one bend on the deck and the large stretching area from the contact point and small stretching area on the sides.

The mean crushing force for Model B is:

$$P_m = s_0(0.134lt + 6.28t^2) \tag{4.3}$$

where:

P_m - mean crushing force;
l - distance from the bow tip to the point of application of the load;
t - bow shell plate thickness (0.21mm and 1.2mm are the two values used in this study);

This model considers only the upper bow and not the bulb.

4.5.2 Gerard

Gerard developed a semi-empirical method for the estimation of crushing loads of bow structures based on the correlation of the results of a series of panel tests with various stiffener types [43].

This method is very conservative. It predicts loads that are approximately 50% higher than the experimental results. The maximum crushing strength σ_c, according to Gerard is given by the following equation:

$$s_c = s_0 b_g \left[\left(nt^2 / A \right) \sqrt{E / s_y} \right]^m \tag{4.4}$$

The total crushing load is then:

$$P_c = s_c A \tag{4.5}$$

where:

σ_y - yield stress;
σ_0 - compressive flow stress (incluses strain rate effects);
E - Young's Modulus;
β_g, m - coefficients depending on edge restraint. The values applied are for undistorted edges. β_g=0.56, m=0.85
n - sum of cuts and flanges for cross-section under consideration (Figure 38);
t - average thickness for the cross-section under consideration;
A - cross-sectional area

The strain rate is:

$$\dot{e} = v_x / s \tag{4.6}$$

where:

v_x - velocity in longitudinal direction during impact;
s - frame spacing

The magnitude of the dynamic flow stress is:

$$s_0(\dot{e}) = 1.29 s_{0_s} \dot{e}^{0.037} \tag{4.7}$$

where σ_{0s} is the static ultimate strength of the material.

The load formula given above predicts the maximum crushing load of plated structures within ± 10% of the experimental results. One of the major drawbacks of the model is that it has been derived from the crushing of fairly simple and regular plate constructions where the range of plating to stiffener thickness ratios and stiffener spacing are limited. Normal bow structures consist of a number of plate panels of different dimensions and stiffener sizes.

4.5.3 Amdahl

Amdahl developed a model using intersection elements, correlated against model test results [23,44,45]. Amdahl's method is a modified Wierzbicki [20] method, based on the energy dissipated during plastic deformation of basic structural elements such as angles, T-sections and cruciforms (Section 2.2.2.3). The total crushing load of a specific structure is obtained by adding up all the basic elements' crushing loads.

Amdahl's procedure, as simplified by Pedersen, provides the following equation for the average crushing strength [22]:

$$s_c = 2.42 s_0 [n_{AT} t^2 / A]^{0.67} [0.87 + 1.27 \frac{n_c + 0.31 n_T}{n_{AT}} (\frac{A}{(n_c + 0.31 n_T) t^2})^{0.25}]^{0.67} \quad (4.8)$$

The total crushing load is found by multiplying σ_c by the associated cross-sectional area of the deformed material:

$$P_c = \sigma_c A \quad (4.9)$$

where:

- σ_c - crushing strength of the bow;
- σ_0 - ultimate strength of steel (incl. strain rate effects);
- t - average thickness of the cross-section under consideration;
- A - cross-sectional area of the deformed steel material;
- n_c - number of cruciforms in the cross-section (Figure 38);
- n_T - number of T-sections in the cross-section (Figure 38);
- n_{AT} - number of angle- and T-sections in the cross-section (Figure 38)

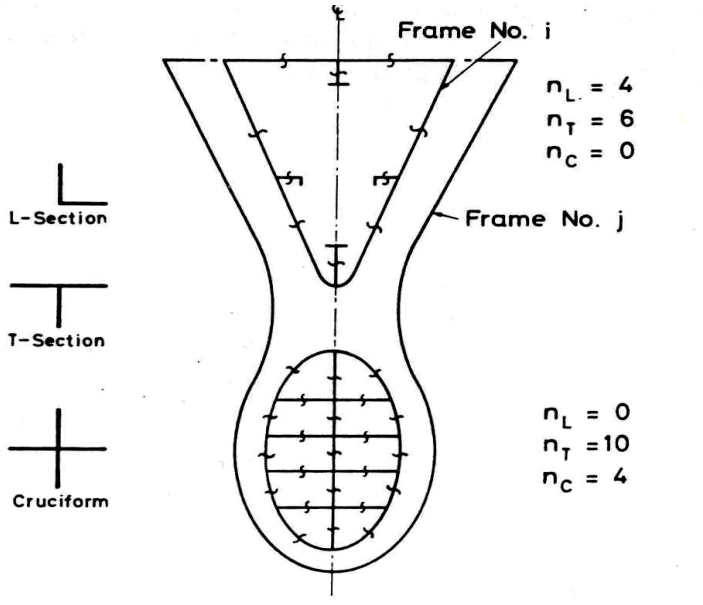

Figure 38 - Method of cross-sections to determine the number of intersections [22]

4.5.4 Yang and Caldwell

Yang and Caldwell also model the bow section as an assembly of basic elements, as shown in Figure 38, using a modified Wierzbicki method [20].

The mean crushing force P_m is the sum of the minimum energy results for all elements contacted in the bow:

$$P_m = 1.178 s_0 / H \sum^{n_T} b_i t_i^2 + 0.215 s_0 H \sum^{n_A+n_T} t_i + 6.935 s_0 \sum^{n_A+n_T} t_i^2 + 0.265 s_0 H \sum^{n_T} t_i$$

$$+ 0.589 s_0 \sum^{n_T} t_i^2 + 0.75 s_0 H \sum^{n_C} \sum^{4} t_i + 0.375 s_0 \sum^{n_C} \sum^{4} t_i^2 \qquad (4.10)$$

where:

P_m	-	mean crushing load of the structure;
σ_0	-	flow stress based on the mean value of yield and ultimate stress;
b_i	-	width of the ith plate flange;
t_I	-	thickness of the ith plate flange;
H	-	folding length of the distorted plate flanges;
n_c	-	number of cruciforms in the cross-section (Figure 38);
n_T	-	number of T-sections in the cross-section (Figure 38);
n_{AT}	-	number of angle- and T-sections in the cross-section (Figure 38);
n_f	-	number of flanges of angles, T-sections and cruciforms

The theory is applied to a tanker collision with a concrete bridge pier. In the results of the analysis, the mean crushing strength of the bow structure exceeds test results by 10%. Figure 39 shows Pedersen's comparison of force-penetration curves developed using Gerard's, Amdahl's and Yang and Caldwell's methods [22].

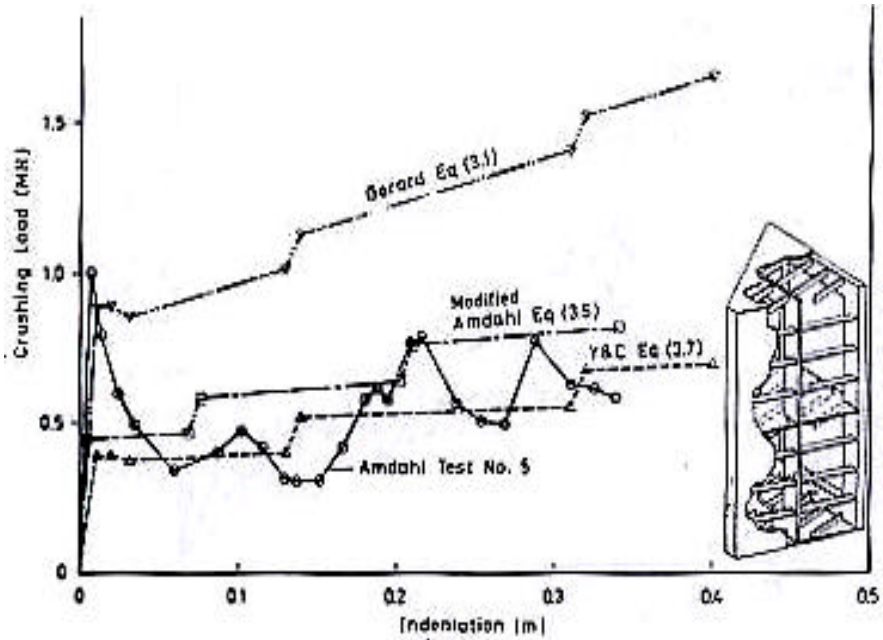

Figure 39 – Comparison of Gerard's, Amdahl's and Yang and Caldwell's Results [22]

As can be seen in Figure 39, Gerard's results are conservative and predict 50% higher loads as compared to Amdahl's and Yang and Caldwell's results for larger penetrations. For small penetrations, Gerard's results agree well with Amdahl's results.

4.5.5 Pedersen

Pedersen presents a method for estimating the collision forces between conventional merchant vessels and large volume offshore structures [22]. The main emphasis is on impact loads on fixed offshore structures due to bow collisions. The crushing loads are determined as a function of vessel size, vessel speed, bow profile, collision angles and eccentric impacts. Pedersen discusses the various methods and theories for calculating crush loads during collisions, including Amdahl, Gerard and Yang and Caldwell. He applies these methods to six different ships in order to compare and validate the theories.

After a series of numerical calculations simulating model tests, Pedersen concludes that Gerard's results are approximately 50% higher than the experimental results as shown in Figure 39. Amdahl, and Yang and Caldwell provide similar results with Amdahl being somewhat more conservative.

Six different ships are considered in a series of calculations using the Amdahl and Yang and Caldwell equations: 1) 150,000 dwt Bulk Carrier; 2) 40,000 dwt containership; 3) 3000 dwt general cargo vessel; 4) 2000 dwt tanker; 5) 1000 dwt pallet carrier; and 6) 500 dwt coaster. All these ships have bulbous bows.

Figure 40 shows the calculated crushing load-indentation curves using Amdahl's modified method and Yang and Caldwell's method for the 150,000 dwt bulk vessel in a fully loaded condition, striking head-on with a rigid wall at an initial impact speed of 18 knots. Similar results are obtained for the 40,000 dwt container vessel for a head-on collision with a rigid wall at a speed of 12.9 m/s.

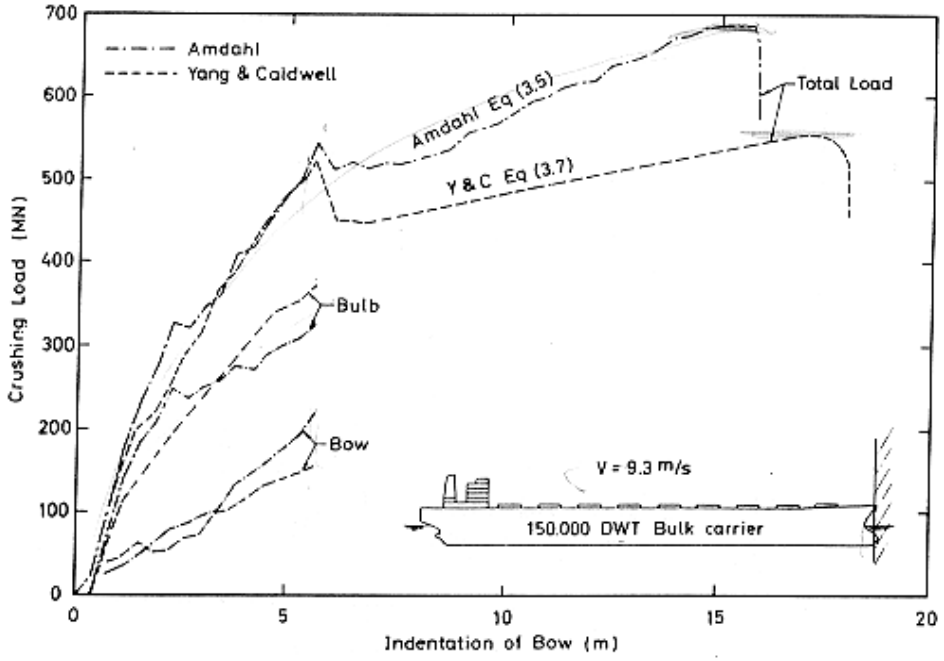

Figure 40 – Force-indentation curves for 150,000 dwt Bulk Ship [22]

In Figure 40, the force-penetration curve is uncoupled into two curves – one for the upper bow and the other for the bulb. The overall force curve represents a sum of the bow and bulb forces. Pedersen suggests that the force-penetration curve can be approximated using a sine curve, the peak of which represents the maximum bow crushing force and the quarter period is the impact duration as given in Equation (4.12) and Equation (4.13).

Based on these six ships, an empirical expression is derived to estimate maximum bow collision load, as a function of strain rate, impact velocity, vessel displacement and vessel length. For a vessel between 500 dwt and 300,000 dwt the crushing load is given by:

$$\begin{aligned} P_{bow} &= P_0 \bar{L}[\bar{E}_{imp} + (5.0 - \bar{L})\bar{L}^{1.6}]^{0.5} \quad \text{for} \quad \bar{E}_{imp} \geq \bar{L}^{2.6} \\ P_{bow} &= 2.24 P_0 [\bar{E}_{imp} \bar{L}]^{0.5} \quad \text{for} \quad \bar{E}_{imp} < \bar{L}^{2.6} \end{aligned} \tag{4.11}$$

where:

$\bar{L}$ = L_{pp}/275 m;

$\bar{E}_{imp}$ = E_{imp}/1425 MN and E_{imp} = ½ m_x V^2_0; and:

P_{bow} - maximum collision load in MN;
P_o - reference collision load equal to 210 MN;
E_{imp} - energy to be absorbed by plastic deformations;
L_{pp} - length of the vessel (m);
m_x - mass plus added mass (5%) w.r.t longitudinal position (10^6 kg);
V_o - initial speed of the vessel in ms^{-1}

The maximum indentation S_{max} is:

$$S_{\max} = \frac{p}{2}\frac{E_{imp}}{P_{bow}} \tag{4.12}$$

and the associated impact duration is:

$$T_0 \approx 1.67 \frac{S_{\max}}{V_0} \tag{4.13}$$

Table 3 - Pedersen Collision Data [22]

Vessel size	500 DWT	1000 DWT	2000 DWT	3000 DWT	270,000† DWT
L_{pp} (m)	41.00	53.80	69.00	78.00	330.7
B_m (m)	9.00	11.00	12.30	16.00	51.80
D (m)	6.40	6.70	8.60	10.50	27.60
Mass (10^3 kg)	886	1650	3020	4600	312.384
V_0 ($m\,s^{-1}$)	5.0	5.5	7.0	7.5	7.5
P_{bow} Eqn (3.10) (MN)	15.3 (21)‡	25.0 (24)‡	39.9 (32)‡	50.7 (72)‡	859.2 (900)‡
s_{max} Eqn (3.12) (m)	1.19 (1.1)‡	1.64 (2.0)‡	3.06 (3.3)‡	4.21 (3.6)‡	16.82 (17.00)‡
T_0 Eqn (3.13) (s)	0.40 (0.35)‡	0.50 (0.67)‡	0.73 (0.85)‡	0.94 (0.93)‡	3.76 (4.0)‡
P_{bow} W–G Eqn (3.14) (MN)	19.7	27.8	39.4	48.2	457.3
P_{bow} US-Guide Eqn (3.15) (MN)	13.4	20.9	37.6	49.3	467.7

Table 3, Table 4 and Table 5 list bow collision load results for seven different vessels based on the Pedersen empirical equations provided above. The collision loads in the tables vary between 20 and 900 MN, which is a variation caused by the variation of vessel size and impact energy.

Table 4 - Pedersen Collision Data for 150000 dwt Bulk Carrier [22]

Vessel size	150,000 DWT			
L_{pp} (m)	274.0			
B_m (m)	47.0			
D (m)	21.6			
Mass (10^3 kg)	174,900			
V_0 (m s^{-1})	9.3	7.7	5.2	2.6
P_{bow} Eqn (3.10)	646.7	584.4	500.5	309.9
(MN)	(570–680)†	{514}‡	{462}‡	{270}‡
s_{max} Eqn (3.12)	19.3	14.6	7.8	3.2
(m)	(16–18)†	{14.6}‡	{8.4}‡	{3.8}‡
T_0 Eqn (3.13)	3.46	3.17	2.50	2.2
(s)	(3.0–3.5)†	{3.35}‡	{2.79}‡	{2.41}‡
P_{bow} S–S Eqn (3.14) (MN)	340.8	—	—	—
P_{bow} US-Guide Eqn (3.15) (MN)	432.2	357.9	241.7	120.8

Table 5 - Pedersen Collision Data for 40000 dwt Container Ship [22]

Vessel size	40,000 DWT		
L_{pp} (m)	211.5		
B_m (m)	32.2		
D (m)	21.0		
Mass (10^3 kg)	54,000		
V_0 (m s^{-1})	12.9	9.3	5.2
P_{bow} Eqn (3.10)	398.6	342.6	294.2
(MN)	(350–450)†	{345}‡	{224}‡
s_{max} Eqn (3.12)	18.6	11.2	4.1
(m)	(15–19)†	{10.5}‡	{5.2}‡
T_0 Eqn (3.13)	2.41	2.02	1.31
(s)	(2.0–2.6)†	{1.95}‡	{1.72}‡
P_{bow} S–S Eqn (3.14) (MN)	176.0	—	—
P_{bow} US-Guide Eqn (3.15) (MN)	309.6	223.2	124.8

The empirical equations are also used to obtain plots of bow crushing force, crushing distance and collision duration as functions of ship size and velocity, as seen in Figure 41, Figure 42 and Figure 43.

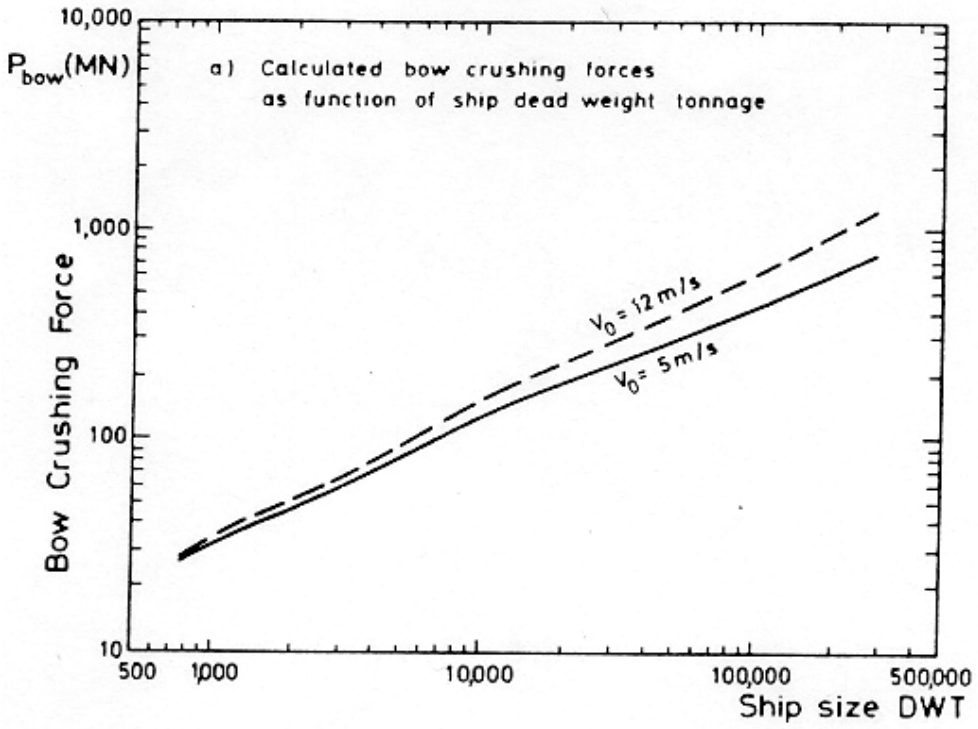

Figure 41 – F vs. dwt for different speeds [22]

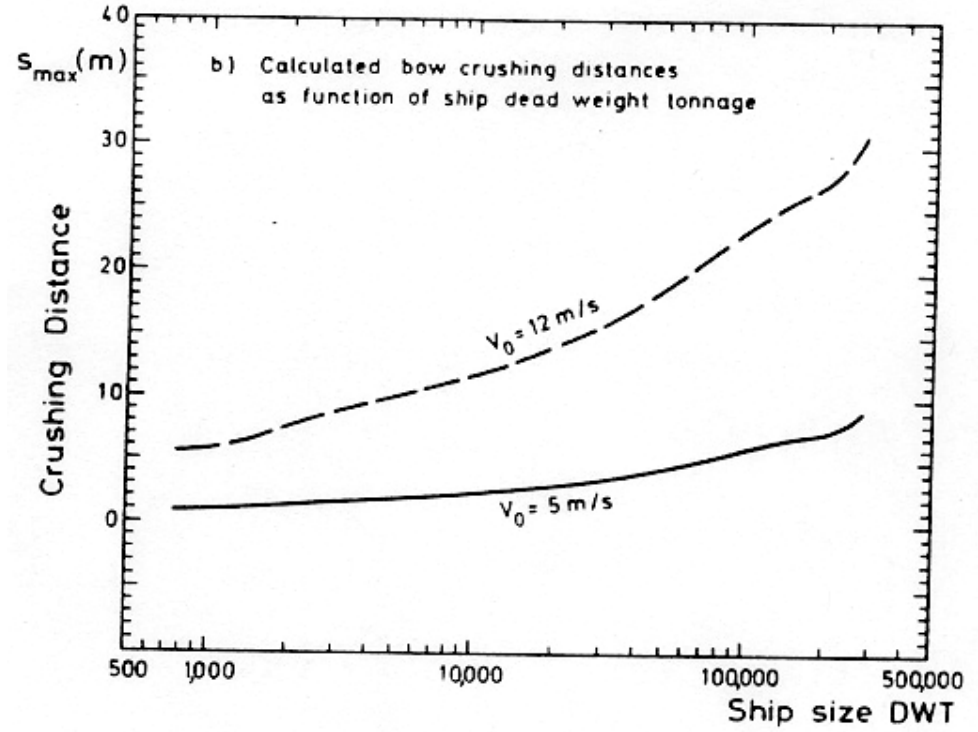

Figure 42 – Crushing distance vs. dwt for different speeds [22]

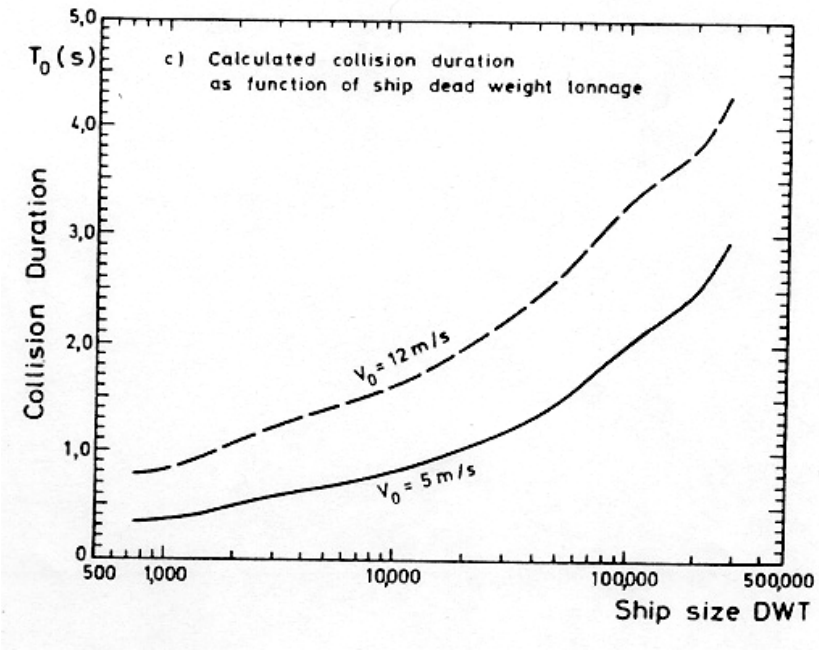

Figure 43 - Collision duration vs. dwt for different speeds [22]

4.5.6 Transversely-Stiffened Bow Model

Lehmann and Yu provide a model specifically developed for transversely-stiffened bows [46]. Their method is based on crushing of conical shell structures. The shell plating of a transversely-stiffened bulb or bow is modeled as a series of short conical shells with different cone angles. The average crushing load for each cone is:

$$F_C = 2.09 s_0 t^2 \left(\frac{2pR_i}{L} + \frac{L}{t} + p + 2j \right) \tan j + 1 \qquad (4.14)$$

where:

σ_0	-	material ultimate strength
t	-	plate thickness
L	-	frame spacing
R_i	-	effective radius
φ	-	conic angle

Internal element intersections are treated using the Amdahl formula, Equation 4.8.

4.5.7 Lutzen., Simonsen, and Pedersen

Lutzen., Simonsen, and Pedersen divide the bow used in their study into two parts, a conventional bow and a bulb [47]. Variables describing the bow (shown in Figure 44) are:

j	-	stem angle
B	-	ship breadth
H_{deck}	-	uppermost deck height
B_d,B_b	-	deck and bottom coefficients

The horizontal shape of the deck and bottom is assumed to be parabolic. The bulb is assumed to have the form of an elliptic parabola.

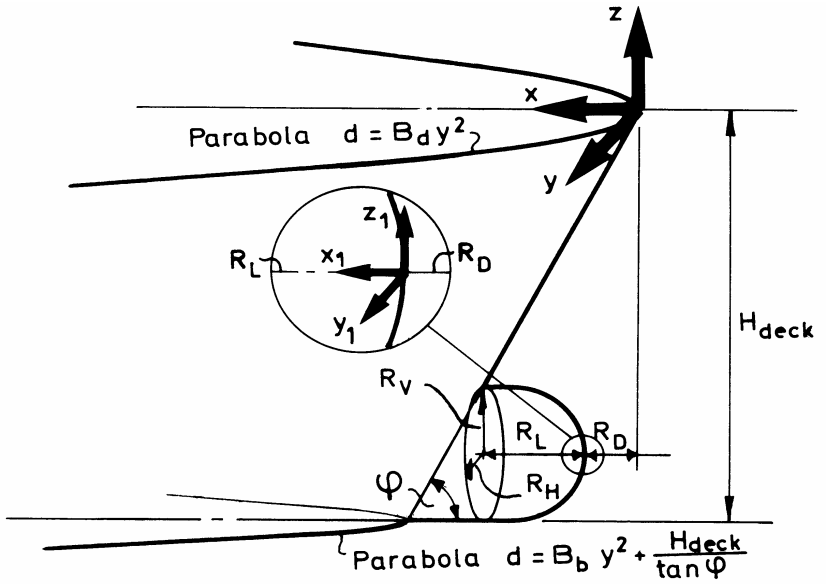

Figure 44 - DTU Bow Model [47]

Longitudinally-stiffened bow stiffness is modeled based a modification of Amdahl's method [22], Equation (4.2). Transversely-stiffened bow stiffness is based on Lehmann and Yu, Equation (4.14). The total crushing load is found by multiplying the associated cross-sectional area of the deformed steel material. Crushing load results for a transversely-stiffened 51800 dwt bulk carrier are shown in Figure 45 where the plot Eq. 1 uses Amdahl's method and Eq. 2 uses Lehmann and Yu. Although the results appear similar, they are different in initial stiffness (less than 1 meter deformation) where Lehmann and Yu predict much lower stiffness consistent with transverse stiffeners. Lehmann and Yu is the preferred method for transversely-stiffened bows.

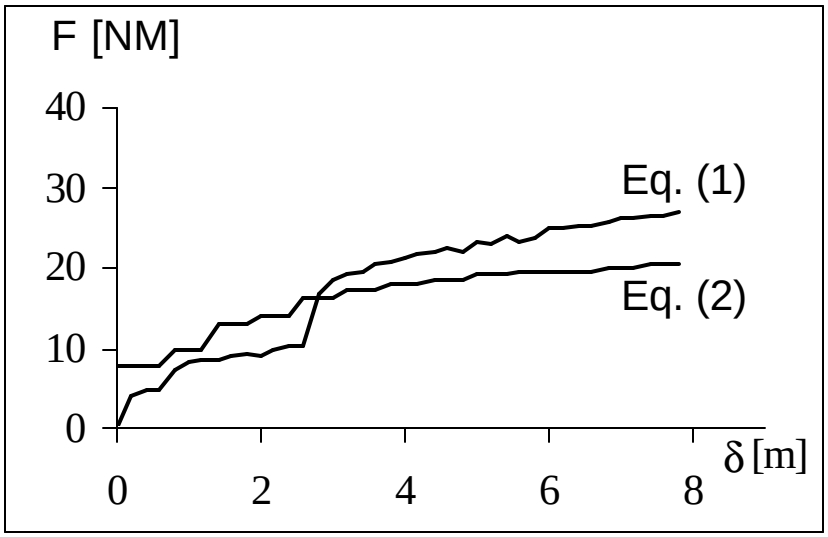

Figure 45 - Crushing Load Results for 51800 dwt Bulk Carrier [47]

Figure 46 compares the force-deformation curves for a 40000 dwt Container Vessel (longitudinally stiffened) and a 51800 dwt Bulk Carrier (transversely stiffened), both calculated using Amdahl's method. The significant difference in stiffness for large deformations is very obvious in this figure.

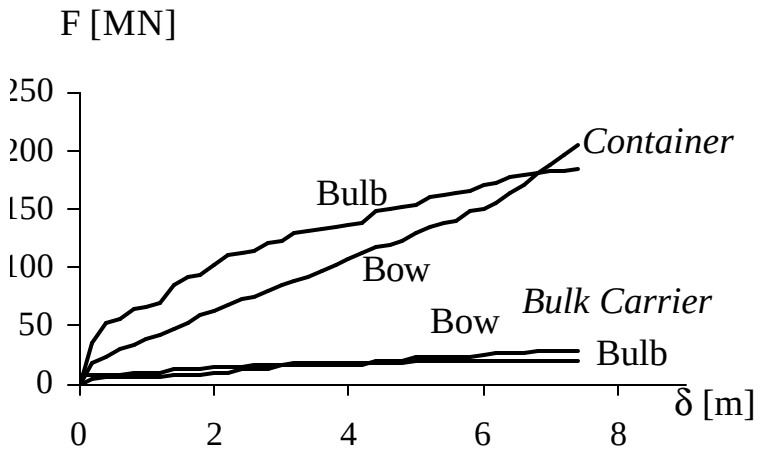

Figure 46 - Force-Deflection Comparing Longitudinally and Transversely- Stiffened Bows [47]

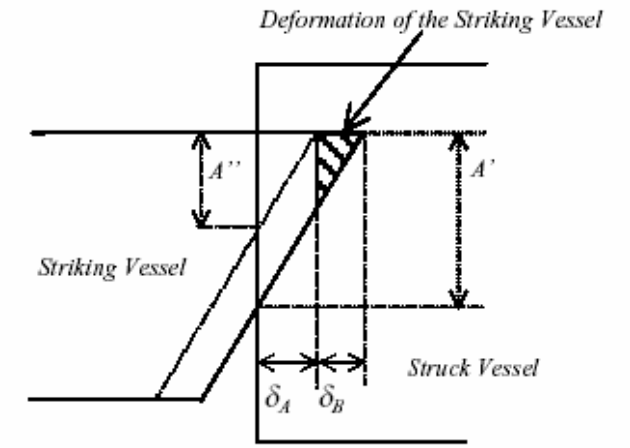

Figure 47 - DTU Model Ship Collision Interaction [47]

The analysis is carried out in penetration steps as shown in Figure 47. Only one of the striking or struck ships can be deformed in each step. By comparing the crushing forces for the bow and the side, it is determined which vessel deforms during the step. The following calculations are performed:

1. Force-Penetration curve $F_{struck}(d_A)$ for the struck vessel, where the striking vessel is rigid.
2. Force-Penetration curve $F_{striking}(d_B)$ for the striking vessel, where the struck vessel is rigid.

Their interaction is taken into account by comparing the forces F_A and F_B, which are determined as follows:

Struck vessel: $$F_A = F_{Struck}(d_A)\frac{A'}{A''} \tag{4.15}$$

Striking vessel: $$F_B = F_{Striking}(d_A + d_B)$$

where:

F_A	-	force to crush the struck vessel
F_B	-	force to crush the striking vessel
F_{struck}	-	force from force-penetration curve for struck vessel; striking vessel rigid
$F_{striking}$	-	force from force-penetration curve for striking vessel; struck vessel rigid
d_A	-	penetration into the struck vessel
d_B	-	deformation of the striking vessel
A'	-	cross-sectional area of striking vessel at a distance d_A+d_B from bow tip
A''	-	cross-sectional area of striking vessel at a distance d_A from bow tip

The forces on the struck and the striking vessel F_A and F_B are compared:

- If $F_A > F_B$ - Deformation of the striking vessel, d_B is increased
- If $F_B > F_A$ - Deformation of struck vessel, d_A is increased

This method was applied to a range of ships listed in Table 6. All striking ships in this analysis have longitudinally-stiffened bows. It can be seen that the bows of the smaller striking ships are much less stiff than the sides of the larger struck ships. Bow damage is most important in these cases. In large ship striking large ship collisions, bows are virtually rigid and side damage dominates. This indicates that bow stiffness increases with ship size, consistent with Equation (4.11).

Table 6 - Percent of Total Absorbed Energy Dissipated in the Bow [47]

Striking Vessel / Struck Vessel	Bulk Carrier 150,000 DWT	Container Vessel 40,000 DWT	General Cargo 3,000 DWT	Tanker 2,000 DWT	Coaster 500 DWT
Tanker L = 103m	0	0	0	24	97
Tanker L=198m	0	0	36	95	89
Tanker L=317m	0	0	52	99	94
RoRo L=58m	0	0	0	98	91
RoRo L=150m	0	0	20	48	82
RoRo L=180m	0	0	0.4	46	86

4.5.8 Kierkegaard

Kierkegaard also develops a mathematical model for force-indentation relations for high-energy collisions involving bow structures based on Wierzbicki [37,48,20]. Stiffened plates are included explicitly in the crushing mechanism. The crushing force is calculated in a simple time simulation, where the strain rate effect on flow stress is also included. The structure is crushed from the front and the simulation procedure is able to handle rigid body motions of crushed and non-crushed structure. In complex ship bow structures, the crushing mechanisms are not fully compatible as the common folding length in each transverse section could result in an unrealistically high collision force when stiffeners are involved. The mechanisms for the basic elements are extended to apply to a complex bow structure. This method is applied and compared to crushing tests of bow models given in the literature by Arita [49], Amdahl [23] and Hagiwara [39].

Hagiwara's test model is a 1/5-scale bow of a 17,000 dwt cargo ship, which is typical of a small ship having transverse framing. For simplicity of fabrication, Kierkegaard's model omits some of the inner structural members, as seen in Figure 35. The flow stress is taken to be 250 MN/m^2 and the quasi-static crushing is simulated using a constant speed $V_0 = 10^{-4}$ m/s as in the test. The simulation is done in 1400 steps. The calculated results shown in Figure 36 agree very well with the test results.

4.6 Deformable Bows in Finite Element Analysis

4.6.1 Valsgard and Pettersen

Valsgard and Pettersen's collision damage calculation considers the vertical variation in the stiffness of the striking bow [50]. A bulbous bow is modeled. Bow stiffness is represented as a set of non-linear springs (Figure 48) evaluated using a semi-empirical approach.

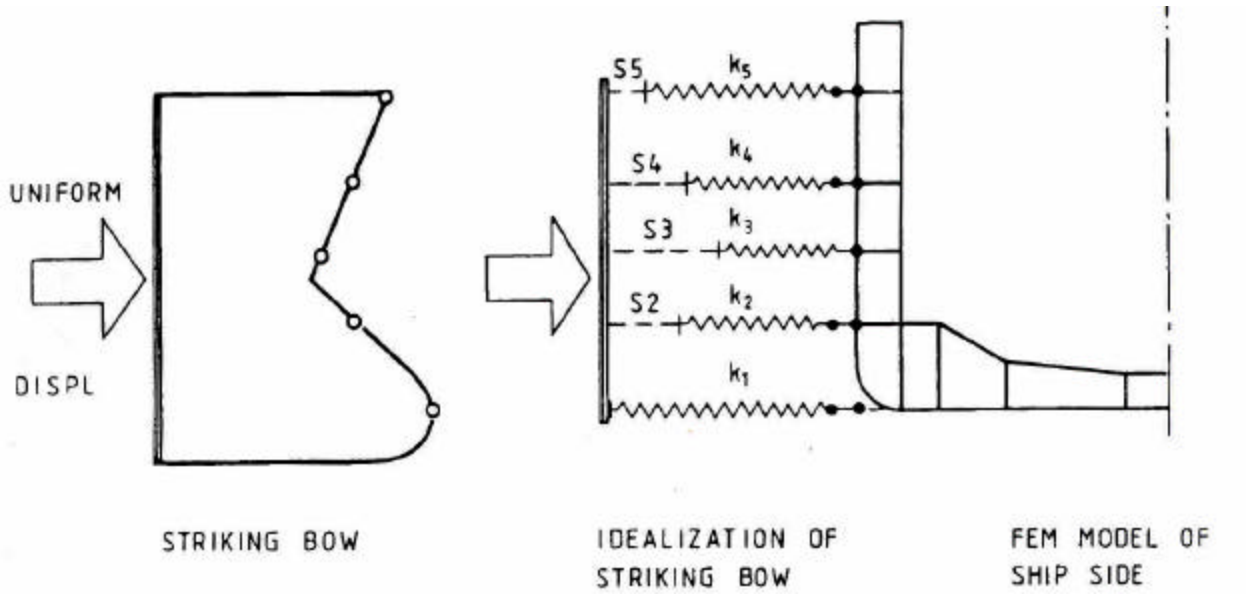

Figure 48 - Idealization of striking bow by a set of non-linear springs [50]

The struck ship has zero speed before the collision. After the collision, both ships have a common speed, as determined by conservation of momentum. It is a right angle collision with one degree of freedom only. The impact energy is absorbed by both the side and the bow structures. The calculated stiffness characteristics (load vs. indentation) are used in determining the damage and energy absorption in each part. Various longitudinal striking positions and striking speeds are investigated.

The striking bow is simulated by a set of non-linear springs (k1-k5) with associated slacks (S2-S5) which represent the geometrical bow form. These springs are attached to the nodes in the ship's side in which the stiffness characteristics are determined by a nonlinear simplified FE procedure. In this way the relative damage and energy absorption of the side and the bow are determined. The results depend on the relative stiffness of the bow and for this reason, results for two different bow stiffnesses are calculated in this study.

The spring constants of the bow are represented as discrete linear functions of force-deformation values supplied as input to the computer program. Non-linear bow springs for the striking bow were modeled by Bach-Gansmo and Valsgard [51] for 10 vertical levels in the ship bow. These springs are established by using a combination of crippling loads determined from Gerard's test [22] and elastic buckling loads. The load-deformation behavior of the structural elements in the bow is then constructed as proposed by Chang et.al. [52], as shown in Figure 49. The relative stiffness of the ship's side and the bow determines which structure suffers the most damage in a collision.

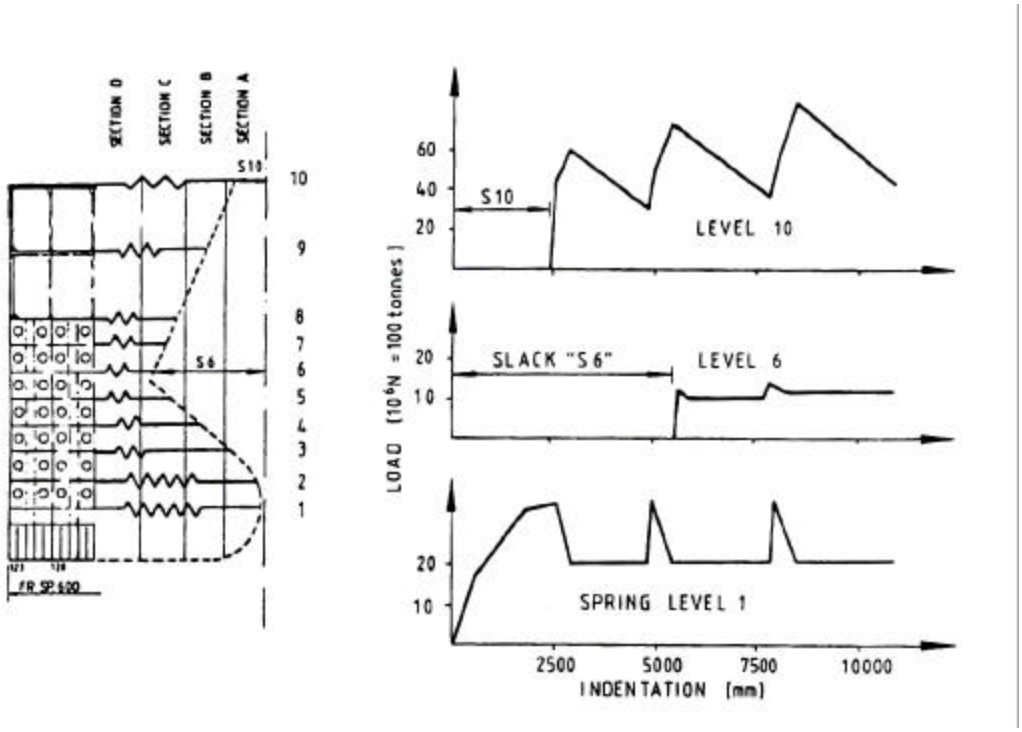

Figure 49- Approximation of bow stiffness with non-linear springs [50]

The results show that the bow of the striking ship in this case absorbs about 55% of the total energy, as compared to 15% when the stiffness of the striking ship's bow is assumed to be ten times the actual stiffness.

4.7 Bow Summary

Table 7 summarizes the various bow models described in the sections above.

Table 7 – Comparison of important features of various bow models

Model	Rigid	Deformable	Closed-Form Equation	FE-Based	Empirical	Intersection Elements	Bow Infinite Wedge
Minorsky [9]		✓	✓		✓		
Hutchison [12]	✓						✓
Ito [27]	✓		✓		✓		
Wierzbicki [20]	✓		✓			✓	
Simonsen [10]	✓			✓	✓	✓	
SIMCOL 0.1 – 2.0 [35]	✓						✓
SIMCOL 2.1 [35]	✓						
Woisin [17]		✓			✓		
Kim [40]		✓	✓		✓		
Gerard [43]		✓	✓			✓	
Amdahl [44,45]		✓	✓			✓	
Kierkegaard [48]		✓		✓	✓	✓	
Kitamura and Akita [38]		✓			✓		
Hagawara [39]		✓			✓		
Yang and Caldwell [24]		✓	✓			✓	
Pedersen [22]		✓	✓				
Lutzen et. al. [47]		✓	✓			✓	
Valsgard, Pettersen [50]		✓		✓		✓	

4.8 Bow Hypothesis

An objective of this study is to identify a simple, but sufficient bow model for use in SIMCOL. Vakkalanka made the following hypothesis and set out to prove it using existing research, actual collision data, and finite element analysis [55]:

> "The almost universal assumption of a rigid striking ship bow in ship collision analysis is not valid. Differences in striking ship bow stiffness, draft, bow height and shape have an important influence on the allocation of absorbed energy between striking and struck ships and the extent of damage in the struck ship. The energy absorbed by the striking ship can be significant and varies in different collision scenarios."

Xia [56] and Sajdak have continued this work.

The reanalysis of Minorsky's results in Table 2 shows that the percentage of energy absorbed by the striking ship in real collision cases is significant and is not constant. Using finite element analysis, Valsgard and Pettersen modeled a collision with a double hull struck ship and deformable striking bow that absorbed 55% of the total absorbed energy. After increasing the bow stiffness to ten times the estimated value, the bow still absorbed 15% of the total absorbed energy. Using closed-form equations for bow stiffness, Lutzen., Simonsen, and Pedersen [47] show that bow energy absorption for a large striking ship with a longitudinally-stiffened bow is small. Bow energy absorption for smaller striking ships and for striking ships with transversely-stiffened bows is significant and variable.

SIMCOL 2.1 assumes a rigid wedge-shaped bow. This is very advantageous for probabilistic analysis because of its simplicity and single variable (bow angle). However, based on the above, this is not an adequate assumption for large (150K dwt) struck ships. Most of the ships in the worldwide striking ship population are much smaller and their bows will deform on impact with a large ship. The bow absorbed energy is also not a constant fraction of the total so it cannot be subtracted a priori. The upper bow behaves very differently than the bulb in collision and may be raked.

4.9 Future SIMCOL Bow Recommendation

Based the above citations and analysis, the simple SIMCOL bow model must be modified to consider the most important characteristics of striking ship bows encountered in the worldwide ship population. This must be done with care to minimize unnecessary complexity. In the next version of SIMCOL (3.0), the following changes to the bow model will be implemented:

- The bow geometry will be modeled using an upper and lower wedge. The upper wedge may be raked and will model only the upper bow. The lower wedge will not be raked and will model the bulb. Each may have different bow angles.
- The upper and lower wedges will be deformable, each with a different stiffness or force/deflection relationship. Section 5.5 provides some preliminary bow analysis modeling comparing the Amdahl and Yang and Caldwell equation results to LSDYNA results. It is anticipated that similar analysis will be performed for a range of longitudinally stiffened and transversely stiffened striking ship bows (3K-150K dwt). The

force/deflection relationships for these bows colliding with a rigid wall will be analyzed and a simplified stiffness model will be developed.

- In a given time step, the deformation to accommodate the external motion will be applied separately to the struck and striking ship in a pre-calculation. The ship that deforms with the lowest absorbed energy will deform in the time step. The other will not deform.
- It will be assumed that the shape of the striking ship bow does not change although its absorbed energy will be calculated assuming it does. A contact area adjustment method similar to Equation (4.15) will be used to compensate for this simplifying assumption.

CHAPTER 5 Finite Element Modeling of Ship Collisions

Finite element modeling of ship collisions cannot be performed with confidence without significant research, experimentation and validation of modeling techniques, element and material models, and careful model parameter value selection. The casual and undisciplined application of commercial software may produce impressive pictures, but be entirely wrong. The open literature and even detailed technical reports on the subject do not provide sufficient detail, analysis and validation to reproduce or defend many analyses. "Calibration" of model parameters to one or two validation cases does not insure accuracy for other analyses. Simply stated, you can make a finite element analysis tell you whatever you want with pretty pictures to defend its accuracy.

This Chapter provides a structured approach to determine valid modeling techniques, element and material models, and model parameter values for modeling ship collisions using LSDYNA. LSDYNA is a general-purpose, explicit finite element program used to analyze the nonlinear dynamic response of three-dimensional inelastic structures. It has fully automated contact analysis capability and error-checking features [30,31,32]. It was developed primarily for automotive collision applications, but can also be used for ship to ship collisions. It performs a fully dynamic analysis, not quasi-static. Crash behavior has large displacements, and is very non-linear with multiple point contact and rupture. Explicit time integration is best for these problems. The use of small time-steps is required for stability, but explicit integration does not require inversion of a large stiffness matrix as is required with implicit methods. Explicit integration also allows discontinuous failure criteria such as rupture strain. The run time required for an explicit code is approximately proportional to the number of nodes vice the square of the number of nodes as with implicit codes. Many parameters in LSDYNA can only be adjusted using the LSDYNA card deck file. In this Chapter, these parameters are indicated with an asterisk (*). Unless otherwise discussed, LSDYNA default values should be used.

FEM variables requiring particular consideration include: element type, mesh size, boundary conditions, contact type, failure strain, strain rate dependency, friction and other material properties. A very coarse finite element mesh using primarily panel elements to save CPU time also requires close attention to hour glassing and an effective algorithm for smearing stiffeners in panel thickness.

5.1 Process

The basic procedure for modeling in LSDYNA is:

- Create a model using the FEMB pre-processor.
- Run the LSDYNA collision simulation using the model.
- Use the post- and/or graph-processor to obtain/review the simulation results.

A detailed procedure flow chart is provided in Figure 50.

Engineering Technology Associates FEMB (Finite Element Model Builder) is used for modeling and pre-processing. FEMB's CAD interface allows the input of CAD line data from CAD packages like AutoCAD. Once the CAD line data is received, FEMB can be used to manipulate both line and surface data. If CAD data is not available, the Geometry Builder in FEMB can be

used to create points, lines, splines and surfaces, and to automesh and build a finite element model. The FEMB model is also used to define elements. The elements are assigned to parts, with specific material properties and other element properties. Boundary conditions and interface parameters are also defined for the collision simulation.

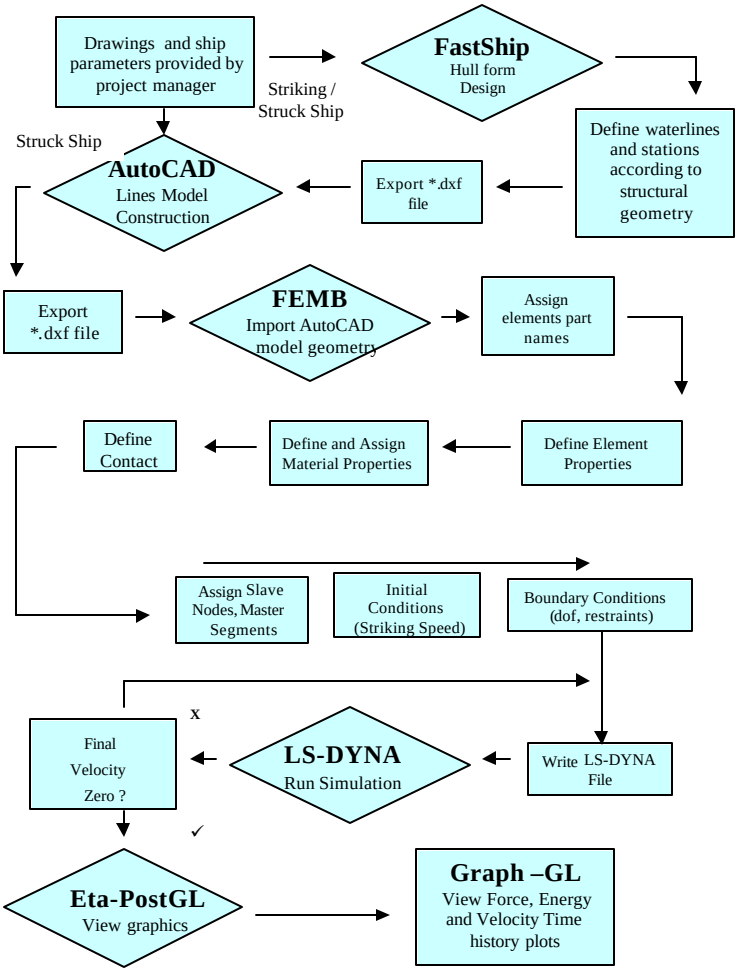

Figure 50 - LSDYNA Modeling and Simulation Process

5.2 Geometry and Model Overview

In this project, LSDYNA is used to model collisions between a striking ship and a rigid wall and a striking ship and a struck oil tanker. In some cases the striking ship bow is assumed to be rigid and in other cases the bow is deformable. The ships modeled in this project include a 150K dwt Bulk Carrier (BC150) (striking ship) and a 150K dwt Double Hull Tanker (DH150) (struck ship). They are described in detail in Chapter 6.

Figure 51 shows a striking ship to rigid wall collision as modeled in LSDYNA. The striking ship geometry is developed from an AutoCad model, Figure 52. It includes a detailed bow model forward of the collision bulkhead and lumped beam elements aft of the collision bulkhead. The detailed portion of the bow model is shown in Figure 53 with side-shell, deck, longitudinal

bulkhead and primary girder components modeled using meshed shell elements. Stiffeners are smeared into plates. Smeared (equivalent) thickness calculations are described in Appendix A.

In order to simplify the geometry of transverse frames, they are modeled as "stiff" transverse bulkheads using panel elements. The thickness (stiffness) of these panels was increased progressively (to 50mm) until transverse deformation was very small. Collision results compare well with results using detailed transverse frame models. The collision bulkhead is the boundary between the detailed portion of the bow and the remainder of the striking ship. It is also modeled as a "stiff" transverse bulkhead. Fully rigid transverse frames and bulkheads were found to cause very high stresses and premature failure at their interface with the side shell and deck panel elements. They are not used. The remainder of the striking ship is modeled using "stiff" Hughes-Liu beam elements and concentrated masses such that the total mass and mass moment of inertia are the same as in the actual ship (including actual mass and added mass in the collision direction). This is discussed in Section 5.3. The total cross sectional area of the longitudinal beam elements in this part of the model is determined such their sum is equal to the total longitudinal structure sectional area at the collision bulkhead in the real ship. Again, fully rigid beams were found to cause very high stresses and premature failure at their interface with the panel elements so stiff deformable beam elements are used.

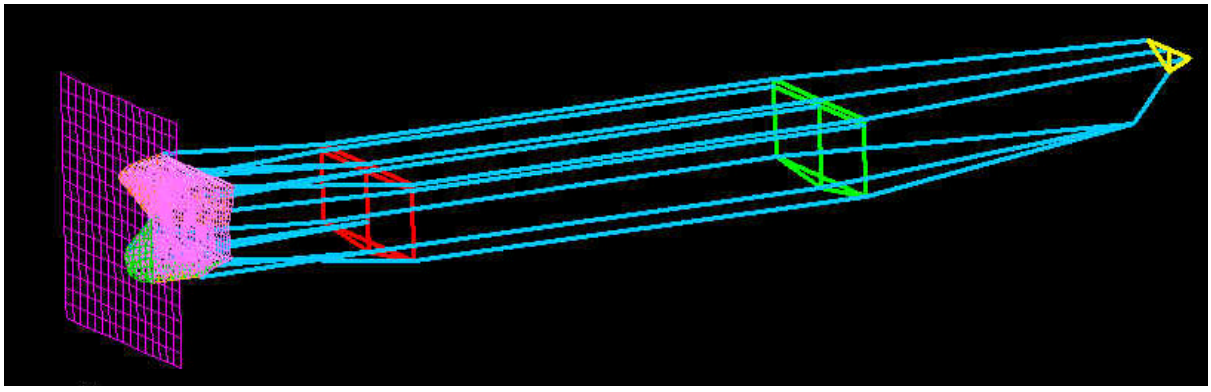

Figure 51 – BC150 Striking Rigid Wall in LSDYNA

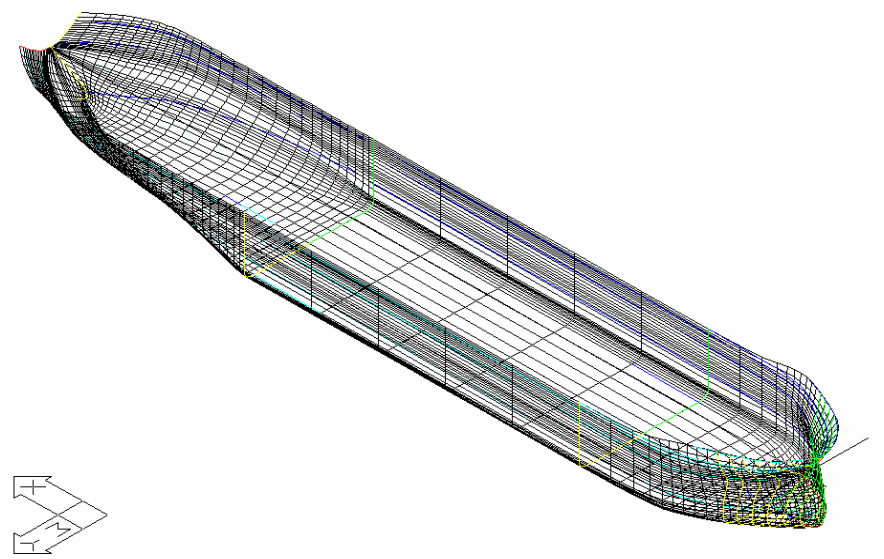

Figure 52 - 150K dwt Bulk Carrier (BC150) Hull Form Modeled in AUTOCAD

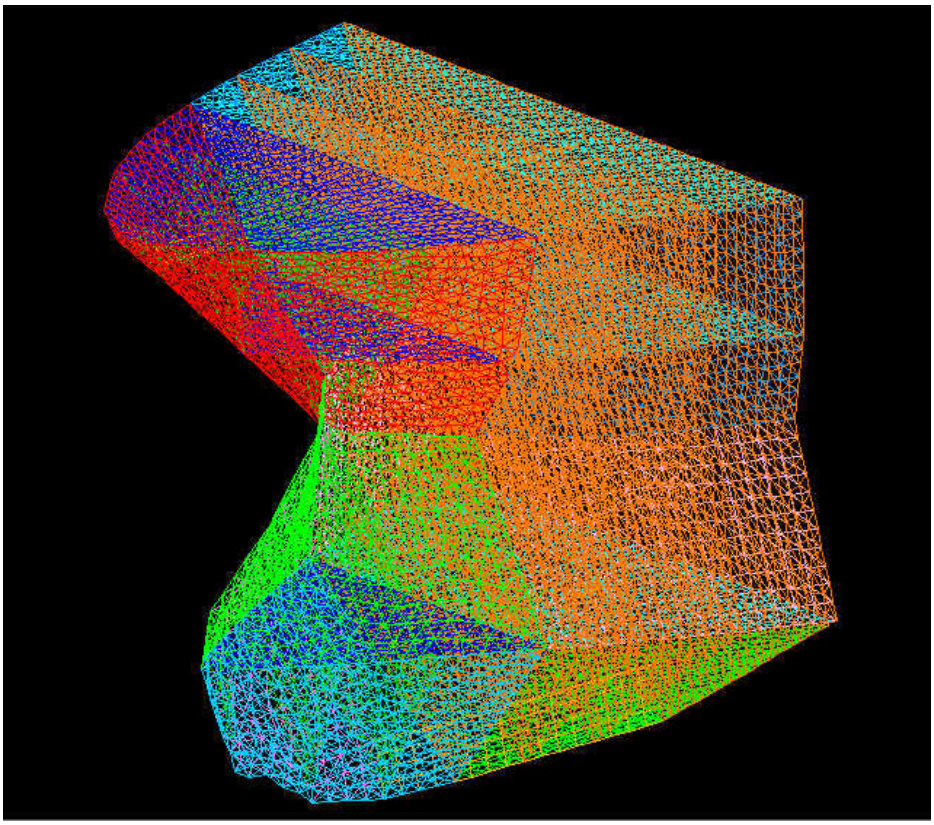

Figure 53 - BC150 Bow Model

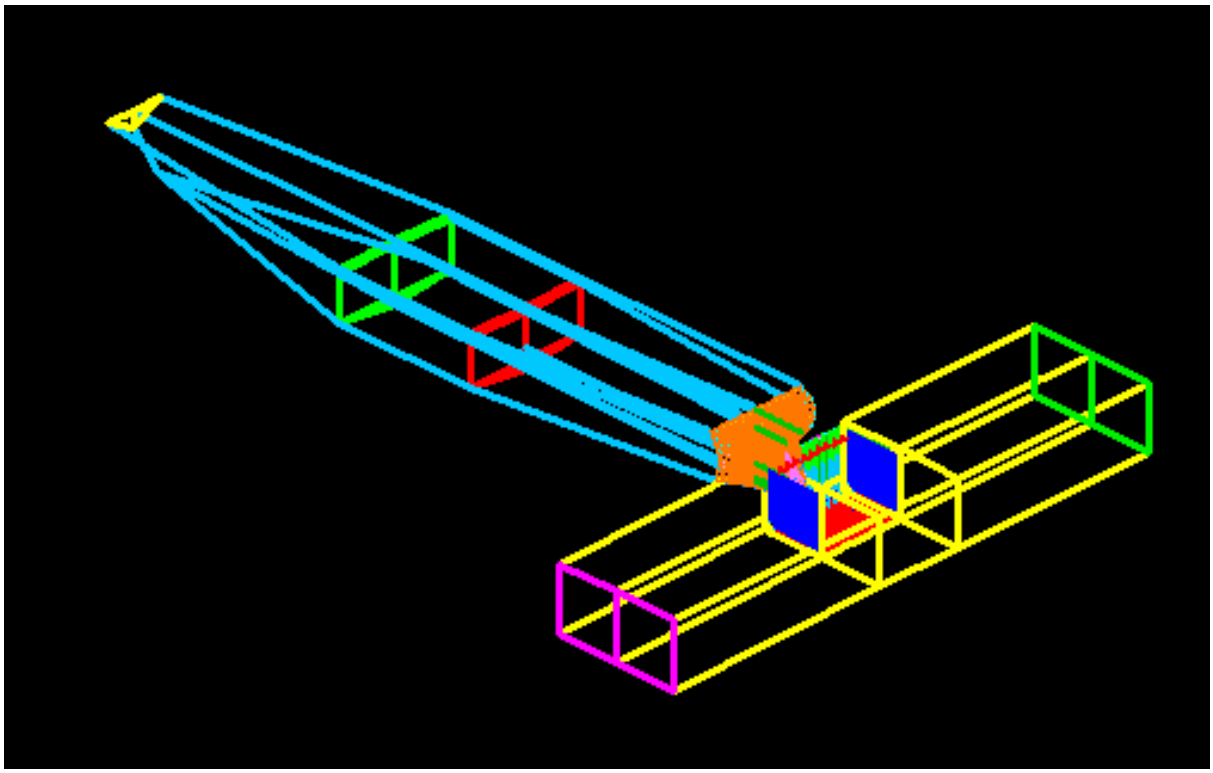

Figure 54 – BC150 Striking 150K dwt Double Hull Tanker (DH150) in LSDYNA

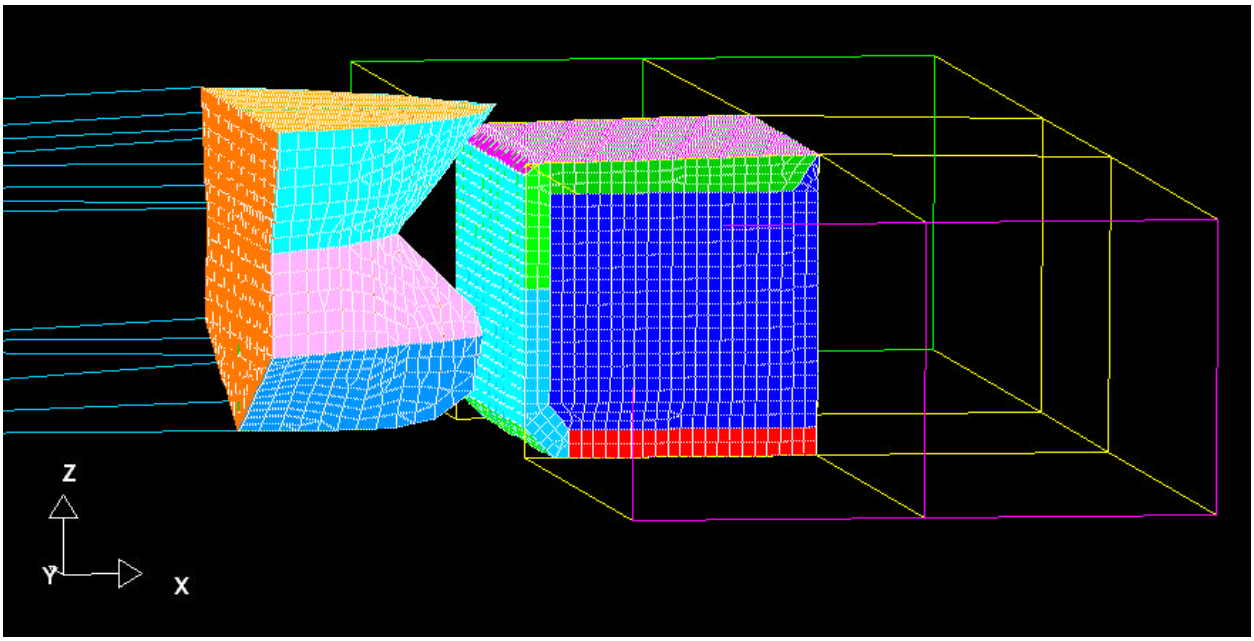

Figure 55 – BC150 Striking DH150

Figure 54 and Figure 55 show a striking ship and struck ship collision modeled in LSDYNA. The striking ship is modeled as in the rigid wall collision described above. The struck ship is modeled with only one side of the struck cargo tank in detail. Figure 56 and Figure 57 show the struck cargo tank section. The struck section includes shells, webs, transverse and longitudinal bulkheads and stringers modeled as panel elements. Stiffeners are smeared into the plate thickness. Smeared (equivalent) thickness calculations are provided in Appendix A.

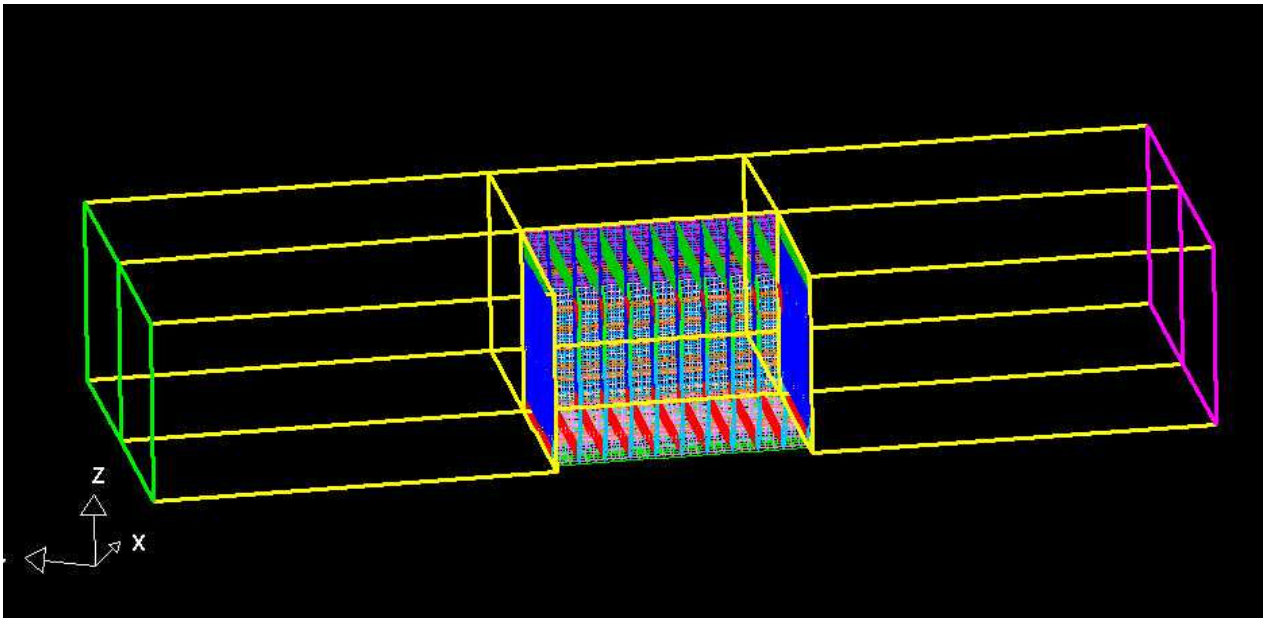

Figure 56 – LSDYNA DH150 Struck Ship Model

The remainder of the struck ship is modeled using Hughes-Liu beam elements and concentrated masses, as with the bow model. This is based on the assumption that in ship collision cases local structural response dominates the collision results. Dimensions of the longitudinal lumped beam

elements are selected to model the horizontal moment of inertia at midship. This allows some flexibility for hull girder horizontal bending (HGHB), although with a large struck ship, horizontal bending in collision is very small [57]. Forward and aft transverse bulkheads are at the boundaries between the detailed cargo tank model and the remainder of the struck ship. In order to simplify the geometry of the boundary transverse bulkheads, they are modeled as "stiff" transverse bulkheads using panel elements only. When a transverse bulkhead is in way of or close to the collision contact, detailed tank structure is modeled on both sides of a detailed transverse bulkhead and the stiff bulkhead boundary is moved to the opposite end of the additional tank. The centerline bulkhead model is also modeled using a very stiff bulkhead unless it is in way of or close to the collision contact. When close to the collision contact the centerline bulkhead model is based on real ship scantlings and geometry, but backed with stiff beam elements that connect to nodes on the opposite deck edge at each frame, deck and stringer. Again, fully rigid beams were found to cause very high stresses and premature failure at their interface with the panel elements so stiff deformable beam elements are used.

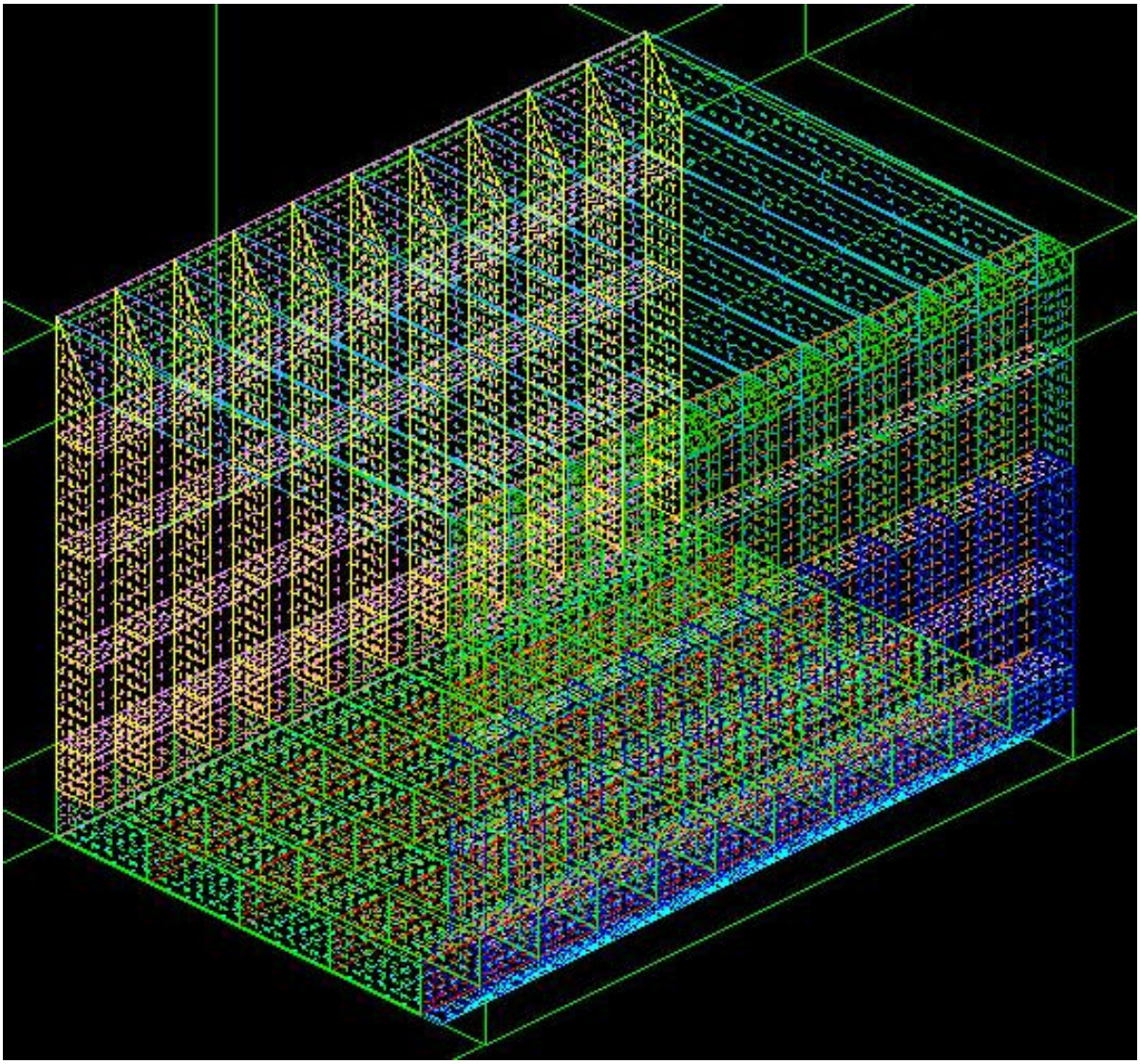

Figure 57 - LSDYNA DH150 Struck Section

5.3 External Dynamics and Constraints

The LSDYNA simulation is used to model both the internal structural response in collision and the external ship dynamics including hydrodynamics. To save CPU time, an inertia-equivalent method is used vice an explicit calculation of the fluid-structure interaction [58]. Masses and mass moments of inertia in surge, sway and yaw represent the virtual masses (actual plus added mass) for each ship. The masses of the striking ship outside of the bow are assumed to be concentrated in three transverse section parts shown in Figure 51 in red, green and yellow (MSTERN, MASS1 and MASS2). The masses of the bow parts are summed and the remaining mass is adjusted by assigning an appropriate mass density to the MSTERN, MASS1 and MASS2 parts so that the total mass of the striking ship model is equivalent to the mass of the actual ship plus the added mass in surge. The locations of the forward two transverse masses (MASS1 and MASS2) are determined by matching the required added mass moment of inertia in yaw. A similar procedure is followed for the struck ship. Spreadsheets used to calculate this mass and moment balance are provided in Appendix B.

The motion of the striking ship is prevented in the 3, 4 and 5 directions (translation in the Z-axis, rotation around the X-axis and Y-axis or heave, pitch, and roll) by constraining the nodes in the collision bulkhead in these directions. These constraints allow the striking ship model to be very simple and provide for a faster solution. The striking ship motions in heave, pitch, and roll are relatively small and less significant in a collision event. The motions of the struck ship are also constrained in these directions, allowing only sway, surge and yaw by constraining the nodes in the boundary transverse bulkheads in these directions. This effectively limits ship global motion to the horizontal plane, but allows deformed sections a full six degrees of freedom.

Added mass values vary over the duration of the collision and depend on hull form [13]. For model simplicity, mid-range values are typically used or average added mass coefficients may be used where:

$$\begin{aligned} a_{11} &= c_{11} m_s \\ a_{22} &= c_{22} m_s \\ a_{33} &= c_{33} I_{s33} \end{aligned} \tag{5.1}$$

Coefficients values used in this report were selected to standardize results when compared to other models, specifically Pedersen [14], Simonsen [10] and Paik [29]. Assumed added mass coefficients are 0.05 in surge (c_{11}), 0.85 in sway (c_{22}) and 0.21 in yaw (c_{33}).

5.4 FEA Parameters

Lemmen and Vredeveldt [59] used LSDYNA to model full-scale collision tests. Their report identifies variable values that provide results consistent with their test results. Servis et. al. [60] and Naar [61] also provide some excellent general guidance.

5.4.1 Element Types

LSDYNA has many element types to choose from. In order to save CPU time, we have avoided solid modeling and a fine mesh in favor of shell and beam elements and a coarse mesh. The

Hughes-Liu beam element is used for all struck and striking ship model beam elements. Hughes-Liu elements are designed not to fracture and provide out of plane bending not provided by truss elements. Belytschko-Tsay shell elements are used for all plate panels in both the struck and striking ship models. This element uses a local coordinate system that deforms with the element and provides a higher degree of numerical accuracy than a standard shell element at a lower time cost. Numerous runs with other element types available in LSDYNA were not as satisfactory. Single point (reduced), standard Gauss integration is used and the panel reference location is taken at mid-plane.

ISTUPD(*) is the flag to set the shell thickness change option. Shell thickness may change in a collision due to membrane strain. The stretching of shell plating is important between the webs and also between the transverse bulkheads. A membrane model is used in SIMCOL, but in LSDYNA we do not treat the shell as a pure membrane. In-plane membrane strains are considered together with other in-plane strains. The ISTUPD variable is set to the default of 0 to disallow for the membrane strain.

NIP is the number of through-thickness integration points. Lemmen and Vredeveldt found that two or three integration points through the thickness were sufficient. Hourglassing, numerical deformation modes other than rigid body that do not contribute to strains at the integration points (Figure 58), were not a problem with their small mesh (80x80mm). The LSDYNA manual recommends that the hourglass energy be less than 10% of the internal energy. Otherwise, other methods should be used, such as triangle-elements instead of quadrilateral-elements or fully integrated elements instead of reduced integration elements. In our project, an examination of the effect of integration points on the absorbed energy was performed using Charpy-V notch test experiments and collision simulations. Unless there was a significant hour-glassing (numerical error) problem, results were found to be relatively insensitive to the number of integration points. Therefore, NIP = 2 is used for most analyses. If hour-glassing problems are encountered, NIP is increased to 3.

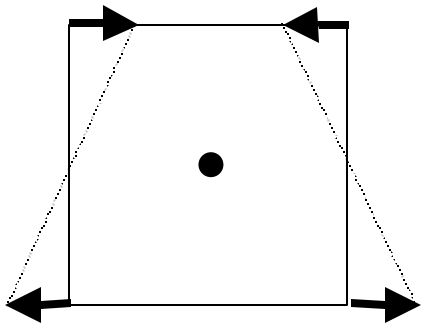

Figure 58 – Hour-glassing

QH is the hourglass coefficient. This value is the maximum acceptable percent of allowed hourglassing. For ship collision analysis we accept the recommended default value of 0.1. If the hourglass energy exceeds 10%, LSDYNA will display a warning and attempt to reduce hour-glassing by reducing the time step and invoking various numerical correction algorithms.

HGEN is the flag for selection of the hourglass energy calculation. Our ship collision analysis uses hourglass energy as a check for computational error, and the HGEN variable is set to 2. This turns on the hourglass energy calculation.

5.4.2 Mesh

Starting with the line model of the ship hull geometry, surfaces are created over the lines, partitioning and joining surfaces consistent with major structural members. Next the surfaces are auto-meshed in FEMB with a minimum element dimension of 0.5 meters and a maximum element dimension of 1.5 meters. Element dimensions less than 0.5 meters are processing time prohibitive. Element dimensions larger than 1.5 meters fail to capture important structural characteristics and hull curvature. Hourglassing is also an important concern with large mesh sizes and must be monitored closely. Finally, mesh problems are repaired manually. The resulting length to thickness (L/t) ratio is typically 30:1 to 40:1.

Convergence tests are required to determine if the coarse mesh model is sufficient to capture important structural characteristics and converge to a correct model solution. Large mesh sizes require less computer time, but the mesh size must be small enough for reasonable accuracy. Figure 59 shows the results of a typical convergence test for the DH150/BH150 collision model. Above 20000 elements, the results become reasonably stable. Below this number there is significant variation. 20000 elements represents a mesh with L/t ratio of approximately 40:1 or in this model an element length of approximately one meter.

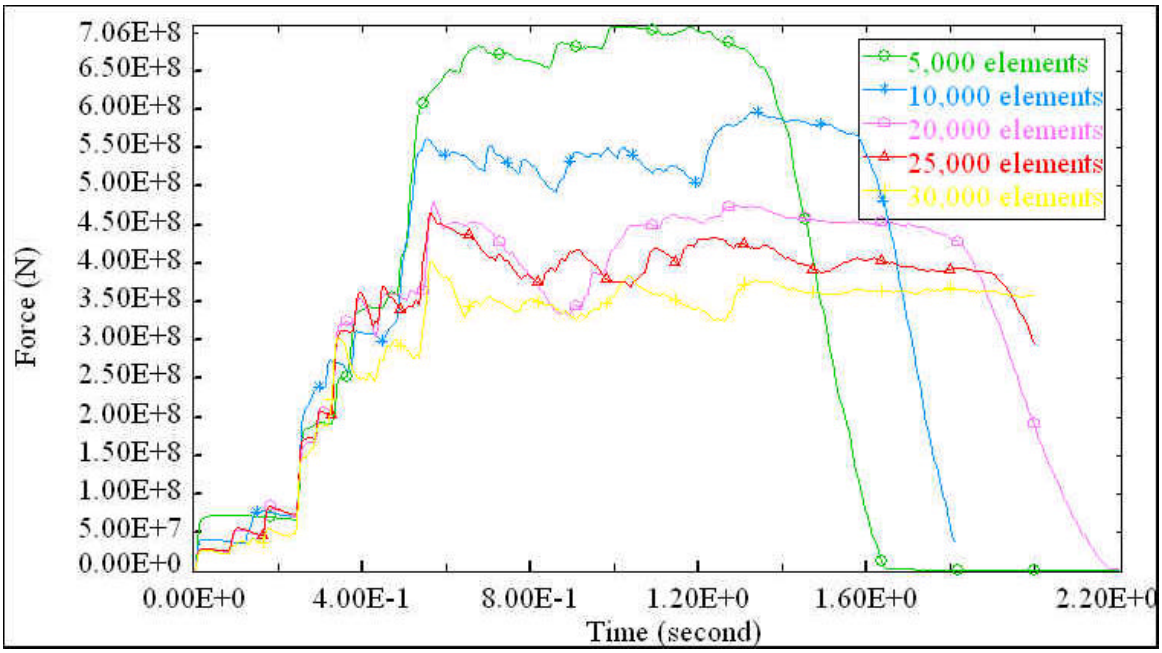

Figure 59 - Force-Time Curves With Different Number of Elements (150CW7)

IRNXX is the shell plate normal update option. IRNXX is the flag that directs LSDYNA to calculate the element's outward surface normal at every iteration or cycle, every n set cycles, only upon restart, or not at all. The ship collision analysis results in large deformations and the outward normals need to be calculated continuously to maintain accurate results. Accept the default value of –1 to indicate that the outward surface normals are calculated every cycle.

5.4.3 Contact Type and Friction

Three types of striking to struck ship contact are available in LSDYNA. After many analyses using all three of these contact types, Type 5 was found to provide the best simulation of actual damage geometry (folding, crushing, and tearing). Its results were stable and consistent. Figure

60 shows how Type 5 contact is defined in LSDYNA. The red dots and lines indicate slave nodes and segments (surfaces), and the blue dots and lines indicate master nodes and segments. Slave nodes are usually taken to be mesh nodes in the struck ship and master nodes are taken to be mesh nodes in the striking ship.

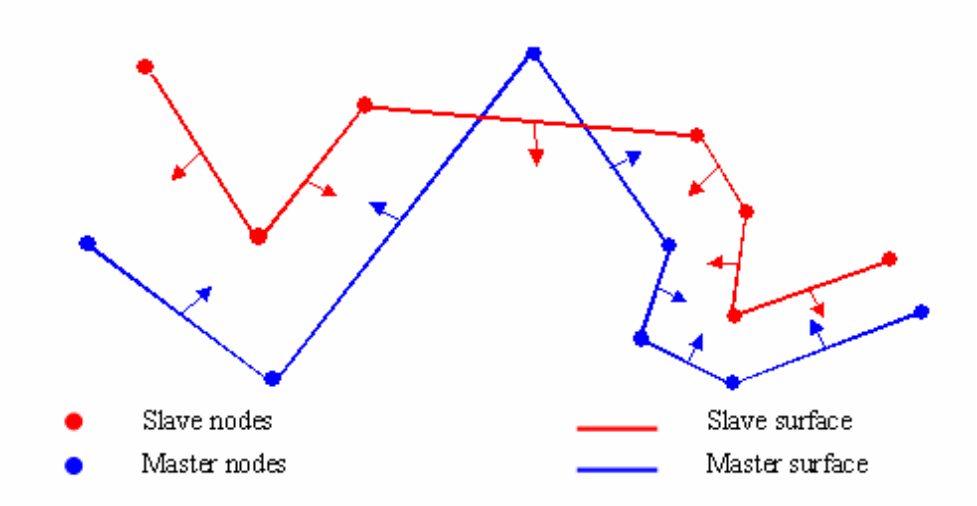

Figure 60 - LSDYNA Contact Algorithms

In Type 5 contact, slave nodes are constrained to be on the positive side of master segments (side of outward pointing normal). Slave nodes are prevented from going through the master surface. Both surfaces are allowed to deform, but only the slave surface is allowed to rupture.

In cases with a bow striking a rigid wall, slave nodes are taken to be mesh nodes in the striking ship bow and master nodes are in the rigid wall.

SLSFAC is an interface numerical scale factor used to effectively decrease the time step locally in areas of large deformations until failure occurs. The LSDYNA default is 0.1, but this value may be too low for large deformation problems like ship collisions. By progressively increasing this parameter (similar to locally decreasing the time step) results stablized with an **SLSFAC** value of 0.2 or greater. This value was used in all subsequent analyses.

The correct consideration of friction in a ship-ship collision model is also important. As friction is increased the penetration of the striking ship into the struck ship is decreased or the absorbed energy per unit penetration is increased. Several considerations of friction and various static and dynamic friction coefficient values are reported in the literature. The most common value found in the literature for the dynamic friction coefficient is 0.3 [22,59,62,63,64,65]. Reported dynamic coefficients of friction vary from 0.0 to as high as 0.6 and static coefficients are reported at values between 0.5 and 0.8 [28,66,67,68,69]. Wisniewski et al [70] modeled collisions with a 40K dwt container ship striking a 105K dwt double hull crude oil carrier using ABAQUS-EXPLICIT. The dynamic coefficient of friction was varied from 0.0 to 0.6 in a parametric study. Plots of Wisniewski's results are provided in Figure 61 where it is shown that the higher the friction coefficient the faster the loss of kinetic energy of the striking ship. The difference between the friction curves for 0.3 and 0.6 is much smaller than between the curves for 0.0 and 0.3. As a result Wisniewski states that "the effect of friction will not increase significantly for larger values of the coefficient."

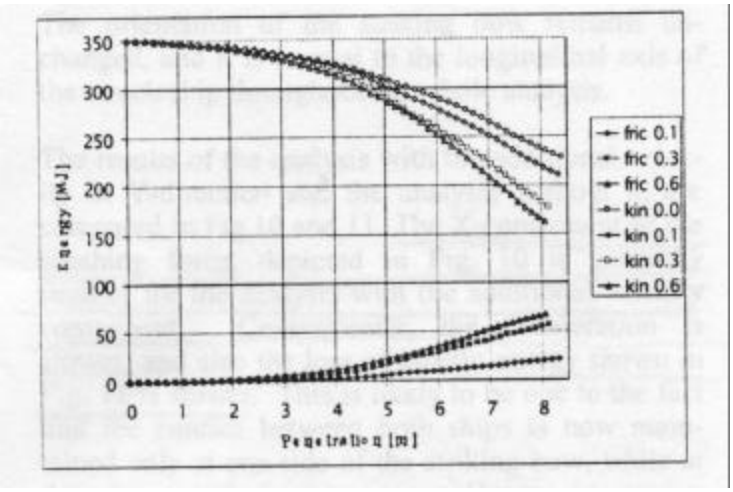

Figure 61 - Friction and Kinetic Energy vs. Penetration [70]

The friction model in LSDYNA is based on the Coulomb friction relation given by Equation (5.2):

$$m_c = FD + (FS - FD)e^{-DC \cdot ABS(V_{rel})} \tag{5.2}$$

where:

μ_c = coulomb friction coefficient
FS = static coefficient of friction for mild steel on steel
FD = dynamic coefficient of friction for mild steel on steel
$\mathbf{V_{rel}}$ = relative velocity of contact surfaces
DC = exponential friction decay coefficient

The LSDYNA User's Manual [71] suggests a value of 0.74 for the static friction coefficient (FS) of dry mild steel on steel. An average value from the literature for FS of wet mild steel on steel is 0.7. The LSDYNA User's Manual suggests a value of 0.57 for the dynamic friction coefficient (FD) of dry mild steel on steel. An average value from the literature fir FD is 0.3. Figure 62 shows the Coulomb Friction value as a function of the change in relative velocity of the contact surfaces in meters per second with a DC value of 7.0. By increasing the value of DC the value of the relative velocity at which the steel on steel contact acts in a dynamic manner is decreased, i.e. the rate of change from the static friction coefficient to the dynamic is increased. Values selected for these coefficients in this project are FS = 0.7, FD = 0.3 and DC = 7.0.

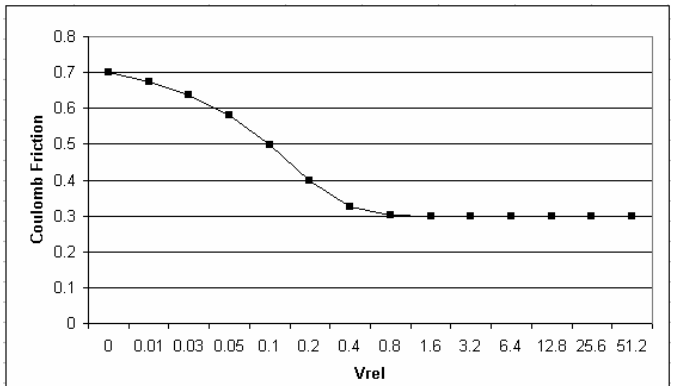

Figure 62 - Coulomb Friction vs. Relative Velocity of Contact Surfaces

5.4.4 Time

The analysis may be stopped when a minimum time step (DTMIN), minimum percent energy change (ENDENG) or minimum percent mass change (ENDMAS) is reached., but these indicators do not give positive control and sometimes the simulation will stop prematurely or go on for ever. The analysis may also be stopped by setting the termination time (ENDTIM) or the termination cycle (ENDCYC). For our analyses, the variable ENDTIM is used. The lowest value of ENDTIM is desired to reduce the overall time cost of the analysis, but ENDTIM should be large enough to ensure completion of the collision event. An initial guess at the ENDTIM value is made using Equation (5.1) where a maximum penetration of 5 meters is assumed.

$$ENDTIM = \frac{DBI + 5.0}{V_B} \tag{5.3}$$

where:

DBI = distance between the forward most point of the striking bow and the impact location on the struck vessel (m) at t = 0

V_B = velocity of the striking vessel in the surge direction in (m/s) at t = 0

To check for completion of the collision event, the Force vs. Penetration plot should look similar to the curves in Figure 63 where force returns to zero at the end of the collision event.

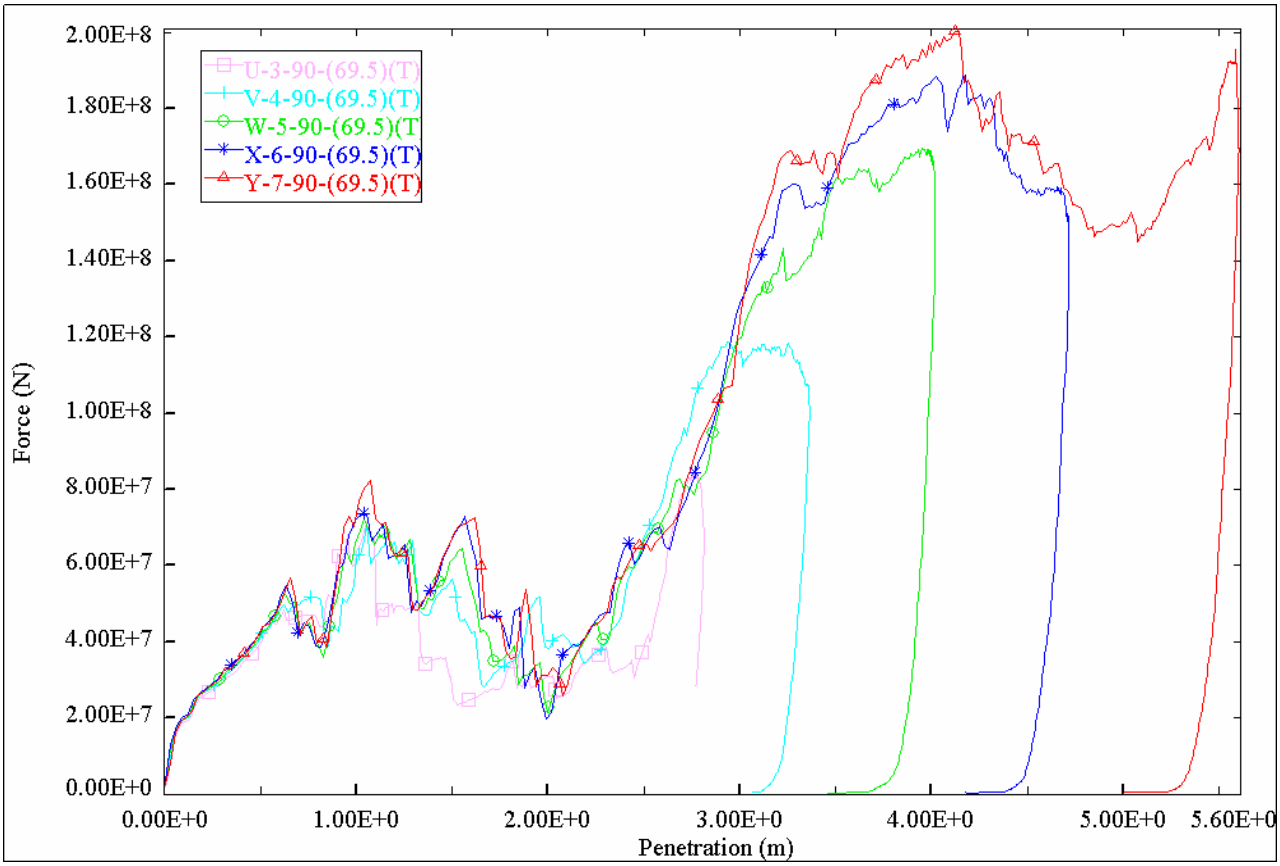

Figure 63 - Force vs. Penetration Plots

5.5 Material Properties

5.5.1 Material Types and Mechanical Properties

Only three of many (nearly 100) material types available in LSDYNA were found to be suitable or necessary for ship collision analyses:

- Type 24 – Elastic/Plastic Isotropic with Piecewise Linear Plasticity – This material type allows strain rate effects and complete material fracture. All panels in the struck ship are modeled using LSDYNA Material Type 24. Material behavior is specified using the following parameters: Young's modulus, yield stress, tangent modulus, failure strain and Cowper and Symonds strain rate parameters.
- Type 3 – Elastic/Plastic Isotropic with Kinematic Plastic Hardening - All beams in the struck and striking ship and panels in the striking ship are modeled using LSDYNA Material Type 3. Material Type 3 is used in the striking ship because of the "No Fracture" behavior in its stress-strain curve shown in Figure 64. It was found that Master Elements modeled with Material Type 24 confuse the contact algorithm when these elements fracture. Model elements away from damaged areas must remain intact for model integrity. The use of Type 3 material avoids these problems.
- Type 20 – Rigid – Material Type 20 is used in special model cases specifying a rigid wall or a rigid bow. Rigid elements are bypassed in deformation processing and are very time efficient.

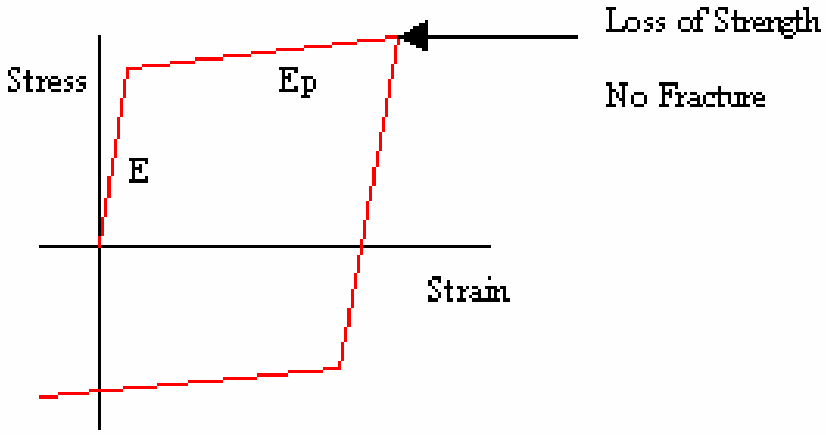

Figure 64 - Kinematic/Isotropic Elastic Plastic Material Stress-Strain Curve

Lemmen and Vredeveldt used Material Type 24. They considered 2 failure criteria: 1) criteria with bending (CB) - elements fail at specific integration points (stress then set to zero) when specific integration point equivalent plastic strain reaches the failure value - fails layer by layer; and 2) criteria with membrane strains only (CM) - stresses at all element integration points are set to zero when equivalent plastic strain reaches the failure value in the central layer – the element fails over its full thickness. CB was found to provide results more consistent with their tests and is used in this project.

Parameter values for modeling ABS materials Grade A and B, AH32 and AH36 using Material Types 3 and 24 are listed in Table 8 and Table 9.

Table 8 - Material Type 3 Definitions

NAME	(Material Name)	M3GB	M3GAH32	M3GAH36
TYPE	(Material Type)	3	3	3
MID	(Material Identification Number)	601	602	603
RO	(Material Density)	7.78E+03	7.83E+03	7.85E+03
E	(Material Modulus of Elasticity)	1.90E+11	2.00E+11	2.10E+11
PR	(Material Poissons Ratio)	0.281	0.292	0.303
SIGY	(Material Tension Yeild Stress)	2.35E+08	3.15E+08	3.55E+08
ETAN	(Material Tangent Modulus)	3.75E+09	3.05E+09	3.22E+09
BETA	(Material Hardening Parameter)	0	0	0
SRC	(Cowper-Symmonds Strain Rate Parameter C)	40.4	40.4	40.4
SRP	(Cowper-Symmonds Strain Rate Parameter P)	5	5	5
FS	(Material Failure Strain)	0	0	0
VP	(Material Formulation for rate effects)	0	0	0

ETAN is the slope of the Bilinear stress strain curve (also called the Hardening Modulus). Because both Material Types 3 and 24 are used as elastic-plastic with linear hardening models in the ship collision analysis the value of ETAN must be specified. The suggested value of ETAN for each material is derived from Equation (5.4):

$$\mathrm{ETAN} = \frac{\mathrm{SIGU} - \mathrm{SIGY}}{\mathrm{FAIL}} \tag{5.4}$$

SIGU is the ultimate strength of the material in tension. The values of SIGU are taken to be 450 Mpa for ABS GR. B, 490 Mpa for ABS GR. AH32 and 540 Mpa for ABS GR. AH36, MSTRIKE, MSTRUCK, HSTRIKE, HSTRUCK.

SIGY is the material tension yield stress as defined by ABS Rule Requirements for Materials and Welding 2001.

BETA is a value between 0 and 1 where 0 corresponds to kinematic hardening and 1 corresponds to isotropic hardening.

Figure 65 shows the resulting stress verses strain curves for Type 3 and Type 24 Material at each grade.

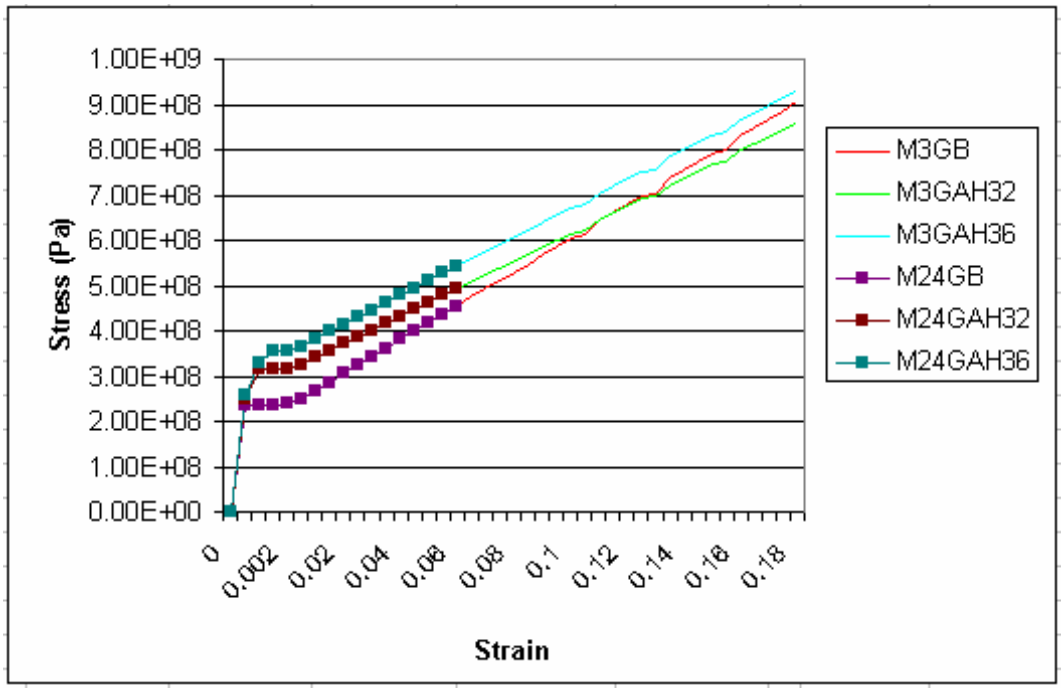

Figure 65 - Material Types 3 and 24 Stress/Strain Curves

FAIL is the failure strain. If Failure Strain is equal to 0, no element failure and deletion is considered for this material. Failure strain is discussed in Section 5.5.1.2. When the plastic strain reaches the value of FAIL, the element is deleted from the calculation.

VP is the material strain rate formulation flag. If VP = 0, the yield stress is scaled via the Cowper Symmonds model, if VP = 1, then a viscoplastic formulation is used.

TDEL is the minimum time step size for the automatic deletion of an element regardless of failure. When the calculated required time step for proper numerical evaluation of this element is below TDEL the element is deleted automatically.

LCSS or LCSR is a load curve identification number. If this value is defined greater than zero (I.E. the user has entered a complete effective stress verses plastic strain table defining a curve) then the values EPS1 – EPS8, ES1 – ES8 and ETAN are ignored.

EPS1 through EPS8 and corresponding values **ES1 through ES8** are optional if SIGY is defined. This option allows an eight point piecewise linear approximation of the effective stress verses plastic strain plot. If however, this option is used then EPS1 = 0 corresponding to the initial yield stress. If this option is used SIGY and ETAN are ignored and may be entered as zero.

Table 10 lists the material property values used to model the BC150 striking ship. Table 11 and Table 12 list the material property values used to model the DH150 struck ship.

5.5.2 Strain Rate

The effect of stain rate on yield strength is modeled using the Cowper and Symonds strain rate model. Lemmen and Vredeveldt [59] found this model to give good results. The influence of

material inertia forces was found to be negligible, ie., other than the effect of strain rate, material properties are not sensitive to velocity.

Table 9 - Material Type 24 Definitions

MATERIAL TYPE 24				
NAME	(Material Name)	M24GB	M24GAH32	M24GAH36
TYPE	(Material Type)	24	24	24
MID	(Material Identification Number)	701	702	703
RO	(Material Density)	7.78E+03	7.83E+03	7.85E+03
E	(Material Modulus of Elasticity)	1.90E+11	2.00E+11	2.10E+11
PR	(Material Poissons Ratio)	0.281	0.292	0.303
SIGY	(Material Tension Yeild Stress)	2.35E+08	3.15E+08	3.55E+08
ETAN	(Material Tangent Modulus)	3.75E+09	3.05E+09	3.22E+09
FAIL	(Plastic Strain to Failure)	0.0574	0.0574	0.0574
TDEL	(Minimum Time Step Size for Automatic Deletion)	0	0	0
C	(Cowper-Symmonds Strain Rate Parameter C)	40.4	40.4	40.4
P	(Cowper-Symmonds Strain Rate Parameter P)	5	5	5
LCSS	(Load Curve Identification Number for Effective Stress verses Plastic Strain)	0	0	0
LCSR	(Load Curve Identification Number for Strain Rate Scaling Effect on Yeild Stress)	0	0	0
VP	(Material Formulation for rate effects)	0	0	0
EPS1	(Effective Plastic Strain Value 1)	0	0	0
EPS2	(Effective Plastic Strain Value 2)	0	0	0
EPS3	(Effective Plastic Strain Value 3)	0	0	0
EPS4	(Effective Plastic Strain Value 4)	0	0	0
EPS5	(Effective Plastic Strain Value 5)	0	0	0
EPS6	(Effective Plastic Strain Value 6)	0	0	0
EPS7	(Effective Plastic Strain Value 7)	0	0	0
EPS8	(Effective Plastic Strain Value 8)	0	0	0
ES1	(Corresponding Yeild Stress Value to EPS1)	0	0	0
ES2	(Corresponding Yeild Stress Value to EPS2)	0	0	0
ES3	(Corresponding Yeild Stress Value to EPS3)	0	0	0
ES4	(Corresponding Yeild Stress Value to EPS4)	0	0	0
ES5	(Corresponding Yeild Stress Value to EPS5)	0	0	0
ES6	(Corresponding Yeild Stress Value to EPS6)	0	0	0
ES7	(Corresponding Yeild Stress Value to EPS7)	0	0	0
ES8	(Corresponding Yeild Stress Value to EPS8)	0	0	0

Table 10 – Mass and Material Properties for the BC150

Material Property Name	**Deformable**	**Mass**
Material Type	Type 3	Type 3
Mass Density	7.85E+03	7.85E+03
Youngs Modulus	2.09E+11	2.09E+11
Poissons Ratio	2.80E-01	2.80E-01
Yeild Stress	4.57E+08	4.57E+08
Tangent Modulus	4.57E+08	4.57E+08
Failure Pl. Strain	1.50E-01	1.50E-01
Step Size for el. Del.	0	0
Strain Rate Para: C	4.00E+01	4.00E+01
Strain Rate Para: P	5	5

Table 11 - DH150 Material Details

MATERIAL	HT32	MILD	RIGID1	MASSF	MASSA
Type	24	24	3	3	3
Mass Density	7.8500E+03	7.8500E+03	2.7620E+05	1.82E+05	1.82E+05
Youngs Modulus	2.0900E+11	2.0900E+11	2.0900E+11	2.0900E+11	2.0900E+11
Poissons Ratio	2.8000E-01	2.8000E-01	2.8000E-01	2.8000E-01	2.8000E-01
Yeild Stress	4.5700E+08	4.5670E+08	4.5670E+08	4.5670E+08	4.5670E+08
Tangent Modulus	4.5700E+08	4.5670E+08	NOT APPLICABLE	NOT APPLICABLE	NOT APPLICABLE
Failure Plain Strain	1.5000E-01	1.5000E-01	NOT APPLICABLE	NOT APPLICABLE	NOT APPLICABLE
Step Size for Element Deletion	0.0000E+00	0.0000E+00	NOT APPLICABLE	NOT APPLICABLE	NOT APPLICABLE
Hardening Modulus	NOT APPLICABLE	NOT APPLICABLE	0.0000E+00	0.0000E+00	0.0000E+00
Hardening Parameter	NOT APPLICABLE	NOT APPLICABLE	0.0000E+00	0.0000E+00	0.0000E+00
Strain Rate Parameter C	4.0000E+01	4.0000E+01	0.0000E+00	0.0000E+00	0.0000E+00
Strain Rate Parameter P	5.0000E+00	5.0000E+00	0.0000E+00	0.0000E+00	0.0000E+00
LCSS	0.0000E+00	0.0000E+00	NOT APPLICABLE	NOT APPLICABLE	NOT APPLICABLE
LCSR	0.0000E+00	0.0000E+00	NOT APPLICABLE	NOT APPLICABLE	NOT APPLICABLE
Effective Strain/Stress 1	0.0000E+00	0.0000E+00	NOT APPLICABLE	NOT APPLICABLE	NOT APPLICABLE
Effective Strain/Stress 2	0.0000E+00	0.0000E+00	NOT APPLICABLE	NOT APPLICABLE	NOT APPLICABLE
Effective Strain/Stress 3	0.0000E+00	0.0000E+00	NOT APPLICABLE	NOT APPLICABLE	NOT APPLICABLE
Effective Strain/Stress 4	0.0000E+00	0.0000E+00	NOT APPLICABLE	NOT APPLICABLE	NOT APPLICABLE
Effective Strain/Stress 5	0.0000E+00	0.0000E+00	NOT APPLICABLE	NOT APPLICABLE	NOT APPLICABLE
Effective Strain/Stress 6	0.0000E+00	0.0000E+00	NOT APPLICABLE	NOT APPLICABLE	NOT APPLICABLE
Effective Strain/Stress 7	0.0000E+00	0.0000E+00	NOT APPLICABLE	NOT APPLICABLE	NOT APPLICABLE
Effective Strain/Stress 8	0.0000E+00	0.0000E+00	NOT APPLICABLE	NOT APPLICABLE	NOT APPLICABLE
Failure Strain	NOT APPLICABLE	NOT APPLICABLE	0.0000E+00	0.0000E+00	0.0000E+00

Table 12 - DH150 Material and Property Assignments

DH150 Striking Ship In Brief:		
PART	Property	Material
DECK	DECK	HT32
BOTT	BOTT	HT32
INNBOTT	INNBOTT	HT32
SIDESHEL	SIDESHEL	MILD
INN_SKIN	INN_SKIN	MILD
BULKHEAD	BULKHEAD	MILD
STRINGER	STRINGER	MILD
FLR_GIRDER	FLR_GIRDER	MILD
DEC_TRAN	DEC_TRAN	MILD
VERTWEB	VERTWEB	MILD
FLR_TRAN	FLR_TRAN	MILD
WEBUP	WEBUP	MILD
WEBLOW	WEBLOW	MILD
BLOCK	BLOCKA	RIGID1
MASSAFT	MASSAFT	MASSF
MASFORW	MASSAFT	MASSA
TRBULKHD	TRBULKHD	MILD
BRACKET	DEC_TRAN	MILD

The Cowper-Symonds constitutive equation, Equation (5.5), is widely used and has been found adequate for many theoretical and numerical calculations [29]:

$$s_D = s_y \left[1 + \left(\frac{e_r}{C} \right)^{\frac{1}{P}} \right] \tag{5.5}$$

where:

s_D = dynamic yield stress
s_y = material static yield stress
e_r = strain rate =
C, P = material constants

The material properties C and P are most often taken as 40.4 sec^{-1} and 5.0 respectively for mild steel [28,29,72]. Paik et al. [28] used C equal to 3200 sec^{-1} and P equal to 5.0 for high tensile steel materials based on unidentified test data. These values of C and P for mild steel and high strength steel are used in this project. Ship to ship collision strain rates in this project reach

maximum values of approximately 0.1 sec^{-1}. This results in a dynamic yield stress that is 1.3 times the static yield stress in mild steel and can have a significant effect on the results.

5.5.3 Failure Strain

For Material Type 24, when the plastic strain reaches the value of FAIL, the element is deleted from the calculation. Static tension tests of mild steel performed by Naar et al [61] and by Lehmann et. al. [69] indicate a failure strain of 18%. Wisniewski et. al. [70] reports a material failure strain of 17% for both mild steel and high tensile steel. Simonsen and Lauridsen [73] report a material failure strain of 19% determined via a tension test on mild steel. Kitamura [57] reports that, "a lot of material tests have shown that [failure strain] of ordinary mild steel is about 30%". Servis et al [60] report a tested material failure strain for mild steel at 46.1%. These citations represent a wide range of values.

Comparison of FEM results to experimental results for a range of experiments shows that the necessary numerical failure strain (the value required in an FEM to match experimental data) is a function of element size [29,57,59,60,61,69,72,73,74,75]. Research performed to determine this relationship shows significant scatter (Figure 66). The general trend indicates that the larger the element size the smaller the necessary numerical failure strain.

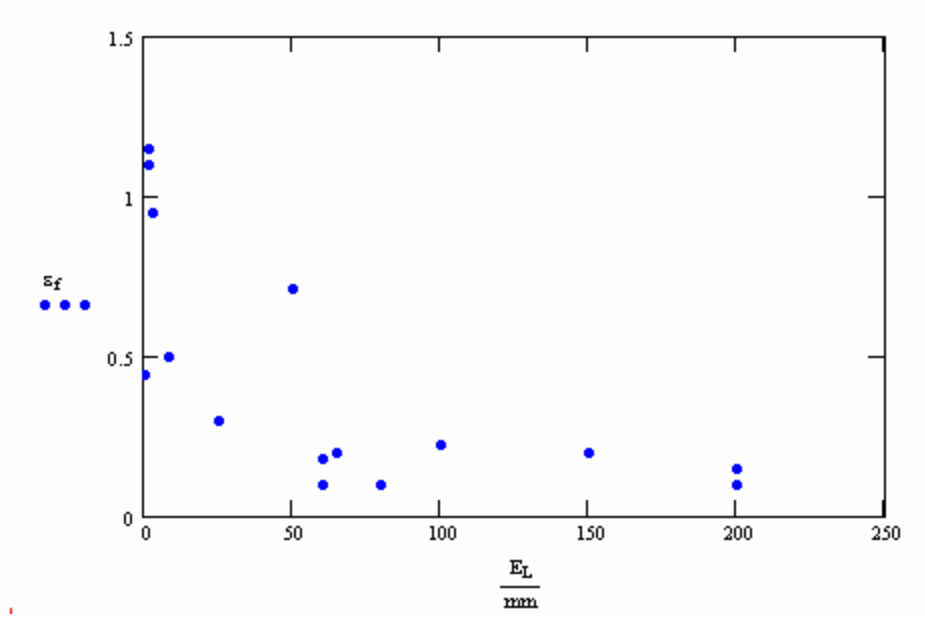

Figure 66 – Failure Strain as a Function of FEM Element Size

Paik and Pederson [29] and Kitamura [57] explain that lower values of failure strain are used with larger element sizes to numerically account for stress concentration factors such as cracks, corrosion and impact loadings etc… within the model that larger size elements do not properly capture. Paik and Pederson also state that "ship collisions are essentially dynamic problems and dynamic effects may not be neglected." For this reason, the use of static or quasi-static experiments to validate the numerical failure strain to be used within a dynamic model is suspect.

To account for the dynamic effects on failure strain, Paik and Pederson [28,29] use an inverse Cowper-Symonds equation, Equation (5.6) to determine the numerical failure strain.

$$\frac{\varepsilon_{fd}}{\varepsilon_f} = \left[1 + \left(\frac{\varepsilon_r}{C}\right)^{\frac{1}{P}}\right]^{-1} \tag{5.6}$$

where:

e_{fd} = dynamic failure strain
e_r = strain rate
C and P = Cowper-Symonds material property coefficients
ef = static failure strain = 10%

The 10% value of the static failure strain was determined to provide the best results when matching a quasi-static penetration of a cone into a circular plate. However, dynamic tests were not performed to validate the dynamic relation expressed in Equation (5.6).

Kitamura [57] performed a series of dynamic drop tests and quasi-static penetrations where either scale models were struck repeatedly by a free falling rigid bow model of 8.44 tons, or slowly indented by the same rigid bow. Figure 67 shows the failure strain necessary to model these tests using FEA. It is not clear whether these results were developed based on the dynamic tests or the quasi-static tests.

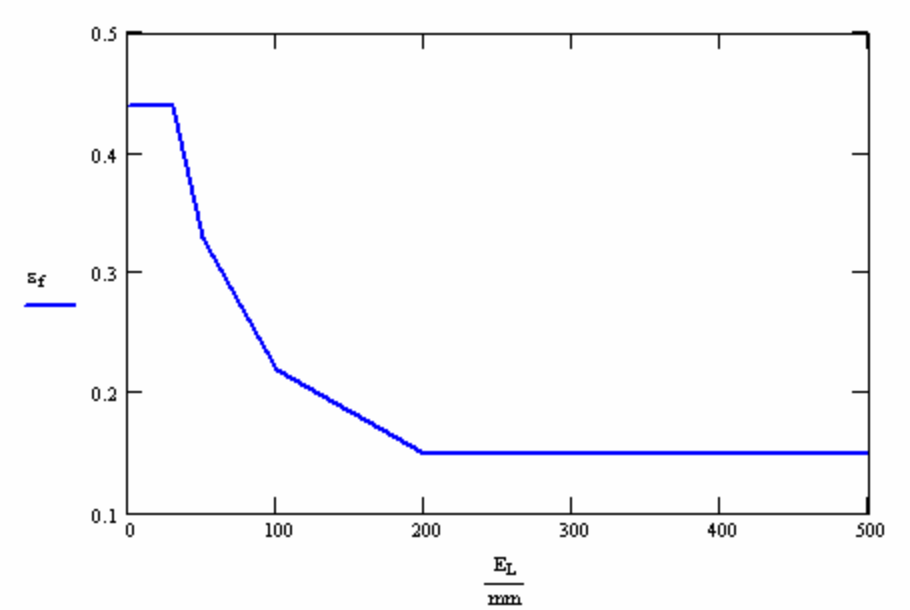

Figure 67 - Kitamura Necessary Failure Strain Results [57]

In this project, a Charpy-V-Notch (CVN) test is used to examine the relationship between the element edge length and dynamic numerical failure strain. This is a simple dynamic test to which a finite element model can be implemented.

The Charpy-V-Notch (CVN) test measures the total absorbed energy (Charpy energy) prior to fracture when impacting a material sample using a pendulum device as shown in Figure 68. A pendulum of a known mass is released from a known height and allowed to swing into the material sample located at the bottom of the pendulum's arc. The absorbed energy is calculated by measuring the height to which the pendulum swings after the impact.

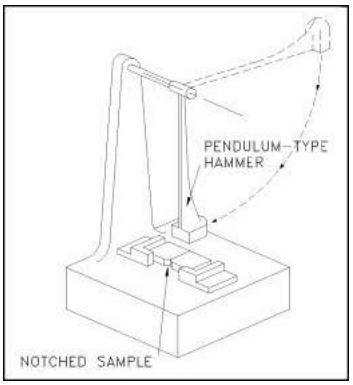

Figure 68 - Charpy-V-Notch (CVN) Test

The standard size of a CVN test specimen is specified by ASTM E23 and has the dimensions shown in Figure 69. The long dimension of the sample (55-mm) is cut parallel to the rolling direction of the steel.

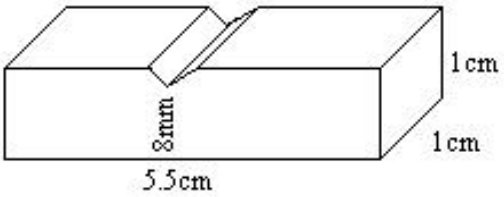

Figure 69 - Charpy-V-Notch (CVN) Sample Dimension

CVN Impact tests conducted on ABS GR. B materials at various temperatures by Francis, Cook and Nagy [76] yield the impact energy verses temperature plot shown in Figure 70. The transition from brittle to ductile behavior for these results occurs at 0 degrees Fahrenheit and the upper shelf impact energy (absorbed energy in full ductile behavior range) is approximately 57 ft-lb or 77.0 Joules.

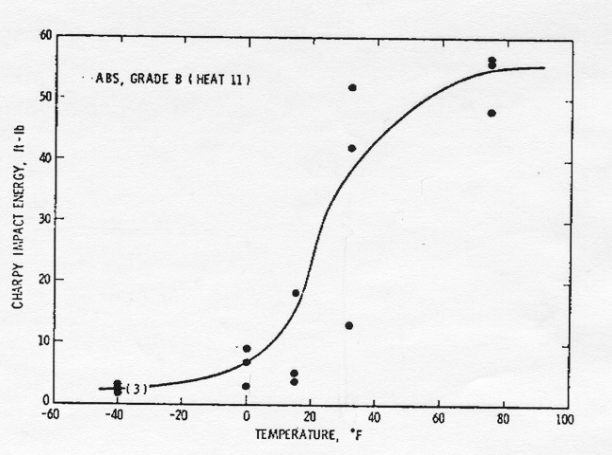

Figure 70 – Charpy Energy [76]

Figure 70 shows a large statistical error. Another SSC Study [77] reports an upper shelf impact energy of 112 ft-lb for the same material. Reproducibility is a common problem between facilities.

In this project, LSDYNA is used to model the CVN test results presented in Figure 70. The FEA absorbed energy is compared to the upper shelf absorbed energy from the Francis, Cook and Nagy [76] test (ABS GR. B – 57 ft-lbs). The finite element model of the CVN test specimen consists of a flat plate with a varying number of elements, fixed on either end, with a constant width of 10 mm and length of 55 mm (Figure 71 and Figure 72). The pendulum is modeled using a rigid shape matching the dimensions specified by ASTM E23. The test specimen is modeled based on material properties for ABS Grade B mild steel (Table 14) using a Piecewise-Linear-Isotropic-Plastic static stress strain curve defined by the points given in Table 14.

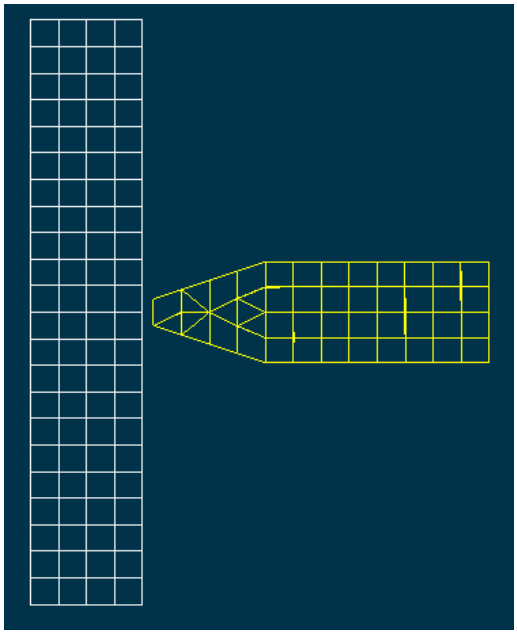

Figure 71 – CVN FEM

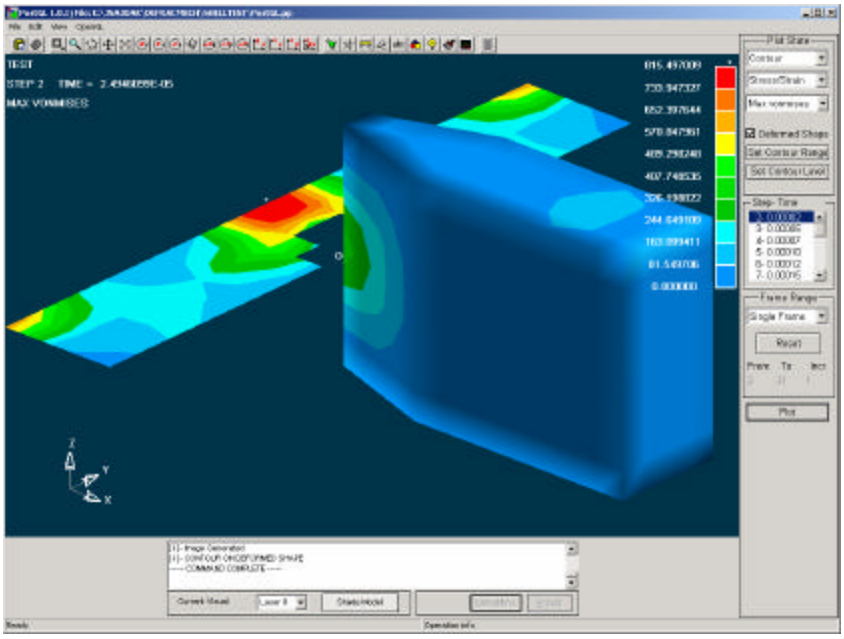

Figure 72 - CVN FEM

Table 13 - ABS Grade B Mild Steel Properties

Youngs Modulus	2.1E+5 MPa
Poissons Ratio	0.303
Yield Stress	2.35E+2 MPa
Cowper-Symonds Strain Rate Parameter C	40.4 sec^{-1}
Cowper-Symonds Strain Rate Parameter P	5
Mass Density	7.85E-9 $tonne/mm^3$

Table 14 – Stress-Strain Curve Definition

Strain	Stress (Mpa)
0.000E+0	2.350E+2
4.888E-2	2.350E+2
9.888E-2	3.517E+2
1.988E-1	4.276E+2
2.488E-1	4.138E+2
2.988E-1	3.793E+2
3.788E-1	3.103E+2
1.000E+0	0.000E+0

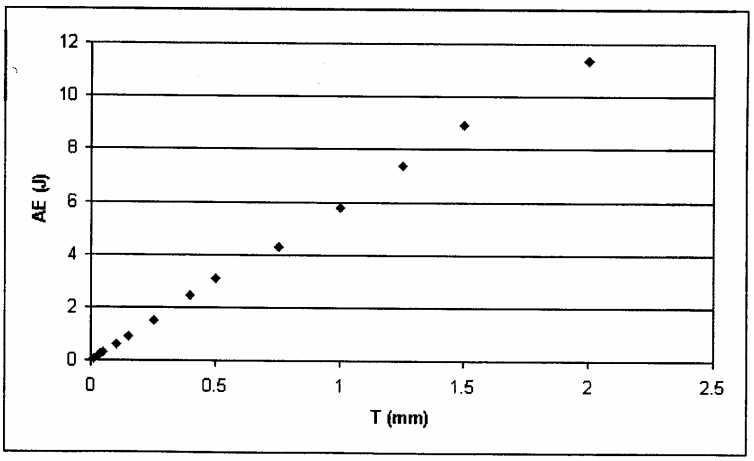

Figure 73 - FEA Charpy Energy versus Sample Thickness

For a given element type (Belytschko-Tsay shell element), and with all material properties except failure strain held constant, the FEA absorbed energy is a function of t, L and FS only. For a given failure strain and element length, the absorbed energy is a linear function of thickness as shown in Figure 73. Using dimensional analysis, AE/t is a function of the dimensionless parameters L/t and FS, Equation (5.7):

$$AE/t = F(L/t,FS) \tag{5.7}$$

By maintaining a constant failure strain of 5% in the LSDYNA CVN model, and varying the average element edge length and material thickness, numerical convergence of the AE/t parameter to a single value is shown to occur for L/t ratios greater than 2.5 (Figure 74). When L/t = 2.5, the FEA absorbed energy is only a function of the assumed failure strain and the sample thickness, and not element size. The panel model is sufficient in this regime.

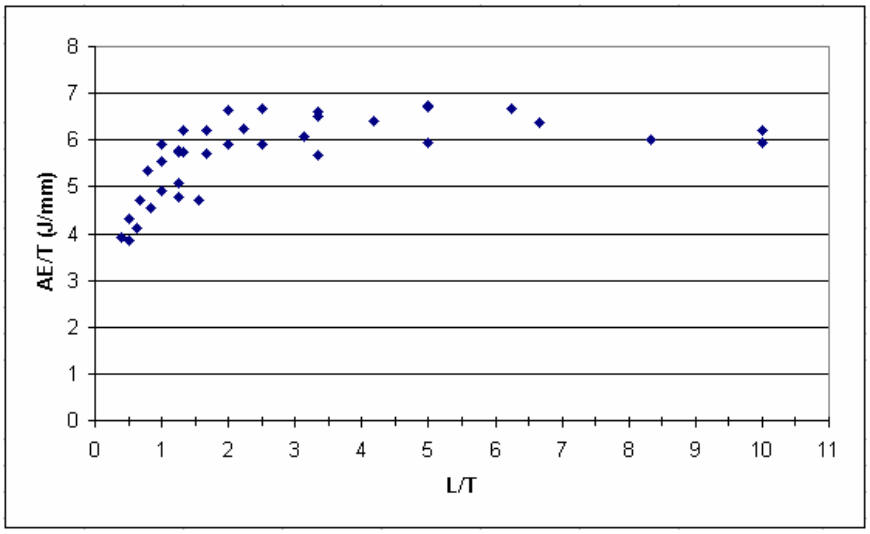

Figure 74 - FEA Charpy Energy versus L/t Ratio

Examination of the effect of failure strain (FS) on FEA absorbed energy, where the element thickness is 10 mm and L/t is 10.0, shows that the absorbed energy is linearly related to the failure strain (Figure 75), where AE is the absorbed energy in Joules divided by 10 and FS is the failure strain.

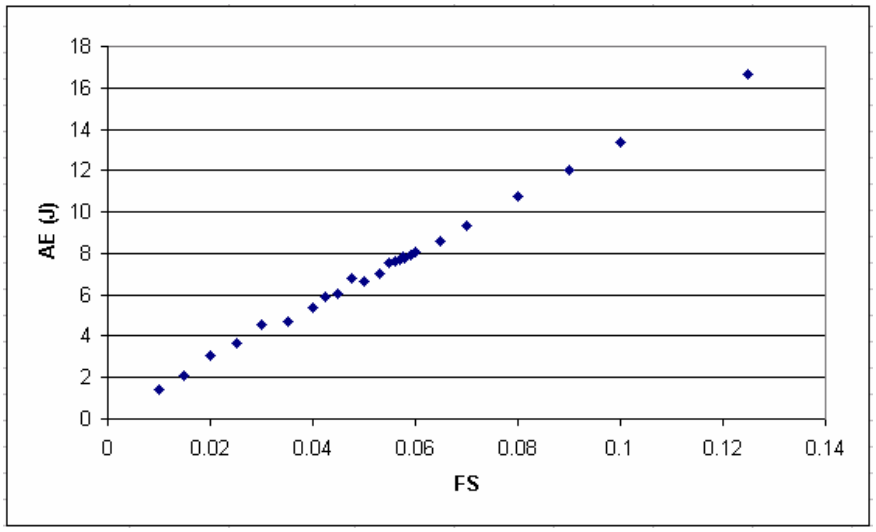

Figure 75 - FEA Charpy Energy versus Failure Strain (FS)

The numerical failure strain required to properly model a CVN test of ABS Gr. B mild steel using Belytchko-tsay elements (upper shelf energy = 77 Joules) is 5.74% when L/t = 2.5. Examination of larger structures must be performed to ensure the applicability of the above functional energy convergence method to large dynamic ship to ship collisions.

5.6 Typical Results

Numerical results for the LSDYNA collision simulation runs are provided and discussed with the other models in Section 6.3. Figure 76 shows typical upper bow deformation consistent with the photographs in Figure 37. Figure 77 through Figure 79 show typical shell damage results predicted by the model. Figure 80 through Figure 82 show bow penetration into the double side with damage to adjacent webs.

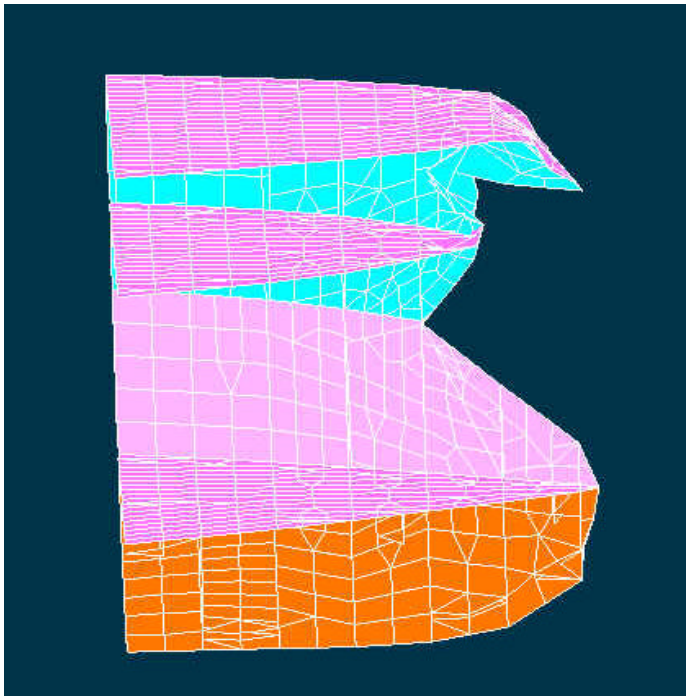

Figure 76- Folding-Down Upper Bow of Conventional Bow Model

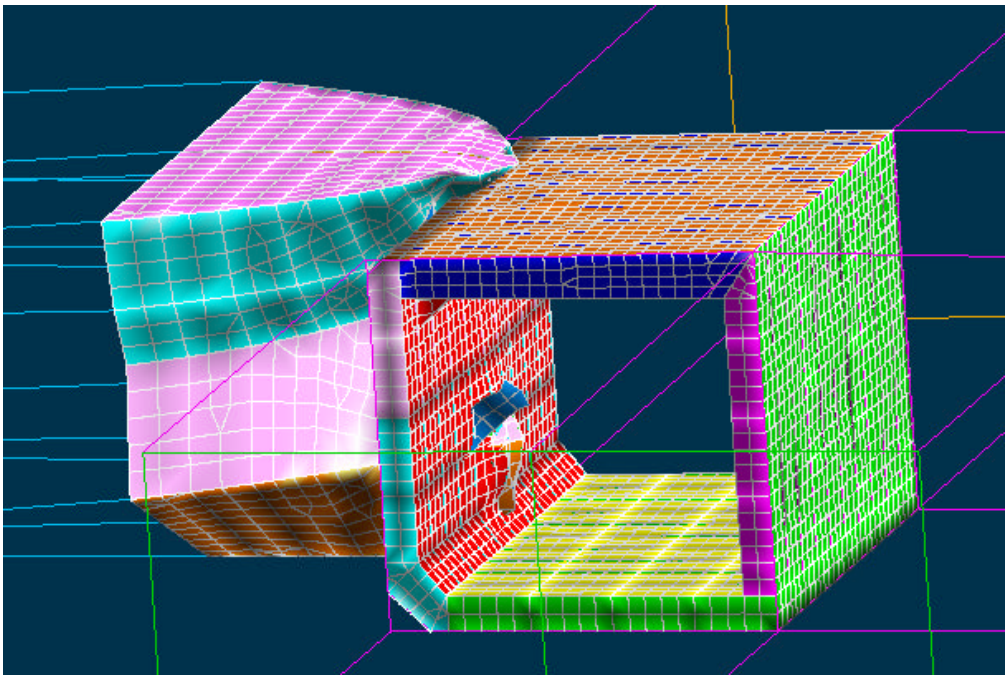

Figure 77 – Ship to Ship Collision Simulation

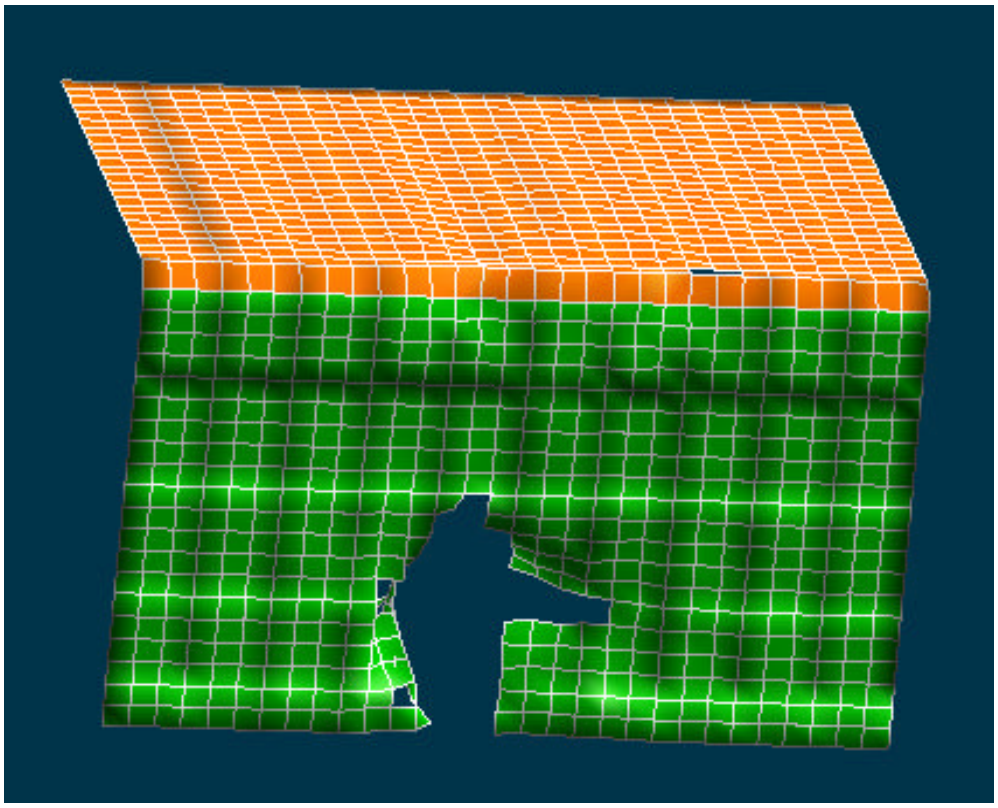

Figure 78 - Damaged Outer Shell and Deck for Double Hull Tanker

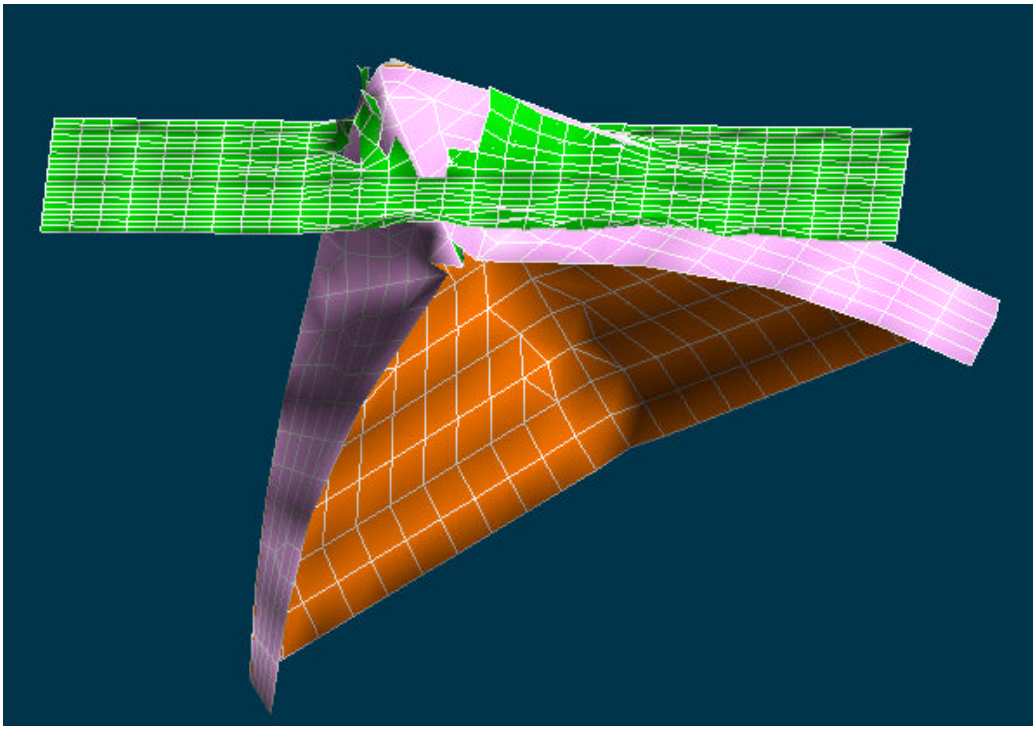

Figure 79 - Bulb of Striking Ship Penetrating Outer Shell of Struck Ship

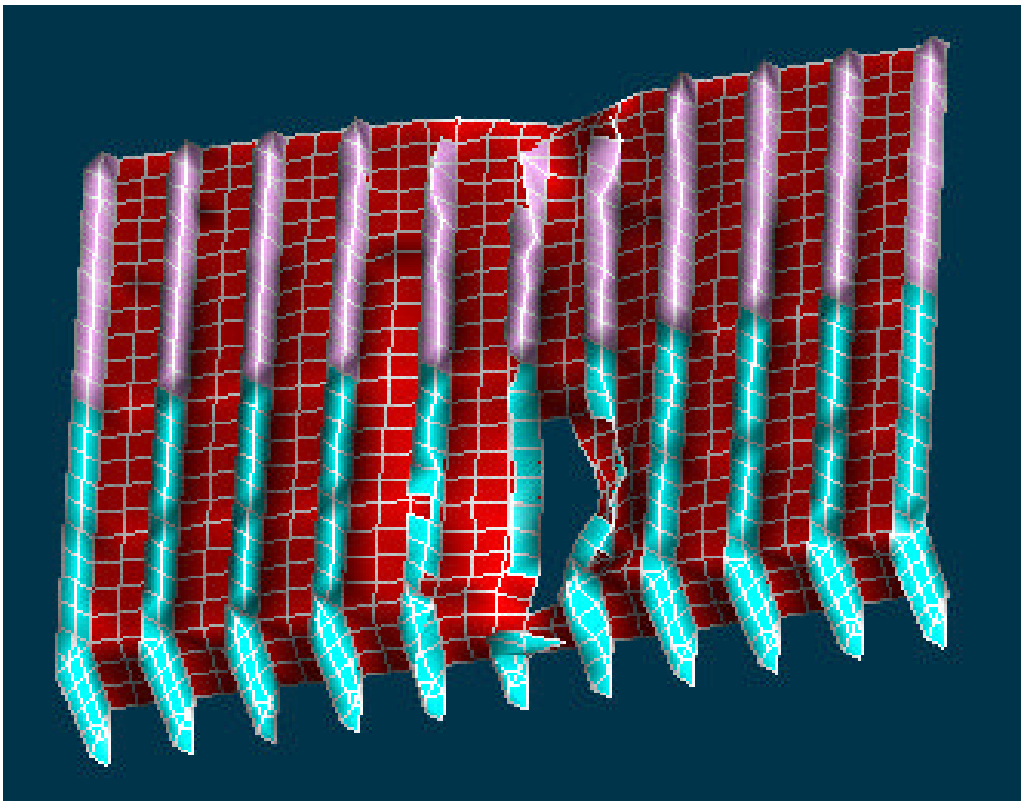

Figure 80 - Damaged Web and Shell of DH150

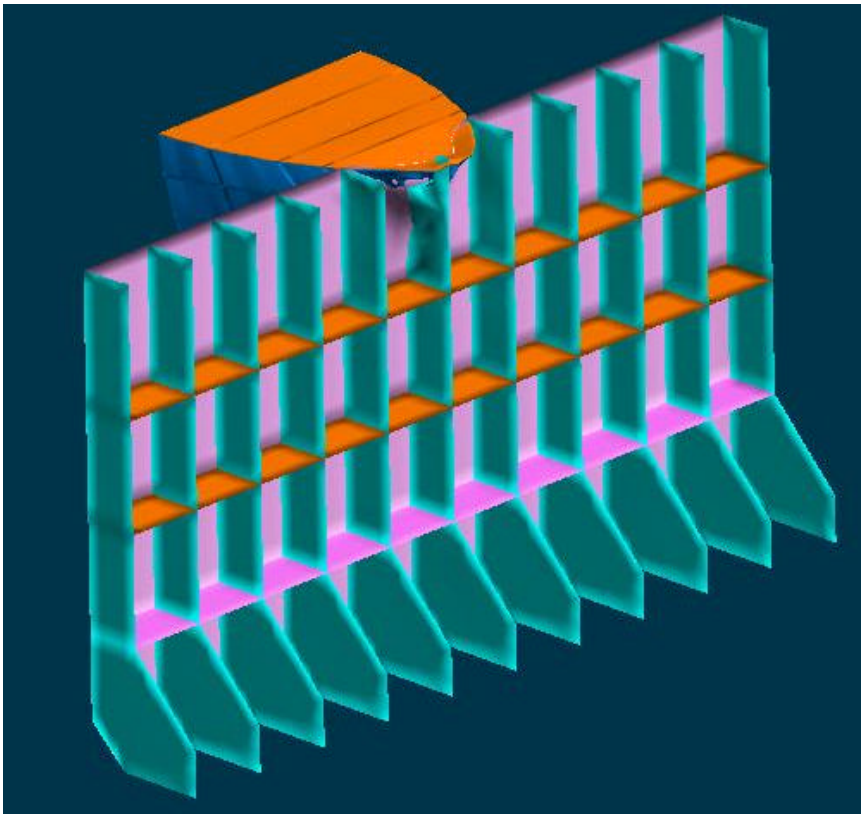

Figure 81 - Damaged Web and Shell of DH150

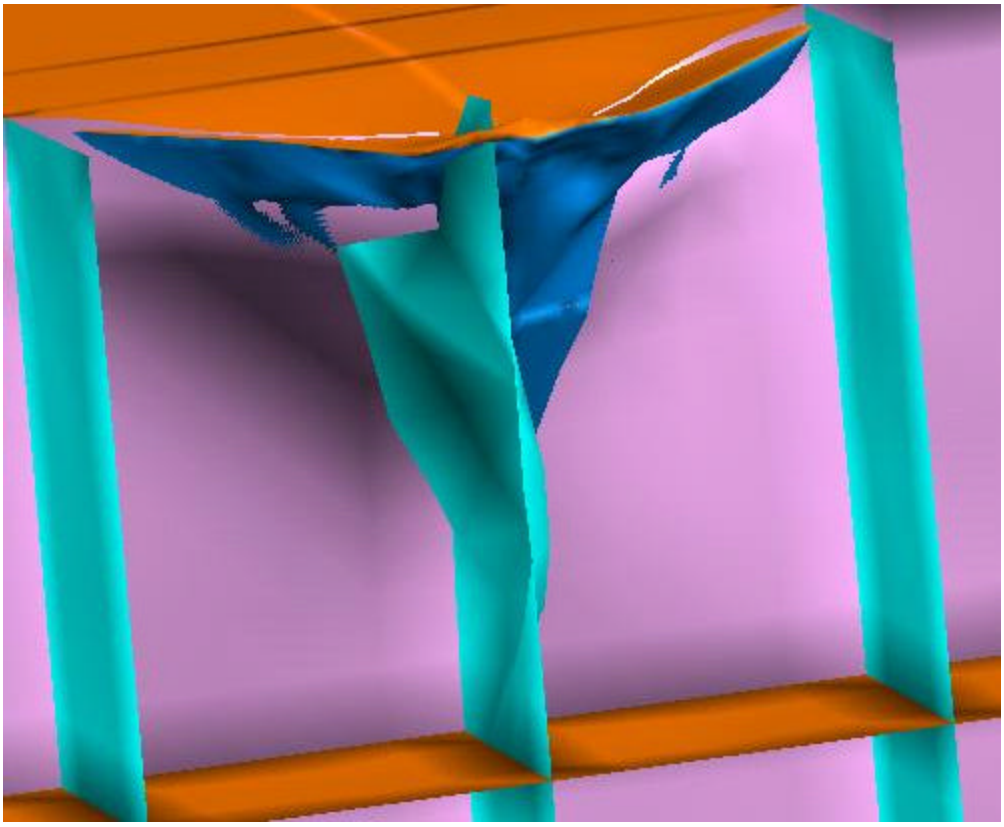

Figure 82 - Damaged Web and Shell of DH150

CHAPTER 6 SIMCOL Model Validation

Due to the lack of sufficient actual or model test data for proper SIMCOL model validation, preliminary validation is accomplished by comparison to other simplified and finite element results. The other simplified models include DAMAGE (MIT), ALPS/SCOL (Pusan National University, Korea), and a DTU (Technical University of Denmark) model. Finite element analysis is accomplished using LSDYNA. These four models take very different approaches to solving and coupling the internal and external collision problems. Although not a formal validation, comparison and agreement between these models provides useful insight into their performance and increases confidence in the validity of their results.

6.1 Other Simplified Models

6.1.1 DAMAGE (MIT)

The DAMAGE 4.0 collision module solves the external problem uncoupled from the internal problem, and applies the calculated absorbed energy to plastic deformation of the struck ship. Structural components, motions, masses etc. are described in ship coordinate systems local to each ship and in one global coordinate system. Degrees of freedom in DAMAGE include striking ship surge and struck ship sway and yaw.

DAMAGE 4.0 assumes that:

- Both ships are perpendicular before and during impact, i.e. only right angle collisions are considered.
- The forward motion of the struck ship is zero.
- The striking ship bow is rigid.

Based on conservation of linear momentum, angular momentum and energy, the model calculates ship velocities after impact and the loss of kinetic energy available for structural deformation. This is the external problem.

To determine the side deformation, the striking ship is moved into the struck ship in small increments. In each increment, the total resistance forces for penetration into the side are estimated and the incremental plastic deformation work is calculated. The bow is moved forward until the total work is equal to the loss of kinetic energy. DAMAGE 4.0 considers the material and structural scantlings of all major structural components of the side structure.

The model for the internal mechanics is based on the direct contact deformation of super-elements. The super-elements and mechanisms used to model the side in DAMAGE are:

- Shell and inner side plating (laterally loaded plastic membrane)
- Deck and girder crushing
- Beam loaded by a concentrated load
- X-, L- and T-form intersections crushed in the axial direction

The bow geometry is defined using eight parameters. Figure 83 shows an example of a typical bow geometry.

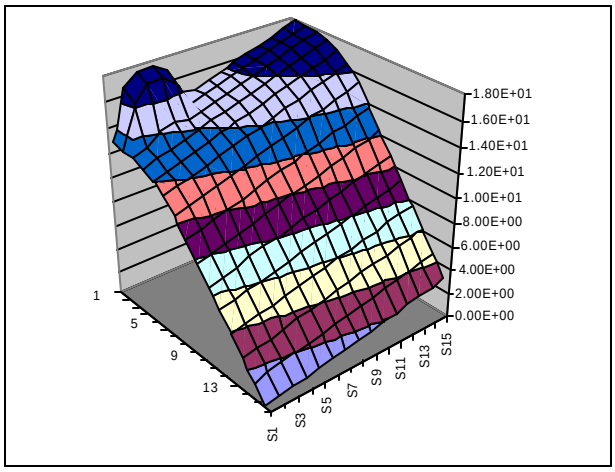

Figure 83 - DAMAGE Bow Geometry

6.1.2 ALPS/SCOL (Pusan National University, Korea)

ALPS/SCOL is a coarse-mesh 3-D non-linear finite element code using super-elements based on the Idealized Structural Unit Method (ISUM) [28,29]. The geometry of the striking and the struck ships is described in a global (three-dimensional) rectangular coordinate system. The stress in an ISUM unit is described in a local element coordinate system. ALPS/SCOL considers sway and yaw of the struck ship with the following assumptions:

- The added masses of the striking and the struck ships are calculated based on ships of similar type and size using a linear strip theory-based computer program.
- The striking ship is assumed to be rigid.
- The analysis of the external and the internal dynamics is undertaken separately.
- The longitudinal velocity of the struck ship is not considered.

Since ALPS/SCOL is based on a simplified 3-D nonlinear finite element approach, damage in three directions (penetration, vertical and horizontal damage) is considered. The geometry of the striking ship bow shape is described by gap/contact elements. One cargo hold of the struck ship is taken as the extent of the struck ship analysis. ISUM stiffened panel units are used to model the struck vessel structure.

The geometry of the struck ship is described using 600 rectangular or triangular ISUM units. If the deformation of the struck ship is symmetric, the total degrees of freedom in the numerical model are reduced by half. Each node has 3 degrees of freedom. Figure 84 shows damage calculated in a typical ALPS/SCOL simulation.

Design data required for the striking ship includes a detailed bow geometry description, length, beam, depth, draft and displacement. Design data for the struck ship includes, length, beam, depth, draft and displacement, transverse bulkhead location, COG, and detailed structural design and scantlings. Scenario data required includes striking ship velocity and longitudinal location of impact in the struck ship.

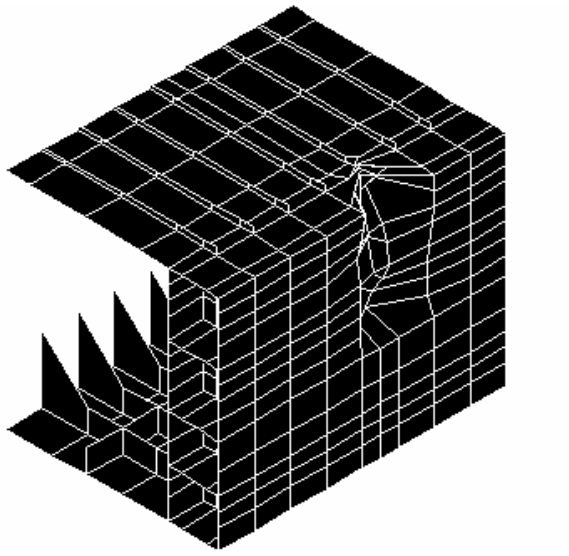

Figure 84 - Damage from ALPS/SCOL Simulation

6.1.3 DTU Model

The Technical University of Denmark (DTU) model also solves the external problem uncoupled from the internal problem, and applies the calculated absorbed energy to plastic deformation of the struck ship.

Solution of the external dynamics is accomplished based on an analytical method developed by Pedersen and Zhang [14]. This method estimates the fraction of the kinetic energy that is available for deformation of the ship structure. The energy loss for dissipation by structural deformation is expressed in closed-form expressions. The procedure is based on a rigid body mechanism, where it is assumed that there is negligible strain energy for deformation outside the contact region, and that the contact region is local and small. This implies that the collision can be considered instantaneous as each body is assumed to exert an impulsive force on the other at the point of contact. The model includes friction between the impacting surfaces so those situations with glancing blows can be identified. Both ships have three degrees of freedom: surge, sway and yaw. The interaction between the ships and the surrounding water is approximated by simple added mass coefficients, which are assumed to remain constant during the collision.

The loss in kinetic energy by the method is determined in two directions, perpendicular and parallel to the side of the struck ship. Both right and oblique angle collisions are considered and both vessels may have velocity before the collision.

The model for the internal mechanics is based on a set of super-elements, where each element represents a structural component. The calculation method is based on the principle that the area of the struck vessel affected by the collision is restricted to the area touched by the striking vessel. The super-elements and mechanisms are:

- Lateral plate deflection and rupture. Large deflections are assumed; this implies that the bending resistance can be neglected
- Crushing of structure intersection elements (X- or T-elements)

- In-plane crushing and tearing of plates
- Beam deflection and rupture

The design data for the struck vessel includes length, beam depth, draft, displacement, COG and detailed structural design and scantlings. The bow of the striking vessel is assumed to be rigid. The basic data for describing the striking ship bow are stem angle, breadth and bow height. The horizontal shape of the deck and the bottom are assumed to be parabolic. If the striking vessel is equipped with a bulb, this is assumed to have the form of an elliptic parabola. Scenario data required includes striking and struck ship velocity, collision angle and longitudinal location of impact at the struck vessel.

6.2 Validation Cases

In order to assess SIMCOL's consistency and sensitivity, SIMCOL results are compared to the results of the other simplified models and LSDYNA for a range of collision cases. Three validation case matrices are used. Table 15 lists the data for each matrix.

Table 15 - Validation Cases

	Struck Ship Speed (knt)	Striking Ship Speed (knt)	Collision Angle (deg)	Strike Location (m fwd MS)
Matrix 1	0	3,4,5,6,7	90	-62.5,29.5, 3.5,36.5, 69.5,102.5
Matrix 2	0	3,4,5,6,7	90	1.85,2.675, 3.5,4.325, 5.15
Matrix 3	0	3,4,5,6,7	45,60,75, 105,120,135	3.5

The struck tanker design in all of these cases is a 150000 dwt double-hull tanker (DH150). It's dimensions are consistent with the dimensions of the 150000 dwt reference tanker in the IMO Interim Guidelines [4]. HECSALV and SafeHull are used to develop the details of the design, and to insure that the arrangement satisfies IMO regulations and the structural design satisfies ABS classification requirements. The 150000 dwt struck tanker design is shown in Figure 85. Table 16 and Table 17 list the principal characteristics and structural data for this design. The striking ship in all cases is a 150000 dwt bulk carrier (BC150) that has been used by other researchers in collision studies [22]. The striking ship principal characteristics are listed in Table

18 and its bow profile is shown in . The vertical alignment of these two ships at the start of the collision event is shown in Figure 87.

The first test matrix considers damage for a series of strike locations on the web at the center of each struck ship cargo tank. This represents a large global variation in strike longitudinal location. The second test matrix considers damage for a series of strike locations on either side of the web at the center of the midship cargo tank. This represents a relatively small local variation in location on and between webs. The third test matrix considers damage for a series of collision angles with a strike location on the web at the center of the midship cargo tank.

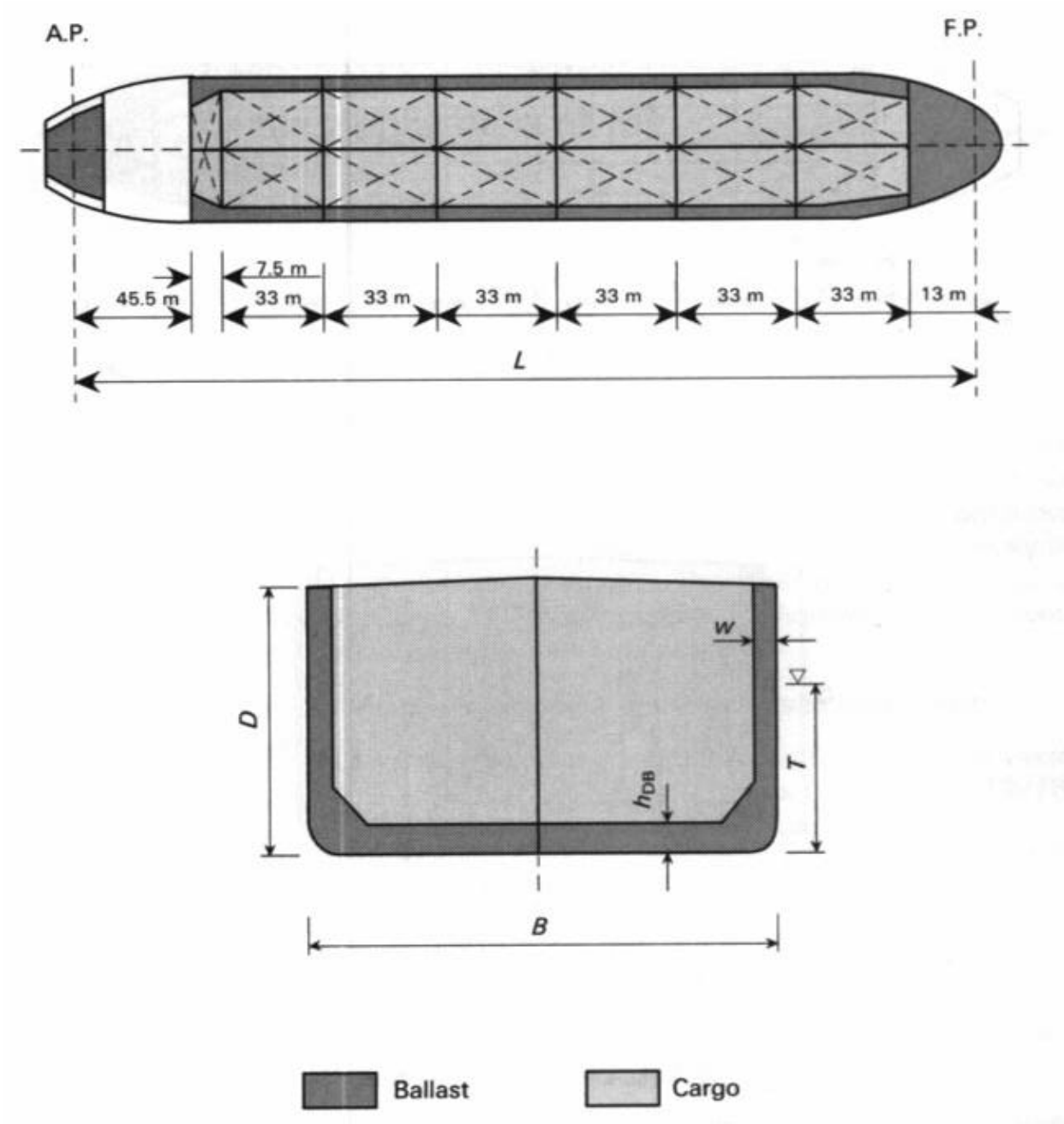

Figure 85 - Struck Ship Design [3]

Table 16 - Struck Ship Principal Characteristics

Deadweight, tonnes	150,000
Length *L*, m	264.00
Breadth *B*, m	48.00
Depth *D*, m	24.00
Draft *T*, m	16.80
Double Bottom Ht h_{DB}, m	2.32
Double Hull Width *W*, m	2.00
Displacement, tonnes	178,867

Table 17 – Stuck Ship Structural Characteristics

Ship		150,000 dwt double hull tanker
Web Frame Spacing L_s, m		3.30
Smeared Thickness t_h, mm	Deck	47.32
	Inner Bottom	26.92
	Bottom	28.29
	Stringers	3 ⌖15.34
Smeared Thickness t_v, mm	Side Shell	21.92
	Inner Skin	22.94
	Bulkhead	22.28
Web Thickness t_w, mm	Upper	12.00
	Lower	18.00

Table 18 - Striking Ship Principal Characteristics

Ship Type	150,000 dwt bulk carrier
Length *L*, m	274.00
Breadth *B*, m	47.00
Depth *D*, m	21.60
Bow Height *H*, m	26.00
Draft *T*, m	15.96
Displacement, tonnes	174,850
Half Entrance Angle, α	38°

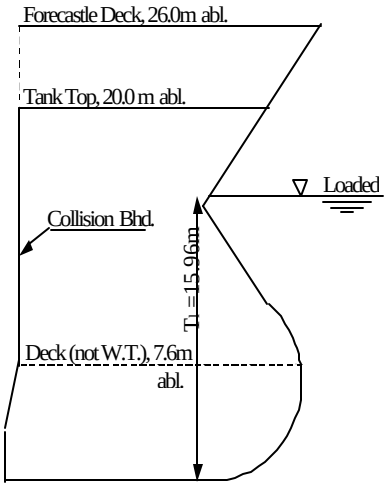

Figure 86 – Striking Ship Bow Profile

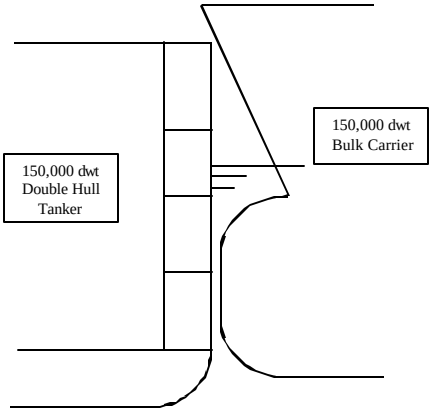

Figure 87 - Collision Strike Vertical Alignment

6.3 Validation Results

Validation results for struck ship penetrations are shown in Figures Figure 88 through Figure 93. The figures show transverse penetration into the struck ship as a function of the particular variables in each matrix. The results show good agreement in penetration magnitude between the models. DAMAGE generally predicts the lowest penetration, and ALPS/SCOL generally predicts the highest. SIMCOL results fall between these extremes.

Figure 88 and Figure 89 (Matrix 1) show the effect of the external dynamics. More energy is absorbed in strikes around midship causing more penetration because less kinetic energy is dissipated in struck ship yaw. All of the models capture this trend.

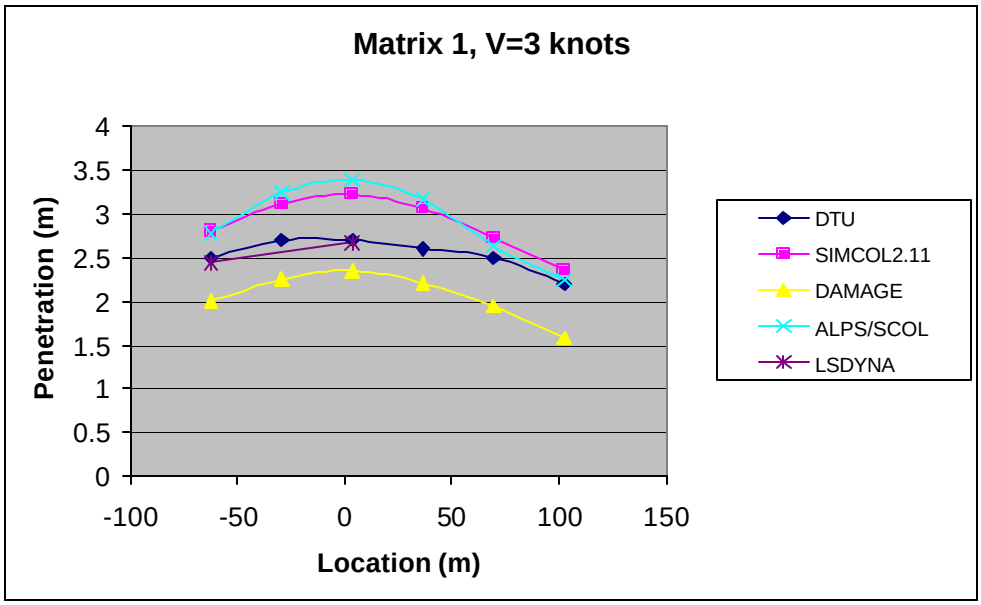

Figure 88 – Matrix 1 Low Energy Collision

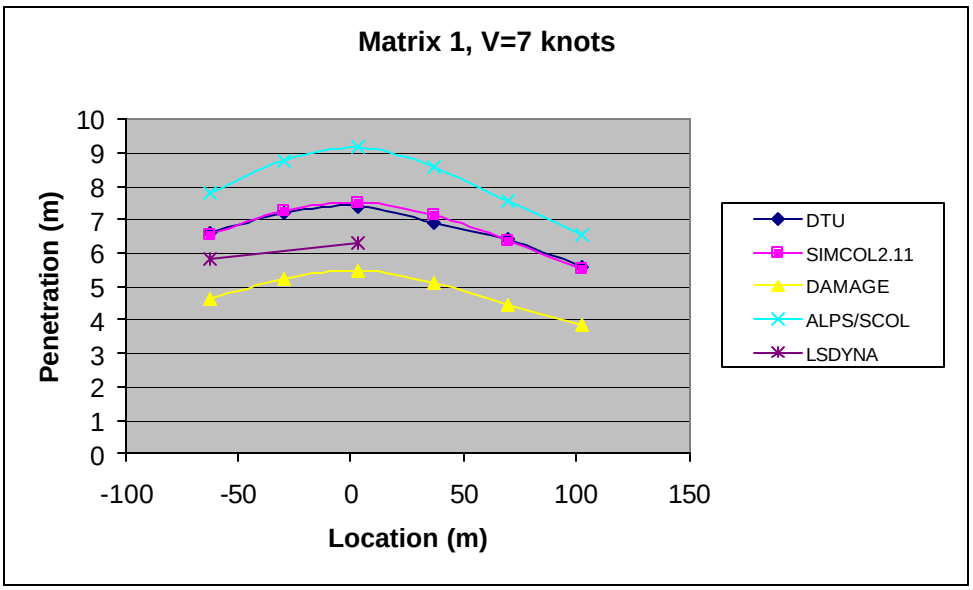

Figure 89 – Matrix 1 High Energy Collision

Although the Matrix 2 results for the different models are similar in magnitude, Figure 90 and Figure 91 show different trends for strikes on the web. SIMCOL predicts higher penetration on the web because of bending failures between the web and the shell and the web and the inner hull. The web is effectively driven into the hull. The other models do not capture this mechanism.

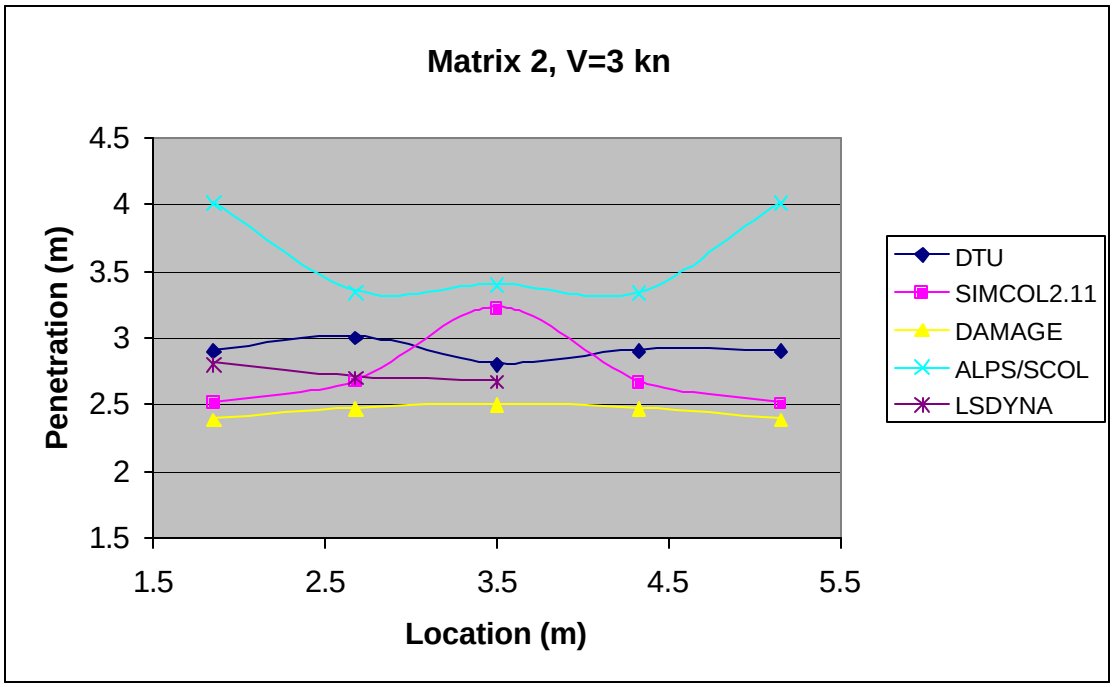

Figure 90 – Matrix 2 Low Energy Collision

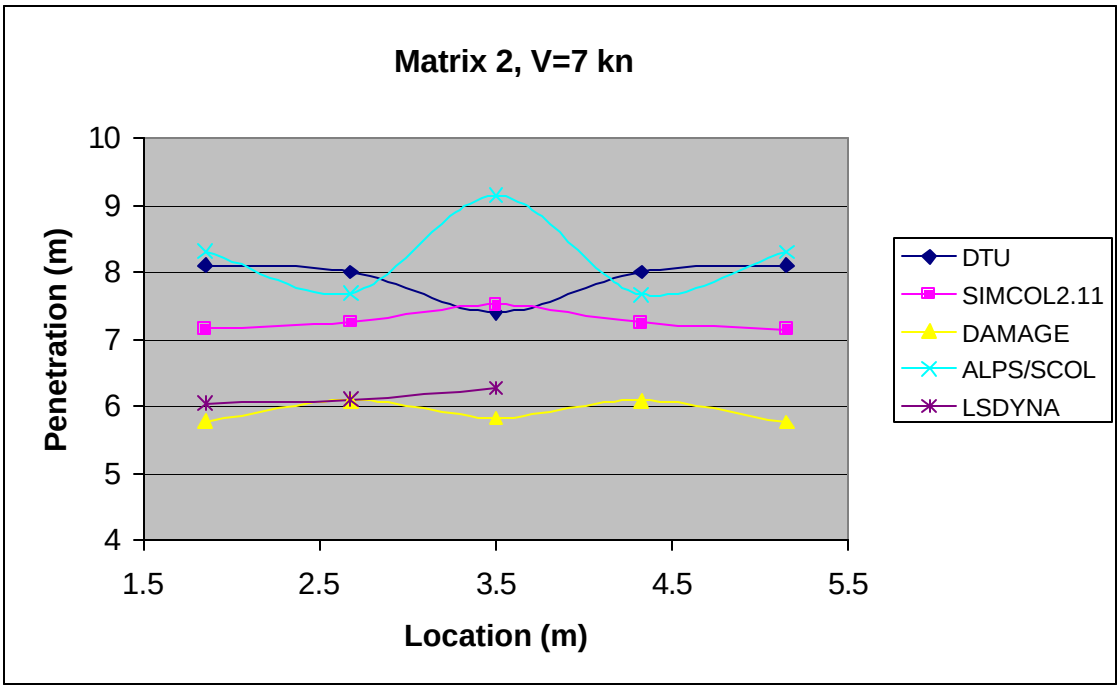

Figure 91 – Matrix 2 High Energy Collision

Figure 92 and Figure 93 (Matrix 3) also show the effect of the external dynamics. More energy is absorbed in right angle collisions and there is more penetration in these cases. Kinetic energy is not dissipated in struck ship yaw. All of the models capture this trend. The current version of DAMAGE is only able to consider right angle collisions, so DAMAGE is not used in Matrix 3.

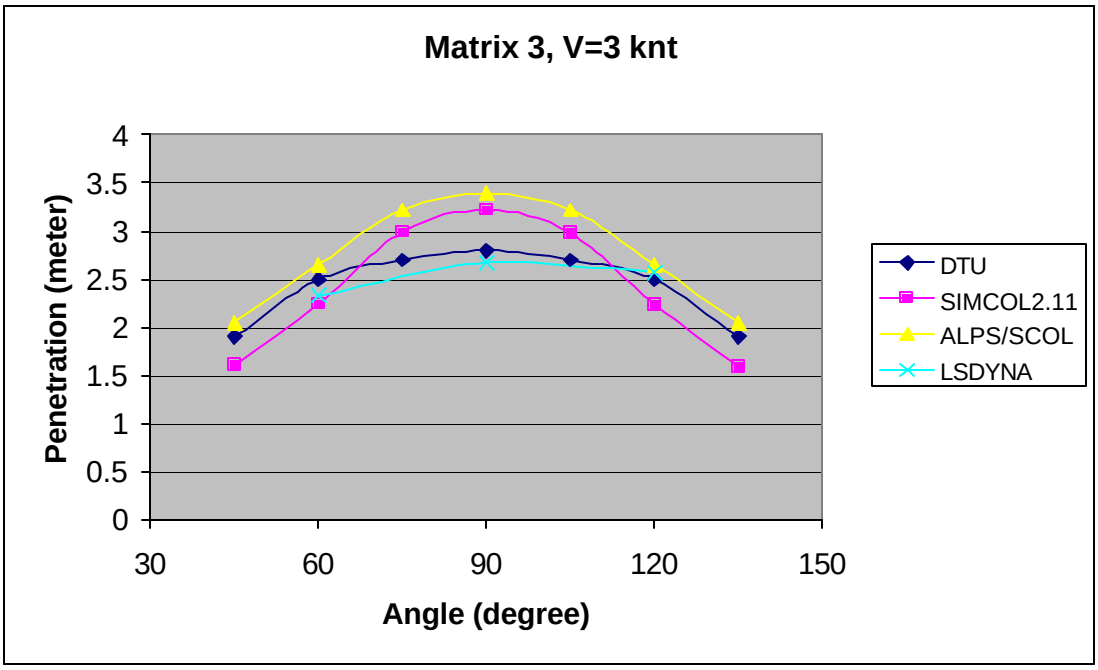

Figure 92 – Matrix 3 Low Energy Collision

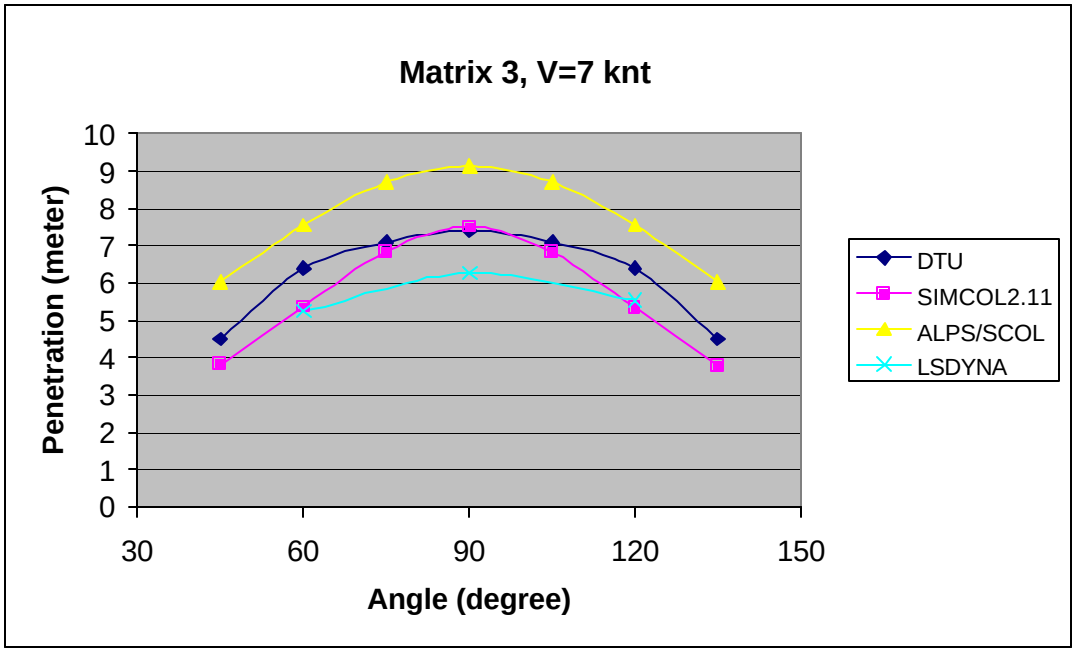

Figure 93 – Matrix 3 High Energy Collision

Although not a validation, the results from five very different models are remarkably similar, and this increases confidence in their results. SIMCOL results are less homogeneous for different scenarios because of SIMCOL's coupling to external mechanics. The SIMCOL bow geometry may be oversimplified, but at least for these test cases, it provides consistent and sufficient results. The advantage of this simplified geometry is its single parameter description (half-entrance angle) which facilitates its application for probabilistic analysis.

CHAPTER 7 Probabilistic Modeling of the Collision

Collisions are high consequence, low probability events. Because of this high consequence, most collisions involve litigation and sometimes years of legal proceedings. The focus of these proceedings is frequently on human error vice a precise technical analysis of what happened and what resulted. For these reasons, complete technical data describing the struck and striking ship, the collision event, and the resulting damage is very difficult to obtain even when it exists.

Data required by SIMCOL 2.1 to describe the collision event include:

- Struck ship design parameters
- Struck ship variables – speed, trim, draft or displacement
- Event variables - collision angle (ϕ), strike location (l)
- Striking ship variables – type, dwt, speed, displacement, length, beam, bow half-entrance angle (HEA), draft at bow

Except for the struck ship design parameters, these are all random variables with varying degrees of dependency, some discrete and some continuous. Two primary data sources are used in this study to determine the probabilities and probability density functions necessary to define these random variables:

- 1998 Sandia Report [78].
- 1993 Lloyd's Worldwide Ship data [79].

The Sandia Report [78] considers collision data from 4 sources:

1. Lloyd's Casualty Data for 1973 to 1993 – contains 30,000 incident reports of which 1947 were ship to ship collision events, 702 of which occurred in ports. This data was used primarily to estimate the probability and geographical location of collisions and fires that could harm nuclear flasks. It did not include specific scenario and technical data. It is not directly applicable to collision scenarios.
2. ORI Analysis, 1980 [80] – includes a summary of data from cargo vessel accidents in 1974 and 1975 for 78000 transits of ships over 5000 gross tons. Most of this data is from the USCG Commercial Vessel Casualty File. It includes 216 collisions for ships in US waters or US ships in international waters. 8 collisions of tankers and cargo ships and other tanker accidents from the ECO World Tanker Accident file are also included. This totals 1122 cargo ship accidents. 115 are struck cargo ship collisions with more than 90 percent of these in inland and coastal waters. The study addresses the probability of various accident types.
3. ORI Analysis, 1981 [81] – Includes the probability of striking ship displacement, speed, collision angle and collision location for struck cargo ship collisions.
4. Engineering Computer Optecnomics, Inc (ECO) World Fleet Data.

Applicable subsets of this data are described here.

7.1 Collision Probability

The Lloyd's accident data referenced in the Sandia Report [78] is extensive. Although it provides little detail on the collision scenario and damage, the statistics on geographical location and probability of occurrence are informative. Figure 94 and Figure 95 show that collisions occur primarily in near-shore areas where there is a high concentration of ships approaching ports. This is not surprising. Collision probabilities per nautical mile sailed are approximately 2×10^{-7}. Collision frequency per port call is approximately 4×10^{-5}.

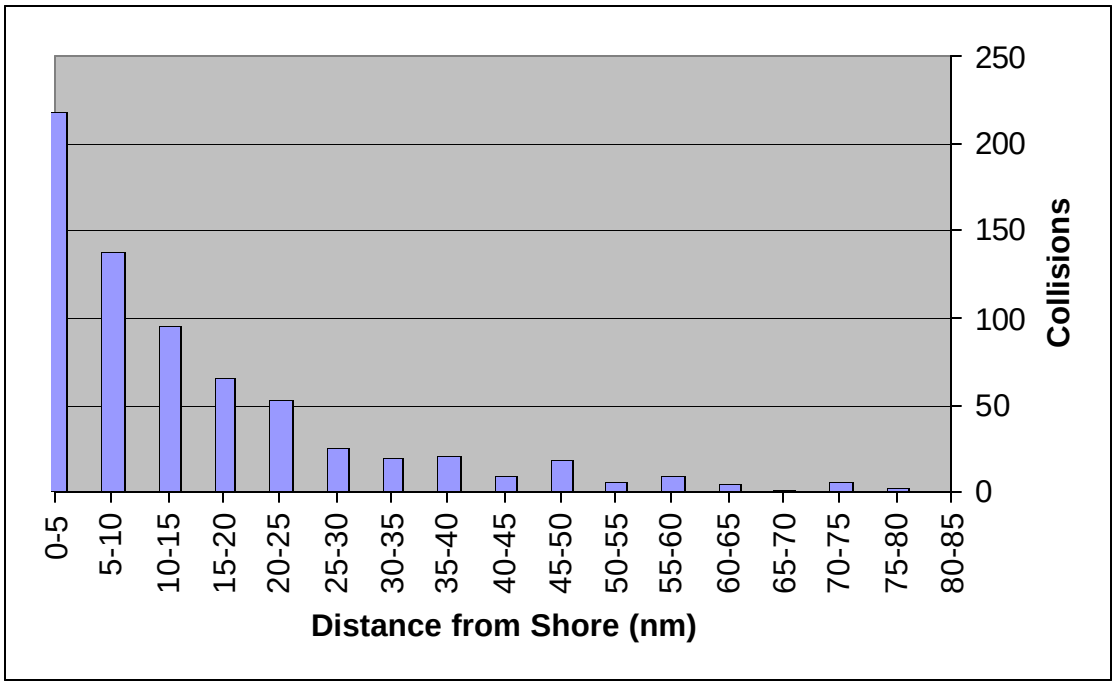

Figure 94 - Collisions, 1973-1993 All Ships Worldwide [78]

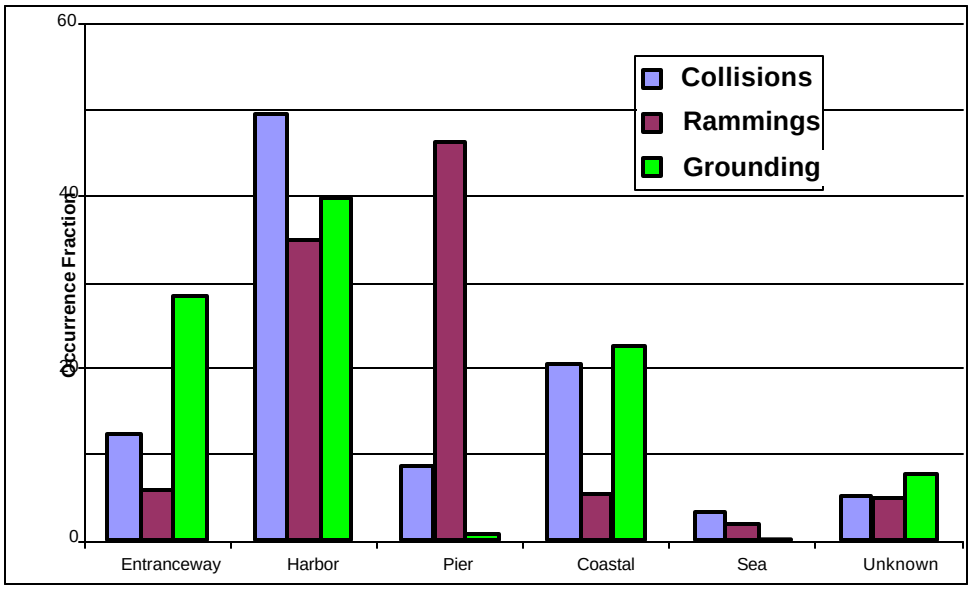

Figure 95 - Accident Location [78] – Worldwide Tanker Data, 1969-1974

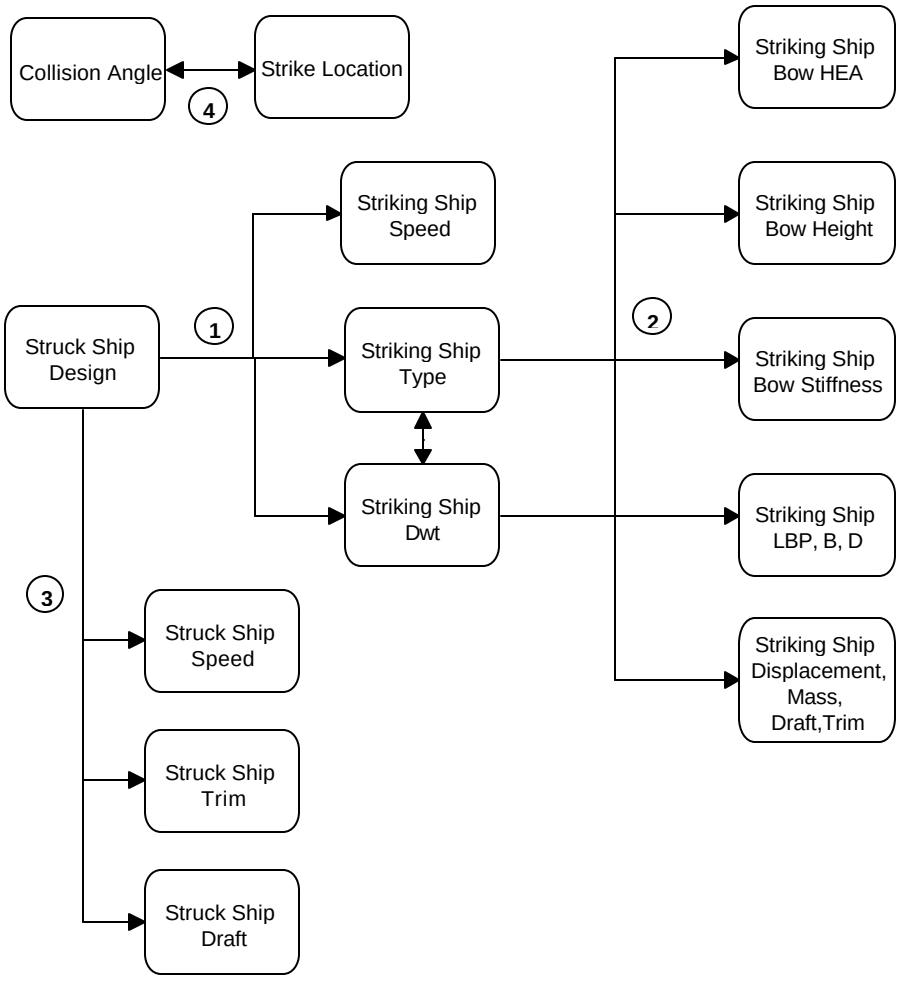

Figure 96 – Collision Event Variables

7.2 Collision Event Random Variables

Collision event random variables are not expected to be fully independent, but their interdependence is difficult to quantify because of limited collision data. Figure 96 provides a framework for defining the relationship of scenario variables. Available data are incomplete to fully quantify this relationship. Strike location must often be inferred from the damage description because a reliable record of the precise location is not available. Ship heading and speed prior to the collision are often included in accident reports, but collision angle and ship speed at the moment of collision are frequently not included or only estimated and described imprecisely. Expected dependencies, labeled Numbers 1 through 4 in Figure 96, are:

1. Striking ship type and displacement. This data may come from actual collision events or from ship encounter data. Worldwide ship characteristics may also be used if it is assumed that a given struck ship encounters a representative sample of all worldwide ships. Actual collision data is very limited and encounter data is difficult to obtain. This report develops the striking ship type probability and the corresponding striking ship displacement probability density functions from worldwide data. The striking ship type is treated as an

independent random variable, and a unique striking ship displacement probability density function is developed for each type. It is expected that there should be some degree of bias for striking ships to be similar in size and type to struck ships. Similar ships operate on similar routes. This bias would not be reflected in worldwide data. Data required to access the extent of this bias is very limited. The striking ship collision speed is also treated as an independent random variable. Its probability density function is developed from actual collision data. Collision speed is the striking ship speed at the moment of collision, and is not strongly dependent on service speed. It depends primarily on actions taken just prior to collision and its probability density function is assumed to be the same for all ships.

2. Striking ship principal characteristics. Other striking ship principal characteristics are treated as dependent variables, and they are derived from striking ship displacement and type based on regression analysis of worldwide ship data. Given a specific type and displacement of striking ship, other principal characteristics are strongly related. Principal characteristics include length, beam, draft, bow half entrance angle, bow height, and bow stiffness or structural design.
3. Struck ship draft, trim and speed. A specific struck ship with known design characteristics in a specific trade will have specific distributions for draft, trim and speed. In this report, full load draft and zero trim are assumed. Struck ship speed is treated as an independent random variable. The probability density function for struck ship speed is developed from actual collision data.
4. Collision angle and strike location. When two ships are maneuvering to avoid a collision (in-extremis), it is expected that the resulting collision angle and strike locations are related, but there is insufficient data to quantify this relationship. In this report, they are treated as independent random variables. The probability density functions for collision angle and strike location are developed from actual collision data.

7.2.1 Striking Ship Type and Displacement

Figure 97 provides probabilities of the struck ship encountering specific ship types. These probabilities are based on the fraction of each ship type in the worldwide population in 1993 [79]. Each of the general types includes a number of more specific types:

- Tankers – includes crude and product tankers, ore/oil carriers, LPG tankers, chemical tankers, LNG tankers, and oil/bulk/ore carriers
- Bulk carriers - includes dry bulkers, ore carriers, fish carriers, coal carriers, bulk/timber carriers, cement carriers and wood chip carriers
- Freighters – includes general freighters and refrigerated freighters
- Passenger – includes passenger and combo passenger/cargo ships
- Containerships – includes containerships, car carriers, container/RO-ROs, ROROs, bulk/car carriers, and bulk/containerships

It is likely that particular ships are more likely to meet ships of the same type since they travel the same routes, but this relationship could not be established with available data. Additional collision data must be obtained to establish this relationship.

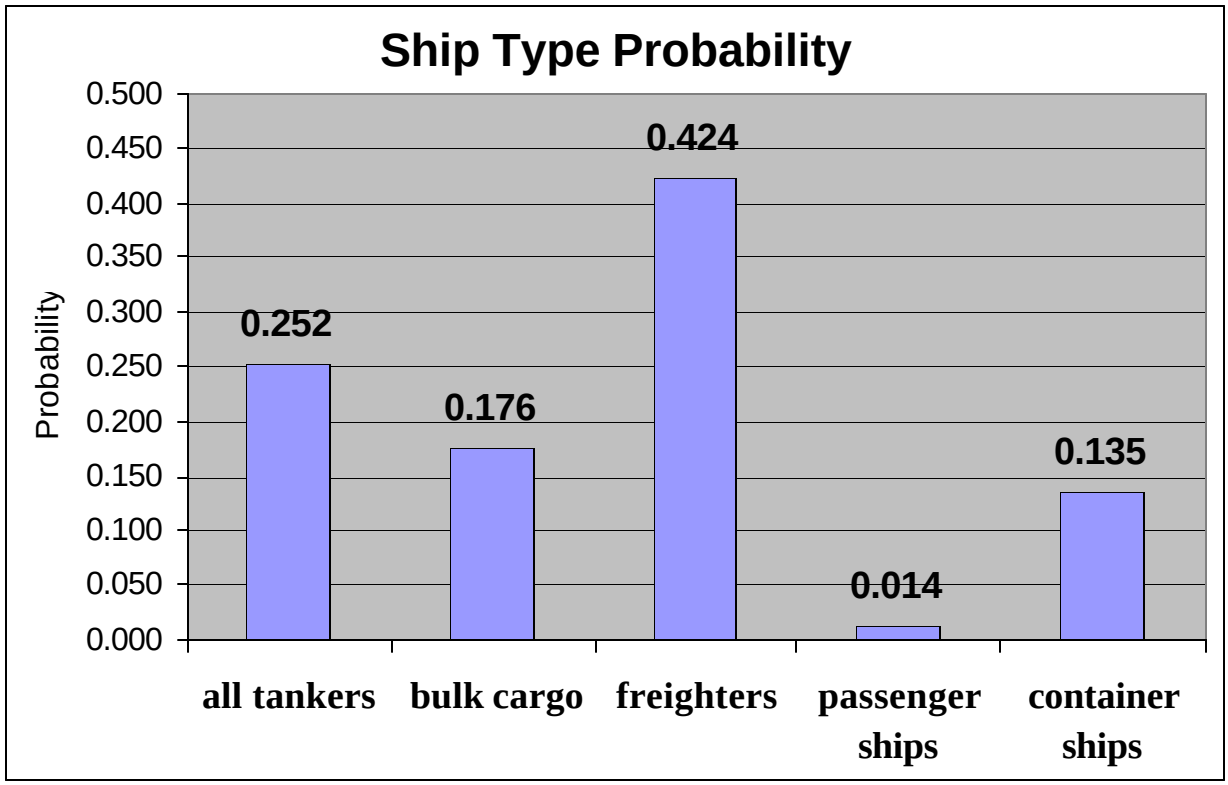

Figure 97 – Ship Type Probability [79]

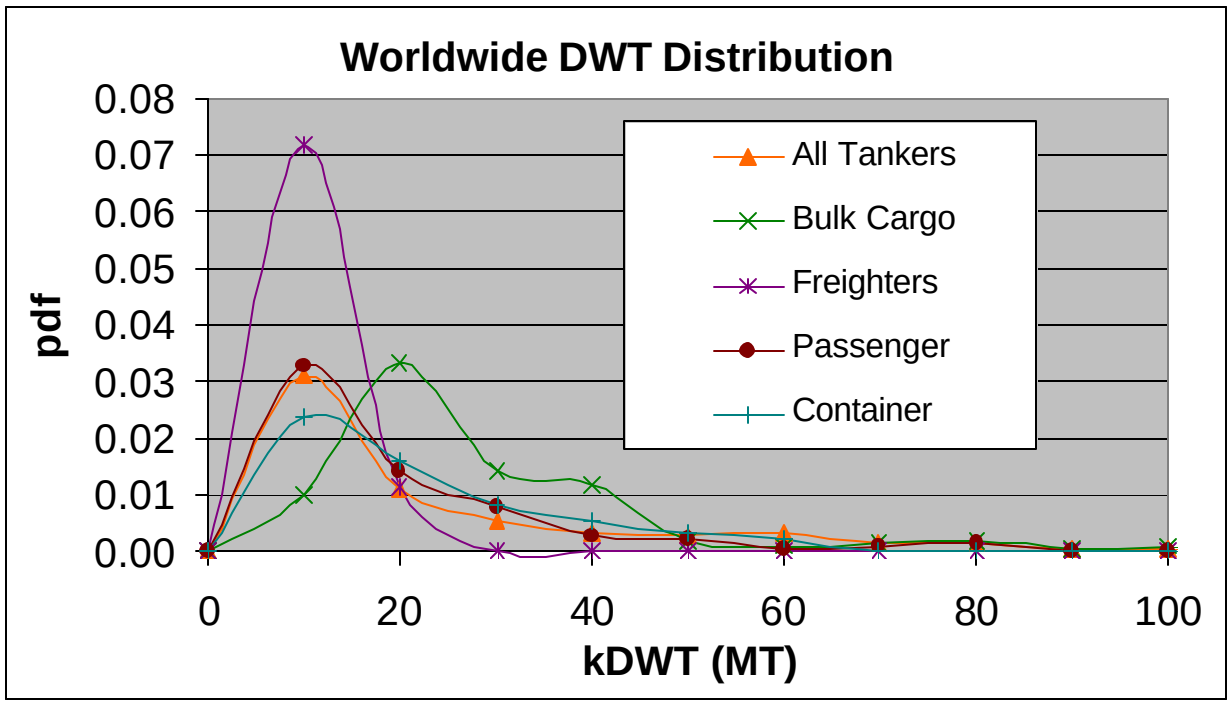

Figure 98 - Striking Ship Displacement, Worldwide Distribution

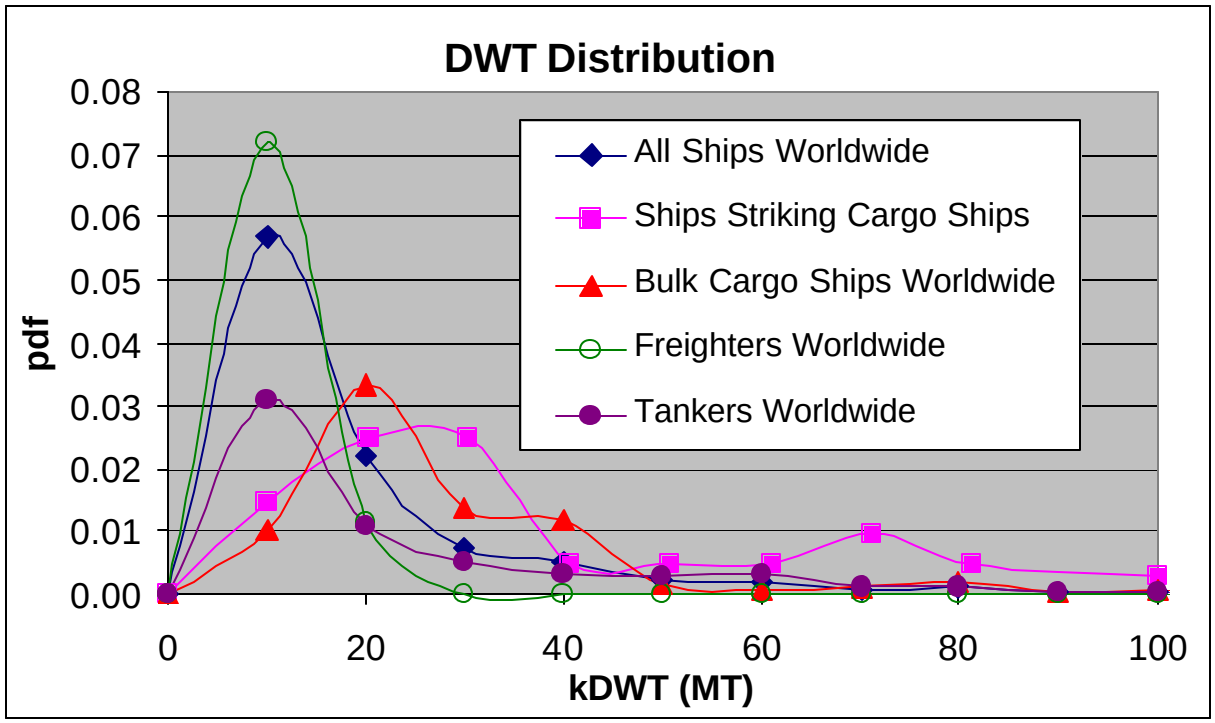

Figure 99 – Displacement of Ships Striking Bulk Carriers [78]

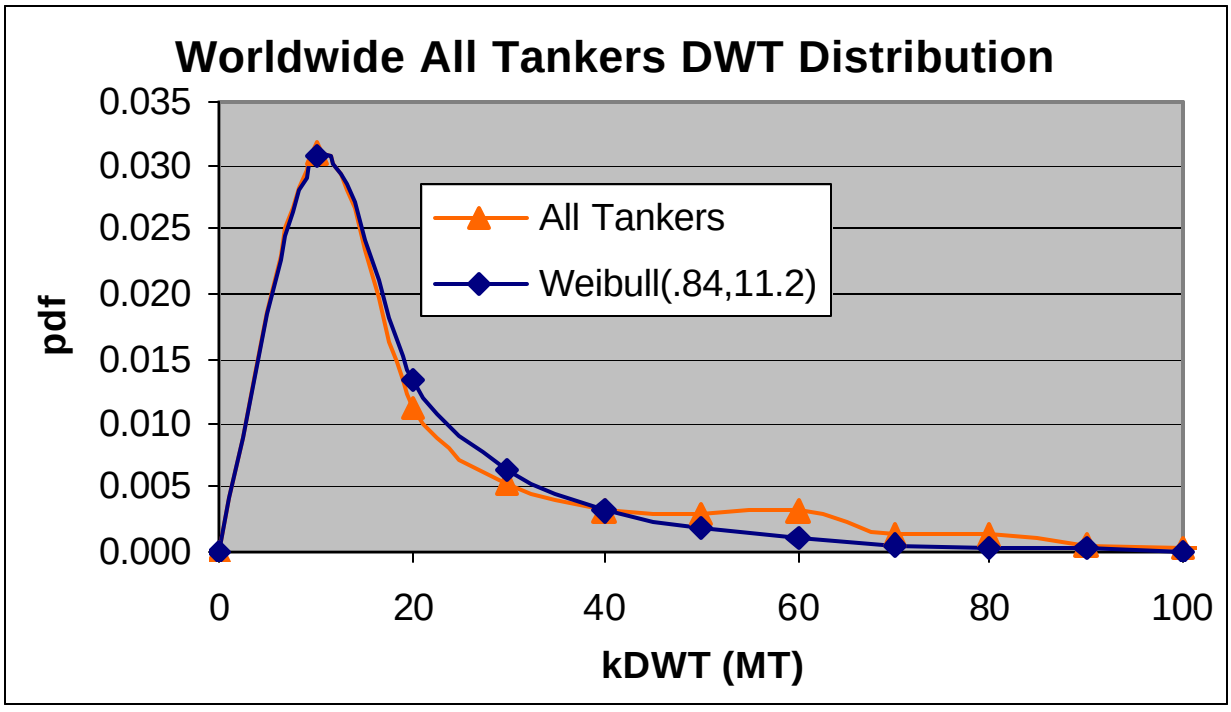

Figure 100 - Striking Ship Displacement - All Tankers

Figure 98 shows the worldwide distributions of displacement for each of these ship types and all ships [79]. The distributions are significantly different and must be applied individually to each ship type. Figure 99 shows the displacement distribution for ships striking bulk cargo ships obtained from the Sandia collision data [78]. This is actual collision data. There is a significant

difference between the all-ships worldwide distribution and the striking ship distributions. The cargo ship striking ship distribution is similar to the cargo ship distribution with a bias to larger ships. Unfortunately, the Sandia data is not sufficient to establish a general rule or striking ship displacement pdf for all ship types. The worldwide displacement distributions are used in the study.

Figure 100 through Figure 104 show the displacement distributions and a best-fit distribution for each type. Table 19 provides a summary of parameter values for these distributions.

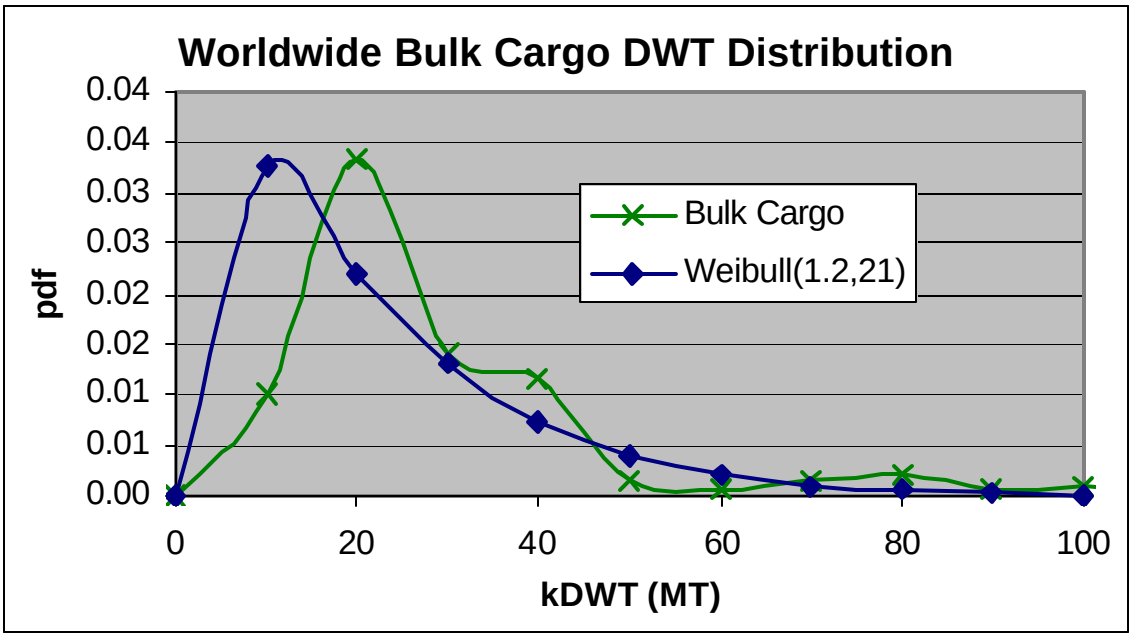

Figure 101 - Striking Ship Displacement - Bulk Cargo Ships

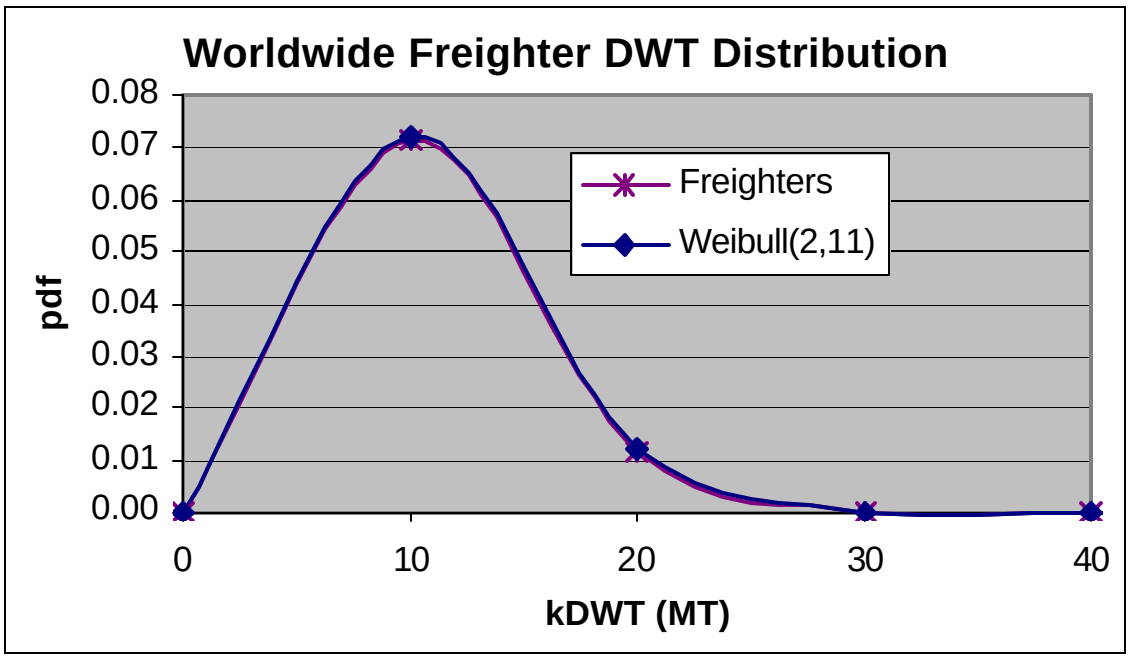

Figure 102 - Striking Ship Displacement - Freighters

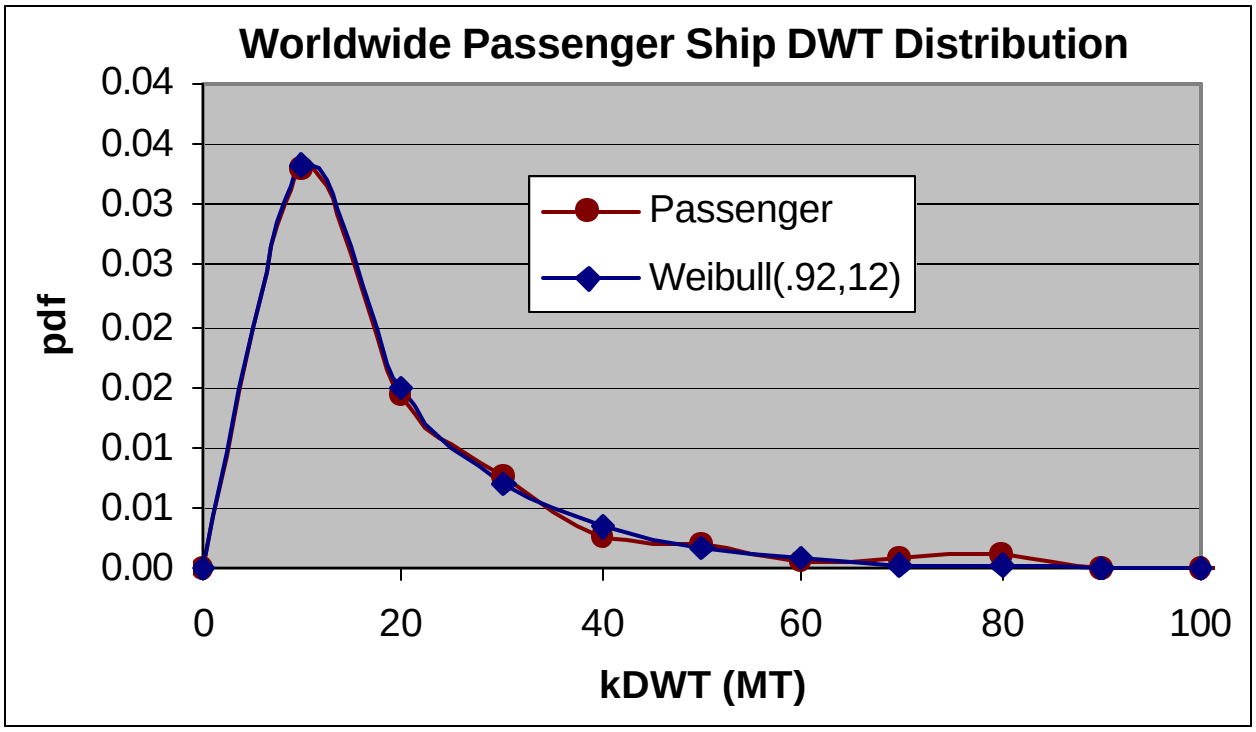

Figure 103 - Striking Ship Displacement - Passenger Ships

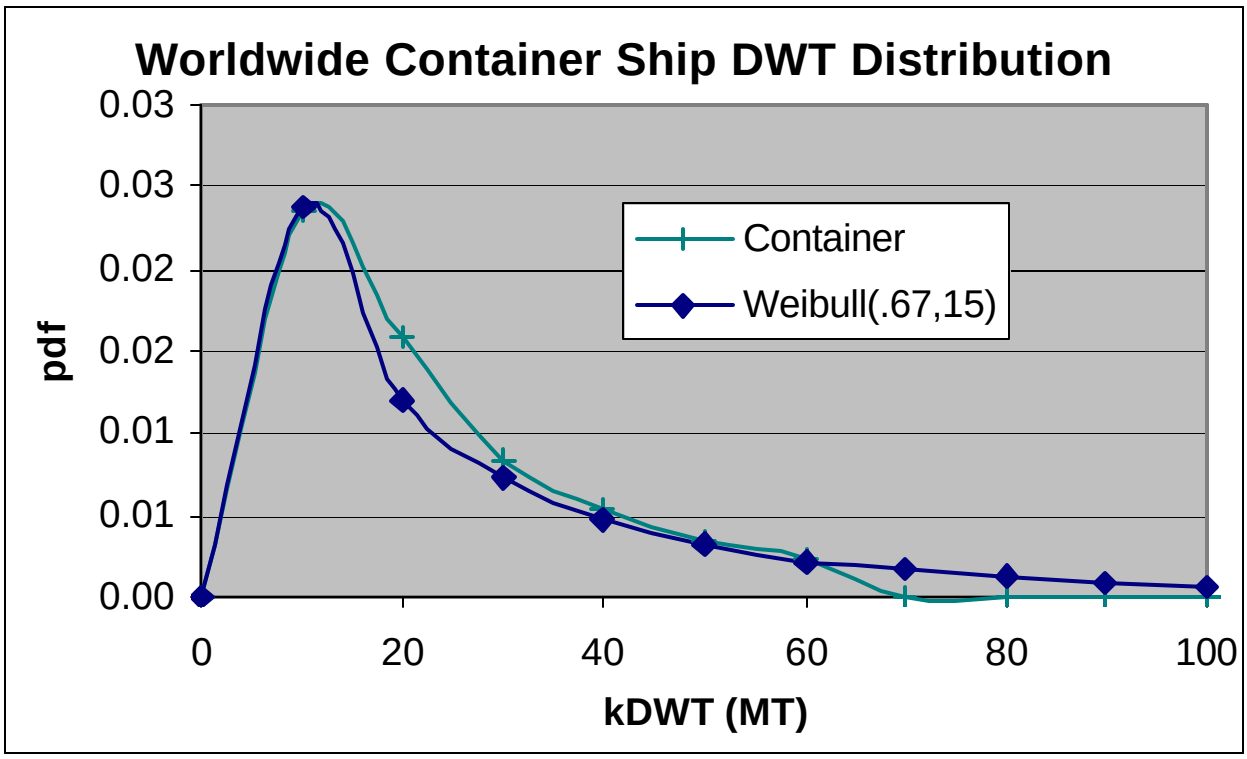

Figure 104 - Striking Ship Displacement - Container Ships

Table 19 - Striking Ship Type and Displacement

Ship Type	Probability of Encounter	Displacement pdf	Weibull a	Weibull b	Mean (kMT)	s (kMT)	Displacement Range (MT)
Tanker	0.252	Weibull	0.84	11.2	12.277	14.688	699-273550
Bulk carrier	0.176	Weibull	1.20	21.0	19.754	16.532	1082-129325
Freighter	0.424	Weibull	2.00	11.0	9.748	5.096	500-41600
Passenger ship	0.014	Weibull	0.92	12.0	12.479	13.579	997-76049
Container ship	0.135	Weibull	0.67	15.0	19.836	30.52	1137-58889

Collision speed is the striking ship speed at the moment of collision, and is not strongly related to service speed. It depends primarily on actions taken just prior to collision. Collision speed data must be collected from actual collision events. Figure 105 is a plot of data derived from the Sandia Report [80] and limited USCG tanker collision data [82]. An approximate Weibull distribution ($\alpha = 2.2$, $\beta = 6.5$) is fit to this data. The mean of this distribution is substantially less than service speed(s), and indicates significant adjustment in speed prior to the actual collision event.

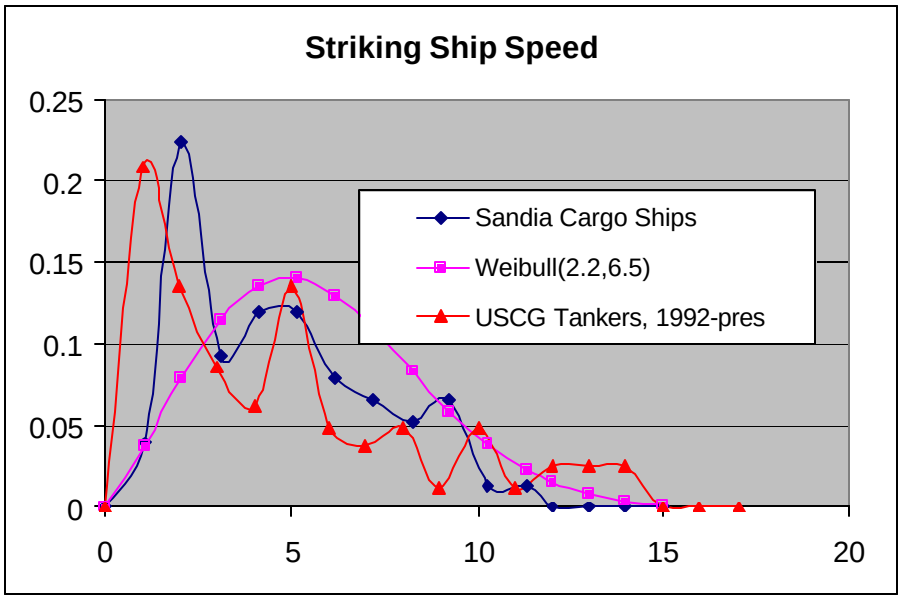

Figure 105 – Striking Ship Speed [80,82]

7.2.2 Striking Ship Characteristics

In this section, data and regression curves are presented for deriving striking ship half-entrance angle, length, beam, draft, and bow height from striking ship type and displacement.

Bow half-entrance angle is not a standard ship principal characteristic. A limited number of drawings were reviewed in the Sandia Study [78]. Table 20 and Figure 106 present the results of this analysis. The trends in this data are difficult to explain and the data is insufficient to derive

pdfs. Table 21 provides single values derived from Table 20 for each type of ship. These values are used in this study.

Lloyd's worldwide data [79] is used to specify the remaining principal characteristics as a function of ship type and displacement. This data is plotted in Figure 107 through Figure 127 and summarized in Table 21. A simple power function is used to fit this data.

Table 20 - Bow Half Entrance Angle (all ships)

Displacement	Bow Half Entrance Angle, (Degrees)			
(tonne)	Tanker	Cargo	Container	Passenger
0-10160	28	29	17	17
10160-20320	30	20	17	17
20320-30480	30	20	17	17
30480-40640	38	20	17	17
40640-50800	38	20	17	17
50800-60960	38	20	17	17
60960-71120	38	20	17	17
71120-81280	38	20	17	17
81280-above	38	20	17	17

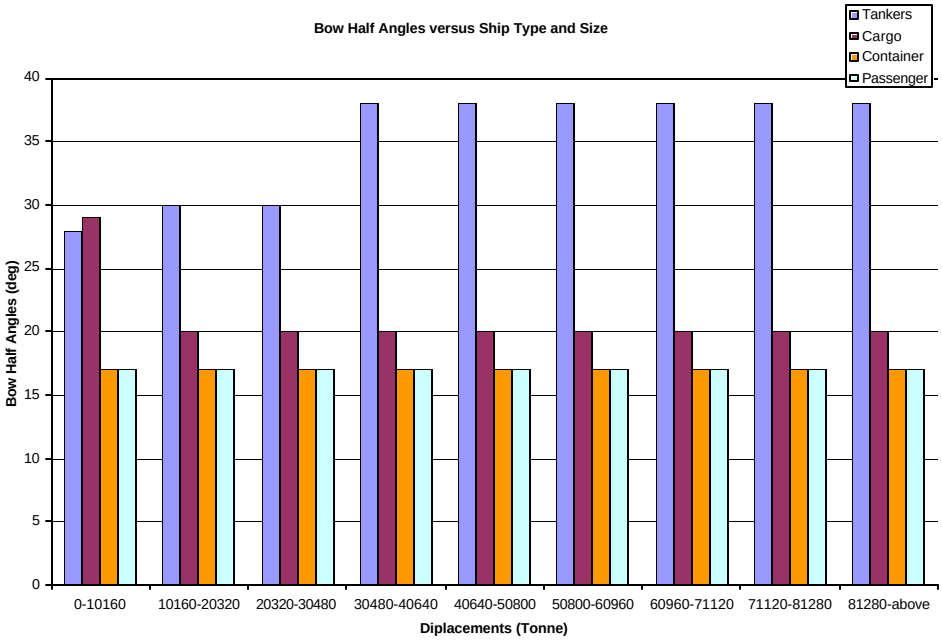

Figure 106 - Bow Half Entrance Angle (all ships by type, design practice) [78]

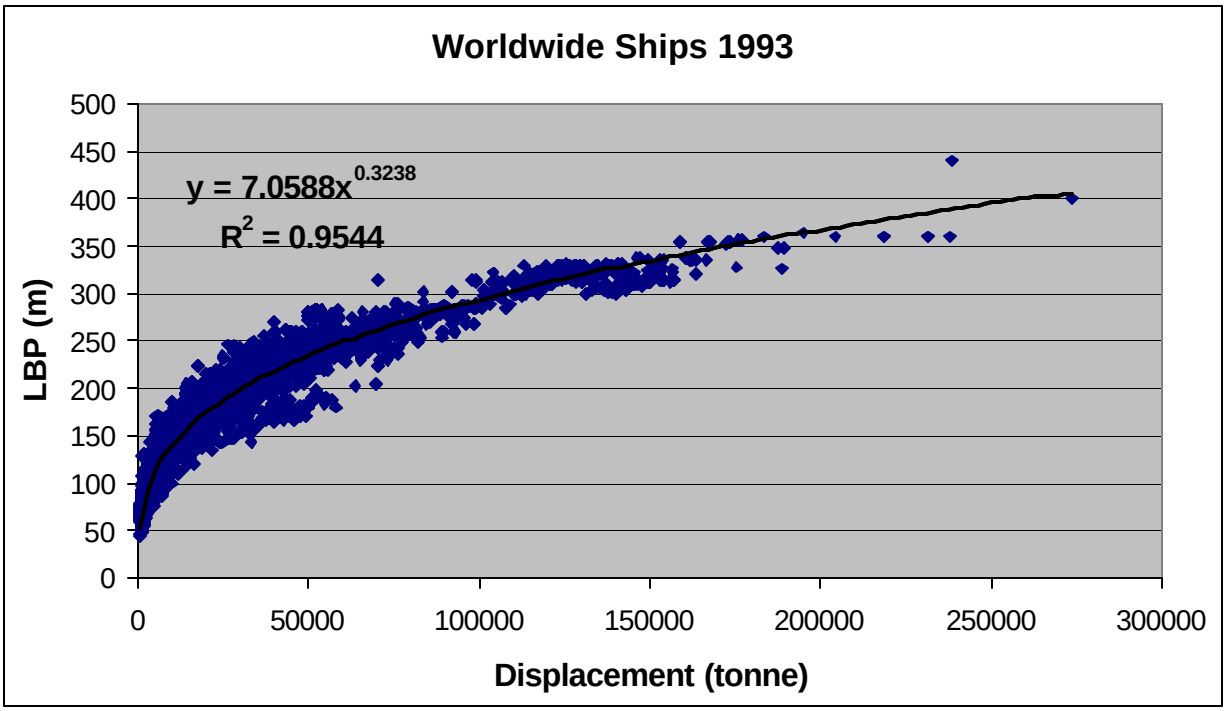

Figure 107 – All Ships Length vs. Displacement [79]

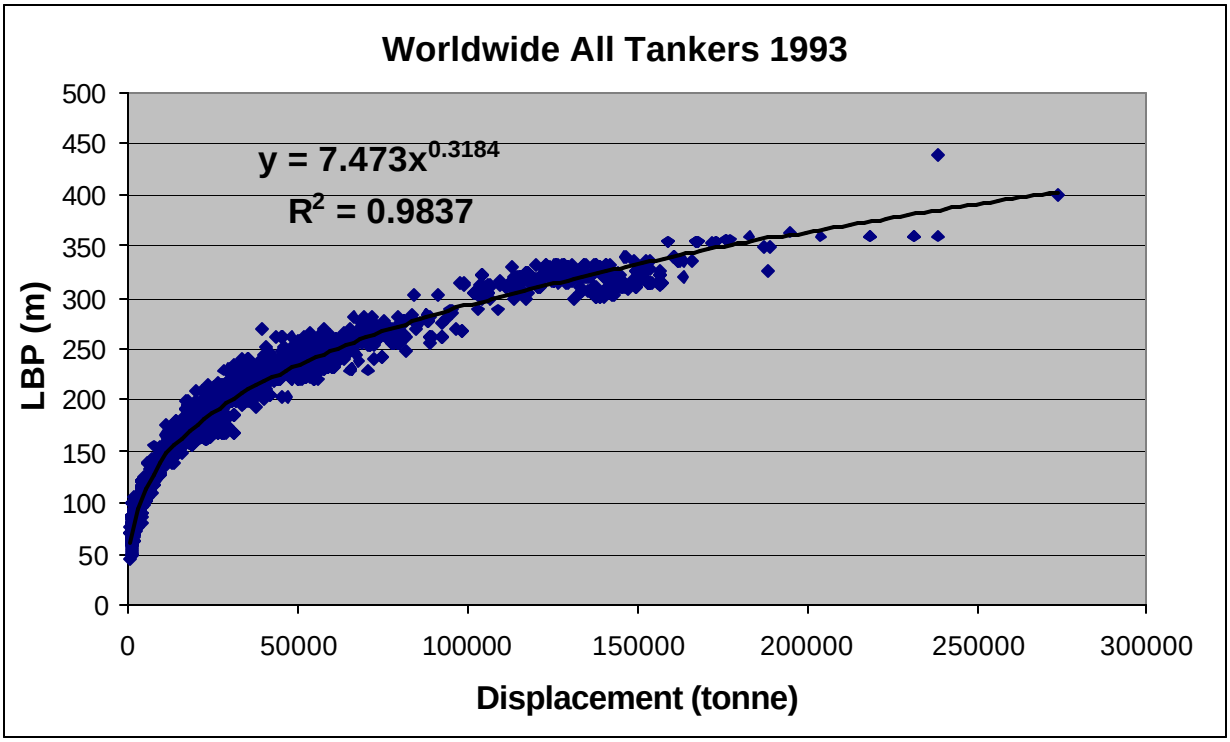

Figure 108 – All Tankers Length vs. Displacement [79]

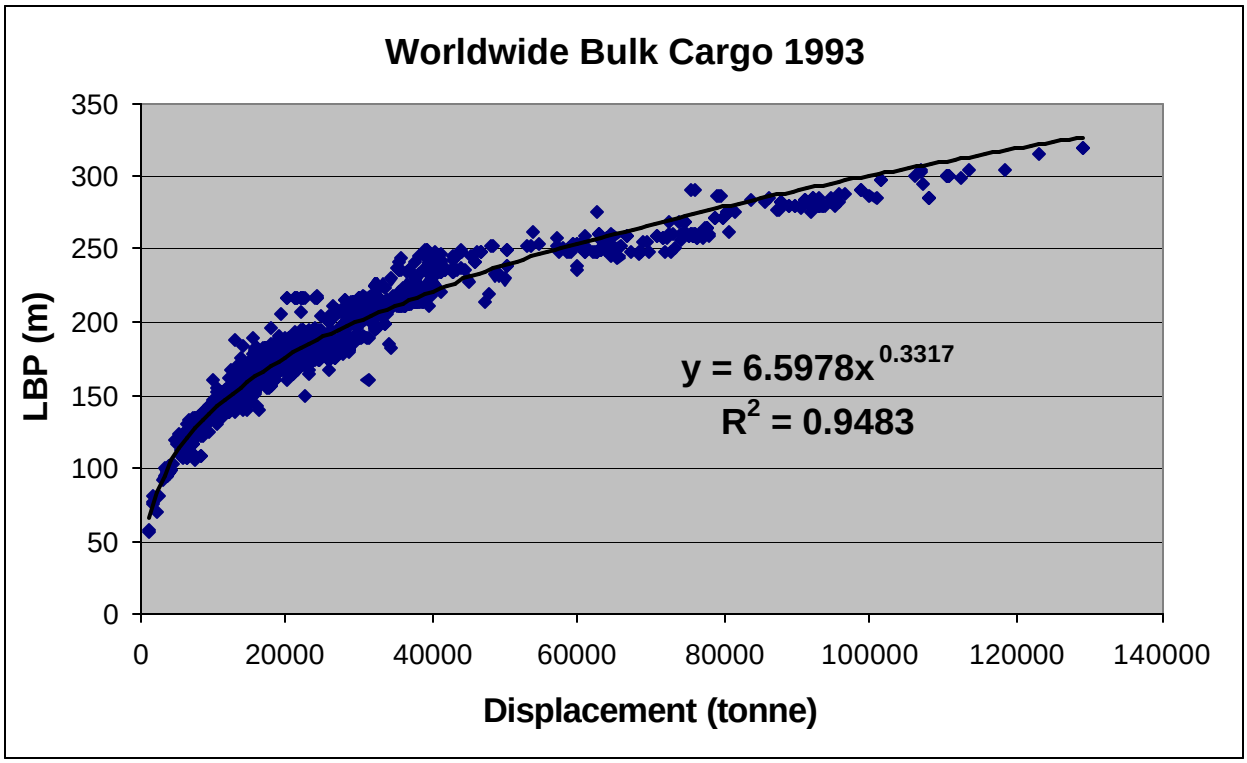

Figure 109 – Bulk Cargo Ships Length vs. Displacement [79]

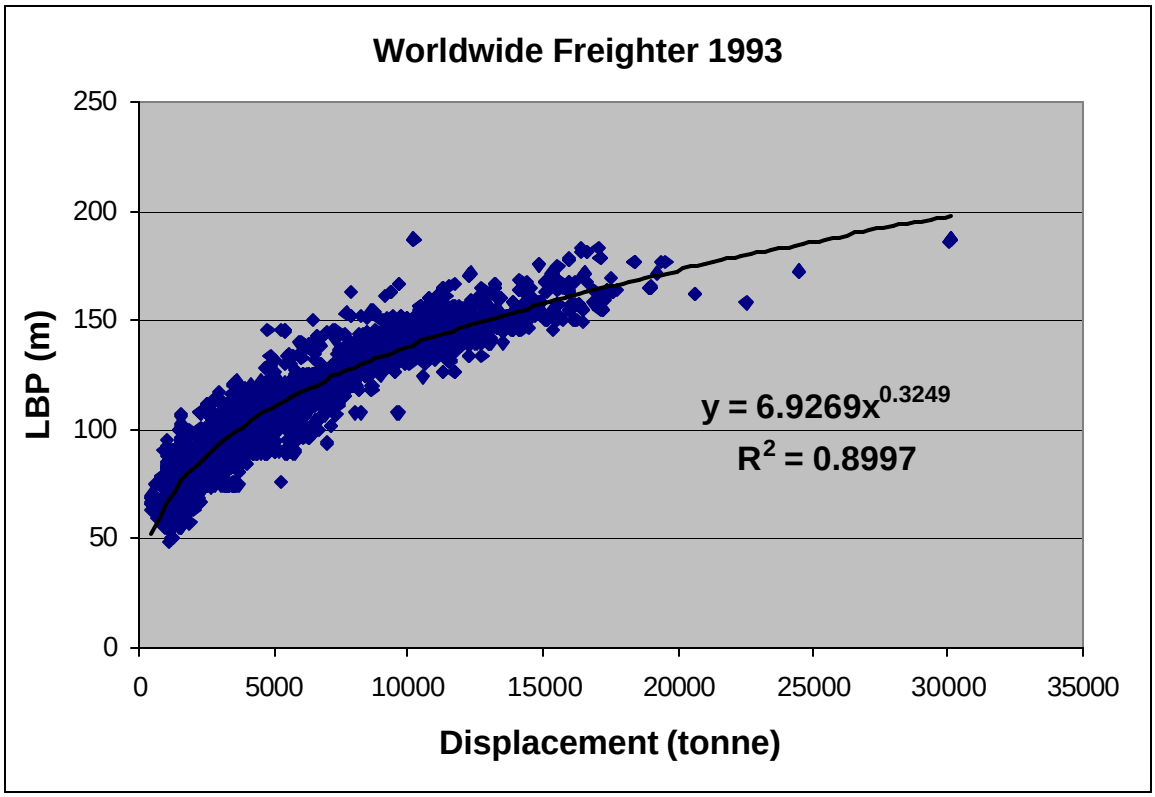

Figure 110 – Freighter Length vs. Displacement

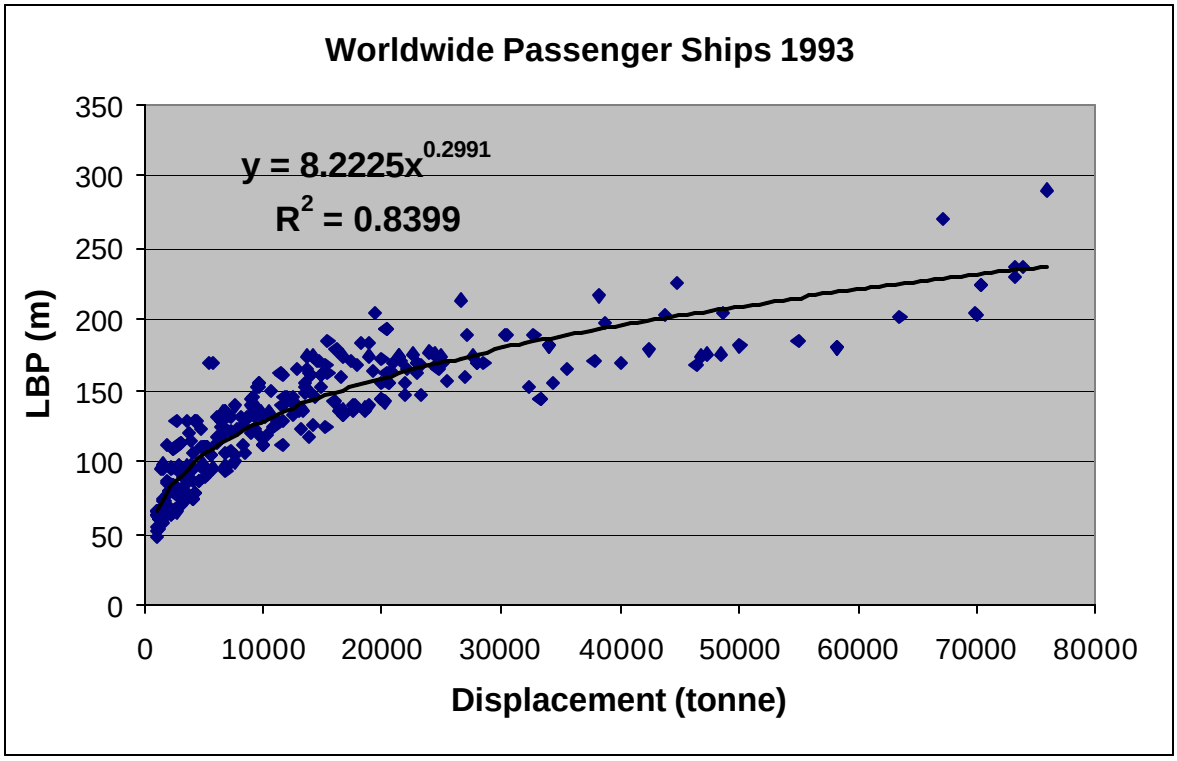

Figure 111 – Passenger Ship Length vs. Displacement [79]

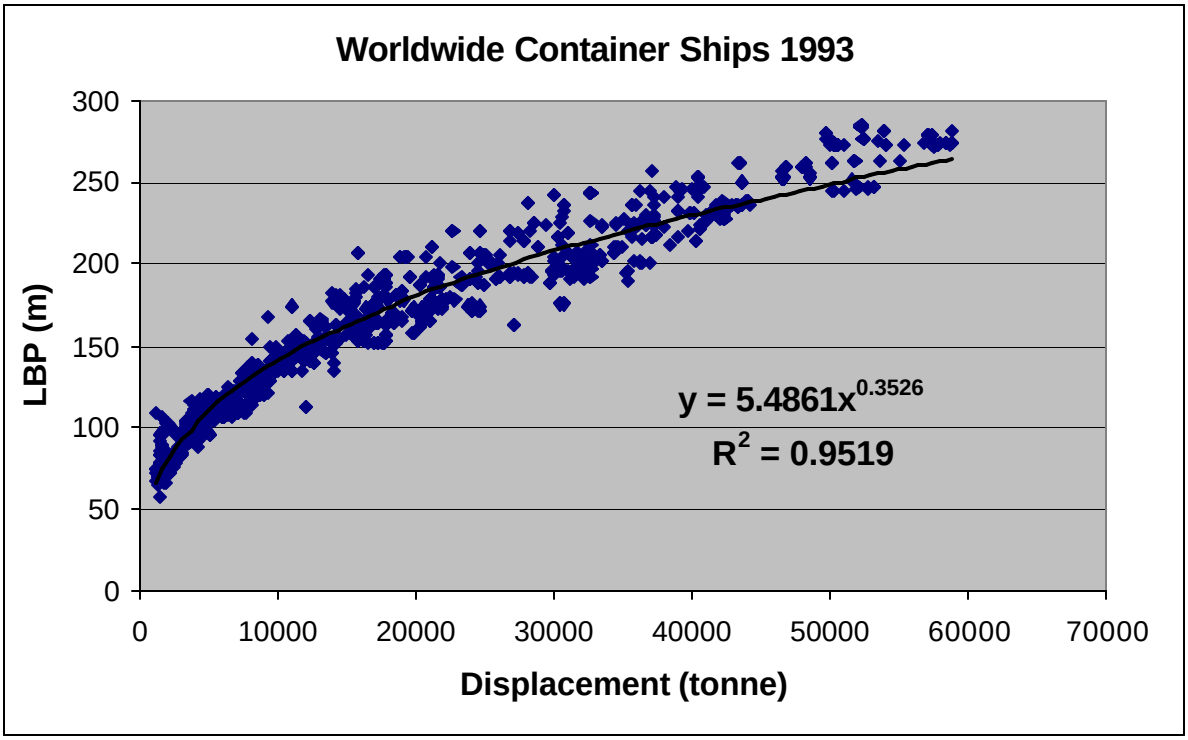

Figure 112 – Container Ship Length vs. Displacement [79]

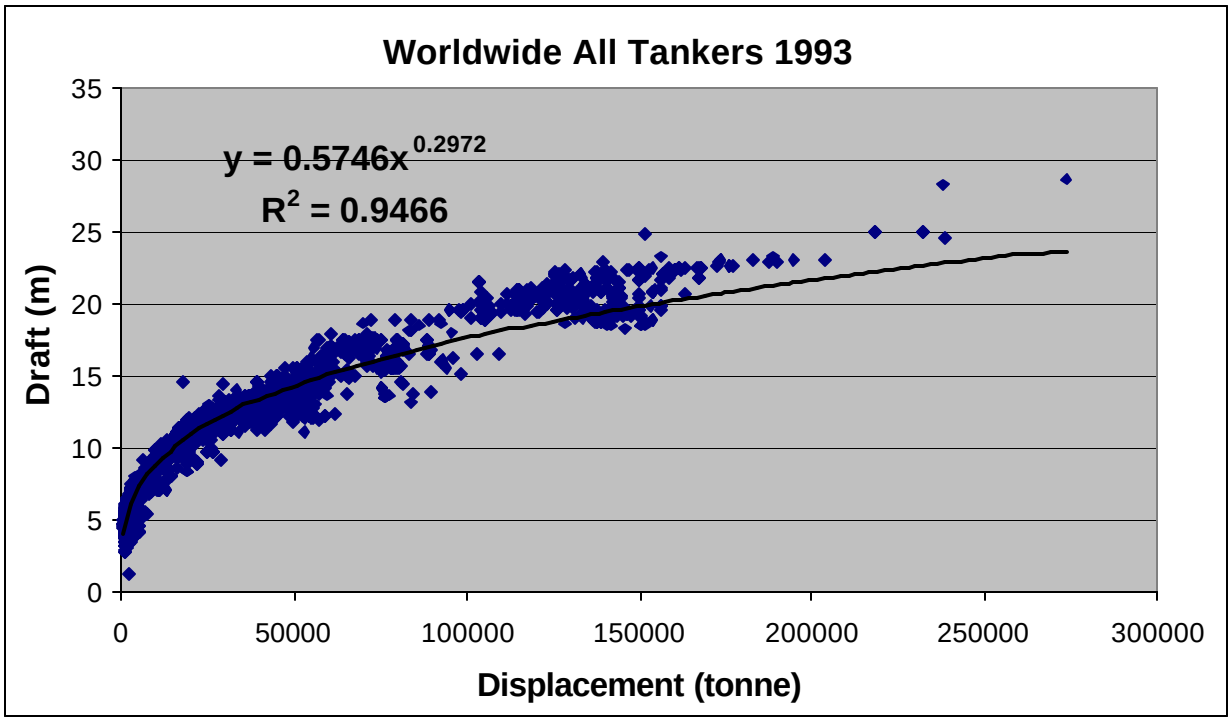

Figure 113 – All-Tankers Full Load Draft vs. Displacement [79]

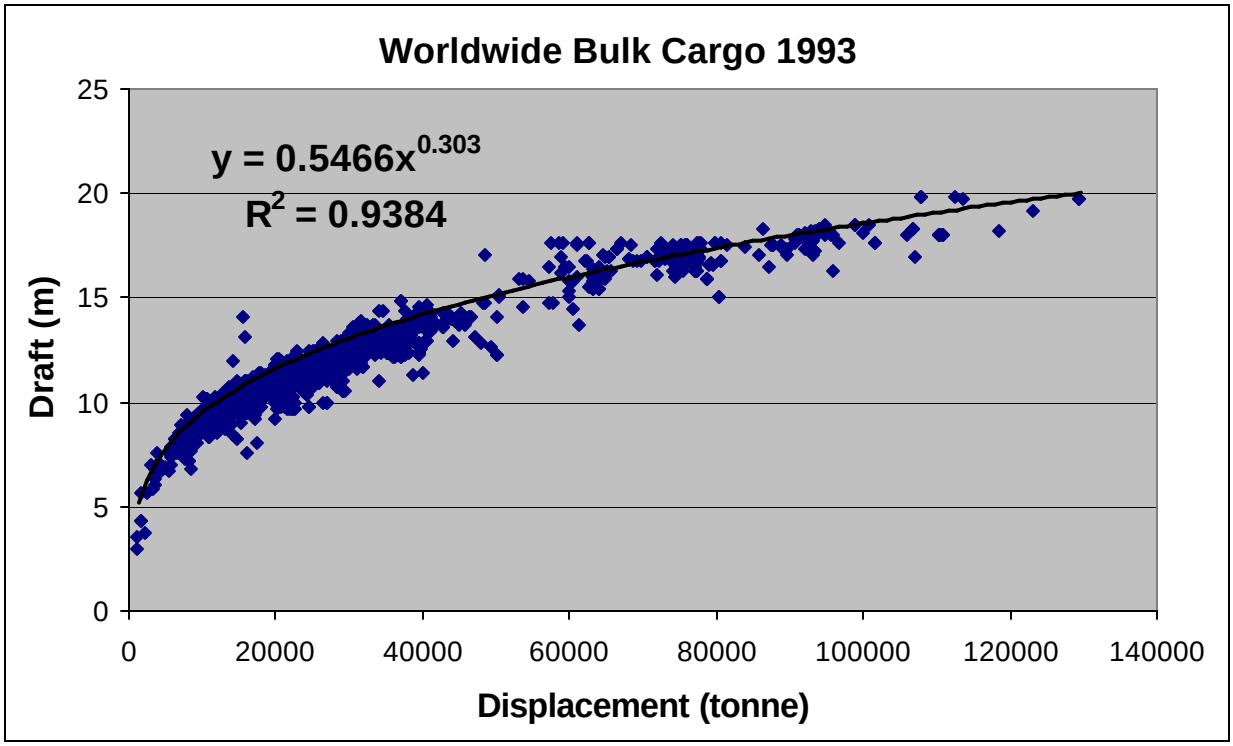

Figure 114 – Bulk Cargo Ship Full Load Draft vs. Displacement [79]

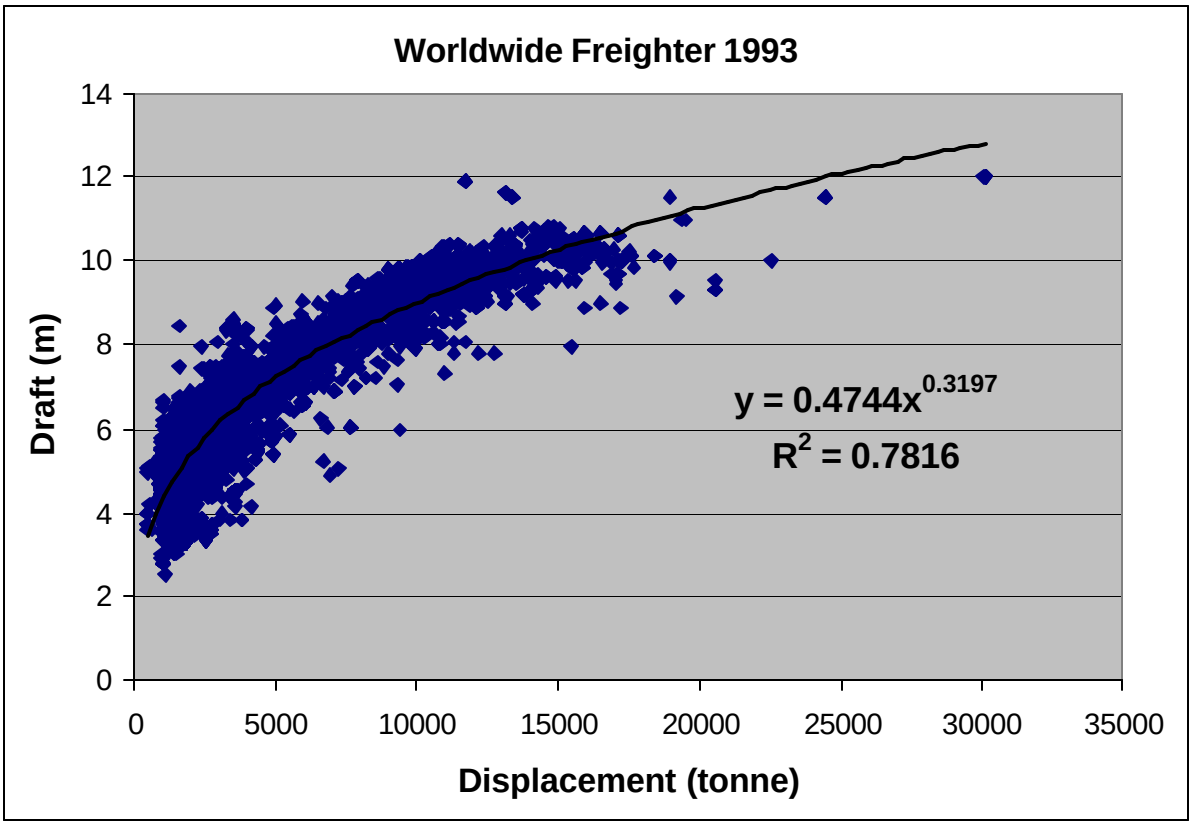

Figure 115 – Freighter Full Load Draft vs. Displacement [79]

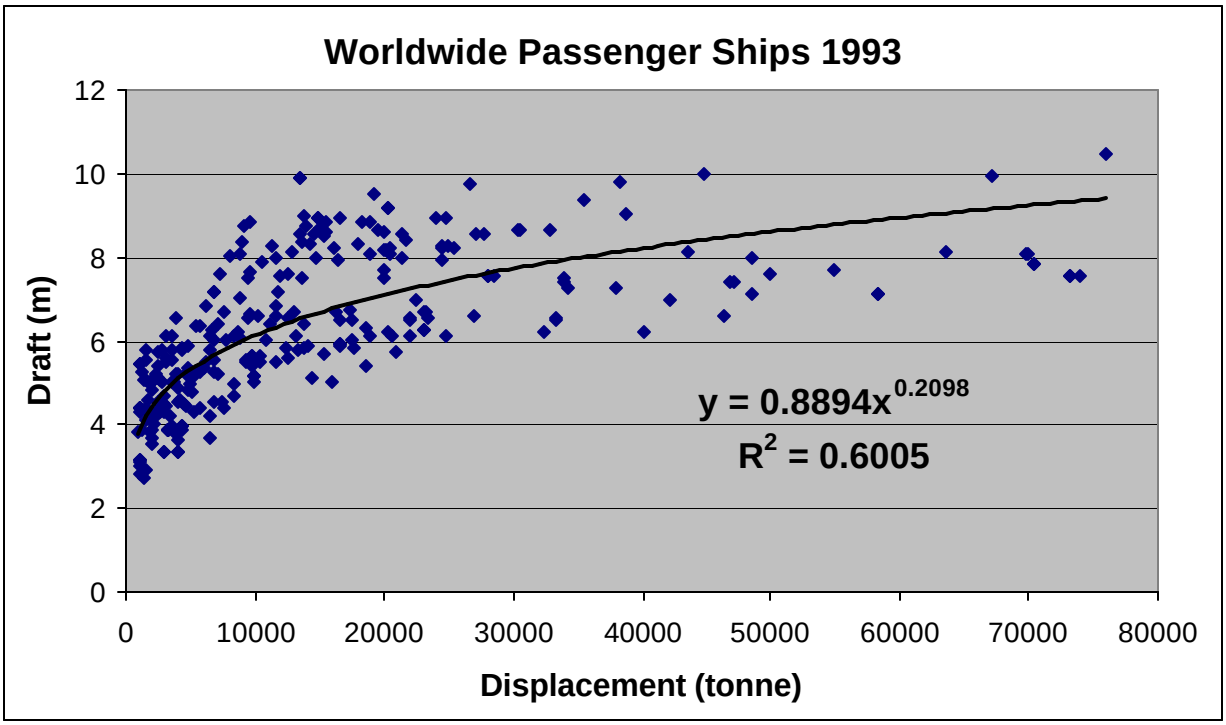

Figure 116 – Passenger Ship Full Load Draft vs. Displacement [79]

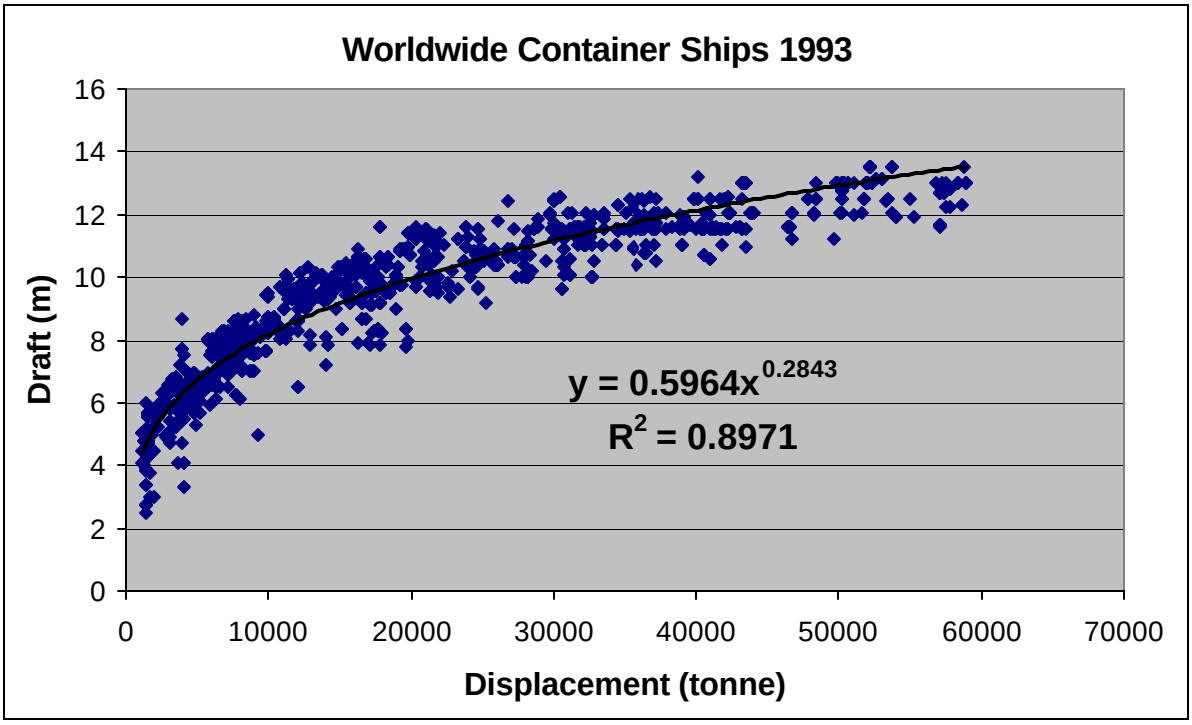

Figure 117 – Container Ship Full Load Draft vs. Displacement [79]

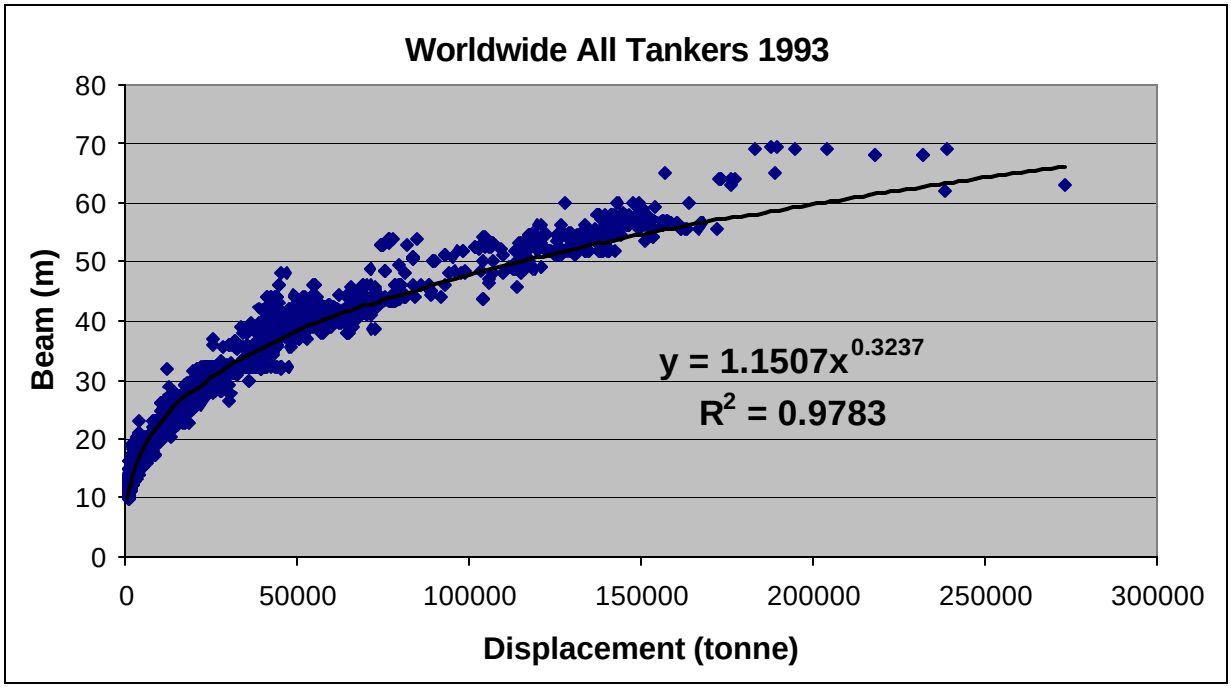

Figure 118 – All Tankers Beam vs. Displacement [79]

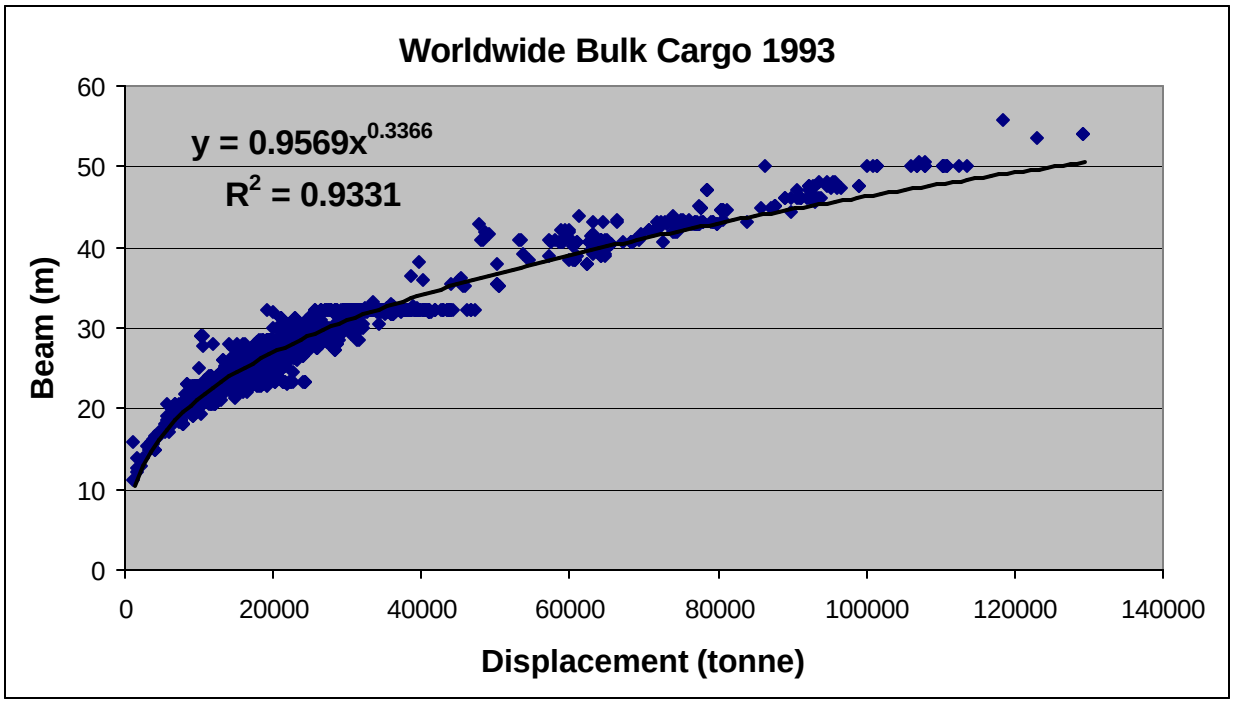

Figure 119 – Bulk Cargo Ship Beam vs. Displacement [79]

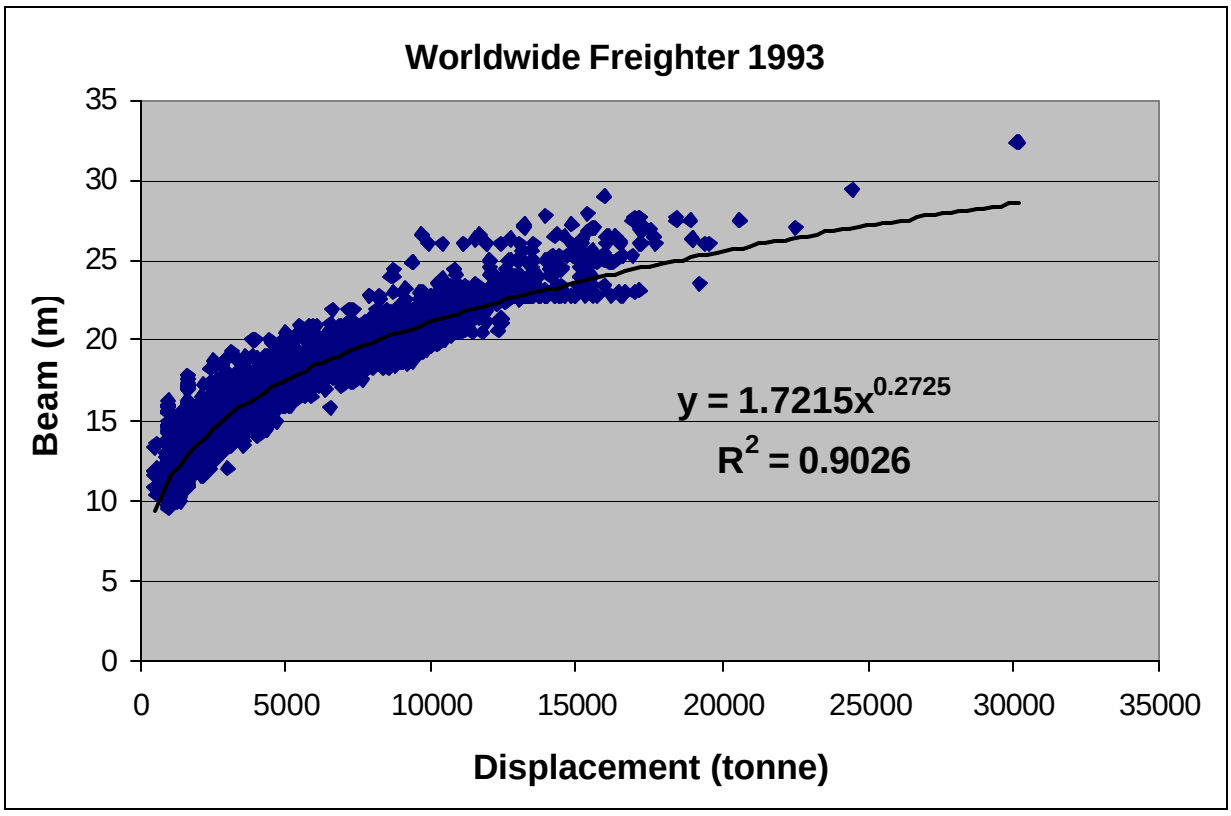

Figure 120 – Freighter Beam vs. Displacement [79]

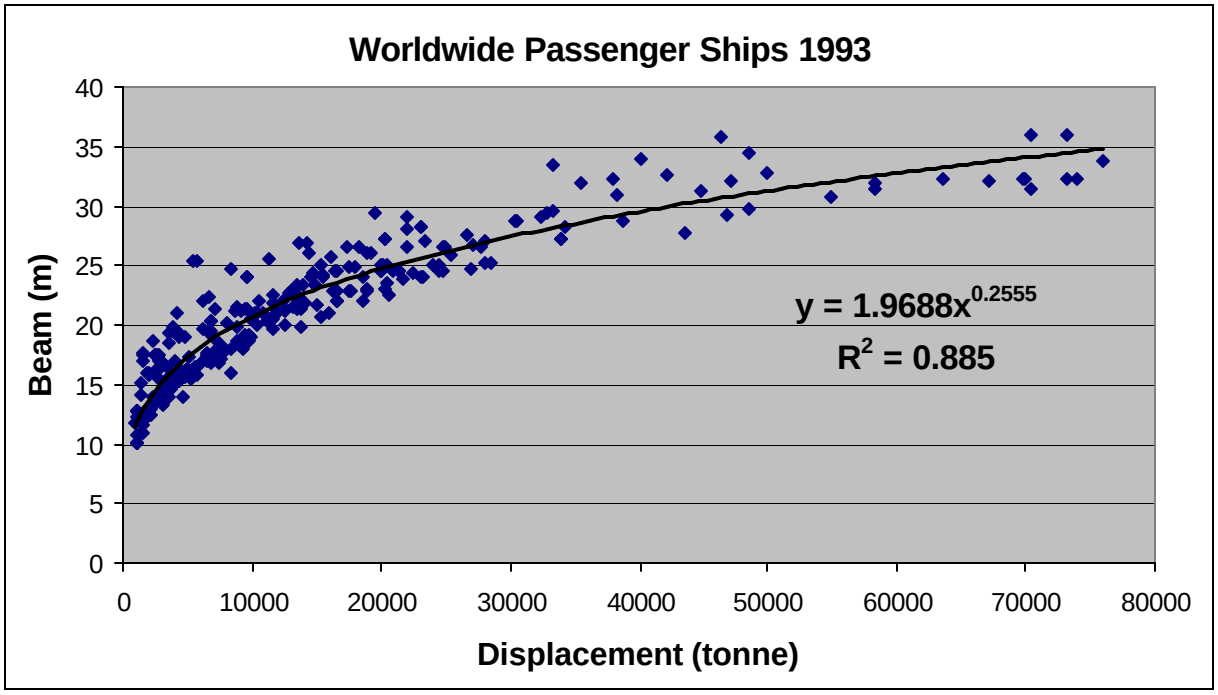

Figure 121 – Passenger Ship Beam vs. Displacement [79]

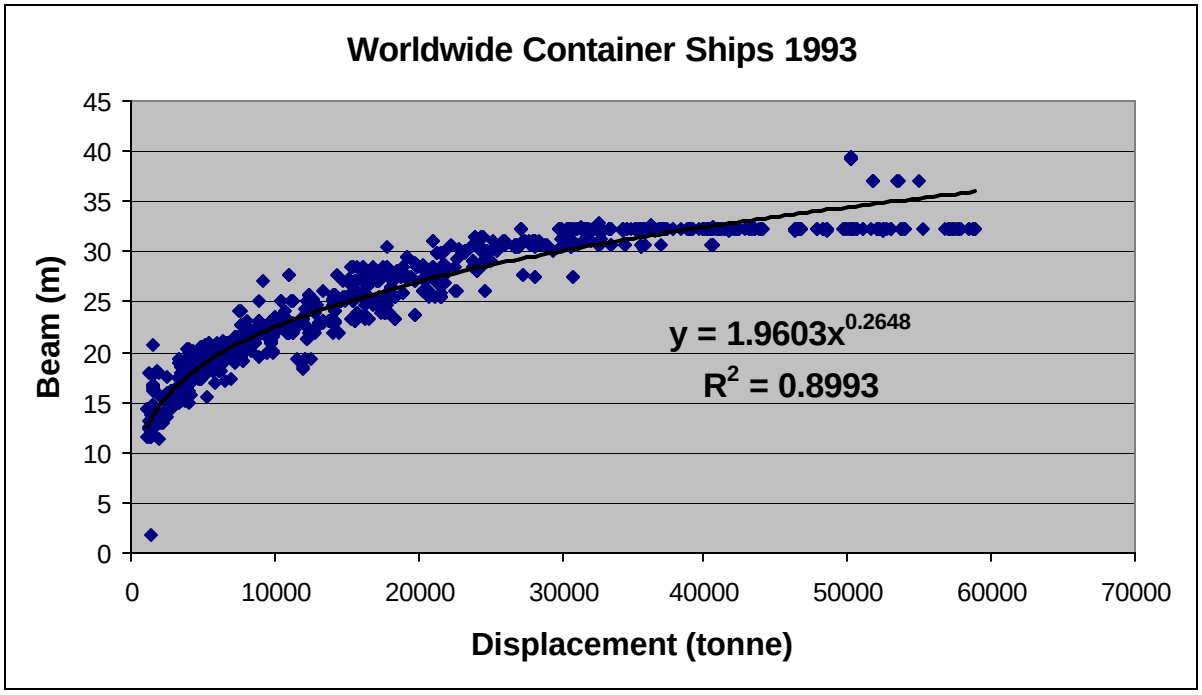

Figure 122 – Container Ship Beam vs. Displacement [79]

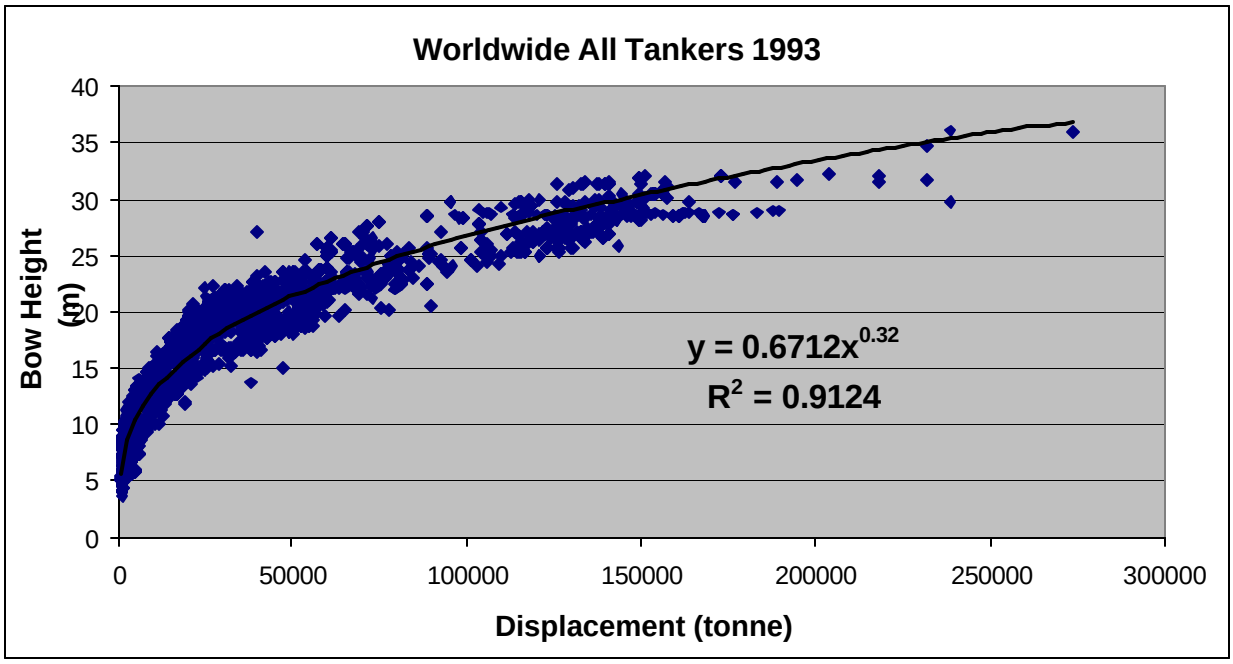

Figure 123 – All Tankers Bow Height vs. Displacement [79]

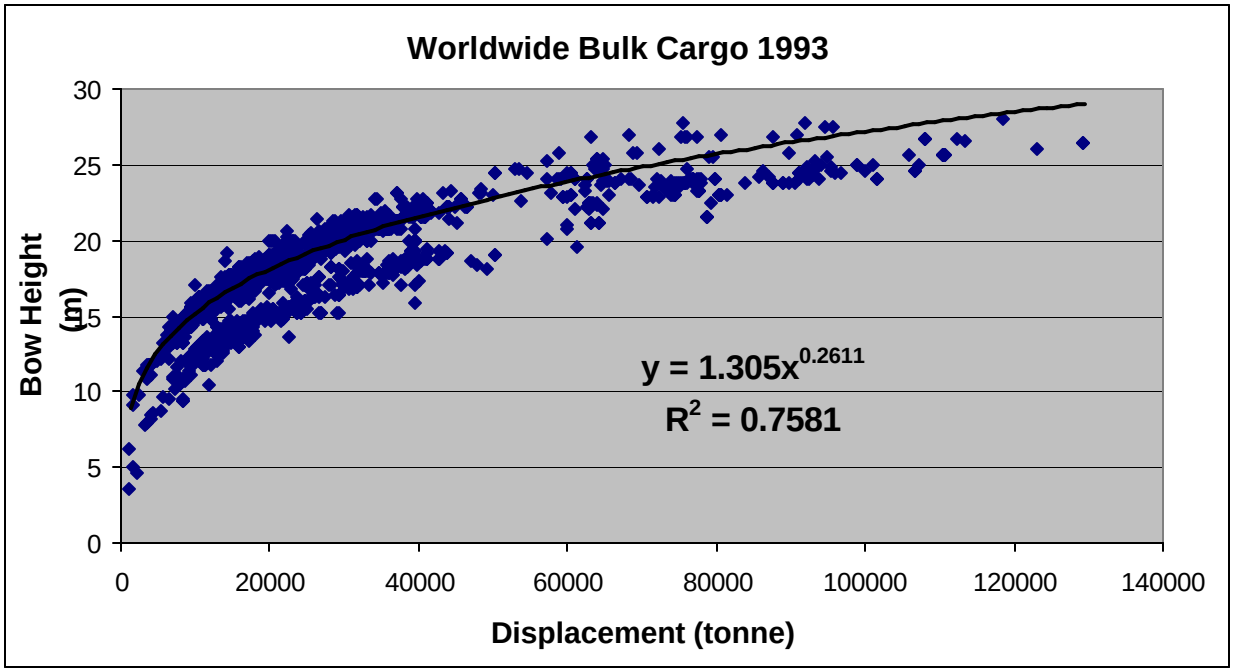

Figure 124 – Bulk Cargo Ship Bow Height vs. Displacement [79]

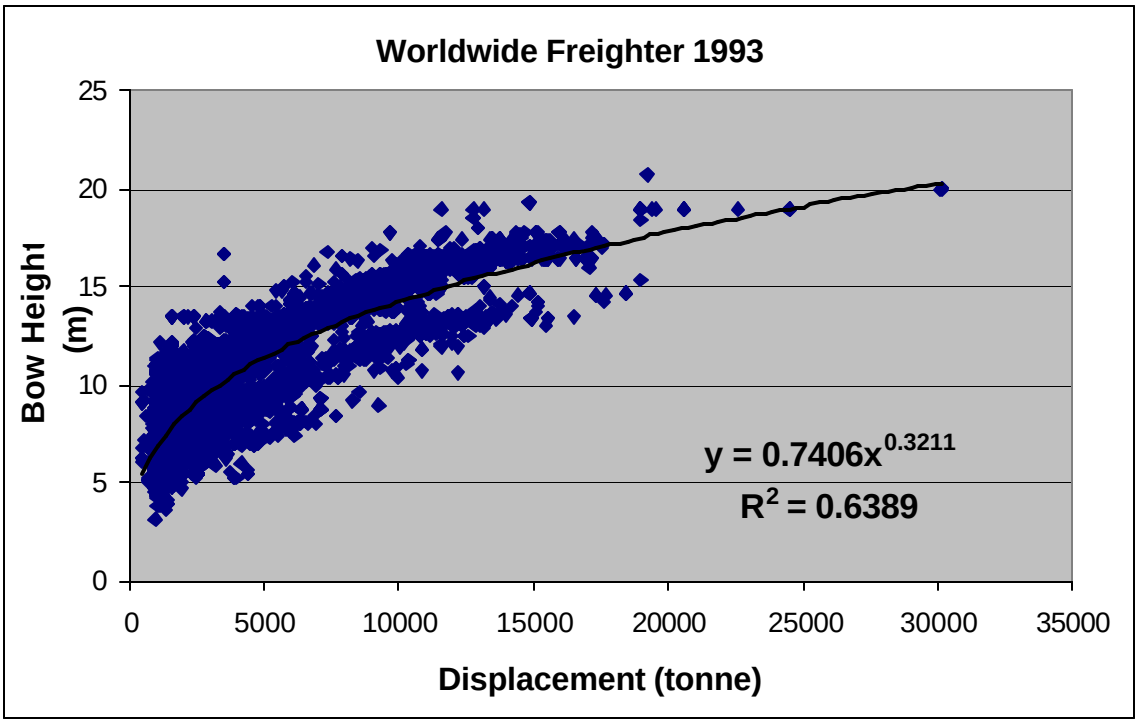

Figure 125 – Freighter Bow Height vs. Displacement [70]

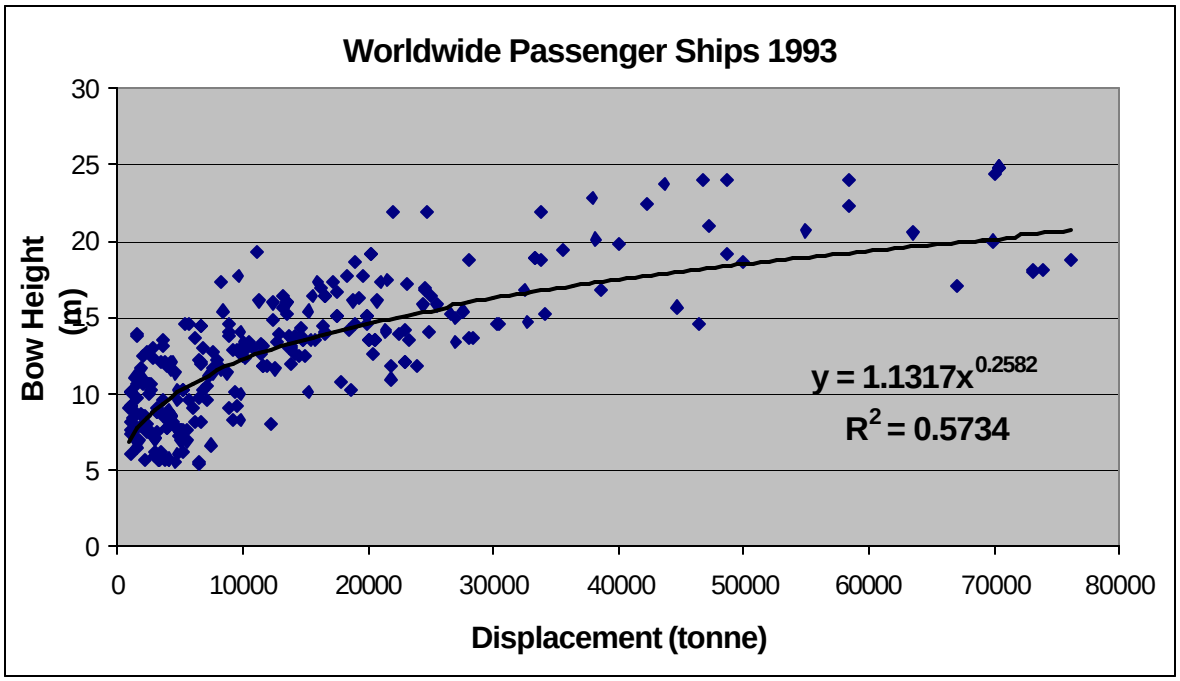

Figure 126 – Passenger Ship Bow Height vs. Displacement [79]

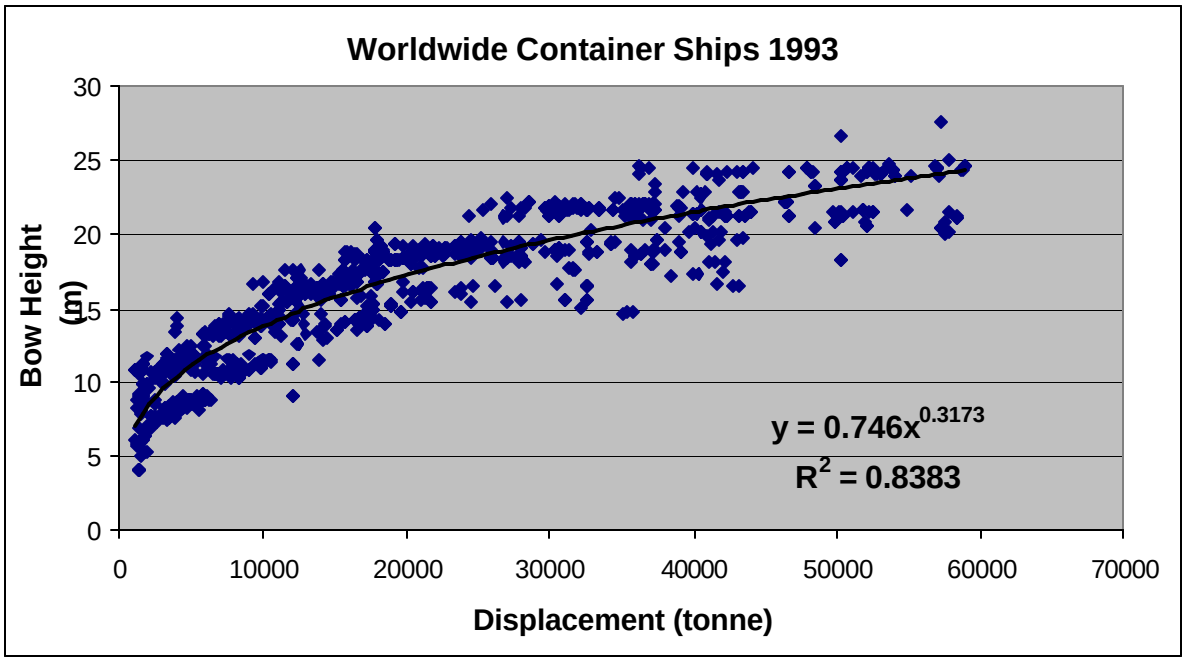

Figure 127 – Container Ship Bow Height vs. Displacement [79]

Table 21 - Striking Ship Characteristics

Ship Type	LBP		Beam		Draft		Bow Height		HEA
	Coef	Power	Coef	Power	Coef	Power	Coef	Power	
Tanker	7.473	.3184	1.1507	.3237	.5746	.2972	.6712	.3200	38
Bulk carrier	6.598	.3317	.9569	.3366	.5466	.3030	1.305	.2611	20
Freighter	6.927	.3249	1.7215	.2725	.4744	.3197	.7406	.3211	20
Passenger ship	8.223	.2991	1.9688	.2555	.8894	.2098	1.1317	.2582	17
Container ship	5.486	.3526	1.9603	.2648	.5964	.2843	.7460	.3173	17

7.2.3 Struck Ship Variables

Figure 128 is a plot of struck ship speed data derived from USCG tanker collision data [82]. The struck ship collision speed distribution is also very different from service speed. Struck ships are frequently moored or at anchor as is indicated by the significant pdf value at zero speed. An exponential distribution ($\alpha = 0.584$) is fit to this data.

Full load displacement and draft with zero trim are assumed for the struck ship.

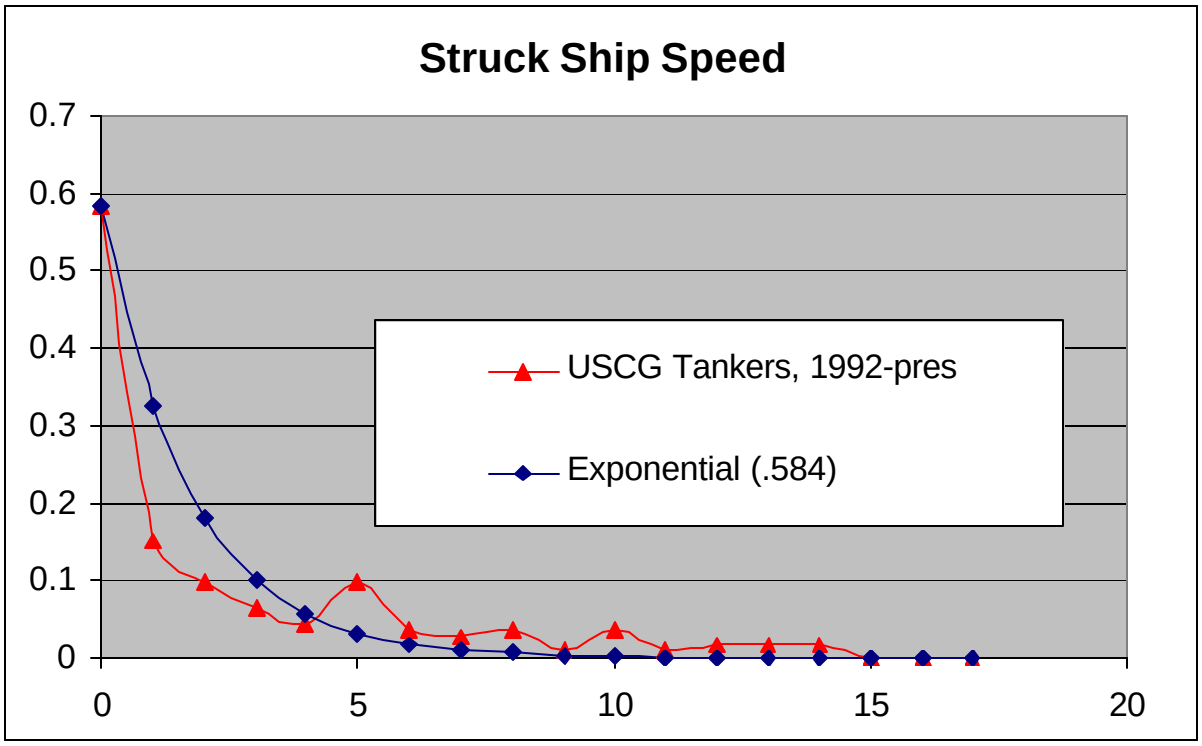

Figure 128 - Struck Ship Speed [82]

7.2.4 Collision Scenario Variables

Figure 129 is a plot of collision angle data derived from the Sandia Report [78]. An approximate Normal distribution (μ = 90 degrees, σ = 28.97 degrees) is fit to this data and is used to select collision angle in the Monte Carlo simulation. At more oblique angles, there is a higher probability of ships passing each other or only striking a glancing blow. These cases are frequently not reported.

The current IMO pdf for longitudinal strike location specifies a constant value over the entire length of the stuck ship [4]. The constant pdf was chosen for convenience and because of the limited available data. Figure 130 shows a bar chart of the actual data used to develop the IMO pdf and data gathered for cargo ships in the Sandia Study [78]. This data does not indicate a constant pdf. The IMO data is from 56 of 200 significant collision events for which the strike location was known. The Sandia data indicates a somewhat higher probability of midship and forward strike compared to the IMO data. The IMO probabilities are used in this study.

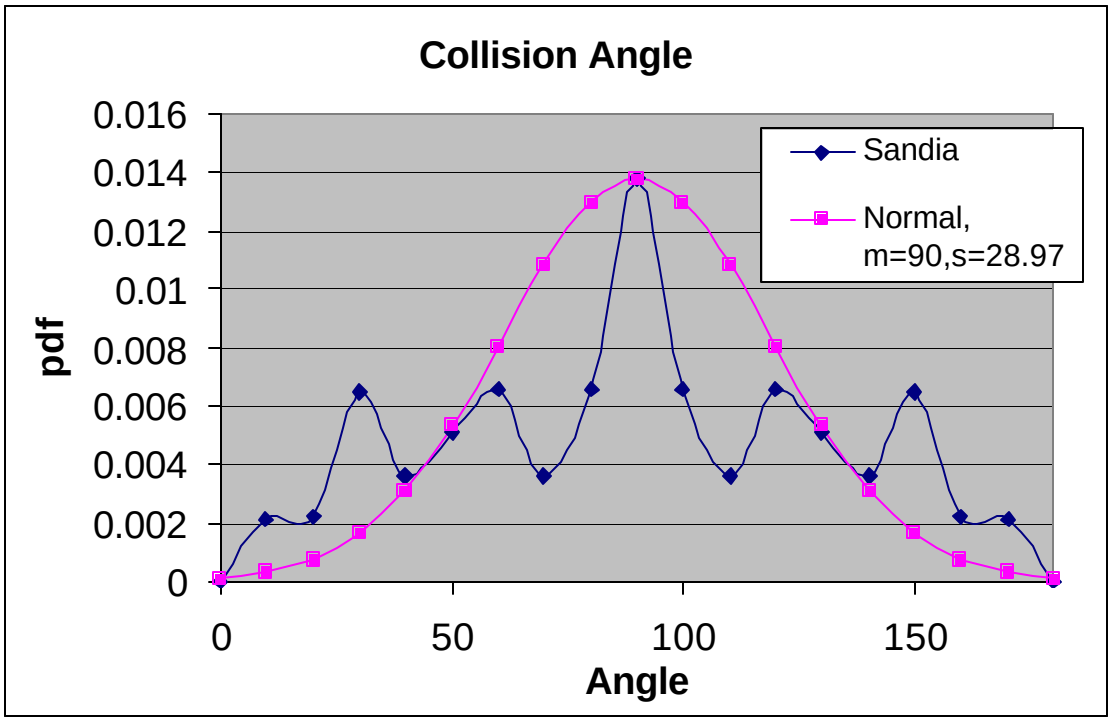

Figure 129 – Collision Angle pdf

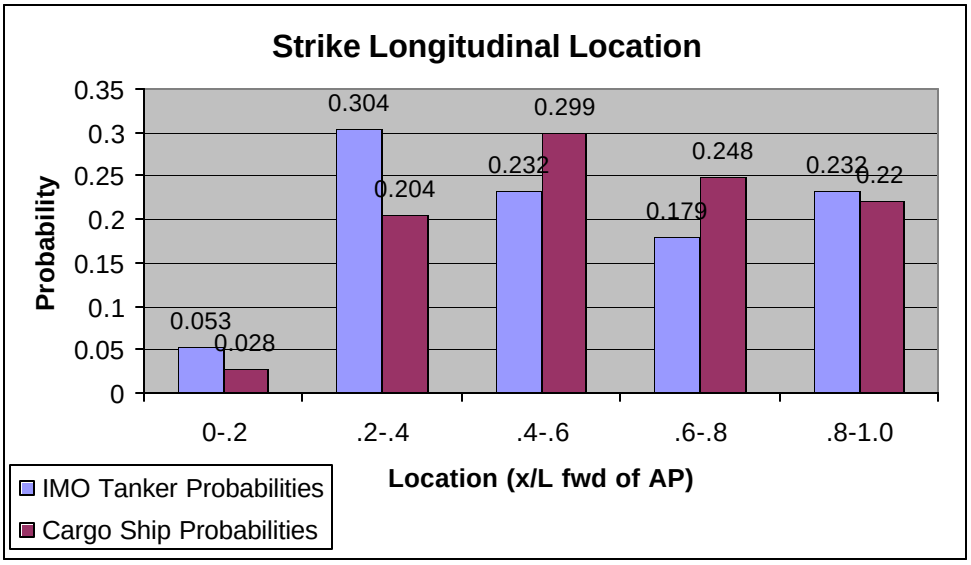

Figure 130 - Longitudinal Side Damage Probabilities [78]

7.3 Uncoupling of Internal and External Dynamics

A potential simplification for the collision scenario definition requires that the external ship dynamics problem be solved uncoupled from the internal deformation problem. This allows

multiple collision scenario random variable definitions to be replaced by pdfs for transverse and longitudinal absorbed energy only. This section examines the validity of this simplification.

Pedersen and Zhang [14] derive expressions for absorbed energy uncoupled from internal mechanics as described in Section 2.1.2.2. Absorbed energy must be calculated in SIMCOL by multiplying transverse force by transverse displacement and longitudinal force by longitudinal displacement for each time step, and then summing for all time steps until the end of the collision event. The relationship between longitudinal and transverse forces is very dependent on the internal deformation of the structure and their relationship varies from time step to time step as the struck ship s penetrated.

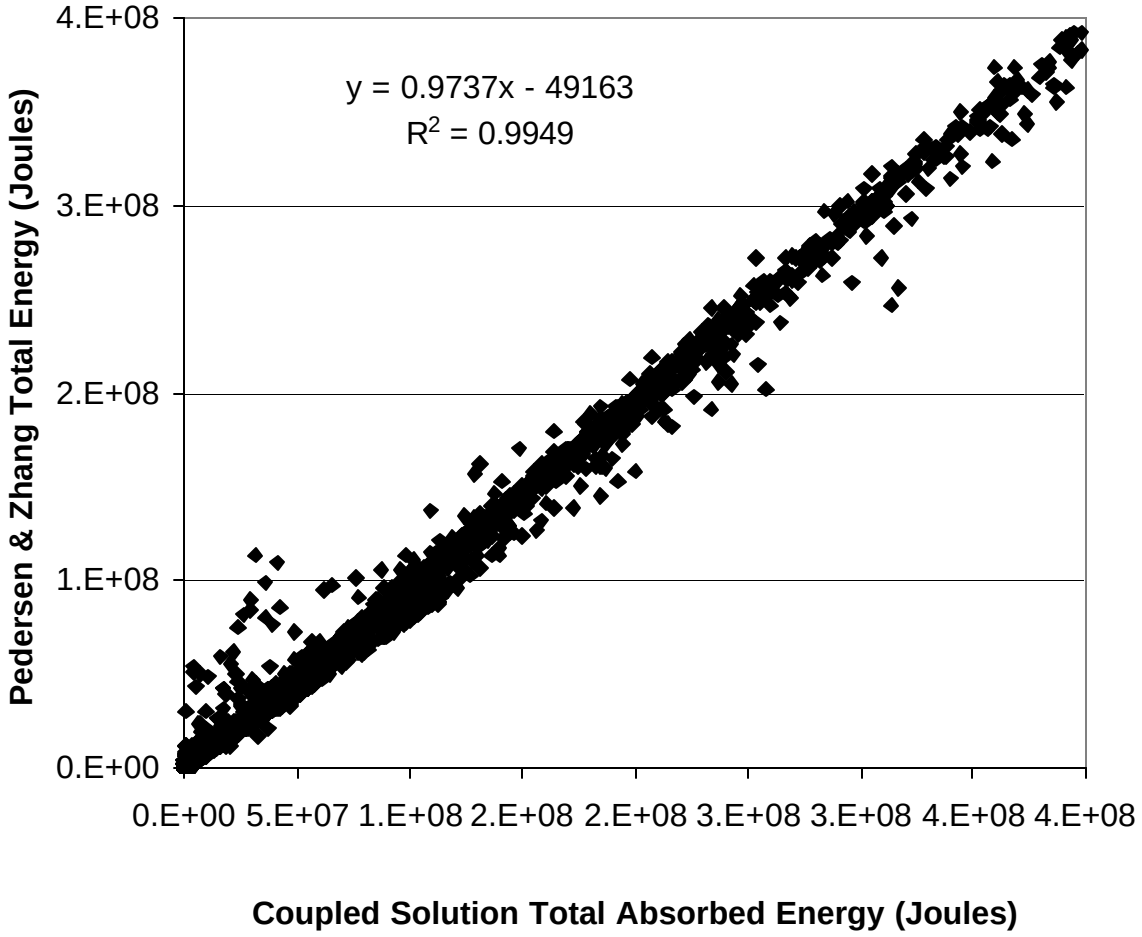

Figure 131 - Total Absorbed Energy

Figure 131 through Figure 133 compare absorbed energy calculated using the Pedersen and Zhang method to energy calculated using SIMCOL. Total absorbed energy shown in Figure 131 is very similar in the two cases, particularly considering the significant difference in the two methods. The longitudinal and transverse components show a larger difference, particularly in the longitudinal direction. This may result from differences in structural resistance in the transverse and longitudinal directions, which in SIMCOL varies during the collision process. The difference in longitudinal absorbed energy is potentially significant because once the structure is penetrated, longitudinal damage extent determines the number of compartments that are opened

to the sea. This has a significant effect on damage stability and oil outflow. Using uncoupled methods to predict absorbed longitudinal energy may not provide sufficient accuracy for this calculation.

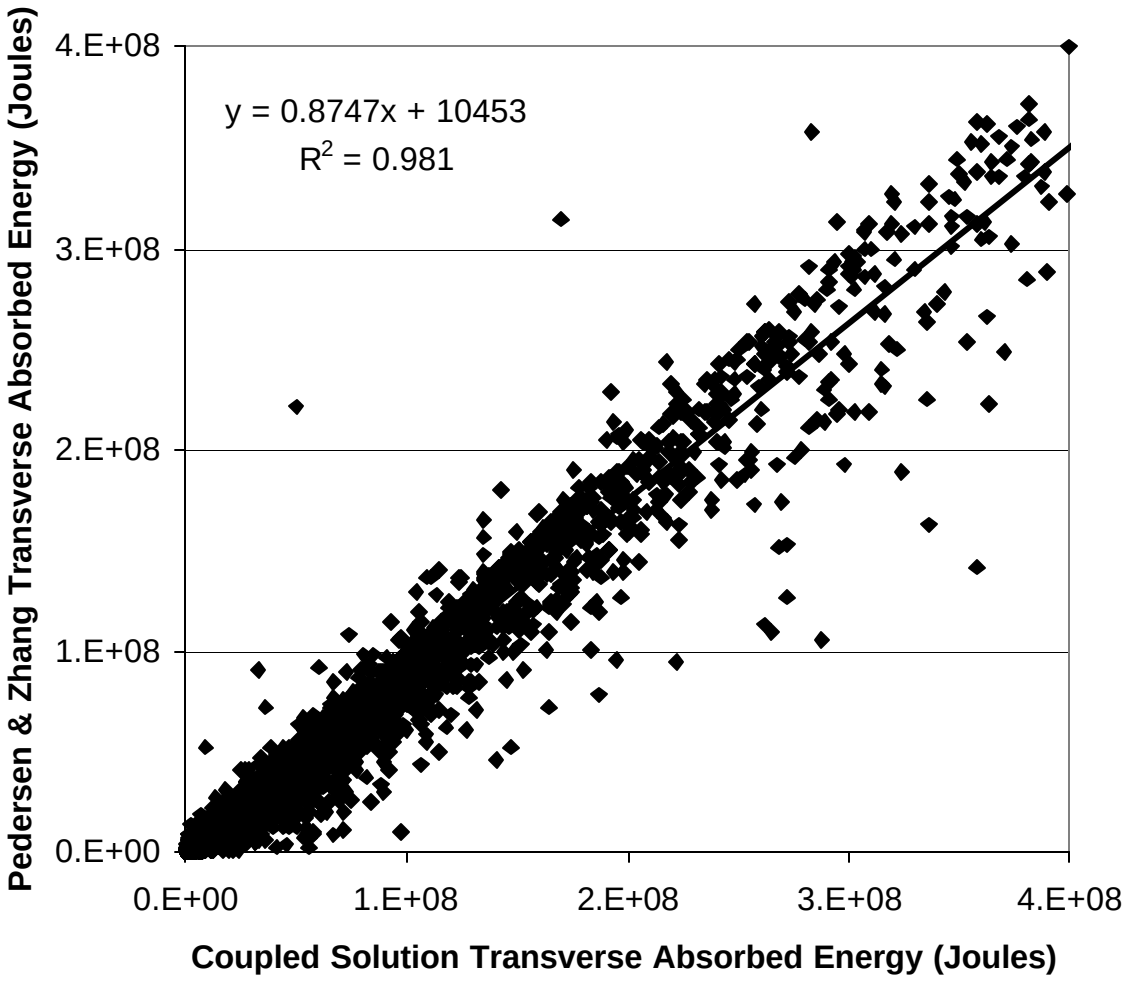

Figure 132 - Transverse absorbed energy

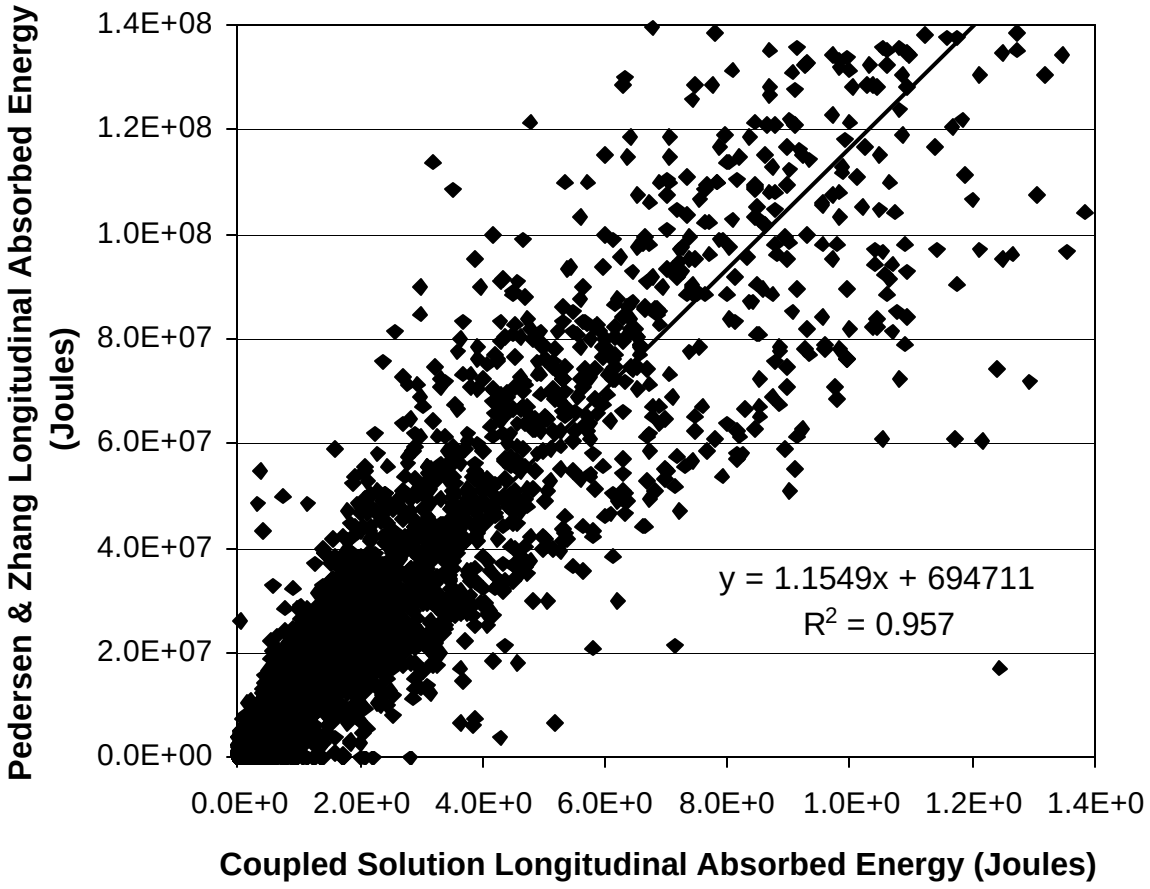

Figure 133 - Longitudinal absorbed energy

CHAPTER 8 SIMCOL Oil Outflow Application

8.1 Struck Ships

The crashworthiness of four struck ships is considered in a probabilistic oil outflow (given a collision) analysis. The struck ships include two 150000 dwt ships, one single hull (SH150) and one double hull (DH150), and two 45000 dwt ships, one single hull (SH45) and one double hull (DH45). SIMCOL input data for these ships are provided in Table 22 and Table 23.

Table 22 - Struck Ship Principal Characteristics

	DH150	SH150	DH45	SH45
Displacement, MT	151861	152395	47448	47547
Length, m	261.0	266.3	190.5	201.2
Breadth, m	50.0	50	29.26	27.4
Depth, m	25.1	25.1	15.24	14.3
Draft, m	16.76	16.76	10.58	10.6
Double bottom height, m	3.34	NA	2.1	NA
Double hull width, m	3.34	NA	2.438	NA

Table 23 – Stuck Ship Structural Characteristics

	DH150	SH150	DH45	SH45
Web frame spacing ,mm	5.2	5.2	3.505	3.89
Smeared deck thickness, mm	29.4	28.2	27.6	30.5
Smeared inner bottom thickness, mm	37.1	NA	27.8	NA
Smeared bottom thickness, mm	36.6	44.2	34	38.5
Smeared stringer thickness, mm	14.9	NA	NA	NA
Smeared side shell thickness, mm	26.7	27.8	24.5	23.6
Smeared inner side thickness, mm	28.1	NA	20.1	NA
Smeared long bhd thickness, mm	25.1	24.5	20	33.4
Smeared upper web thickness, mm	12.5	12.5	12.7	19
Smeared lower web thickness, mm	14.5	16	12.7	19

The collision variable probabilities and probability density functions provided in Chapter 7 are used to develop 10000 collision cases which are applied to the four struck ship designs, for a total of 40000 SIMCOL runs. SIMCOL calculates damage penetration, damage length and oil outflow for each of these runs. A summary of these results is provided in Section 8.2.

8.2 Results

Ten thousand collision cases selected using the assumptions, probabilities and probability density functions specified in Chapter 7 are applied to each of the four ships described in Section 8.1. Damage penetration, damage length and oil outflow are calculated using SIMCOL. Results are summarized in Table 24 and Figure 134 through Figure 136. These results consider all cases, including those with zero outflows and no penetration.

Table 24 – SIMCOL Output Summary

	SH150	DH150	SH45	DH45
Mean penetration (m)	2.28	1.39	1.57	1.28
Mean outflow (m3)	4039	1686	1179	496
Mean damage length (m)	3.87	2.52	2.81	2.29

Table 24 lists mean values for damage length, damage penetration, and oil outflow for each of the four ships. The results are consistent with expected trends. Single hull penetration and damage length exceed the corresponding double hull values at both displacements. This reflects the inherent ability of the double hull to absorb more energy for a given penetration. Damage penetration and length are less for the lower displacement ships. This is due to the collision external dynamics. The smaller ships are accelerated to higher transverse velocities after collision and less kinetic energy is absorbed in structural deformation. Double hull mean outflow is less than the corresponding single hull value at both displacements. This is a result of the lesser double hull damage and the requirement to penetrate and rupture the inner hull of the double hull before spilling oil. Protectively-located ballast tanks in the single hull are not sufficient to reverse the double hull advantages. Outflow is less for the lower displacement ships because individual tanks are smaller and in most cases only single tanks are penetrated.

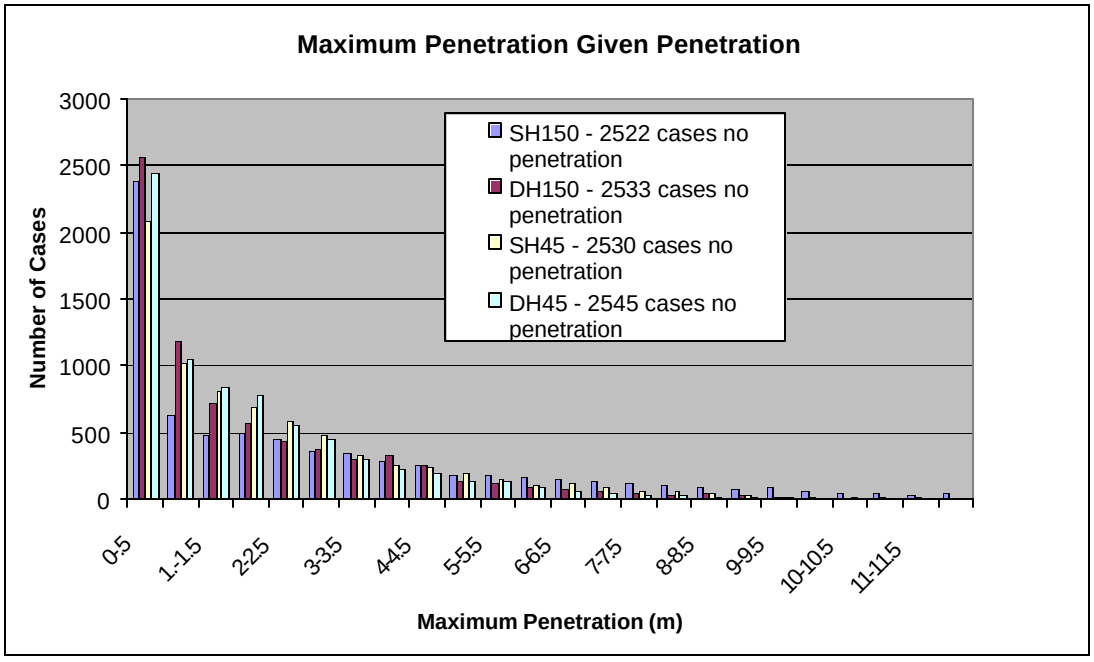

Figure 134 - Penetration Results

Damage penetration and length results are shown in Figure 134 and Figure 135. These results are also consistent with expected trends. The double hull ships have more small penetrations than the corresponding single hull ships. Most penetrations in the SH150 are less than 10 meters. This is consistent with the B/5 rule of thumb. Most penetrations in the SH45 are less than 8 meters. This is slightly above the B/5 rule of thumb. Penetration in the double hull ships is less than the corresponding single hull ships. B/6 would be a better rule of thumb for penetration in these double hull ships.

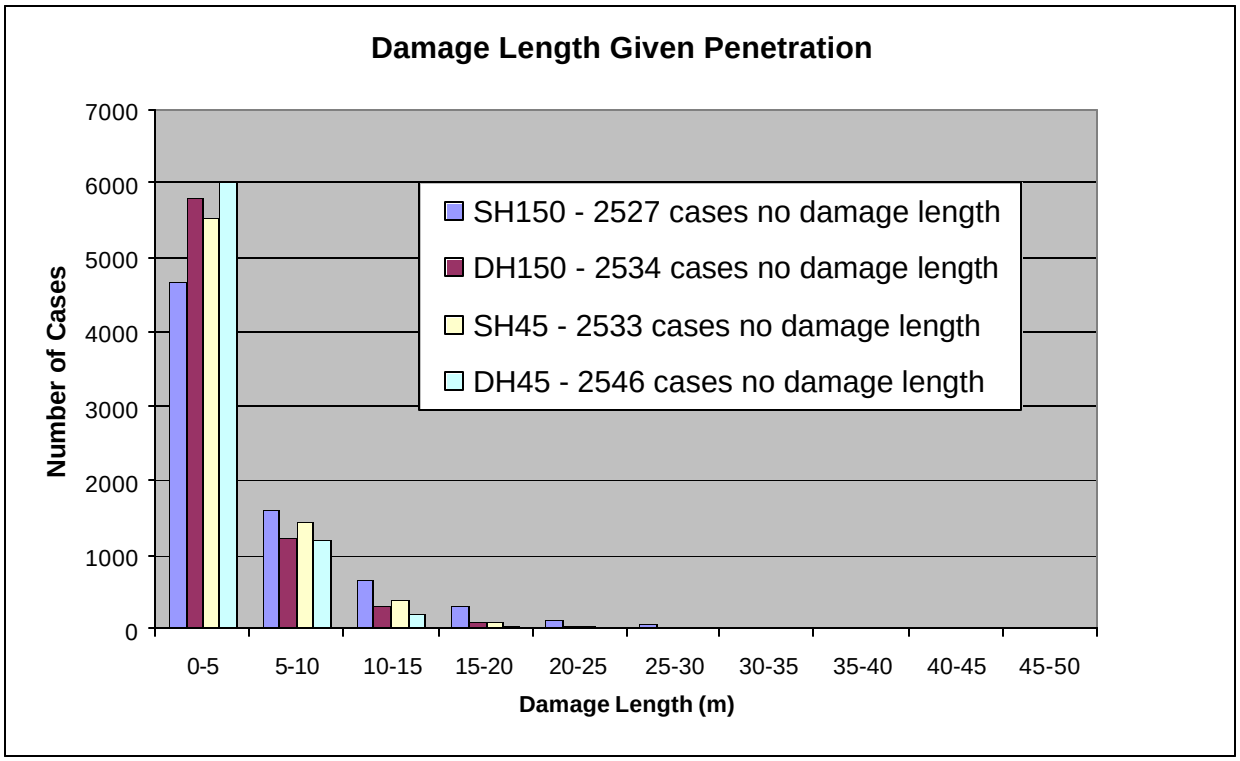

Figure 135 – Damage Length Results

Oil outflow results are shown in Figure 136. These results appear to be much less uniform than in grounding because side damage outflow occurs in total tank increments and tank sizes are very different in the four ships. The largest tank in the DH150 is 14674 cubic meters. Figure 136 shows that there are a number of DH150 cases where more than one cargo tank is penetrated. There are a few cases that penetrate to the 21566 cubic meter centerline tank in SH150. The small ships have more small spills. Individual outflow results for each ship are shown in Figure 137 through Figure 140. Figure 141 and Figure 142 show the difference in outflow between single and double hull ships of the same size.

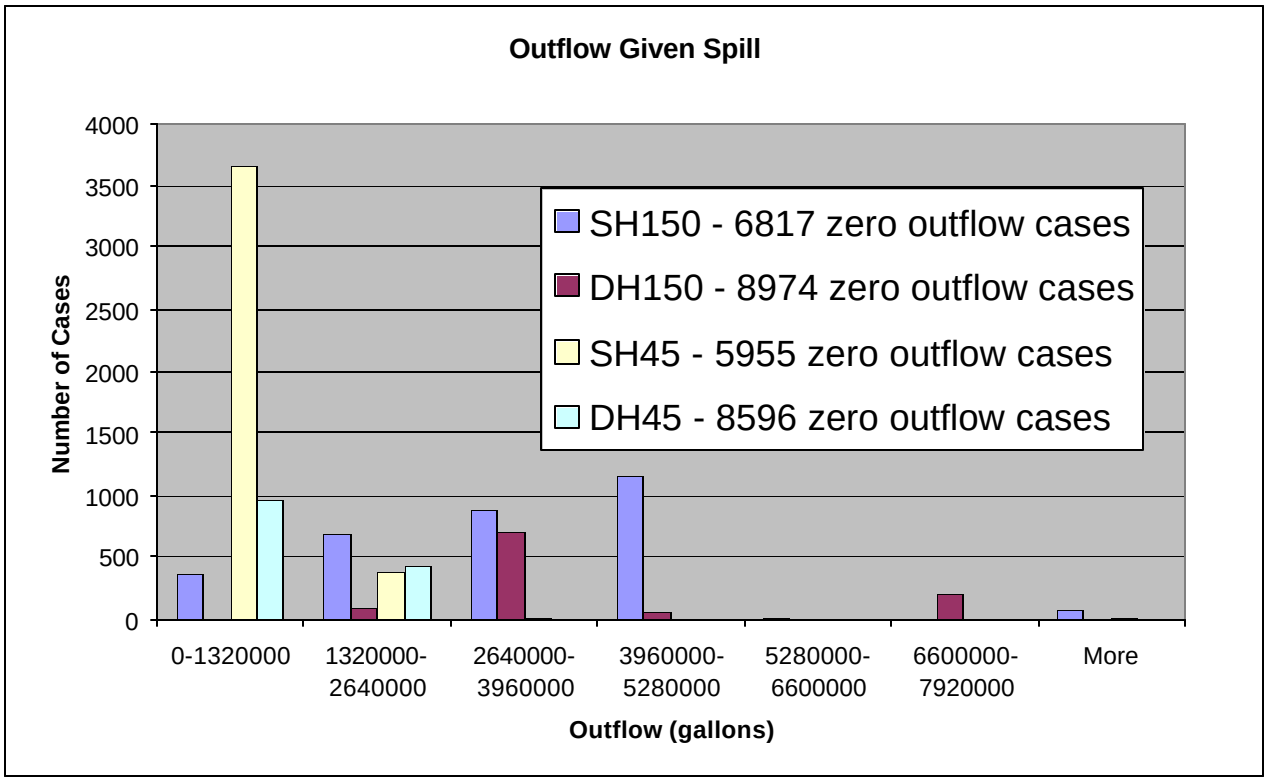

Figure 136 – Outflow Results

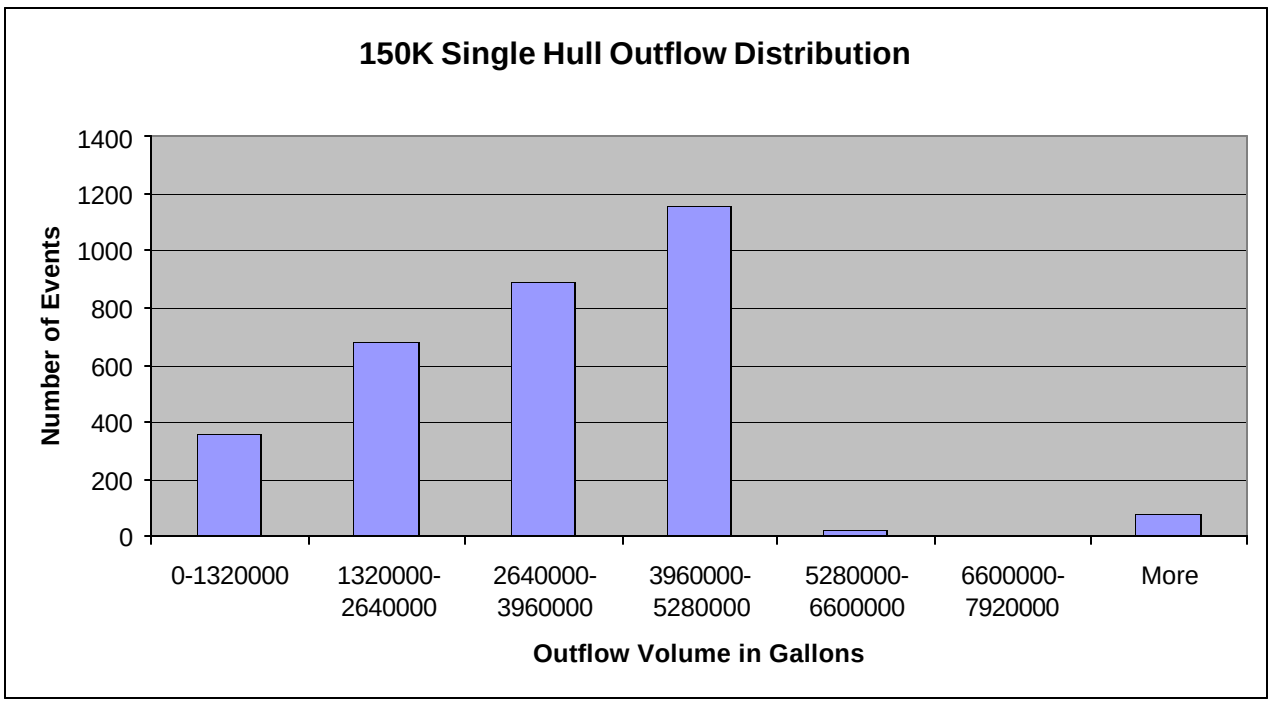

Figure 137 - SH150 Outflow Results

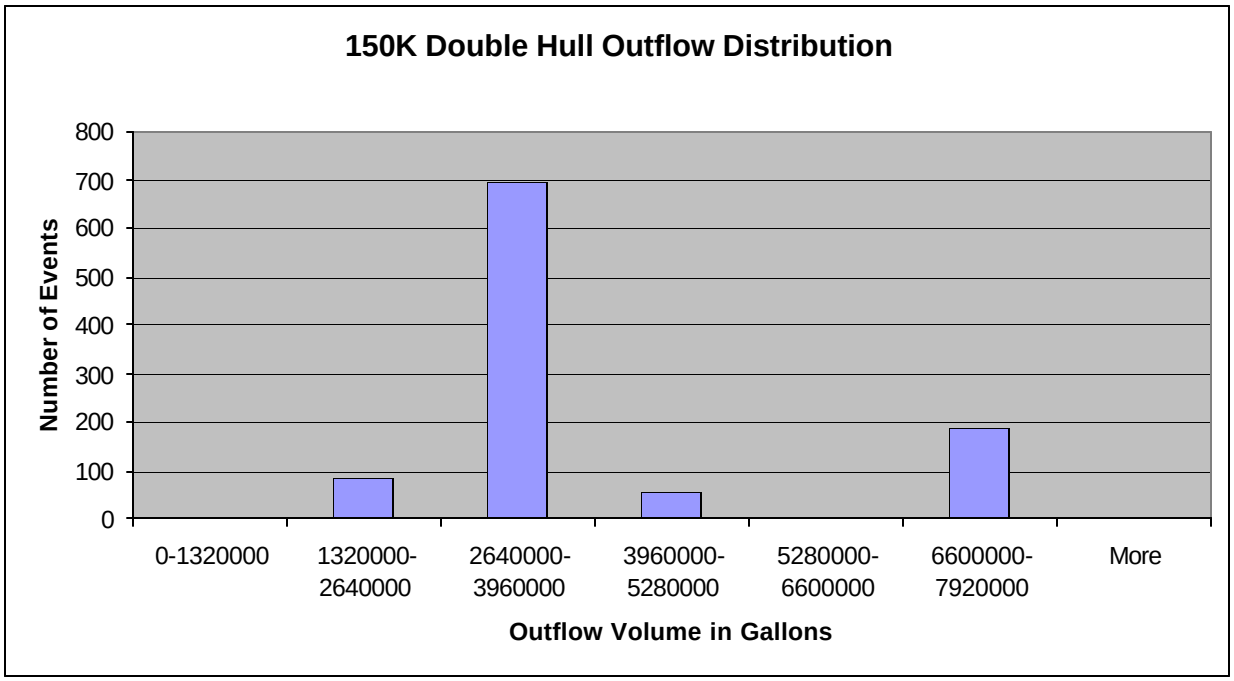

Figure 138 - DH150 Outflow Results

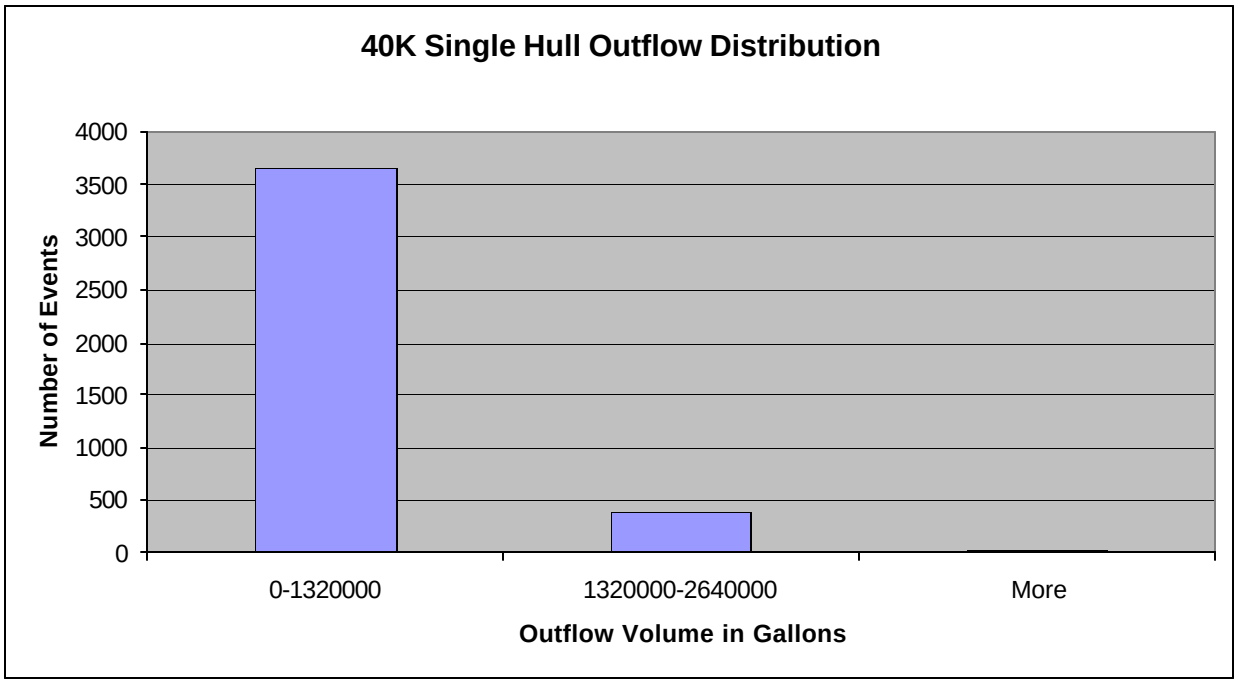

Figure 139 - SH45 Outflow Results

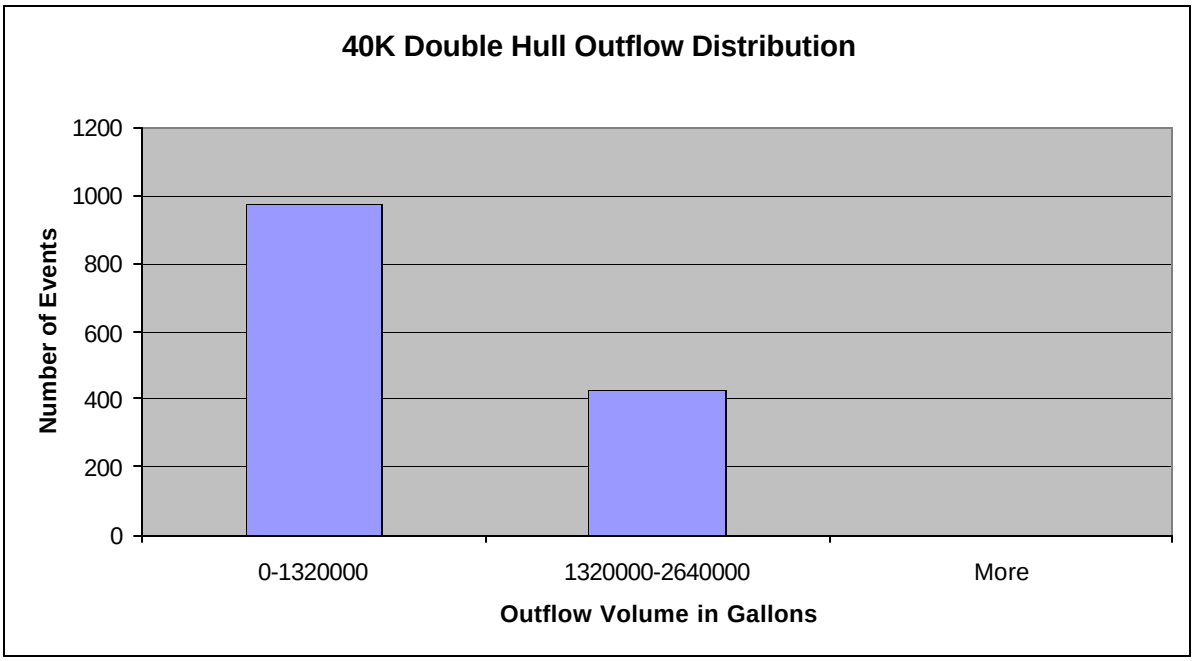

Figure 140 - DH45 Outflow Results

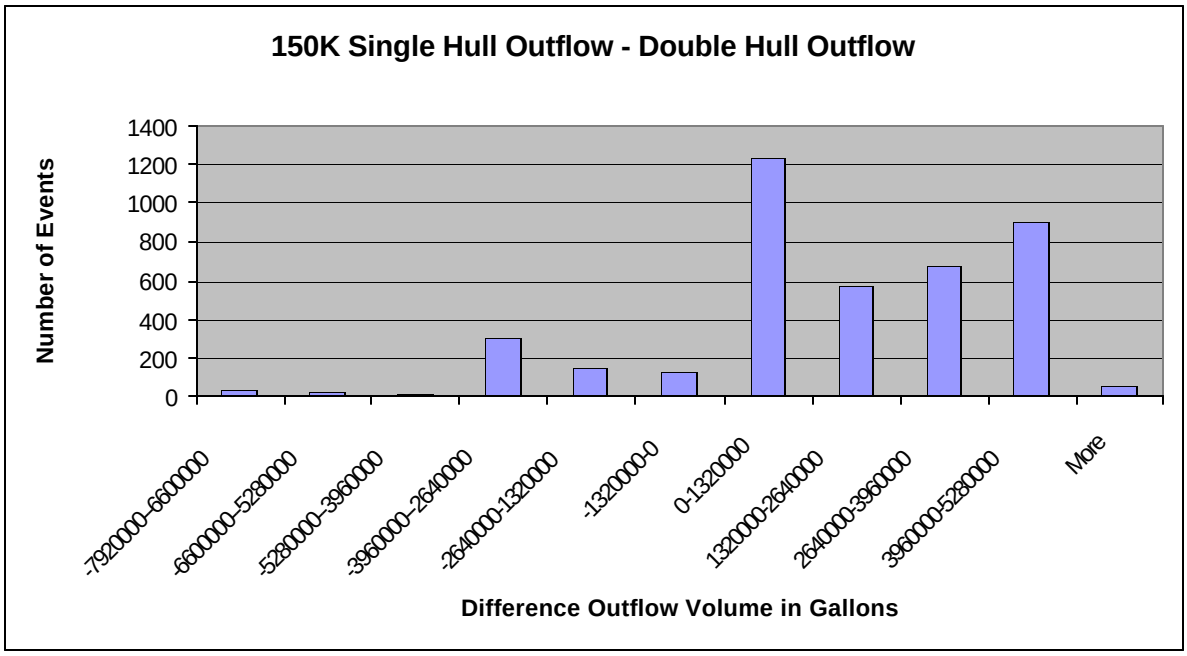

Figure 141 - 150K Tanker Outflow Difference Results

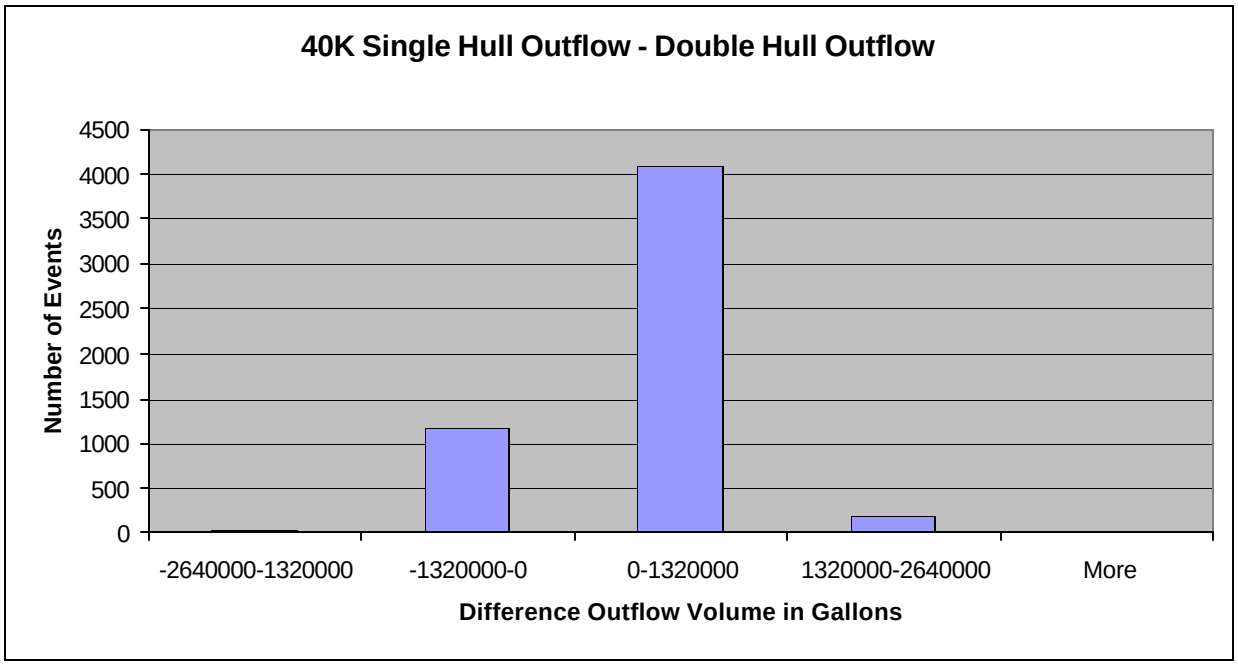

Figure 142 - 45K Tanker Outflow Difference Results

CHAPTER 9 Conclusions and Future Work

This study takes a first step in predicting side damage and oil outflow in ship collisions. It provides a rational probabilistic method for defining collision cases, provides a preliminary validation of a simplified collision model, and provides preliminary results comparing damage and oil outflow for two sizes of single hull and double hull tankers.

The most significant product of this study is the demonstration of a rational process. There will certainly be future improvements to the collision statistical description and to collision and outflow models, but this process works. It provides an important piece of the overall framework for assessing the environmental performance of tankers. The proposed methodology provides a practical means of considering structural design in a regulatory framework, and when implemented will improve the safety and environmental performance of ships.

The following specific tasks were completed using SIMCOL in support of this project:

1. Completed the development of SIMCOL Version 2.11.
2. Developed the capability to model collision events using LSDYNA.
3. Preliminary validation of SIMCOL. Due to the lack of sufficient actual or test data for proper model validation, preliminary validation was accomplished by comparison to results from two other simplified models and two finite element models.
4. Defined probabilistic oil tanker collision events. Probabilities and probability density functions were developed for important collision event parameters.
5. Predicted probabilistic structural damage and oil outflow for four notional oil tankers. Collision damage and outflow were calculated for ten thousand collision events. Mean values and response surfaces were developed for each tanker. Sensitivity to collision scenario variables was explored.

This work continues. Significant future work planned includes:

1. Develop and include a simplified deformable bow model in SIMCOL. Include bow characteristics in the probabilistic collision scenario description. Assess the impact of this change on probabilistic collision damage and oil outflow predictions.
2. Continue to collect collision case data that may be used to validate LSDYNA and SIMCOL collision models. Perform additional validation.
3. Use LSDYNA to study collision damage impacting transverse bulkheads with particular emphasis on the effect of transverse bulkheads on longitudinal extent of damage. Develop a simplified model for the structural response of transverse bulkheads in collision and incorporate into SIMCOL.
4. Apply this methodology to the structural optimization of a tanker design for crashworthiness. Analyze the effect of various structural design parameters on crashworthiness.
5. Apply SIMCOL to calculate probabilistic collision damage for a range of ship types and designs typical of the worldwide population. Compare damage pdfs to those obtained based on data from the IMO data base and to those predicted using the DTU model.

References

[1] Sirkar, J., Ameer, P., Brown, A.J., Goss, P., Michel, K., Willis, W., "A Framework for Assessing the Environmental Performance of Tankers in Accidental Grounding and Collision", *SNAME Transactions **105**, 253-295*, 1997.

[2] Rawson, C., Crake, K. and Brown, A.J., "Assessing the Environmental Performance of Tankers in Accidental Grounding and Collision", *SNAME Transactions **106**, 41-58*, 1998.

[3] Brown, A.J. and Amrozowicz, M., "Tanker Environmental Risk - Putting the Pieces Together", SNAME/SNAJ International Conference on Designs and Methodologies for Collision and Grounding Protection of Ships, August 1996.

[4] IMO, "Interim Guidelines for Approval of Alternative Methods of Design and Construction of Oil Tankers under Regulation 13F(5) of Annex I of MARPOL 73/78", Resolution MEPC.66 (37), Adopted September 14, 1995.

[5] Jones, N., "A Literature Survey on the Collision and grounding Protection of Ships", Ship Structure Committee Report No. SSC-283, 1979.

[6] Giannotti, J.G., Jones, N., Genalis, P. and Van Mater, P.R., "Critical Evaluations of Low-Energy Ship Collision - Damage Theories and Design Methodologies, Volume I: Evaluation and Recommendations", Ship Structure Committee Report No. SSC-284, 1979.

[7] Giannotti, J.G., Jones, N., Genalis, P. and Van Mater, P.R., "Critical Evaluations of Low-Energy Ship Collision - Damage Theories and Design Methodologies, Volume II: Literature Search and Review", Ship Structure Committee Report No. SSC-285, 1979.

[8] ISSC, Report by Specialist Panel V.4 – Structural Design Against Collision and Grounding, Proceedings of the 13th International Ship and Offshore Structures Congress 1997, Trondheim, Norway, 1997.

[9] Minorsky, V.V.,"An Analysis of Ship Collisions with Reference to Protection of Nuclear Power Plants," Journal of Ship Research, 1959.

[10] Simonsen, B.C., "Theory and Validation for the DAMAGE Collision Module", Joint MIT-Industry Program on Tanker Safety, Report No. 67, June 1999.

[11] Crake, K., "Probabilistic Evaluations of Tanker Ship Damage in Grounding Events", Naval Engineer Thesis, MIT, 1995.

[12] Hutchison, B.L., "Barge Collisions, Rammings and Groundings - an Engineering Assessment of the Potential for Damage to Radioactive Material Transport Casks", Report No. SAND85-7165 TTC-05212, 1986.

[13] Zhang, S., "The Mechanics of Ship Collisions", Ph.D. Thesis, Department of Naval Architecture and Offshore Engineering, technical University of Denmark, Lyngby, 1999.

[14] Pedersen, P.T. and Zhang, S., 1998. "On Impact Mechanics in Ship Collisions", Marine Structures, Vol. 11, pp. 429-449.

[15] Reardon, P. and Sprung, J.L., “Validation of Minorsky’s Ship Collision Model and Use of the Model to Estimate the Probability of Damaging a Radioactive Material Transportation Cask During a Ship Collision”, *Proceedings of the International Conference on Design and Methodologies for Collision and Grounding Protection of Ships*, San Francisco, August 1996.

[16] McDermott, J.F., Kline, R.G., Jones, E.L., Maniar, N.M., Chiang, W.P., “Tanker Structural Analysis for Minor Collisions”, *SNAME Transactions*, Vol. 82, pp. 382-414, 1974.

[17] Woisin, G., "Design Against Collision", *International Symposium on Advances in Marine Technology*, Trondheim, Norway, June 1979.

[18] Rosenblatt & Son, Inc, “Tanker Structural Analysis for Minor Collision”, USCG Report, CG-D-72-76, 1975.

[19] Reckling, K.A., "Mechanics of Minor Ship Collisions", *International Journal of Impact Engineering*, Vol. 1, No. 3, pp. 281-299, 1983.

[20] Wierzbicki, T., "Crushing Behavior of Plate Intersections", *Structural Crashworthiness*, edited by A. Jones and T. Wierzbicki, Chapter 3, Butterworth and Co., London, 1983.

[21] Paik, J. and Wierzbicki, T., "A Benchmark Study on Crushing and Cutting of Plated Structures", *Journal of Ship Research*, p. 147, June, 1997.

[22] Pedersen, P.T., et al, "Ship Impacts: Bow Collisions", *International Journal of Impact Engineering*, Vol. 13, No. 2, pp. 163-187, 1993.

[23] Amdahl, J., “Energy Absorption in Ship-Platform Impacts”, Dr. Ing. Thesis, Report No. UR-83-84, The Norwegian Institute of Technology, Trondheim, 1983.

[24] Yang, P.D.C. and Caldwell, J.B., "Collision Energy Absorption in Ships Bow Structures", *International Journal of Impact Engineering*, Vol. 7, No. 2, 1988.

[25] Ito, H., et al, "A Simplified Method to Analyze the Strength of Double Hulled Structures in Collision", *Journal of Society of Naval Architects of Japan*, Vol. 156, pp. 283-295, 1984.

[26] Ito, H., et al, "A Simplified Method to Analyze the Strength of Double Hulled Structures in Collision, 2nd Report", *Journal of Society of Naval Architects of Japan*, Vol. 158, pp. 420-434, 1985.

[27] Ito, H., et al, "A Simplified Method to Analyze the Strength of Double Hulled Structures in Collision, 3rd Report", *Journal of Society of Naval Architects of Japan*, Vol. 160, pp. 401-409, 1986.

[28] Paik, J.K., et al, "On Rational Design of Double Hull Tanker Structures against Collision”, *1999 SNAME Annual Meeting*, 1999.

[29] Paik, J.K. and Pedersen, P.T., "Modeling of the Internal Mechanics in Ship Collisions", *Ocean Engineering*, Vol. 23, No. 2, pp. 107-142, 1996.

[30] Hallquist, J.O (1998), “LSDYNA Examples Manual”, Livermore Software Technology Corporation (LSTC), March 1998.

[31] Hallquist, J.O (1998), “LSDYNA Theoretical Manual”, Livermore Software Technology Corporation (LSTC), May 1998.

[32] Hallquist, J.O (1999), “LSDYNA Keyword Users Manual – Nonlinear Dynamic Structural Analysis of Structures”, Livermore Software Technology Corporation (LSTC), May 1999.

[33] Lenselink, H., and Thung, K.G., “Numerical Simulations of the Dutch-Japanese Full Scale Ship Collision Tests”, Proceedings of Conference on Prediction Methodology of Tanker Structural Failure, ASIS, Tokyo, July 1992.

[34] Wevers, L.J. and Vredeveldt, A.W., "Full Scale Ship Collision Experiments", TNO Report 98-CMC-R0359, 1999.

[35] Chen, D., “Simplified Collision Model (SIMCOL)”, Dept. of Ocean Engineering, Virginia Tech, Master of Science Thesis, May 2000.

[36] Gibbs and Cox, Inc., "Design Criteria and Guide for Design of Nuclear-Powered Merchant Ships", for the US Department of Commerce, MARAD Nuclear Projects Office, January 1960.

[37] Kierkegaard, H., “Ship Collisions with Icebergs”, PhD Thesis, DTU, April 1993.

[38] Kitamura, K. and Akita, M., “A Study on Collision by an Elastic Stem to the Side Structure of Ships”, Trans. SNAJ, 131, 307-317, 1972.

[39] Hagiwara, K., Takanabe, H. and Kawano, H., “A Proposed Method of Predicting Ship Collision Damage”, International Journal of Impact Engineering, No. 1, International Journal of Impact Engineering, No. 1, 1983.

[40] Kim, J.Y., “Crushing of a Bow: Theory vs. Scale Model Tests”, Joint MIT-Industry Program on Tanker Safety, Report No. 69, June 1999.

[41] Kim, J.Y., “Analysis of a Dropped Bow Collision Model”, Joint MIT-Industry Program on Tanker Safety, Report No. 72, May 2000.

[42] Gooding, Peter W. (1999), “Collision with a Crushable Bow”, MIT Thesis, 1999

[43] Gerard, G., ""The Crippling Strength of Compression Elements", *Journal of Aeronautical Science*, 1958.

[44] Amdahl, J. and Kavlie, D., “Experimental and Numerical Simulation of Double Hull Stranding”, Proceedings of the DNV-MIT Workshop on “Mechanics of Ship Collision and Grounding”, Oslo, 1992.

[45] Amdahl, J. and Kavlie, D., “Design of Tankers for Grounding and Collision”, MARIENV ’95, 1995.

[46] Lehmann, E. and Yu, X., “Progressive Folding of Bulbous Bows”, The Sixth International Symposium on Practical Design of Ships and Mobile Units (PRADS), September, 1995.

[47] Lutzen, M., Simonsen, B.C. and Pedersen, P.T., "Rapid Prediction of Damage to Struck and Striking Vessels in a Collision Event", Ship Structure Symposium 2000, Washington D.C., 2000.

[48] Kierkegaard, H., Ship Bow Response in High Energy Collision", Marine Structures, Vol. 6, pp. 359-376, 1993.

[49] Arita, K., “A Probabilistic Assessment on Protective Structures in Ship Collisions”, 63 General Meeting of Ship Research Institute, 1994.

[50] Valsgard, S. and Pettersen, E., "Simplified Non-Linear Analysis of Ship/Ship Collisions", Norwegian Maritime Research, No. 3, pp. 2-17, 1982.

[51] Bach-Gansmo, O. and Valsgard S., "Simplified stiffness evaluation of a bulbous ship bow", Progress report No. 1, DnV, Report No. 81-0437 (Rev. no. 1 of 17.02.82), 1981.

[52] Chang, P.Y., Seibold, F. and Thasantorn, C., "A Rational Methodology for the Prediction of Structural Response due to Collision of Ships.", Paper No. 6, SNAME Annual Meeting, New York, NY, Nov. 13-15, 1980.

[53] Wang, G., Katsuyuki, S., Ohtsubo, H. (1995), "Predicting Collision Strength of Bow Structure", Marienv 95

[54] Suzuki, K., Ohtsubo, H. (1995), "Crushing Strength of Ship Bow Structure - Calculation of Absorbed Energy and Optimal Design", Marienv95

[55] Vakkalanka, Suryanarayana, "Simplified Bow Model for a Striking Ship in Collision", Dept. of Ocean Engineering, Virginia Tech, Master of Science Thesis, July 2000.

[56] Xia, Jianjun, "Finite Element Analysis of Ship Collisions", Department of Ocean Engineering, Virginia Tech, Master of Science Thesis, May 2001.

[57] Kitamura, O., "FEM Approach to the Simulation of Collision and Grounding Damage", 2nd International Conference on Collision and Grounding of Ships, Copenhagen, Denmark, July, 2001.

[58] Gu, Y. and Wang, Z.L., "An Inertia Equivalent Model for Numerical Simulation of Ship-Ship Collisions", 2nd International Conference on Collision and Grounding of Ships, Copenhagen, Denmark, July, 2001.

[59] Lemmen, P.P.M. and Vredeveldt, A.W., "Application of Explicit Finite Element Method in Ship Collision Analysis", TNO Report 93-CMC-R1153, 1 December 1993.

[60] Servis, D. et. al., "The Implementation of Finite Element Codes for the Simulation of Ship-Ship Collision", 2nd International Conference on Collision and Grounding of Ships, Copenhagen, Denmark, July, 2001.

[61] Naar, H. et. al., "Comparison of the Crashworthiness of Various Bottom and Side Structures", 2nd International Conference on Collision and Grounding of Ships, Copenhagen, Denmark, July, 2001.

[62] Sinmao, M. & Abramowicz, W. "Joint MIT-Industry Report #66." MIT Department of Ocean Engineering, 1999.

[63] Tikka, K.K. & Chen, Y.J. "Prediction of Structural Response in Grounding", Ship Structure Symposium 2000, Washington D.C., 2000.

[64] Simonsen, B.C. "Ship Grounding on Rock – I.", Marine Structures, 10, pp. 519-562, 1997.

[65] Kitamura, O. "Buffer Bow Design for the Improved Safety of Ships", Ship Structure Symposium 2000, Washington D.C., 2000.

[66] "Machinery's Handbook 25, Twenty Fifth Edition." Industrial Press Inc., 1996.

[67] Simonsen, B.C. & Wierzbicki, T. "Joint MIT-Industry Report #59." MIT Department of Ocean Engineering, 1999.

[68] Shibue, T., Abe, A. and Fujita, K. "The Effect of the Strut Arrangement on the Energy Absorption of Side Structure in Collision", 2nd International Conference on Collision and Grounding of Ships, Copenhagen, Denmark, July, 2001.

[69] Lehmann, E. & Peschmann, J. "Energy Absorption by the Steel Structure of Ships in the Event of Collisions", 2nd International Conference on Collision and Grounding of Ships, Copenhagen, Denmark, July, 2001.

[70] Wisniewski, K., Kolakowski, P., Rozmarynowski, B. & Gierlinski, J.T. "Dynamic FE simulation of damage in ships collision", 2nd International Conference on Collision and Grounding of Ships, Copenhagen, Denmark, July, 2001.

[71] "LSDYNA USER'S MANUAL", Livermore Software Technology Corporation, 2001.

[72] Lemmen, P.M., Vredeveldt, A.W., and Pinkster, J.A., "Design Analysis for Grounding Experiments", SNAME/SNAJ International Conference on Designs and Methodologies for Collision and Grounding Protection of Ships, San Francisco, August 1996.

[73] Simonsen and Lauridsen. "Energy Absorption and Ductile Failure in Metal Sheets Under Lateral Indentation by a Sphere."

[74] Kitamura, O., "Comparative Study on Collision Resistance of Side Structure", Marine Technology, Vol. 34, No. 4, pp.293-308, October 1997.

[75] Servis, D.P., and Samuelides, M., "Ship Collision Analysis Using Finite Elements", Safer Euroro Spring Meeting, Nantes Greece, 28 April 1999.

[76] Francis, P.H., Cook, T.S., and Nagy, A., Ship Structure Committee Report Number 276 (SSC-276), 1978.

[77] R.L. Rothman & R.E. Monroe, Ship Structure Committee Report Number 235 (SSC-235), 1973.

[78] Sandia National Laboratories, *Data and Methods for the Assessment of the Risks Associated with the Maritime Transport of Radioactive Materials Results of the SeaRAM Program Studies*, SAND98-1171/2, Albuquerque, NM, May 1998.

[79] Lloyds Worldwide Ship data, provided by MARAD, 1993.

[80] ORI, *Hazardous Environment Experienced by Radioactive Material Packages Transported by Water*, Silver Spring, MD, October 1980.

[81] ORI, *Accident Severities Experienced by Radioactive Material Packages Transported by Water*, Silver Spring, MD, November 1981.

[82] USCG Ship Casualty Data, 1982-1990.

Appendix A – Smeared Plate Thickness Calculation

DH150 Smeared Thickness:

SEQ	ID		B	THK	CORROSION	Stif A	Stif SPAC	MATID	TOTAL AREA	SMEARED THK
NO		DESCRIPTION	m	cm	(mm)	cm2	(m)		(cm^2)	(m)
1	KPL-01	KEEL PLATE	1.8	1.9	1	342	0.85	2		
2	BTM-01	BOTTOM	3.3	1.7	1	561	0.85	2		
3	BTM-02	BOTTOM	5.1	1.7	1	867	0.85	2		
4	BTM-03	BOTTOM	5.1	1.7	1	867	0.85	2		
5	BTM-04	BOTTOM	5.1	1.7	1	867	0.85	2		
6	BTM-05	BOTTOM	1.1	1.7	1	187	0.85	2		
7	BLG-01	BILGE	0.976	1.7	1	165.87	2.201	2		
8	BLG-02	BILGE	0.975	1.7	1	165.82	2.927	2		
9	BLG-03	BILGE	0.975	1.7	1	165.82	2.927	2		
10	BLG-04	BILGE	0.976	1.7	1	165.87	2.201	2		
11	BLG-05	BILGE	0.1	1.7	1	17	1.226	2	4371.38	0.0171
12	SHL-01	SIDE	1.85	1.7	1.5	314.5	0.85	2		
13	SHL-02	SIDE	4.25	1.8	1.5	765	0.85	1		
14	SHL-03	SIDE	5.1	1.8	1.5	918	0.85	1		
15	SHL-04	SIDE	5.1	1.8	1.5	918	0.85	1		
16	SHL-05	SIDE	1.45	1.8	1.5	261	0.85	1		
17	SHL-06	SIDE	2.55	2	1.5	510	0.85	2	3686.5	0.0182
18	GWR-01	GUNWALE	0.1	2	2	20	0.7	2		
19	GWR-02	GUNWALE	0.518	2	2	103.53	0.518	2		
20	GWR-03	GUNWALE	0.518	2	2	103.52	0.518	2		
21	GWR-04	GUNWALE	0.518	2	2	103.53	0.718	2		
22	GWR-05	GUNWALE	0.15	2	2	30.01	0.718	2		
23	DEC-01	UPPER DECK	0.85	2	2	170.05	0.8	2		
24	DEC-02	UPPER DECK	20.805	1.9	1	3953.04	0.855	2		
25	DEC-03	UPPER DECK	1.2	1.9	1	228	0.855	2	4711.68	0.0191
26	INB-01	INNER BOTTOM	5.1	1.7	1.5	867	0.85	2		
27	INB-02	INNER BOTTOM	5.1	1.7	1.5	867	0.85	2		
28	INB-03	INNER BOTTOM	5.1	1.7	1.5	867	0.85	2		
29	INB-04	INNER BOTTOM	5.1	1.7	1.5	867	0.85	2	3468	0.0170
30	INS-01	I.S. BULKHEAD	2.68	2	1.5	536	0.9	2		
31	INS-02	I.S. BULKHEAD	4.25	1.8	1.5	765	0.85	2		
32	INS-03	I.S. BULKHEAD	5.1	1.9	1.5	969	0.85	1		
33	INS-04	I.S. BULKHEAD	5.1	1.6	1.5	816	0.85	1		
34	INS-05	I.S. BULKHEAD	1.45	1.65	1.5	239.25	0.85	1		
35	INS-06	I.S. BULKHEAD	3.673	1.8	1.5	661.14	0.873	2	3986.39	0.0179
36	CTR-01	C.L. BULKHEAD	1.6	1.6	1	128	0.75	2		
37	CTR-02	C.L. BULKHEAD	1.4	1.65	1	115.5	0.75	1		
38	CTR-03	C.L. BULKHEAD	1.8	1.65	1	148.5	0.85	1		
39	CTR-04	C.L. BULKHEAD	3.2	1.6	1	256	0.85	1		
40	CTR-05	C.L. BULKHEAD	3.2	1.5	1	240	0.85	1		
41	CTR-06	C.L. BULKHEAD	6.4	1.5	1	480	0.85	1		
42	CTR-07	C.L. BULKHEAD	4.6	1.8	1	414	0.975	2	1782	0.0080
43	BGR-01	W.T.BTM.GIRDEF	2.3	1.8	2	207	0.8	2	207	0.0090
44	NBG-01	N-TIGHT B. GDR	0.85	1.4	2	119	0.8	2		
45	NBG-02	N-TIGHT B. GDR	0.6	0	2	0	0.8	2		
46	NBG-03	N-TIGHT B. GDR	0.85	1.4	2	119	0.8	2		
47	NBG-04	N-TIGHT B. GDR	0.85	1.4	2	119	0.8	2		
48	NBG-05	N-TIGHT B. GDR	0.6	0	2	0	0.8	2		
49	NBG-06	N-TIGHT B. GDR	0.85	1.4	2	119	0.8	2		
50	NBG-07	N-TIGHT B. GDR	0.85	1.5	2	127.5	0.8	2		
51	NBG-08	N-TIGHT B. GDR	0.6	0	2	0	0.7	2		
52	NBG-09	N-TIGHT B. GDR	0.85	1.5	2	127.5	0.8	2		
53	NBG-10	N-TIGHT B. GDR	0.85	1.5	2	127.5	0.8	2		
54	NBG-11	N-TIGHT B. GDR	0.6	0	2	0	0.7	2		
55	NBG-12	N-TIGHT B. GDR	0.85	1.5	2	127.5	0.8	2	986	0.0145
56	NTS-01	NON-TIGHT STR	0.7	1.2	2	84	0.7	1		
57	NTS-02	NON-TIGHT STR	0.6	0	2	0	0.7	1		
58	NTS-03	NON-TIGHT STR	0.7	1.2	2	84	0.7	1		
59	NTS-04	NON-TIGHT STR	0.7	1.2	2	84	0.7	1		
60	NTS-05	NON-TIGHT STR	0.6	0	2	0	0.7	1		
61	NTS-06	NON-TIGHT STR	0.7	1.2	2	84	0.7	1		
62	NTS-07	NON-TIGHT STR	0.7	1.2	2	84	0.7	1		
63	NTS-08	NON-TIGHT STR	0.6	0	2	0	0.7	1		
64	NTS-09	NON-TIGHT STR	0.7	1.2	2	84	0.7	1		
65	NTS-10	NON-TIGHT STR	0.6	1.2	2	72	0.8	1		
66	NTS-11	NON-TIGHT STR	0.7	0	2	0	0.8	1		
67	NTS-12	NON-TIGHT STR	0.7	1.2	2	84	0.8	1	660	0.0120

Appendix B – Mass and Moment of Inertia Calculations

BC150 Mass & Moment Calculation Spreadsheet

Definition	Variable	Value	Units	Notes	Assumptions
Total Mass of Vessel	M	1.7774E+08	Kg	Constant	
Needed A11	A11n	1.9551E+08	Kg	A11c -- A11n	
Length Between Perpendiculars	LBP	2.7426E+02	m	Constant	
Length of BOW	Lb	2.1873E+01	m	Constant	
Total Beam Length in HULL	Lh	2.5676E+03	m	Constant	
Total Beam Length in MASSMB1	Lb1	2.4728E+02	m	Constant	
Total Beam Length in MASSMB2	Lb2	2.4788E+02	m	Constant	
Total Beam Length in MASSSTERN	Lr	5.2490E+01	m	Constant	
Area Thickness of MASSMB1	Ab1	1.0000E+00	m^2	Constant	
Area Thickness of MASSMB2	Ab2	1.0000E+00	m^2	Constant	
Area Thickness of MASSSTERN	Ar	1.0000E+00	m^2	Constant	
Area Thickness of HULL	Ah	1.0000E+00	m^2	Constant	
Mass Density of HULL	Dh	6.3273E+04	Kg/m^3	Variable	
Mass Density of MASSMB1	Db1	5.7307E+04	Kg/m^3	Variable	
Mass Density of MASSMB2	Db2	5.7307E+04	Kg/m^3	Variable	
Mass Density of MASSSTERN	Dr	5.7307E+04	Kg/m^3	Variable	
Calculated Mass of HULL	Mh	1.6246E+08	Kg		
Calculated Mass of MASSMB1	Mb1	1.4171E+07	Kg		
Calculated Mass of MASSMB2	Mb2	1.4205E+07	Kg		
Calculated Mass of MASSSTERN	Mr	3.0081E+06	Kg		
LS-DYNA Mass of BOW	Mb	1.6670E+06	Kg		
Distance HULL from Midships	Xh	0.0000E+00	m	Always equals zero	1
Distance MASSMB1 from Midships	Xb1	2.7426E+01	m	Constant	
Distance MASSMB2 from Midships	Xb2	2.7426E+01	m	Constant	
Distance MASSSTERN from Midships	Xr	1.3713E+02	m	Constant	
Distance BOW Mass from Midships	Xb	1.2984E+02	m	Constant	
HULL Yaw Moment of Inertia	I66h	1.0184E+12	Kg*m^2	-(1/12)*Mh*LBP^2	
BOW Yaw Moment of Inertia	I66b	0.0000E+00	Kg*m^2	Always equals zero	2
Calculated A11	A11c	1.9551E+08	Kg*m^2	A11c -- A11n	
Needed A66	A66n	1.1244E+12	Kg*m^2	A66c -- A66n	
Calculated A66	A66c	1.1244E+12	Kg*m^2	A66c -- A66n	
LS-DYNA Kinetic Energy HULL	Keh	7.9070E+07	(Kg*m^2)/s^2	Velocity: u - 1m/s	
LS-DYNA Kinetic Energy MASSMB1	Keb1	7.1032E+06	(Kg*m^2)/s^2	Velocity: u - 1m/s	
LS-DYNA Kinetic Energy MASSSTERN	Ker	1.5087E+06	(Kg*m^2)/s^2	Velocity: u - 1m/s	
LS-DYNA Kinetic Energy MASSMB2	Keb2	7.1032E+06	(Kg*m^2)/s^2	Velocity: u - 1m/s	
LS-DYNA Kinetic Energy BOW	Keb	8.3351E+05	(Kg*m^2)/s^2	Velocity: u - 1m/s	
LS-DYNA Mass HULL	Mlh	1.5814E+08	Kg		
LS-DYNA Mass MASSMB1	Mlb1	1.4206E+07	Kg		
LS-DYNA Mass MASSMB2	Mlb2	1.4206E+07	Kg		
LS-DYNA Mass MASSSTERN	Mlr	3.0174E+06	Kg		

Checks	Variation	RMS % Error
A11c -- A11n	0	
A66c -- A66n	0.00E+00	
Mlh--Mh	-4320168.655	-2.6592E-02
Mlb1--Mb1	35430.26624	2.5002E-03
Mlb2--Mb2	1.03E+03	7.2215E-05
Mlr--Mr	9335.452423	3.1035E-03
Total Mass	-4274377.1	kg

Assumptions

1. Center of flotation and center of hull are assumed to be at midships
2. I66b small compared to I66h and not considered to effect results

DH150 Mass & Moment Calculation Spreadsheet

Matching Struck Ship:		DH150			
Definition	**Variable**	**Value**	**Unit**	**Note**	**Assumption**
Total Mass of Vessel	M	178867000	Kg	Constant	
Needed A22	A22n	270089170	Kg	A22c -- A22n	
Length Between Perpendiculars	LBP	274.263	m	Constant	
Length of Cargo BLOCK	L	200	m	Constant	
Total Beam Length in BLOCK	Lb	1481	m	Constant	
Total Beam Length in MASSAFT	La	168	m	Constant	
Total Beam Length in MASSFOR	Lf	168	m	Constant	
Area Thickness of BLOCK	Ab	1	m^2	Constant	
Area Thickness of MASSAFT	Aa	1	m^2	Constant	
Area Thickness of MASSFOR	Af	1	m^2	Constant	
Mass Density of BLOCK	Db	156383.6186	Kg/m^3	Variable	
Mass Density of MASSAFT	Da	106994.6751	Kg/m^3	Variable	
Mass Density of MASSFOR	Df	106994.6751	Kg/m^3	Variable	
Calculated Mass of BLOCK	Mb	231604139.2	Kg		
Calculated Mass of MASSAFT	Ma	17975105.41	Kg		
Calculated Mass of MASSFOR	Mf	17975105.41	Kg		
LS-DYNA Mass of Cargo Section	Mc	2534820	Kg		
Distance BLOCK from Midship	Xb	0	m	Always equals zero	1
Distance MASSAFT from Midship	Xa	100	m	Constant	
Distance MASSFOR from Midship	Xf	100	m	Constant	
Distance Cargo Section Mass from Midship	Xc	0	m	Always equals zero	2
Cargo Section Length	Lc	33	m	Constant	
Cargo Section Breadth	Bc	24	m	Constant	
BLOCK Sway Moment of Inertia	I66b	7.72E+11	Kg*m^2	-(1/12)*Mb*L^2	1
Cargo Section Sway Moment of Inertia	I66c	0	Kg*m^2	Always equals zero	2
Calculated A22	A22c	270089170	Kg*m^2	A22c -- A22n	
Needed A66	A66n	1.13152E+12	Kg*m^2	A66c -- A66n	
Calculated A66	A66c	1.13152E+12	Kg*m^2	A66c -- A66n	
LS-DYNA Kinetic Energy BLOCK	Keb	1.16E+08	(Kg*m^2)/ts^2	Velocity: u - 1m/s	
LS-DYNA Kinetic Energy MASSAFT	Kea	8.99E+06	(Kg*m^2)/ts^2	Velocity: u - 1m/s	
LS-DYNA Kinetic Energy MASSFOR	Kef	8.99E+06	(Kg*m^2)/ts^2	Velocity: u - 1m/s	
LS-DYNA Kinetic Energy Cargo Section	Kec	1.27E+06	(Kg*m^2)/ts^2	Velocity: u - 1m/s	
LS-DYNA Mass BLOCK	Mlb	231616000	Kg		
LS-DYNA Mass MASSAFT	Mla	17976000	Kg		
LS-DYNA Mass MASSFOR	Mlf	17976000	Kg		

Checks	**Variation**	**DYNA % Error**
L -- Xa+Xf	0	
A22c -- A22n	0	
A66c -- A66n	0	
Mb -- Mlb	11860.82802	0.01%
Ma -- Mla	894.5859883	0.00%
Mf -- Mlf	894.5859883	0.00%
Ma -- Mf	0	

Assumptions

1: As Cargo section Location changes, I66b is considered small and thus does not change through parralel axis theorem

2: As Cargo Section Location Changes, I66c and Mc*Xc^2 small and not considered to affect results